

# Phytomining of precious metals from mine wastes

Zakuan Azizi Shamsul Harumain  
Doctor of Philosophy

**University of York**  
**Biology**  
**October 2016**

## Abstract

The increasing demand for precious metals such as palladium and gold for industrial applications has led to the exploration of sustainable environmental-friendly technologies to capture and recycle these metals from mine wastes. Phytomining is an emerging technology that makes use of the ability of plants to extract and accumulate metals from soil and water. Chapter 3 discusses the potential of phytomining to recover palladium from mine waste materials. These studies determined that willow (*Salix* sp.) and miscanthus (*Miscanthus giganteus*) were able to accumulate high levels of palladium in the aerial tissues when grown on synthetic media containing palladium as well as on mine waste materials. The use of chemical lixiviants improved the uptake and translocation of palladium in both willow and miscanthus. The potential of palladium nanoparticle formation in plants as plant-based catalysts was investigated but no palladium nanoparticles were detected when the plants were grown on synthetic mine waste. Chapter 4 evaluates the potential of *merA* gene for mercuric reductase in *Arabidopsis* as a genetic engineering approach to improve tolerance to gold and palladium in plants. In contrast to previously published findings *merA* expression did not increase tolerance of the transgenic plants to toxic levels of gold and palladium. Inhibition studies on purified mercuric reductase further revealed that gold and palladium inhibited the activity of MerA with ionic mercury. In Chapter 5, the potential of synthetic biology strategy was also investigated where the expression of synthetic short peptides, which are shown to be responsible in the formation of various sizes of metal nanoparticles *in vitro*, were found to increase the formation of smaller sized gold nanoparticles (<10 nm diameter) compared to wild type plants when expressed in *Arabidopsis*. Chapter 6 describes the transcriptional response of *Arabidopsis* to precious metals and investigates the potential involvement of heavy metal transporter 5 (*AtHMA5*) in the detoxification mechanism for gold and palladium. *AtHMA5* was found to be strongly up regulated in response to gold and palladium. However, studies with *Arabidopsis hma5-1* mutant knockout lines and yeast heterologous expression studies demonstrated that gold and palladium is not a substrate for *AtHMA5* suggesting that *AtHMA5* is not involved in gold and palladium detoxification. Overall, this work is the first to describe a holistic approach in searching for suitable field applicable plant candidates for phytomining of precious metals such as palladium and gold as well as strategies to improve its uptake, tolerance and nanoparticle formation in plants.

# Table of Contents

<b>Abstract</b> .....	<b>ii</b>
<b>Table of Contents</b> .....	<b>iii</b>
<b>List of Figures</b> .....	<b>vii</b>
<b>List of Tables</b> .....	<b>xvi</b>
<b>Acknowledgements</b> .....	<b>xvii</b>
<b>Author's declaration</b> .....	<b>xviii</b>
<b>Chapter 1: Introduction</b> .....	<b>1</b>
1.1 Precious metals at a glance .....	1
1.2 Mine wastes.....	2
1.2.1 Waste material from mining activities .....	2
1.2.2 Conventional methods of mine waste management.....	4
1.3 Elemental sustainability of precious metals .....	7
1.4 Metal uptake in plants.....	9
1.4.1 Mechanism of metal uptake in plants .....	9
1.4.2 Toxicity of metals in plants .....	11
1.4.3 Detoxification mechanisms for metals in plants.....	13
1.5 Phytoextraction of metals .....	20
1.5.1 Phytomining .....	20
1.5.2 Metal Hyperaccumulator species.....	20
1.5.3 Chemically-assisted or induced phytoextraction .....	24
1.6 Bioengineering to improve phytoextraction .....	26
1.7 Main objective.....	28
Objectives: .....	28
<b>Chapter 2: Materials and methods</b> .....	<b>29</b>
2.1 Materials and suppliers.....	29
2.2 Plant studies .....	29
2.2.1 Seed sterilisation using chlorine gas .....	29
2.2.2 Murashige and Skoog medium for plant growth .....	29
2.2.3 Supplements to plant growth media .....	30
2.3 Bacterial studies .....	30
2.3.1 Growth media used for bacterial growth .....	30
2.4 Yeast studies .....	30
2.4.1 Growth media used for yeast growth .....	30
2.4.2 Yeast selective media.....	30
2.5 Molecular biology studies .....	31
2.5.1 Isolation of genomic DNA from plants (CTAB method) .....	31
2.5.2 Isolation of plasmid.....	31
2.5.3 Purification of DNA / RNA.....	31
2.5.4 DNA sequencing.....	31

2.5.5	Isolation of RNA from plant and yeast .....	31
2.5.6	Reverse transcription of RNA .....	32
2.5.7	Transformation of <i>E. coli</i> .....	32
2.5.8	Transformation of <i>Agrobacterium tumefaciens</i> and <i>Saccharomyces cerevisiae</i> (Electroporation).....	32
2.5.9	Plant transformation .....	32
2.5.10	Real-Time (quantitative) PCR (qPCR).....	33
<b>Chapter 3: Palladium uptake in plants .....</b>		<b>34</b>
3.1	Introduction.....	34
3.1.1	Palladium at a glance .....	34
3.1.2	Palladium mining activity .....	35
3.1.3	Uses of palladium .....	37
3.1.4	Phytomining of palladium from mine wastes .....	40
3.1.5	Use of cyanide to enhance palladium solubilisation .....	41
3.1.6	Field applicable plant species for phytomining of palladium.....	42
3.2	Materials and methods .....	45
3.2.1	Palladium uptake in Arabidopsis .....	45
3.2.2	Palladium uptake in field applicable plant species .....	46
3.2.3	Sample preparation for ICP-MS analysis .....	47
3.2.4	Testing catalytic activity of the plant derived palladium nanoparticles .....	48
3.2.5	Transmission electron microscopy .....	48
3.3	Results.....	49
3.3.1	Palladium uptake in Arabidopsis .....	49
3.3.2	Palladium uptake in mustard .....	55
3.3.3	Palladium uptake in willow.....	61
3.3.4	Growth and uptake of palladium by miscanthus.....	81
3.3.5	Testing catalytic activity.....	84
3.4	Discussion .....	85
3.4.1	Effect of palladium on Arabidopsis .....	85
3.4.2	Field applicable plant species.....	86
<b>Chapter 4: Genetic engineering approach to improve gold and palladium tolerance in plants.....</b>		<b>90</b>
4.1	Introduction .....	90
4.1.1	Genetic engineering to enhance precious metals uptake and tolerance... ..	91
4.1.2	Mercuric reductase .....	92
4.1.3	Expression of bacterial <i>merA</i> in Arabidopsis .....	95
4.2	Materials and methods .....	97
4.2.1	Production of Arabidopsis MerA transgenic lines .....	97
4.2.2	Cloning, expression and purification of MerA recombinant protein in <i>E. coli</i> . .....	97
4.2.3	Germination and root length studies.....	98
4.2.4	Kinetic analysis of MerA with mercury, gold and palladium.....	98
4.3	Results.....	99
4.3.1	Expression of <i>merA</i> in Arabidopsis.....	99
4.3.2	Screening of MerA transgenic lines for mercury resistance .....	100
4.3.3	Screening MerA-expressing plants for tolerance to gold .....	105
4.3.4	Screening MerA-expressing plants for tolerance to palladium .....	108
4.3.5	Metal uptake studies of MerA-expressing plants from soil containing gold and palladium .....	111

4.3.6	Cloning, expression and purification of MerA .....	112
4.3.7	MerA activity assays with mercury .....	115
4.3.8	Enzymatic assay of MerA activity on gold and palladium .....	118
4.3.9	Enzymatic assay of MerA activity on gold and palladium as inhibitors....	119
4.3.10	Effect of gold and palladium on MerA activity with mercury .....	121
4.3.11	Inhibition study of MerA transgenic lines on gold and palladium .....	125
4.4	Discussion .....	130
4.4.1	Genetic engineering to increase formation of metal nanoparticles.....	130
4.4.2	Mercuric reductase .....	131
<b>Chapter 5: The use of peptides to increase formation of gold and palladium nanoparticles in plants .....</b>		<b>134</b>
5.1	Introduction .....	134
5.1.1	Use of peptides for the formation of gold and palladium nanoparticles... 134	134
5.1.2	Metal nanoparticle formation in plants .....	138
5.2	Materials and methods .....	139
5.2.1	Production of transgenic Arabidopsis expressing short synthetic peptides... ..	139
5.2.2	Whole-plant liquid culture experiments.....	141
5.3	Results.....	142
5.3.1	Peptide expressing Arabidopsis lines .....	142
5.3.2	Formation of gold nanoparticles from peptide-expressing transgenic plants .....	144
5.4	Discussion .....	150
<b>Chapter 6: Potential involvement of AtHMA5 in gold and palladium detoxification .....</b>		<b>152</b>
6.1	Introduction .....	152
6.1.1	Microarray analysis of Arabidopsis in response to gold .....	153
6.1.2	Heavy metal ATPase 5.....	156
6.2	Materials and methods .....	167
6.2.1	Hydroponic based experiment settings .....	167
6.2.2	Metal treatment on plants .....	168
6.2.3	RNA extraction from Arabidopsis .....	168
6.2.4	Reverse transcription of plant RNA .....	168
6.2.5	qPCR analysis .....	168
6.2.6	Procurement and verification of the <i>hma5-1</i> knockout mutant .....	171
6.2.7	Cloning of AtHMA5 into pYES2 yeast expression vector .....	171
6.2.8	Transformation of pYES2-AtHMA5 into <i>Saccharomyces cerevisiae</i> .....	172
6.2.9	Transmembrane protein extraction analysis.....	172
6.2.10	Spot analysis experiment .....	173
6.3	Results.....	175
6.3.1	Arabidopsis gene expression in response to palladium .....	175
6.3.2	Characterisation of the Arabidopsis <i>hma5-1</i> mutant .....	178
6.3.3	Growth studies of the <i>hma5-1</i> mutants on copper.....	179
6.3.4	Growth studies of <i>hma5-1</i> mutants on gold.....	182
6.3.5	Growth studies of <i>hma5-1</i> mutants on palladium .....	185
6.3.6	Cloning and expression of AtHMA5 in yeast .....	188
6.3.7	Activity of AtHMA5 on copper .....	190
6.3.8	Activity of AtHMA5 on gold or palladium .....	193

6.3.9 Activity of <i>AfHMA5</i> on excess copper in the presence of gold or palladium .....	196
6.4 Discussion .....	199
<b>Chapter 7: Final discussion .....</b>	<b>204</b>
7.1 Research in context.....	204
7.2 Willow and miscanthus could be used in phytomining of palladium from mine wastes.....	205
7.3 Expression of bacterial <i>merA</i> gene to improve precious metals uptake and tolerance in plants.....	207
7.4 The use of synthetic peptides to increase metal nanoparticle formation in plants. ....	208
7.5 Potential involvement of <i>AfHMA5</i> in detoxification mechanism of palladium and gold in <i>Arabidopsis</i> .....	209
7.6 Future directions.....	211
<b>Appendix .....</b>	<b>213</b>
<b>Abbreviations .....</b>	<b>218</b>
<b>References .....</b>	<b>223</b>

## List of Figures

<b>Figure 1.1:</b> Price comparison between metals within last twelve months.....	1
<b>Figure 1.2:</b> Abandoned Kam Kotia mine wastes storage area in Canada.....	3
<b>Figure 1.3:</b> McArthur River mine wastes dam in Australia.....	3
<b>Figure 1.4:</b> Example of a conventional impoundment technique.....	5
<b>Figure 1.5:</b> In-pit storage technique.....	5
<b>Figure 1.6:</b> Process of depositing backfill mine wastes into a surface borehole.....	6
<b>Figure 1.7:</b> The generic life cycle of a metal.....	8
<b>Figure 1.8:</b> Cross-section of a plant root showing metal uptake pathways.....	10
<b>Figure 1.9:</b> Main transporters of heavy metals in plants with known substrates.....	10
<b>Figure 1.10:</b> Diagram of the intracellular metal detoxification mechanism in plant..	16
<b>Figure 1.11:</b> Phylogenetic tree of heavy metal ATPases in Arabidopsis.....	18
<b>Figure 1.12:</b> Mechanism of processes involved in metal hyperaccumulation.....	21
<b>Figure 1.13:</b> Plant response strategies to increasing metal concentration in soil....	22
<b>Figure 3.1:</b> Distribution of PGM reserves according to countries.....	35
<b>Figure 3.2:</b> Palladium production by year according to major producers.....	36
<b>Figure 3.3:</b> Palladium supply versus demand by year.....	38
<b>Figure 3.4:</b> Schematic diagram of catalytic converter in car exhausts.....	38
<b>Figure 3.5:</b> Palladium demand by automotive sector 2015.....	39
<b>Figure 3.6:</b> Palladium demand according to sector in 2015.....	39
<b>Figure 3.7:</b> Germination studies of Arabidopsis grown on different palladium concentrations.....	49
<b>Figure 3.8:</b> Root lengths of wildtype Arabidopsis grown on different palladium concentrations.....	50
<b>Figure 3.9:</b> Fresh weight of wildtype Arabidopsis grown on different palladium concentration.....	50

<b>Figure 3.10:</b> Appearance of wildtype Arabidopsis grown on various palladium concentrations.....	51
<b>Figure 3.11:</b> Total dry weight of wildtype Arabidopsis shoots grown on different palladium concentrations.....	53
<b>Figure 3.12:</b> Total dry weight of wildtype Arabidopsis shoots grown in soil containing different palladium concentrations.....	53
<b>Figure 3.13:</b> Palladium levels in wildtype Arabidopsis shoots grown in soil containing different palladium concentrations.....	54
<b>Figure 3.14:</b> Palladium levels in wildtype Arabidopsis roots grown in soil containing different palladium concentrations.....	54
<b>Figure 3.15:</b> Appearance of mustard seedlings grown on SOM with and without palladium prior to cyanide treatment.....	56
<b>Figure 3.16:</b> Total biomass of mustard grown on SOM containing different concentrations of palladium.....	56
<b>Figure 3.17:</b> Palladium levels in aerial tissue of mustard grown on SOM containing different concentrations of palladium.....	57
<b>Figure 3.18:</b> Pie charts showing relative percentages of metals found in aerial tissue of mustard germinated and grown on SOM containing different palladium concentrations.....	57
<b>Figure 3.19:</b> Appearance of mustard seedlings growing in mine waste materials containing 20 mg/kg of palladium prior to cyanide treatment.....	59
<b>Figure 3.20:</b> Biomass of aerial tissue of mustard seedlings germinated on mine waste materials.....	60
<b>Figure 3.21:</b> Palladium levels in the aerial tissue of mustard germinated on mine waste materials.....	60
<b>Figure 3.22:</b> Appearance of Super Willow plants prior to transfer to SOM.....	63
<b>Figure 3.23:</b> Super Willow grown in containers containing SOM with various palladium concentrations.....	63
<b>Figure 3.24:</b> Super Willow grown on SOM containing 50 mg/kg of palladium before and after seven days of dosing with 100 mg/kg cyanide.....	64

<b>Figure 3.25:</b> Total leaf dry biomass of Super Willow grown on SOM containing palladium.....	65
<b>Figure 3.26:</b> Palladium levels in the leaf tissues of Super Willow grown on SOM containing palladium.....	65
<b>Figure 3.27:</b> Total stem dry biomass of Super Willow grown on SOM containing palladium.....	66
<b>Figure 3.28:</b> Palladium levels in the stem tissues of Super Willow grown on SOM containing palladium.....	66
<b>Figure 3.29:</b> Palladium levels in the leaf and stem tissues of Super Willow grown on SOM containing different palladium concentrations.....	67
<b>Figure 3.30:</b> Total dry biomass of leaf and stem of Super Willow grown on mine waste materials containing 20 mg/kg palladium.....	69
<b>Figure 3.31:</b> Palladium levels in the leaf and stem tissues of Super Willow grown on mine waste materials containing 20 mg/kg palladium.....	69
<b>Figure 3.32:</b> Levels of metals in Super Willow leaf tissues from plants grown on mine waste materials containing 20 mg/kg of palladium.....	70
<b>Figure 3.33:</b> Levels of palladium and other metals in the stem tissues of Super Willow grown on mine waste materials containing 20 mg/kg of palladium.....	70
<b>Figure 3.34:</b> Total dry weight of leaf and stem tissues from different willow ( <i>Salix</i> spp) grown on SOM dosed with 50 mg/kg palladium.....	72
<b>Figure 3.35:</b> Palladium levels in the leaf and stem tissues of different willow ( <i>Salix</i> spp) species grown on SOM dosed with 50 mg/kg palladium.....	73
<b>Figure 3.36:</b> Total dry weight of leaf tissues from Super Willow and Green Dicks grown on SOM containing 50 mg/kg palladium.....	75
<b>Figure 3.37:</b> Electron micrographs of aerial tissue of willows.....	76
<b>Figure 3.38:</b> EDX-derived spectrum from roots of Super Willow plants grown hydroponically in medium with palladium.....	78
<b>Figure 3.39:</b> EDX-derived spectrum from roots of Super Willow plants grown hydroponically in medium without palladium.....	78

<b>Figure 3.40:</b> EDX-derived spectrum from leaf of Super Willow plants grown on SOM containing 50 mg/kg of palladium without cyanide treatment.....	79
<b>Figure 3.41:</b> EDX-derived spectrum from leaf of Super Willow plants grown on SOM containing 50 mg/kg of palladium with cyanide treatment.....	79
<b>Figure 3.42:</b> EDX-derived spectrum from leaf of Green Dicks willow plants grown on SOM containing 50 mg/kg of palladium without cyanide treatment.....	80
<b>Figure 3.43:</b> EDX-derived spectrum from leaf of Green Dicks willow plants grown on SOM containing 50 mg/kg of palladium with cyanide treatment.....	80
<b>Figure 3.44:</b> Miscanthus plants grown on SOM containing 100 mg/kg of palladium.....	82
<b>Figure 3.45:</b> Total dry weight of shoot and root of miscanthus grown on SOM dosed with 100 mg/kg palladium.....	83
<b>Figure 3.46:</b> Palladium levels in the shoots of miscanthus grown on SOM dosed with 100 mg/kg palladium.....	83
<b>Figure 4.1:</b> Catalytic core structure of MerA.....	94
<b>Figure 4.2:</b> Arabidopsis plants expressing MerA showing resistance to mercury and gold toxicity.....	95
<b>Figure 4.3:</b> Diagram outlining mercury detoxification by MerA in planta.....	96
<b>Figure 4.4:</b> PCR analysis on DNA isolated from transgenic plants.....	99
<b>Figure 4.5:</b> Root lengths of 12 day-old Arabidopsis Col-0 and MerA seedlings on ½ MS (A) media containing 50 µM of mercury.....	101
<b>Figure 4.6:</b> Total fresh weights of 12 day-old Arabidopsis Col-0 and MerA seedlings on ½ MS (A) media containing 50 µM of mercury.....	101
<b>Figure 4.7:</b> Relative expression values of <i>merA</i> transcript level from the MerA seedlings exhibiting the highest resistance to mercury.....	102
<b>Figure 4.8:</b> Appearance of 12 day-old wildtype and MerA seedlings on ½ MS (A) plates containing a range of mercury concentrations.....	103
<b>Figure 4.9:</b> Root lengths of 12 day-old Arabidopsis Col-0 wildtype and MerA seedlings on ½ MS (A) containing increasing concentrations of mercury.....	104

<b>Figure 4.10:</b> Appearance of 12 day-old wildtype and MerA-expressing seedlings on ½ MS (A) plates containing a range of gold concentrations.....	106
<b>Figure 4.11:</b> Root lengths of 12 day-old Arabidopsis Col-0 wildtype and MerA-expressing seedlings on ½ MS (A) media containing increasing concentrations of gold.....	107
<b>Figure 4.12:</b> Total fresh weights 12 day-old Arabidopsis Col-0 wildtype and MerA-expressing seedlings on ½ MS (A) media containing increasing concentrations of gold.....	112
<b>Figure 4.13:</b> Appearance of 12 day-old wildtype and MerA-expressing seedlings on ½ MS (A) plates containing a range of palladium concentrations.....	109
<b>Figure 4.14:</b> Root lengths of 12 day-old Arabidopsis Col-0 wildtype and MerA-expressing seedlings on ½ MS (A) media containing increasing concentrations of palladium.....	110
<b>Figure 4.15:</b> Total fresh weights of 12 day-old Arabidopsis Col-0 wildtype and MerA-expressing seedlings on ½ MS (A) media containing increasing Palladium concentrations.....	110
<b>Figure 4.16:</b> Levels of gold and palladium in the aerial tissues of wildtype and MerA-expressing plants.....	111
<b>Figure 4.17:</b> DNA Agarose gel of amplicons from bacterial colonies transformed with pET16b- <i>merA</i> .....	112
<b>Figure 4.18:</b> Colony PCR to verify <i>merA</i> insertion.....	113
<b>Figure 4.19:</b> SDS-PAGE analysis of MerA expression by E. coli BL21.....	113
<b>Figure 4.20:</b> SDS-PAGE analysis of the expression and purification of MerA.....	114
<b>Figure 4.21:</b> FPLC Purification profile of HIS-tagged MerA.....	114
<b>Figure 4.22:</b> Growth of E. coli BL21 with in LB media with different concentrations of mercury.....	115
<b>Figure 4.23:</b> Michealis-Menten plot showing activity of MerA.....	116
<b>Figure 4.24:</b> Activity of purified MerA with 100 µM Hg as substrate.....	117
<b>Figure 4.25:</b> Activity rate of NADPH oxidation by MerA with 100 µM of mercury, gold and palladium as substrate.....	118

<b>Figure 4.26:</b> Activity rate of NADPH oxidation by MerA with 100 $\mu\text{M}$ of mercury and gold as substrate .....	119
<b>Figure 4.27:</b> Activity rate of NADPH oxidation by MerA with 100 $\mu\text{M}$ of mercury and palladium as substrate.....	120
<b>Figure 4.28</b> Activity of MerA with 100 $\mu\text{M}$ mercury, 50 $\mu\text{M}$ gold and 50 $\mu\text{M}$ palladium as substrate.....	120
<b>Figure 4.29:</b> Michaelis-Menten plots for MerA using mercury as substrate, and a range of gold concentrations.....	121
<b>Figure 4.30:</b> Lineweaver-Burk double reciprocal plots for MerA with different concentrations of gold.....	122
<b>Figure 4.31:</b> Michaelis-Menten plots of MerA using mercury as substrate, and a range of palladium concentrations.....	123
<b>Figure 4.32:</b> Lineweaver-Burk double reciprocal plots for MerA with different concentrations of palladium.....	124
<b>Figure 4.33:</b> Appearance of 12 day-old Arabidopsis Col-0 MerA-expressing seedlings on $\frac{1}{2}$ MS (A) plates containing a range of mercury and gold concentrations.....	126
<b>Figure 4.34:</b> Root lengths of 12 day-old Arabidopsis Col-0 MerA-expressing seedlings on $\frac{1}{2}$ MS (A) media containing 50 $\mu\text{M}$ of mercury and increasing concentration of gold.....	127
<b>Figure 4.35:</b> Appearance of 12 day-old Arabidopsis Col-0 MerA-expressing seedlings on $\frac{1}{2}$ MS (A) plates containing a range of mercury and palladium concentrations.....	128
<b>Figure 4.36:</b> Root lengths of 12 day-old Arabidopsis Col-0 MerA-expressing seedlings on $\frac{1}{2}$ MS (A) media containing 50 $\mu\text{M}$ of mercury and increasing concentration of palladium.....	129
<b>Figure 4.37:</b> Putative diagram of expected MerA mechanism in Arabidopsis root cell in the presence of gold.....	132
<b>Figure 5.1:</b> Bio-panning process for peptides isolation.....	136
<b>Figure 5.2:</b> Peptides for gold nanoparticle formation.....	136
<b>Figure 5.3:</b> TEM images of peptide synthesis of gold nanoparticles.....	137

<b>Figure 5.4:</b> Whole-plant liquid culture experimental settings.....	141
<b>Figure 5.5:</b> Cloning strategy of synthetic peptides.....	142
<b>Figure 5.6:</b> Relative expression of epsilon, alpha, beta and delta transcript levels of transgenic plants.....	143
<b>Figure 5.7:</b> Histogram of frequency distribution of gold nanoparticles and TEM images from epsilon lines after treatment with gold for 24 hours.....	145
<b>Figure 5.8:</b> Histogram of frequency distribution of gold nanoparticles and TEM images from alpha lines after treatment with gold for 24 hours.....	146
<b>Figure 5.9:</b> Histogram of frequency distribution of gold nanoparticles and TEM images from beta lines after treatment with gold for 24 hours.....	147
<b>Figure 5.10:</b> Histogram of frequency distribution of gold nanoparticles and TEM images from delta lines after treatment with gold for 24 hours.....	148
<b>Figure 5.11:</b> Percentage distribution of gold nanoparticle with diameter size less than 10 nm .....	149
<b>Figure 5.12:</b> Percentage distribution of gold nanoparticle with diameter size larger than 30 nm .....	149
<b>Figure 6.1:</b> Comparison of qPCR and microarray gene expression levels in gold-treated Arabidopsis root tissue.....	154
<b>Figure 6.2:</b> Gene expression levels in gold treated Arabidopsis root tissue.....	155
<b>Figure 6.3:</b> Heat map generated from DNA microarray data showing percentage of AtHMA5 gene expression potential in different parts of plant tissues.....	157
<b>Figure 6.4:</b> Schematic view of the predicted topology of AtHMA5.....	158
<b>Figure 6.5:</b> Phylogenetic tree analysis of heavy metal ATPase 5, 6, 7 and 8 from different plant species.....	159
<b>Figure 6.6:</b> Clustal O alignment of amino acid sequences of CsHMA5.2, AtHMA5 and OsHMA5.....	161
<b>Figure 6.7:</b> Mechanism of copper detoxification in Arabidopsis plant root cells....	163
<b>Figure 6.8:</b> Diagram showing different subcellular locations of HMA5s from different plant species in a root cell.....	164
<b>Figure 6.9:</b> Hydroponic growth of Arabidopsis seedlings.....	167

<b>Figure 6.10:</b> Relative expression of ten genes in Arabidopsis roots in response to palladium.....	175
<b>Figure 6.11:</b> Relative expression of heavy metal ATPase genes in Arabidopsis in response to palladium.....	176
<b>Figure 6.12:</b> Relative expression of heavy metal ATPase genes ( <i>AtHMA5, 6, 7, 8</i> ) in Arabidopsis in response to palladium and copper.....	177
<b>Figure 6.13:</b> Diagram of the location of T-DNA .....	178
<b>Figure 6.14:</b> T-DNA inserts within the <i>hma5-1</i> line.....	178
<b>Figure 6.15:</b> Root lengths of 12 day-old Arabidopsis Col-0 wildtype and <i>hma5-1</i> mutant.....	180
<b>Figure 6.16:</b> Total fresh weights 12 day-old Arabidopsis Col-0 wildtype and <i>hma5-1</i> mutant.....	180
<b>Figure 6.17:</b> Appearance of 12 day-old Arabidopsis Col-0 wildtype and <i>hma5-1</i> seedlings on ½ MS (A) with various concentrations of copper.....	181
<b>Figure 6.18:</b> Root lengths of 12 day-old Arabidopsis Col-0 wildtype and <i>hma5-1</i> mutant seedlings on ½ MS (A) media containing increasing gold concentrations..	183
<b>Figure 6.19:</b> Total fresh weights 12 day-old Arabidopsis Col-0 wildtype and <i>hma5-1</i> mutant seedlings on ½ MS (A) media containing increasing gold concentrations..	183
<b>Figure 6.20:</b> Appearance of 12 day-old Arabidopsis Col-0 wildtype and <i>hma5-1</i> seedlings on ½MS (A) with various concentrations of gold.....	184
<b>Figure 6.21:</b> Root lengths of 12 day-old Arabidopsis Col-0 wildtype and <i>hma5-1</i> mutant seedlings on ½ MS (A) media containing increasing palladium concentrations.....	186
<b>Figure 6.22:</b> Total fresh weights 12 day-old Arabidopsis Col-0 wildtype and <i>hma5-1</i> mutant seedlings on ½ MS (A) media containing increasing palladium concentrations.....	186
<b>Figure 6.23:</b> Appearance of 12 day-old Arabidopsis Col-0 wildtype and <i>hma5-1</i> seedlings on ½MS (A) with various concentrations of palladium.....	187
<b>Figure 6.24:</b> Verification of <i>AtHMA5</i> insert via digestion at <i>Xho1</i> and <i>Nde1</i> restriction site of pYES2 vector.....	188

<b>Figure 6.25:</b> Colony PCR of yeast BY4741 expressing pYES2- <i>AthHMA5</i> and empty vector.....	189
<b>Figure 6.26:</b> Growth of yeast BY4741 transformed with pYES2- <i>AthHMA5</i> or pYES2 empty vector after 80 hours of incubation at 30 °C.....	189
<b>Figure 6.27:</b> <i>Ace1</i> functional complementation assay on YSD medium containing various copper concentrations.....	191
<b>Figure 6.28:</b> Growth density of yeast strains on excess copper.....	191
<b>Figure 6.29:</b> <i>Ccc2</i> functional complementation assay on YSD medium containing various media.....	192
<b>Figure 6.30:</b> Spot assay analysis on YSD medium containing gold.....	194
<b>Figure 6.31:</b> Spot assay analysis on YSD medium containing palladium.....	195
<b>Figure 6.32:</b> Spot assay analysis on YSD medium containing 1 mM copper plus various concentrations of gold and gold only.....	197
<b>Figure 6.33:</b> Spot assay analysis on YSD medium containing 1 mM copper plus various concentrations of palladium and palladium only.....	198

## List of Tables

<b>Table 1.1:</b> Potential non-hyperaccumulator plant species for phytomining of metals and bioenergy production.....	23
<b>Table 1.2:</b> Examples of induced hyperaccumulation.....	25
<b>Table 3.1:</b> Properties of palladium.....	34
<b>Table 4.1:</b> $K_m$ and $V_{max}$ values for MerA using mercury as substrate in the presence of gold.....	121
<b>Table 4.2:</b> $K_m$ and $V_{max}$ values for MerA using mercury as substrate in the presence palladium.....	123
<b>Table 5.1:</b> Peptide sequences involved in formation of metal nanoparticles.....	137
<b>Table 5.2:</b> Primers used to synthesise peptides.....	140
<b>Table 6.1:</b> Percentage identities of the <i>AtHMA5</i> proteins.....	160
<b>Table 6.2:</b> Primers for qPCR analysis in response to palladium.....	169
<b>Table 6.3:</b> Primers for qPCR analysis to measure expression analysis of Heavy Metal ATPases in response to palladium.....	170
<b>Table 6.4:</b> Primers for identification of T-DNA insertion in <i>hma5-1</i> lines.....	171
<b>Table A1:</b> Elemental composition of synthetic ore.....	213
<b>Table A2:</b> Analysis for Au and PGMs.....	213
<b>Table A3:</b> Levels of metals in Super Willow grown on mine waste materials containing 20 mg/kg palladium.....	214
<b>Table A4:</b> Quantitative phase analysis on mine feed.....	215
<b>Table A5:</b> Elemental composition of mine waste materials measured by LiBO <sub>2</sub> /Li <sub>2</sub> B <sub>4</sub> O <sub>7</sub> fusion ICP-MS analysis.....	216
<b>Table A6:</b> Elemental composition of mine waste materials measured by leaching in hot (95°C) Aqua Regia for ICP-MS.....	217

## **Acknowledgements**

First and foremost, I would like to thank the Government of Malaysia and the International Islamic University of Malaysia for trusting me and giving me the opportunity to do my PhD here in York. Also, thanks to the Radhika V. Sreedhar family for the hardship fund that I have received at the end of this study period.

My highest appreciation goes to my supervisor, Professor Neil C. Bruce, for accepting me as a student and also allowing me to be a part of this research group as well as for all the help and advice that he has given me, in both academic and non-academic matters. It has such been such a great experience working in this lab and I will definitely use the experience gained here to help and educate the future generations.

I would also like to take this opportunity to express my appreciation to Dr. Elizabeth L. Rylott, for her guidance, endless meetings, critical ideas, jokes, delicious brownies and many more. I am indeed, truly indebted to her and I wish her all the best in her future undertakings.

Appreciation should also be given to my TAP members, Professor Simon McQueen Mason and Dr. Michael Schultze for their guidance and suggestions throughout this work, to Dr. Fraans Maathuis for his support and guidance for the yeast work. Not to forget, to all M2 lab members for such an amazing working experience especially Kyriakos Tzafestas, Maria Razalan, Emily Johnston, Dana Sabir, Joe Bennett, Federico Sabbadin, Chong Chung Shiong and everyone for being such a great, helpful friends. I would also like to thank Luisa, Marcelo, Katrin, Laziana, Henry and Muhi for helping me with the protein purification work, to the Horticultural team (Alison, Chris, Paul and Colin) for taking care of my plants in the walled garden, to Dr. Helen Parker and Andrea Munoz Garcia for the ICP-MS work, to Darren Phillips from the Biorenewables Development Centre, to Dave and Louise for their tireless lab support, as well as to everyone involved directly or indirectly in this work.

Special thanks goes to my parents and in-laws as well as family members, for their endless support, motivation and prayers. Last but not least, I would like to thank my wonderful wife, Mrs. Ilham Hazizan for her endless trust, motivation, support, love and care especially towards our two beautiful daughters, ilma and ilana.

## **Author's declaration**

I declare that I am the sole author of this work and that it is original except where indicated by reference in the text. No part of this work has been submitted for any other degree to any other institution.

Publication arising from this work:

- Harumain, Z.A.S., et al., Towards financially viable phytoextraction and production of palladium nanoparticle-based catalysts (Submitted).

## Chapter 1: Introduction

### 1.1 Precious metals at a glance

Precious metals such as gold, palladium and platinum have high economic value due to their rarity and application in many industries. They are classed together with other platinum group metal (PGM) such as rhodium, osmium, iridium and ruthenium, which are usually found in the same ore deposits. Historically, gold has also been used as a currency and in the production of jewellery, and today, is still widely regarded as a sign of prosperity. Recent advances in science and technology have now also exploited the chemical properties of palladium and platinum, which are now extensively used especially as catalysts in many industrial applications. Due to their high demand, the price of these metals remains high as compared to other, more common, metals which are also used in the industry such as silver, copper, zinc and lead (Figure 1.1).

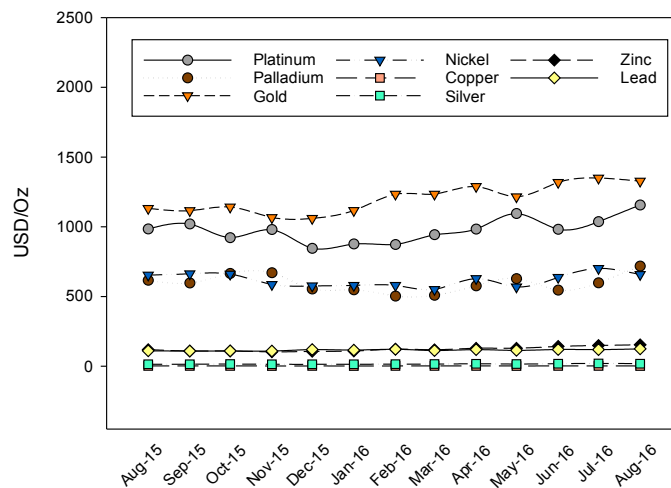


**Figure 1.1:** Price comparison between metals within last twelve months [1].

The mining of these precious metals results in the production of huge amounts of waste material, which can cause environmental problems if storage is unsuitable. These mine wastes often contain significant amounts of precious metals, which are uneconomical to extract using conventional methods. This has led to interest in identifying efficient, economic and environmentally friendly approaches for the recovery of the metals from these wastes. As conventional methods for managing mine wastes are costly, phytomining: the use of plants to extract metal, could offer a more economically practical approach to re-green and remediate mine waste containment areas while also adding economic value by allowing the recovery of these valuable metals.

## **1.2 Mine wastes**

### **1.2.1 Waste material from mining activities**

Mine wastes or tailings are the materials that remains after the processing of ore, ore concentrate or other mined materials to extract marketable components such as metals, minerals or bitumen [2]. Mine wastes generally consist of ground rock, process effluent, sand, clay and water, as well as significant amounts of metal residues that are uneconomical to be extracted using conventional methods. During the mining process, mine wastes are retained in a tailings storage facility. The water from the mine wastes is usually pumped back for re-use in the mining process, while the solid material will remain in the storage facility.

The increasing demand for precious metals by industries has increased mining activities, and inevitably, the amount of mine wastes produced every year. It has been reported that the global amount of mine wastes produced increased from 23 % to 27 % between 2009 and 2011 [3]. For example, an annual report from Norilsk Nickel (the world's biggest palladium producer) stated that 13 million tonnes of waste material containing soils, hard rocks and concentrated mine wastes were disposed in the year 2013 [4].

Environmental concern towards mine wastes management has arisen as mine wastes often contain high levels of relatively toxic metals (eg: arsenic, mercury, cadmium and nickel) [5] as well as polycyclic aromatic hydrocarbons (eg: phenanthrene) [2]. Mine wastes often also contain relatively low levels of organic matter or macronutrients [6, 7], and consequentially do not support the growth and survival of many living organisms, including bacteria [8] and these areas often remain un-vegetated (Figure 1.2 and 1.3). Old mining areas especially, are always associated with metal contamination due to poor waste management and the lack of environmental awareness at that time [9]. Many of these old mining sites now pose a significant threat to human health due to dispersion of toxic metal-containing particulates in air, soil and water. A carefully-maintained storage area for mine wastes is required not just to cater for the huge amount of mine wastes produced, but also to avoid mine wastes, or toxic metals and organics being discharged directly into surface water [5]. Improper mine wastes management can also potentially lead to groundwater and open water contamination.



**Figure 1.2:** Abandoned Kam Kotia mine wastes storage area in Timmins, Ontario, Canada. Picture reproduced from Anderson [10].



**Figure 1.3:** McArthur River mine wastes dam in Australia. Picture reproduced from Bardon [11].

### **1.2.2 Conventional methods of mine waste management**

There are several long-term storage techniques that can be applied to manage waste, including “conventional impoundment”, “in-pit’ or “backfill” techniques.

Conventional impoundment storage illustrated in Figure 1.4, can retain mine waste for a longer period of time and also separate unwanted solids before being discharged [12]. In this process, the embankments are designed to retain water and mine wastes. However, this approach will also increase the potential for flooding [13] and could also cause a significant environmental impact if the embankment fails to sustain the amount of mine wastes stored [14]. In-pit mine wastes storage is the process of backfilling abandoned open pit surface mines with mine wastes (Figure 1.5). Although it may reduce the risk of embankment instability [15], this approach can increase the potential of groundwater contamination [16]. Backfill processing involves mixing the mine wastes with cement, which can then be used as a pillar, supporting the underground mining area (Figure 1.6). Problems associated with dust generation and contamination of surface water can be overcome using this technique, but it does carry a high cost of operation and maintenance, along with the CO<sub>2</sub> release associated with the use of cement [5]. Alternatively, submarine mine wastes disposal can be carried out, whereby the mine wastes are discharged deep into the sea. This technique can sometimes be an option if onshore processes are not possible due to the terrain, high seismic activity, high rain downfall and/or low land availability [5]. However, environmental concern regarding the unpredictable nature of the flow of mine wastes could potentially increase contamination migration within the sea water [17].



**Figure 1.4:** Example of a conventional impoundment technique to store mine waste in mining areas. Picture reproduced from Engels [18].

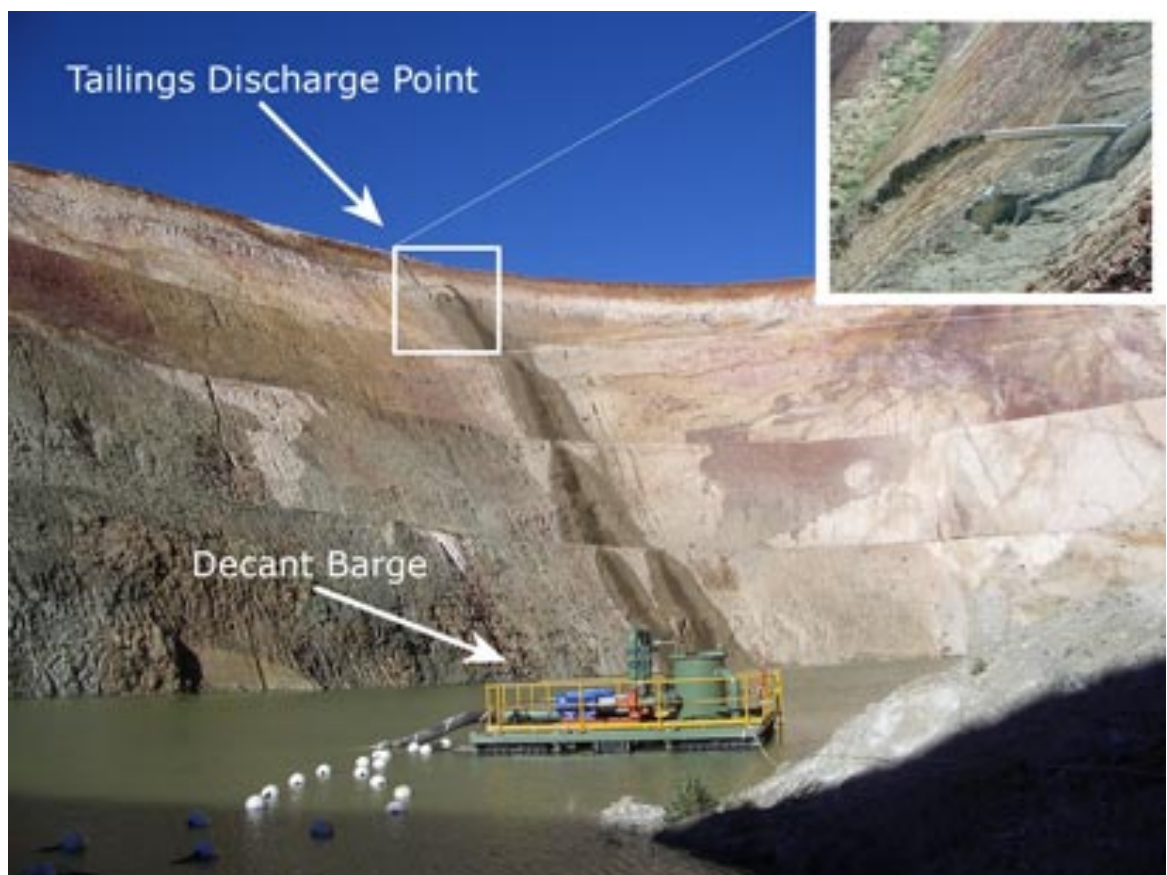


**Figure 1.5:** In-pit storage technique. Picture reproduced from Engels [19].



**Figure 1.6:** Process of depositing backfill mine wastes into a surface borehole. Picture reproduced from Engels [20].

All of these long-term storage approaches have some detrimental impact towards the environment, and as a more environmentally-friendly alternative, phytomining technologies have been proposed to remediate contaminated mining sites using plants. In addition to re-vegetating the contaminated site, the roots and thick aerial vegetation can contribute to site stabilization, reduce surface run-off and lessen wind-borne erosion of toxins. This technology also has the potential to add value, from the harvested plant biomass, which could be used for biofuels, as well as the possibility of recovering additional valuable metals [21], and an emerging technology: producing value-added metal nanoparticle catalysts [22].

### **1.3 Elemental sustainability of precious metals**

The term “elemental sustainability” has been defined by Hunt et al [23] as the idea that every element within the periodic table is guaranteed for use by both current and future generations. There is growing, global appreciation of the importance of sustaining the production of precious metals due to an increase in demand as compared to supply. These precious elements are dispersed and diluted throughout the technosphere making them much more difficult to be recaptured and reused [24]. To solve this problem, multiple efficient approaches to recover and reuse these metals need to be developed.

The life cycle of a metal, as suggested by Reck et al [25], may include mining and milling, smelting, refining, fabricating, manufacturing, use and waste management. Based on the life cycle of a metal as shown in Figure 1.7, there are two stages where recovery opportunities may occur. The first stage is from the mine waste material, which results from the initial mining and processing. Mine wastes are normally voluminous and contain relatively low concentrations of metals. The second stage is from the recycling of discarded metal-containing products. Metals like palladium mainly rely on efficient recycling of waste metal material as the majority of its usage is dominated by the automotive industry especially in the production of catalytic converters [23]. Recycling of palladium from spent autocatalysts using the pyrometallurgical process has become an option for many industries [26]. However, this strategy requires high energy consumption at high cost of operation and maintenance. Additionally, various acidic leaching solutions such as sulphuric acid are also used in this technique, which need expensive, environmentally safe, disposal routes. Therefore, a greener approach, such as phytomining, is needed to recycle precious metals in an environmentally sustainable way to meet the demand from industries.

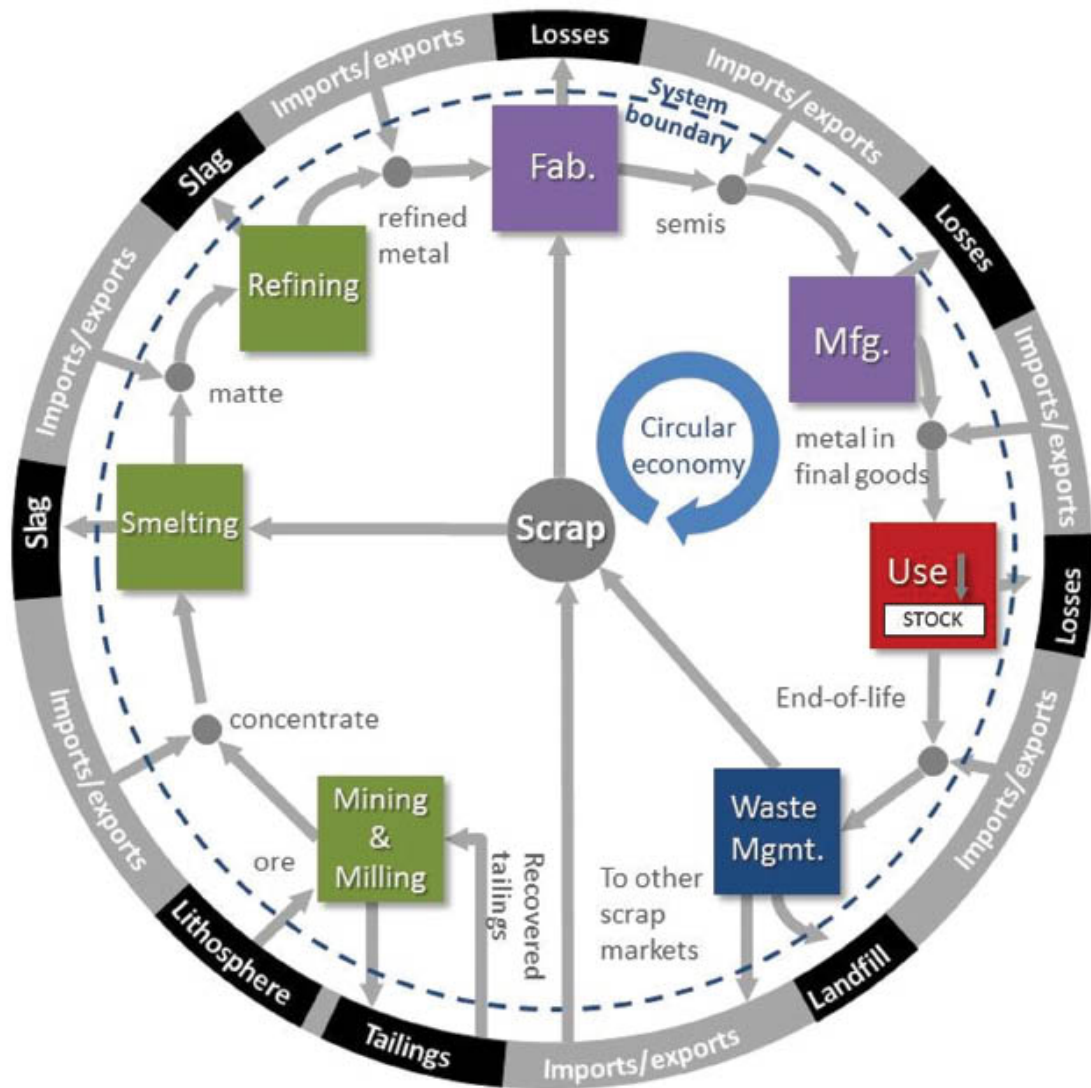


**Figure 1.7:** The generic life cycle of a metal. Life cycle stages include mining and milling; smelting; refining; fabricating (Fab.); manufacturing (Mfg.); use; and waste management and recycling (Waste Mgmt.). The dotted line indicates the boundary of analysis, generally a country or region. Between life stages, the grey circles indicate markets that trade the metal in various forms (concentrate, matte, refined metal, semis, metal as a component of a product). Figure reproduced from Hunt et al [27].

## **1.4 Metal uptake in plants**

### **1.4.1 Mechanism of metal uptake in plants**

Plants possess a remarkable ability to take up transition metals such as copper, zinc and iron from their environment. These metals are essential for growth, for example, copper is an important component of electron-transfer reactions mediated by proteins such as superoxide dismutase, cytochrome oxidase and plastocyanin, while zinc is required as a cofactor for many enzymatic reactions in plant [28]. Interestingly, non-essential metals such as cadmium can also be taken up and accumulated in plant tissues. Prior to uptake, while some metals are readily soluble for uptake, metals that are tightly bound to soil particles can be solubilised by the secretion of chelators such as citrate released from plant roots, or by acidification of the rhizosphere [29]. Subsequent metal uptake and accumulation involves several steps. As shown in Figure 1.8, metals can follow a symplastic, or apoplastic route. In the symplastic route, the metal ions cross the plasma membrane of the root cells through transporters such as channel proteins [28] and diffuse between cells through the plasmodesmata bridges. In the apoplastic route, metal ions travel through the spaces between cells.

To be translocated into the shoots, the metals are transported via the xylem pathway. Metal transporters such as heavy metal ATPases, located at the root pericycle, mediate the transportation of transition metal such as zinc and copper from the cytosol into extracellular compartments before entering xylem [30]. Excess metals in the root cell can also be sequestered and stored by metal transporters into the vacuoles. In order for the metals from the apoplast pathway to be effectively translocated to above ground tissues, the metals will have to enter the xylem by passing through the endodermis cells, mediated by membrane pump or ionic channels due to the presence of casparian strip, which is an impermeable diffusion barrier located in the root apoplast. Then, the flow of the xylem sap moves the metals up to the shoots. Along this route, metals can also be reduced into more stable complexes through chelation with organic acids such as malate, citrate or nicotianamine [31] and also bound to intracellular metallothioneine or specific chaperones [28]. As the metals reach the shoots, they can be stored in a number of locations including the epidermis, mesophyll, cell wall [32] and also sequestered into vacuoles [21]. There are several specific metal transporters and binding proteins that are involved in the uptake, distribution and sequestration of metals in the cell (Figure 1.9).

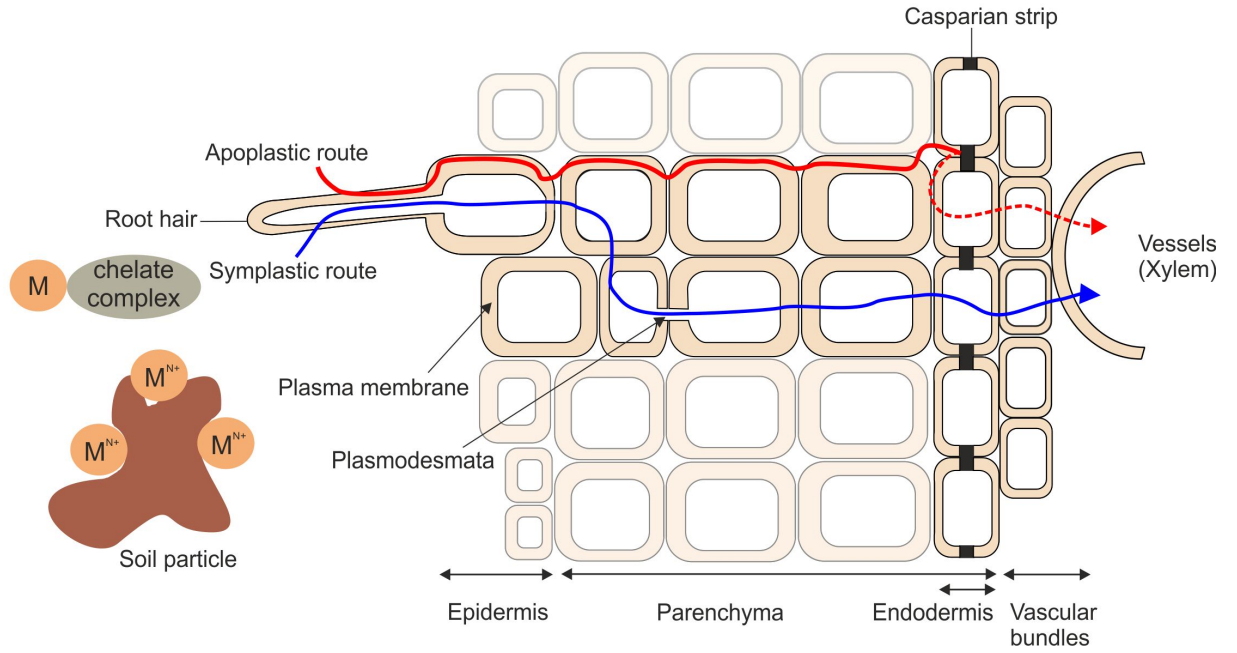


**Figure 1.8:** Cross-section of a plant root showing metal uptake pathways from the soil to the xylem. M = Metal, red line = Apoplastic route, blue line = Symplastic route.

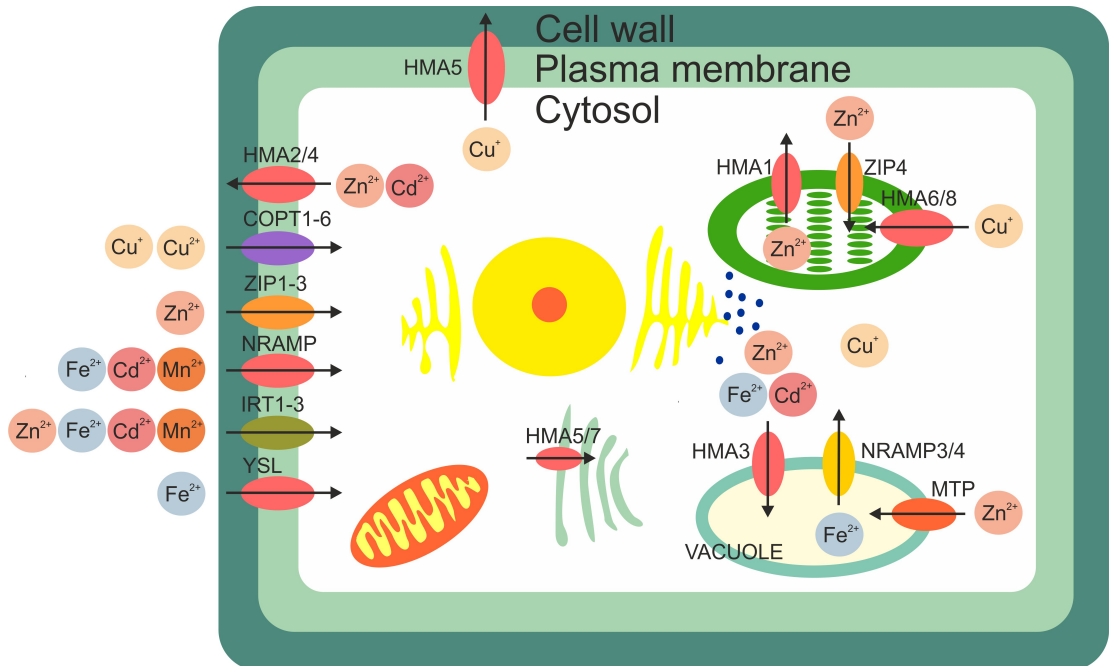


**Figure 1.9:** Main transporters of heavy metals in plants with known substrates. Arrows represent metal movement. Transporters involved: Heavy metal ATPase (HMA), natural resistance associated macrophage proteins (NRAMP), metal tolerance proteins (MTP), yellow stripe1-like proteins (YSL), copper transporters (COPT) and zinc-regulated transporters (ZIP).

### 1.4.2 Toxicity of metals in plants

If the essential metals are absent, plant growth is reduced and deficiency symptoms occur, conversely, high concentrations of these metals can have toxic effects on plant growth [33]. Transition metals such as copper and zinc are important in plants as they are involved in many redox reactions and are also an integral part of many enzyme functions [34]. Copper is reported to be involved as cofactor for a number of oxidases (e.g. amine oxidases, ammonia monooxidase) and also for enzymes related to the elimination of superoxide radicals such as superoxide dismutase and ascorbate oxidase [34]. However, high concentrations of copper have been reported to cause growth retardation and leaf chlorosis in plants [35]. Excess copper may generate reactive oxygen species [36] with this oxidative stress perturbing many plant metabolic pathways [37]. Zinc can also function as a cofactor for important enzymes in plants such as carbonic anhydrase which is responsible for the reversible hydration of carbon dioxide [38] and also for the maintenance of the integrity of ribosomes, by preventing ribosomal RNA from attack by ribonuclease [34, 39]. Nevertheless, high levels of zinc can also inhibit many plant metabolic functions, resulting in retarded growth and earlier senescence [34].

Among the metals considered as non-essential for plant health are nickel, cadmium, lead and mercury as well as precious metals, including palladium and gold. Although in most cases these metals might be present at trace concentrations in the environment, there are areas, such as mine wastes, where they could occur at relatively high levels. In addition, human activities such as mining, agriculture, industry, and the release of domestic effluent can locally increase the level of these metals in soil and water, which could cause toxicity to plants. Nickel is usually present in soil at trace concentrations. However, in serpentine soils, nickel concentrations can be very high (16 mg/kg) [40]. It has been reported that high concentrations of nickel can cause a range of physiological aberrations such as chlorosis, necrosis, inhibition of shoot and root growth in many plant species [41, 42]. Cadmium is also usually present at very low concentrations in soil (0.01-0.7 ppm). At high concentrations, cadmium has been reported to inhibit the uptake, transport and use of several essential elements such as calcium, magnesium and phosphate as well as the uptake of water by plants [43]. Cadmium may also inhibit the activity of nitrate reductase leading to inhibition of the uptake of nitrate and its transport from roots to shoots [44]. Lead, which is one of the most abundant toxic elements in soil, also inhibits seed germination in many plant species. This is

probably due to its inhibition of many enzyme systems such as proteases and amylases [45].

Precious metals like palladium and gold are normally present at very low concentrations in the soil. As a result, there are only a relatively few studies on the phytotoxicity of these metals. Previous reports have suggested that these metals exert toxicity by disrupting protein structure and displacing other essential metals needed for the growth of the plants [36]. Early investigations using *Arabidopsis thaliana* (*Arabidopsis*) germinated on gold chloride, found that the root length and total fresh weight decreased as concentration of gold increased [46]. Gene expression analysis also revealed that *Arabidopsis* plants respond to gold by significantly upregulating genes encoding enzymes involved in metal stress responses such as glutathione transferases, cytochromes P450, glucosyl transferases and peroxidases. In tandem with this response is the downregulation of specific metal transporter genes such as iron regulated transporters, copper transporters and membrane transport proteins [47].

For palladium, a study has reported that this metal causes growth delay and interferes with stem cell elongation in pea (*Pisum sativum*) [48]. Palladium was also found to reduce leaf growth in barley (*Hordeum vulgare* L.) plants [49]. To date, no studies have investigated the transcriptome response to palladium in plants.

### 1.4.3 Detoxification mechanisms for metals in plants

#### 1.4.3.1 Vacuolar compartmentalisation

Plants have developed a number of intracellular detoxification mechanisms to increase their tolerance to environmental pollutants such as heavy metals. Vacuolar compartmentalisation reduces metal stress by sequestering excess metals from the cytosol into vacuole. This mechanism is mediated by transmembrane transporters, which are located at the tonoplast, such as the metal transporting proteins (MTPs), the heavy metal ATPases (HMAs) and the ATP binding cassettes (ABC) (Figure 1.10).

Studies have shown that *AtMTP1* increases zinc tolerance in *Arabidopsis* by sequestering excess zinc into vacuoles [50, 51]. In yeast, *Zrc1* and *Cot1* are vacuolar membrane transporters involved in zinc regulation by sequestering excess zinc into yeast vacuole. It was demonstrated that *AtMTP1* was able to complement the yeast double mutant strain  $\Delta zrc1 cot1$  [50]. In cucumber (*Cucumis sativus*), *CsHMA5.2* is involved in copper detoxification by sequestering excess copper into the vacuole [52]. It was observed the expression of *CsHMA5.2* gene increased tolerance of the yeast mutant strain  $\Delta ace1$  when grown on high concentration of copper. *Ace1* is a copper-binding transcription factor that activates the transcription of the metallothionein genes *Cup1* and *Cup2*, which are involved in copper detoxification mechanism, and the super oxide dismutase *SOD1* [52]. Two ABC transporters (*AtABCC1* & *AtABCC2*) increase plant tolerance to cadmium and mercury with knockout studies revealing that the absence of both transporters leads to growth hypersensitivity when grown in the presence of 40 and 30  $\mu\text{M}$  of cadmium and mercury, respectively [53]. Further subcellular localisation studies also showed that all these transporters: *AtMTP1* [50], *AtABCC1/AtABCC2* [53] and *CsHMA5.2* [52], are located in the vacuolar membrane.

### 1.4.3.2 Metal chelators

As shown in Figure 1.10, natural metal chelators such as glutathione (GSH), phytochelatins (PC) and metallothioneins (MT) are important in metal detoxification mechanism in plants [54, 55]. They bind to free metal ions, buffering metal concentrations in the cytosol and reducing the damage that the free metal ions can cause.

Glutathione is a major sulfhydryl group compound in plants comprising an estimated 0.5 to 10 mM concentration within plant cell compartments [56]. Known primarily for its major role as an antioxidant in plant defence mechanisms against reactive oxygen species [57], GSH is also an essential component in the synthesis of PCs, the metal-binding thiolate peptides that are involved in metal detoxification in plants. Increased metal concentration primarily cadmium as well as silver, lead, zinc, copper, mercury and gold will activate phytochelatin synthase (PS) by binding to the cysteine residue of the N-terminal domain of PS [58]. The PS then uses GSH as substrate for the synthesis of PCs. Previous studies have shown that increased PCs formation confers tolerance to non-essential metals such as cadmium [28], silver [59] and arsenic [60]. Previous work by Howden et al [61] revealed that the disruption of the *AtPCS1* gene encoding PS in Arabidopsis resulted in growth hypersensitivity when the mutant plants were grown on medium containing 0.3  $\mu\text{M}$  of cadmium. In agreement, overexpression of PS increased the accumulation and tolerance to cadmium in Indian mustard (*Brassica juncea*), with 1.5- and 2- fold increase compared to the wildtype [62]. The stable heavy-metal PC complexes are subsequently transported into vacuoles [63], possibly mediated by membrane transporters such as *AtABCC1* and *AtABCC2* [64].

Metallothioneines, like PCs, are cysteine-rich metal chelators that are also involved in metal detoxification in plants. Similar to PCs, MTs also form complexes with metals such as copper, zinc and cadmium via the formation of mercaptide bonds between the cysteine residues present at the N-terminal of the proteins and the metals. In plants, MTs can be further categorised into four different groups on the basis of conserved cysteine residues [65]. Studies carried out on range of plant species have revealed the involvement of MTs in metal tolerance. MTs in Arabidopsis were found to be involved in copper and cadmium tolerance [66]. Tolerance experiments performed on media containing 30  $\mu\text{M}$  of copper or cadmium revealed that the growth of the MT and PT deficient Arabidopsis triple mutant, *mt1a-2-mt1b-1-cad1-3* was more sensitive as compared to the growth of PTs deficient *cad1-3* mutants [66], suggesting that MTs and PTs function cooperatively to protect plants from copper

and cadmium detoxification. Previous work by Gautam et al [67] and Nath et al [68] suggested that MTs in rice (*Oryza sativa*) are involved in arsenic detoxification mechanisms, as the MT genes (*OsMT1* & *OsMT2*) are strongly upregulated in response to arsenic treatment. MT1 was also found to be involved in copper and cadmium detoxification mechanism in pigeon pea (*Cajanus cajan* L.). The expression of *CcMT1* in Arabidopsis plants led to an increased tolerance to copper and cadmium when compared to the wildtype plant [69].

Non-thiol compounds such as organic (citrate and malate) and amino acids (nicotianamine) have extensively been reported to be involved in metal chelation [31, 70-75]. Citrate and malate, which are the intermediates of the tricarboxylic acid cycle (TCA), have been reported to be involved in increasing the tolerance of plants such as canola (*Brassica napus* L.) [71] and barley [72] to aluminium toxicity. These low molecular weight weak-acidic compounds carry a negative charge, which enables them to form complexes with metal ions. The expression of a mitochondrial *CIT1* in yeast increased the cellular and extracellular levels of citrate by 2- to 3- fold and reduced aluminium sensitivity compared to the wildtype [71]. It was also found that the expression of nicotinamine synthase (*TcNAS1*), which is responsible for the production of nicotinamine in alpine penny-cress (*Thlaspi caerulescens*), increased nickel accumulation in Arabidopsis plants by 69 % compared to the wildtype, when the plants were grown in soil containing 700 mg/kg of nickel sulphate [73]. Nicotinamine is a methionine derivative involved in iron homeostasis which is able to bind to many metals *in vitro* [73].

To date, no work has been done on investigating the involvement of metal chelators on precious metal detoxification in plants. As PCs, MTs and non-thiol compounds are mainly known for their involvement in the detoxification of non-essential metals [76], it is possible that they are involved in the detoxification of non-essential noble metals, like gold and platinum group metals (PGMs). However, a search on the microarray expression data for Arabidopsis plants exposed to gold [46] shows that only one putative PS gene (*COBL9*, At5g49270) and one MT (*MT1C*, At1g07610) have altered expression profiles; both are down regulated 2.6 and 3.5-fold respectively, suggesting that PCs and MTs are not involved in the detoxification of gold and PGMs.

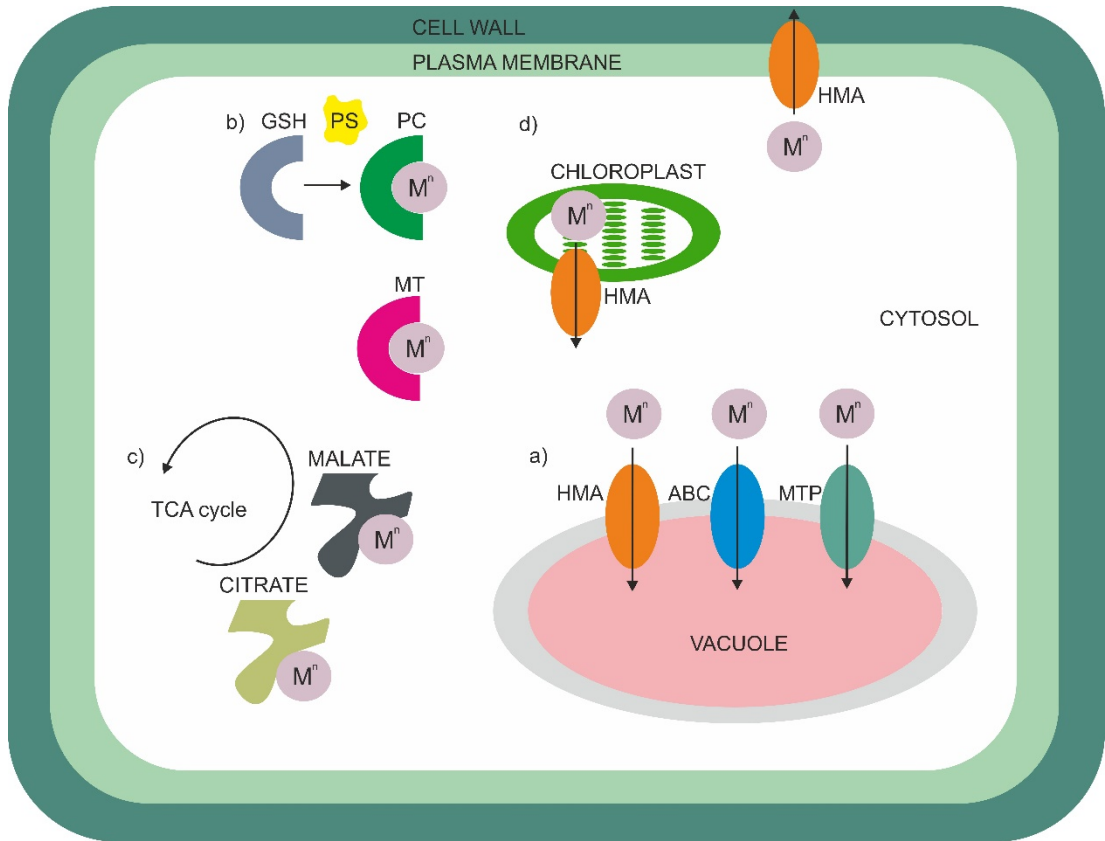


**Figure 1.10:** Diagram of the intracellular metal detoxification mechanism in plant. a) Metal transporters such as *AtHMA3*, *AtABCC2* and *AtMTP1* increase plant tolerance by sequestering excess metals into the vacuole. b) High levels of metals will induce the formation of PCs which are synthesised from GSH in a reaction catalysed by PS. Free metal ions ( $M^n$ ) will be reduced by chelation with PC and also MT. c) Organic acids such as malate and citrate reduce metal stress by forming complexes with free metal ions. d) Membrane transporters such as *AtHMA1*, 2, 4 and 5 increase metal tolerance in plants by pumping metals across the biological membrane.

### 1.4.3.3 Metal transporters

Plants have various transmembrane metal transporters that can reduce the toxic effects caused by high cytoplasmic concentrations of free metals ions. HMA is a P-type ATPase transmembrane pump that is mainly involved in the regulation and transportation of essential and non-essential metals across biological membrane. As the name may suggest, P-type ATPase is an ATP dependent transporter and requires the phosphorylation of an aspartate (D) residue to transport charged substrates across membranes [77]. There are eight HMAs identified in the Arabidopsis genome (*At*HMA) and all have been functionally characterised to some degree. The HMAs have been further categorised in a subfamily, type 1B, which is involved in the transportation of monovalent and divalent cations [78, 79]. HMA transporters possess the general identity of a P-type ATPase transporters: they all present eight transmembrane domains (TMD), two MxCxxC amino terminal metal-binding domains (MBDs), the DKTGTG aspartate phosphorylation site, an ion transduction motif (CPC) and an HP motif [79].

*At*HMA1, 2, 3 and 4 have been grouped together as divalent ion transporters [77, 78] (Figure 1.11). *At*HMA1 is reported to be involved in importing  $Zn^{2+}$  and  $Cu^{2+}$  into the chloroplast of Arabidopsis [80, 81]. *At*HMA2 is responsible for the maintenance of  $Zn^{2+}$  homeostasis in plants, by pumping out excess  $Zn^{2+}$  from the cells [77]. *At*HMA3 increases plant tolerance to  $Cd^{2+}$  and  $Pb^{2+}$  by sequestering these toxic metals into the vacuole [82]. *At*HMA4, which presents high homology to *At*HMA2 (71.3 %) and 3 (71.1 %), has a role in maintaining low levels of  $Cd^{2+}$  and  $Zn^{2+}$  in the cytoplasm, by mediating the transportation of both metals [83]. *At*HMA5, 6, 7 and 8 are grouped together as monovalent transporters, on the basis of their involvement in the translocation of monovalent cations, such as  $Cu^+$  and also  $Ag^+$  [77-80] (Figure 1.11). Transporters *At*HMA5 and 7 are closely related (48.4 %), while *At*HMA6 is more related to *At*HMA8 (43.4 %). *At*HMA5 is involved in copper detoxification mechanisms by pumping out excess copper from the cytoplasm, while its closest homologue, *At*HMA7, is involved in the delivery of copper to ethylene receptors in the plant [79]. The delivery of  $Cu^+$  to the stroma is regulated by *At*HMA6, which is located in the chloroplast envelope. *At*HMA8 is located in the thylakoid and is responsible for the delivery of  $Cu^+$  to plastocyanin for the chloroplast photosynthetic electron transfer chain activity [84].

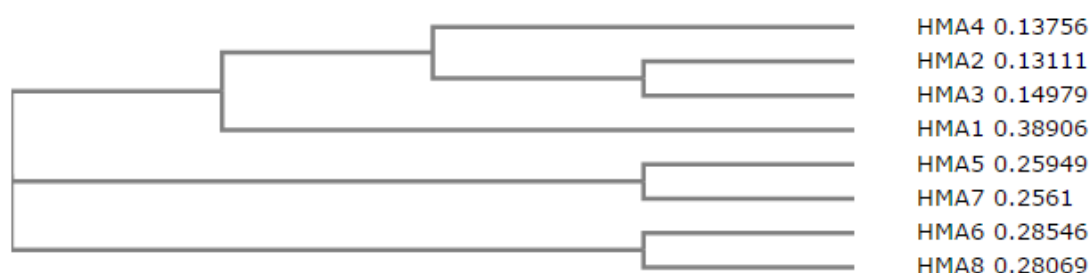


**Figure 1.11:** Neighbourhood-joining phylogenetic tree of heavy metal ATPases in Arabidopsis. The sequences were aligned and the tree was generated using Clustal Omega [85].

Previous studies on *AtHMA1*, 2, 3, 4 and 5 have documented their involvement in excess metal detoxification mechanisms in Arabidopsis (Figure 1.10). To date, information published on *AtHMA6*, 7 and 8 are more focused on intracellular metal trafficking rather than on the (potential) role in metal stress tolerance.

Arabidopsis tolerance to excess  $Zn^{2+}$  concentrations has been reported to be dependent on *AtHMA1*. Previous work carried out by Kim et al [81] demonstrated that *hma1* plants were more sensitive and the shoots and chloroplast of the mutant plants contained significantly higher levels of  $Zn^{2+}$ , compared to the wildtype plants, when grown on media containing excess  $Zn^{2+}$  concentrations (350  $\mu M$ ). These results suggested that *AtHMA1* contributes to  $Zn^{2+}$  detoxification, by reducing the  $Zn^{2+}$  levels in the chloroplast. To support this hypothesis, additional tissue specific and subcellular localisation analyses were conducted, revealing that *AtHMA1* is highly expressed in the shoots (leaves, flowers, stems) and localised in the chloroplast envelope of the plants [81].

*AtHMA2* and *AtHMA4* are strongly related to each other as compared to *AtHMA3*. Both transporters may be functionally redundant and are shown to be strongly induced by  $Zn^{2+}$  and  $Cd^{2+}$  [77, 86]. Earlier work done by Eren and Arguello [77] revealed that high ATPase and phosphorylation activities (> 50 % higher) were observed when  $Zn^{2+}$  and  $Cd^{2+}$  were used as substrates for *AtHMA2* activity, when compared to other metals tested, such as  $Co^{2+}$ ,  $Ni^{2+}$ ,  $Pb^{2+}$  and  $Cu^{2+}$ . Metal content analysis on *hma2* mutant plant tissues showed significantly high levels of  $Zn^{2+}$  and  $Cd^{2+}$  compared to the wildtype, although no significant morphological change could be observed [77]. Similarly, high levels of  $Zn^{2+}$  and  $Cd^{2+}$  were also detected in the roots of *hma4* mutant plants grown on media containing excess  $Zn^{2+}$  (100  $\mu M$ ) and  $Cd^{2+}$  (30  $\mu M$ ) compared to the wildtype [86]. The *hma4* mutant plants also showed

growth hypersensitivity compared to the wildtype when grown on media containing excess  $\text{Cd}^{2+}$  (25  $\mu\text{M}$ ) or  $\text{Zn}^{2+}$  (100  $\mu\text{M}$ ) [87]. Tissue-specific and subcellular localisation analysis on both HMAs revealed that both transporters are highly expressed in the vascular tissue of the roots and localised at the plasma membrane of the root cells, suggesting their function on metal tolerance by transporting excess  $\text{Zn}^{2+}$  and  $\text{Cd}^{2+}$  out from the cytoplasm [78, 86].

Investigations on *AtHMA3* by Morel et al [88] observed that *hma3* mutant plants showed growth hypersensitivity in the presence of excess  $\text{Zn}^{2+}$  (100  $\mu\text{M}$ ) and  $\text{Cd}^{2+}$  (20  $\mu\text{M}$ ) when compared to the wildtype. On the reverse, overexpression of *AtHMA3* significantly increased growth tolerance when compared to the wildtype, when grown on excess  $\text{Zn}^{2+}$  (100  $\mu\text{M}$ ),  $\text{Cd}^{2+}$  (20  $\mu\text{M}$ ),  $\text{Co}^{2+}$  (20  $\mu\text{M}$ ) or  $\text{Pb}^{2+}$  (750  $\mu\text{M}$ ) [88]. However, different from the previous two transporters (*AtHMA2* & 4), subcellular localisation analyses revealed that *AtHMA3* is localised mainly at the tonoplast of the vacuole, suggesting its involvement in sequestering excess metal from the cytosol into the vacuole [88].

Previously, *AtHMA5*, which is a plasma membrane transporter, was shown to increase plant tolerance to excess copper concentrations in plants by transporting excess copper ( $\text{Cu}^+$ ) out from the cytosol [79, 89]. This was demonstrated by growth hypersensitivity and high copper levels observed for the *hma5* mutant plants compared to the wildtype, when grown on excess copper (30  $\mu\text{M}$ ). Interestingly, published data also revealed that in response to gold treatment, *AtHMA5* was significantly upregulated [47]. Since copper shares periodicity with gold and palladium, it could be therefore hypothesised that *AtHMA5* is involved in a detoxification mechanism of gold and palladium in plants. Details and potential involvement of *AtHMA5* on the detoxification mechanism of precious metals are further reviewed in more detail in Chapter 5.

## 1.5 Phytoextraction of metals

Phytoextraction can be defined as a technology whereby plants are used to take up, transport and accumulate metals from the soil into the above ground tissues. To achieve an efficient phytoextraction rate, the plants are required to have the following attributes: fast growth rate, high metal transport rate from roots to shoots, high biomass composition, deep roots and high tolerance of the target metal [90, 91]. The phytoextraction process involves the uptake of metals through adsorption into the root followed by xylem transportation into the aerial tissues. The metals can then be sequestered and stored in the cell wall, into the vacuole, or they can be reduced by cytoplasmic chelation (Figure 1.12).

### 1.5.1 Phytomining

Phytomining, which is a subset of phytoextraction, can be defined as “the *in situ* removal of metals from sub-economic ore bodies or from contaminated mine sites with the additional aim of recovering economic amount of metal from the mine waste” [92, 93]. Conventional mining cannot normally remove 100 % of the desired metal from surrounding minerals [94], thus some of it ends up in the mine wastes. As discussed in Section 1.2, the recovery of precious metals and PGMs from mine wastes may not be cost-efficient, if conventional methods are used. Mine wastes from old now-closed mines are also reported to present very high concentrations of these metals, due to the inefficient recovery techniques applied in the past [94], and many of these old sites have still not been remediated adequately. Chapter 3 explores in more detail the potential use of plants in the phytomining of mine wastes for revegetation and remediation purposes.

### 1.5.2 Metal Hyperaccumulator species

Metal hyperaccumulators are species that can grow in soils containing relatively high concentrations of a metal, taking up and highly concentrating that metal in their tissues. Although many metal hyperaccumulator species have now been identified [92, 95-97], there is only one report of a species able to hyperaccumulate gold. *Berkheyya coddii* was found to accumulate 39 mg/kg of gold from soil containing approximately 0.6 mg/kg of gold ore, after treatment with lixiviant sodium cyanide [92]. No hyperaccumulators of palladium have yet been reported.

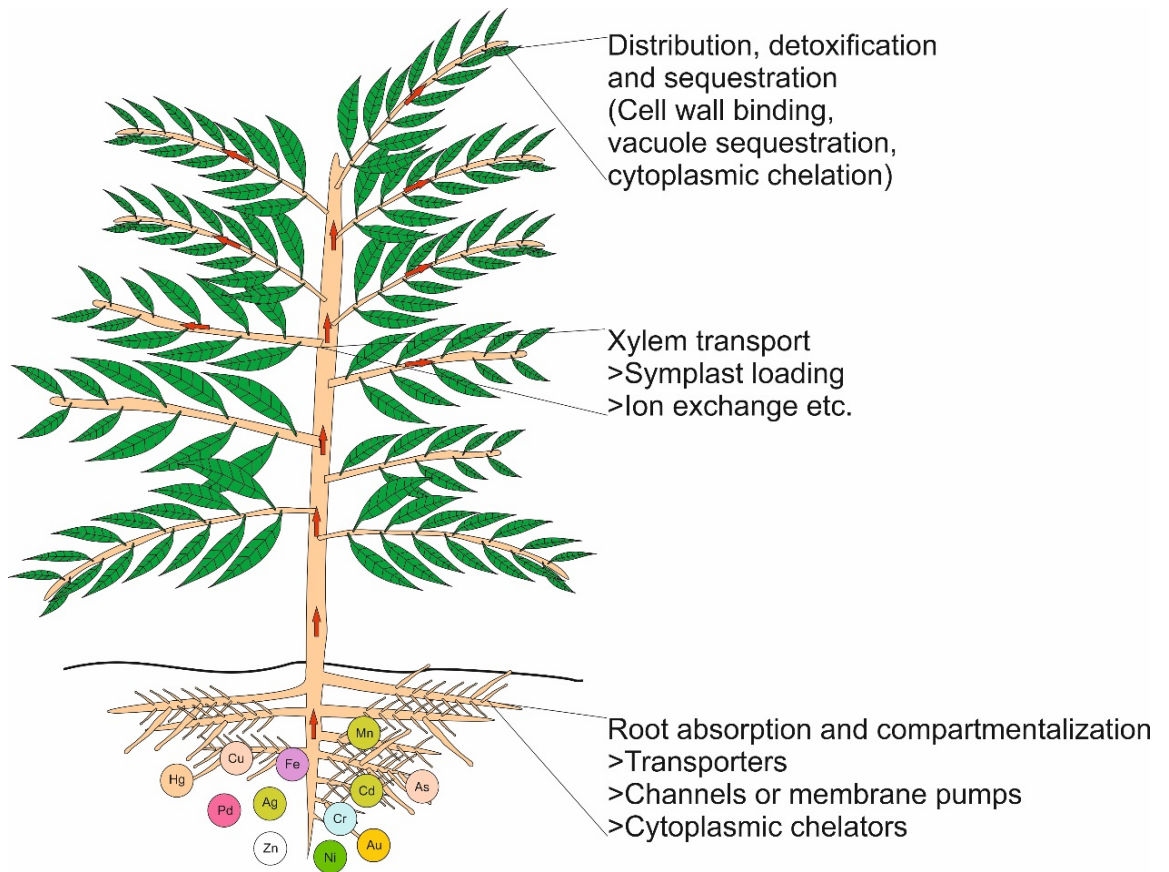


**Figure 1.12:** Mechanism of major processes involved in metal hyperaccumulation by plants. Figure adapted from Sheoran et al [21].

As suggested by Hunt et al [27], plants can be categorised into three groups on the basis of their metal uptake strategy, as shown in Figure 1.13. Metal excluders are plants which are able to accumulate high amounts of metals in roots but will avoid transporting metals to the aerial tissues [98]. Metal indicator plants will accumulate metals in above ground tissues at levels similar to the surrounding soil. Metal hyperaccumulators are plants that accumulate high levels of metals in the aerial tissues.

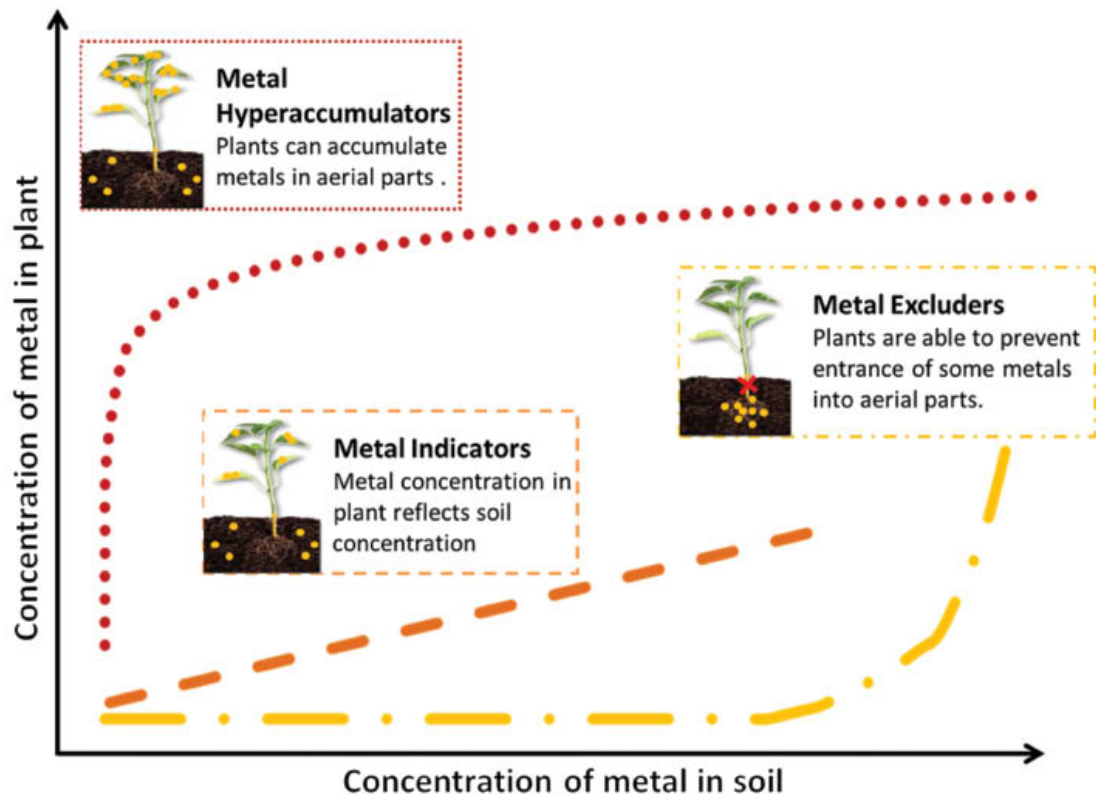


**Figure 1.13:** Three response strategies of plants to an increasing metal concentration in soil: hyperaccumulation (red line), metal indication (orange line) and exclusion (yellow line). Figure reproduced from Hunt et al [27].

Metal hyperaccumulators are the plant species of choice for phytoextraction purposes, as they are capable of accumulating exponentially higher concentrations of metals relative to the metal concentration in the surrounding soil [99]. At least 500 hyper-accumulator plant species have been described so far, belonging to a wide range of families [21, 100] and many of these have been extensively studied for phytoextraction. Known examples are *Arabidopsis halleri* and *T. caerulescens*, which are able to uptake high levels of arsenic, lead, zinc and cadmium [101]. Plant species such as *B. coddii* and *Alysum betolonii* are very efficient at taking up nickel and cobalt from soil [95, 96, 102].

As explained previously in Section 1.2.1, mine wastes often contain features deleterious to plant growth such as high levels of heavy metals and hydrocarbons as well as low nutrient and organic content. In such harsh conditions, plants for phytoextraction purposes should not just be able to take up and accumulate high levels of metals, but should also be capable of growing in these extreme environments. This has led many researchers to investigate the potential use of other, non-hyperaccumulator plant species, such as willow (*Salix* spp.) and miscanthus (*Miscanthus giganteus*, *M. goedaе-uksae* and hybrids) due to their fast growth rates, deep roots and high biomass production. Also in their favour, willow for example, is notably able to withstand the toxicity of a relatively broad range of toxic metals and thrive in some challenging environments [103-110]. Due to their high biomass production, non-hyperaccumulators used for phytoextraction can also be exploited for bioenergy production. As shown in Table 1.1, numbers of non-hyperaccumulator species including willow and miscanthus are now being investigated for their potential to be used in phytomining.

**Table 1.1:** Potential non-hyperaccumulator plant species for phytomining of metals and bioenergy production.

Location	Metals	Plant	Reference
Canada	Ag	<i>Salix miyabeana</i>	[106]
Belgium	Cd, Zn	<i>Salix dasyclados</i>	[105]
Belgium	Cd, Zn	<i>Salix fragilis</i>	[105]
Belgium	Cd, Zn	<i>Salix schwerinii</i>	[105]
China	Cd	<i>Salix aureo-pendula</i>	[111]
China	Cd, Cu, Pb, Zn	<i>Salix matsudana</i>	[112]
China	Cd, Cu, Pb, Zn	<i>Salix fragilis</i>	[112]
United States	Pb	<i>Salix eriocephala</i>	[113]
United States	Pb	<i>Salix nigra</i>	[113]
Sweden	Cd, Cu, Zn	<i>Salix viminalis</i>	[114]
South Korea	As, Cu, Pb, Ni, Cd, Zn	<i>Miscanthus goedaе-uksae</i>	[107]
Italy	Cd	<i>Miscanthus giganteus</i>	[115, 116]
France	Cu, Pb, Zn	<i>Miscanthus giganteus</i>	[117]
Poland	Ni	<i>Miscanthus giganteus</i>	[118]
Poland	Zn	<i>Spartina pectinata</i>	[108]
United States	Fe	<i>Spartina alterniflora</i>	[119]
Spain	Zn, Cd, Fe	<i>Spartina densiflora</i>	[120]

### 1.5.3 Chemically-assisted or induced phytoextraction

One of the biggest challenges in using plants to phytoextract gold and PGMs metals is the low solubility of these elements which limits their availability in soil for uptake by plant root systems. The availability of metals for uptake by the plant greatly relies on the geochemistry of the targeted metal in the soil [27]. It has been demonstrated that the addition of metal chelators such as EDTA [121], N-hydroxyethyl-EDTA (HEDTA) [122], ethylenediamine-N,N'-disuccinic acid (EDDS) [94], nitrilotriacetic acid (NTA), citric acid [75] and thiocyanate [92, 123-126] can significantly increase the uptake and accumulation of metals such as copper, nickel and cadmium (Table 1.2) [75]. These metal chelators induce metal accumulation in plants by forming stable metal chelates or ligand complexes in the soil, which improve the bioavailability of the metal [27, 75]. Such treatment was also found to significantly increase the transportation of metals from the soil to the aerial plant tissue [122], which is an important criterion if phytoextraction is to be commercially viable. However, there are some drawbacks to this approach, especially towards the environment. For example, the use of EDTA increases the concomitant uptake of other heavy metals, such as cadmium [121], lead [122], zinc [122] and chromium [127] together with the targeted metal, limiting the specificity of the approach. Moreover, following the application of EDTA, heavy metals not taken up by the plant can leach into groundwater polluting waterways. This leaching is further enhanced by the low biodegradability rate of EDTA [27, 75] [128]. The use of natural, low molecular weight organic acids (NLMWOA), such as citric acid, to improve metal solubility was found to be an alternative for EDTA [75]. The efficiency of NLMWOAs is questionable, though, as these compounds can be rapidly biodegraded by soil microorganisms [74, 129, 130], resulting in the breakdown of the complexes perhaps even before the metals are taken up by the plants [27]. The use of lixiviants, such as sodium cyanide and ammonium thiocyanate, significantly increase the uptake and translocation of precious metals such as gold in plants [92, 123]. In 1998, Anderson et al [123] published data showing that the application of cyanide to gold-containing soils massively increased the accumulation of gold in *B. juncea* plants. As gold is chemically similar to palladium, the ability of cyanide (in the form of KCN) to induce the uptake of palladium into plants is investigated and discussed in Chapter 3. The feasibility study of using cyanide in metal phytomining is also discussed in that Chapter 3.

**Table 1.2:** Examples of induced hyperaccumulation. Table reproduced from Hunt et al [27].

<b>Family</b>	<b>Species</b>	<b>Metals</b>	<b>Amendment</b>	<b>References</b>
Asteraceae	<i>Helianthus annuus</i>	Cu & Zn	EDDS	[94, 131]
Brassicaceae	<i>Brassica juncea</i>	Cd, Cu, Ni, Pb & Zn	Gallic and citric acid	[75]
Brassicaceae	<i>Brassica juncea</i>	Cd, Cu, Ni, Pb & Zn	EDTA	[121]
Brassicaceae	<i>Brassica juncea</i>	Cd	Citric acid and NTA	[132]
Brassicaceae	<i>Brassica juncea</i>	Au, Ag	NH <sub>4</sub> SCN	[123, 125]
Various	<i>Various</i>	Cd	NTA	[133]
Fabaceae	<i>Pisum sativum</i>	Pb	EDA & HEDTA	[122]
Poaceae	<i>Lolium perenne</i>	Cr, Ni & Zn	EDTA	[127]
Poaceae	<i>Phalaris arundinacea</i>	Cr	EDTA	[127]
Poaceae	<i>Zea mays</i>	Zn	NTA	[134]

## 1.6 Bioengineering to improve phytoextraction

Successful phytoextraction will not just rely on the ability of the plant to take up and accumulate metals from contaminated areas (such as soil and water) into the roots, but also in the ability to successfully translocate them from the roots to the shoots and detoxify them, either by sequestration into the vacuole [82, 83] or by reducing them into less toxic compounds [135]. Many of the metal hyperaccumulator plants are able to translocate and accumulate metals into aerial tissues. However, most of these plants are not suitable for field applications, due to poor agronomic traits, or inability to survive in the specific, and relatively harsh environments found in mine waste [27, 114]. Furthermore, as non-hyperaccumulator plants can be more suitable for growth under such conditions [114, 136], effort is focusing on ways to improve metal uptake and translocation in these species. Genetic engineering could be used to substantially enhance metal phytoextraction in non-hyperaccumulator plants [29].

Metal transporters are required for metal uptake, metal partitioning and metal delivery into subcellular localisation including metal storage in vacuoles. By manipulating these transporters, non-hyperaccumulator plants can be engineered to accumulate and translocate more metals onto the aerial tissues of the plants, while increasing the tolerance of the plant to highly toxic environments. The overexpression of metal transporters was found to increase metal uptake and tolerance in non-metal hyperaccumulating plant species like *Arabidopsis*; for example it was found that the overexpression of endogenous *AtHMA4* (Heavy Metal ATPase 4) enhanced the translocation of zinc and cadmium from the roots to the shoots by 2- and 1- fold per gram of tissue, when compared with the wildtype plant [86]. The overexpression of *Arabidopsis CAX2* (Calcium Vacuolar Transporter 2) was also found to enhance the accumulation of cadmium and manganese in the aerial tissue of transgenic tobacco plants by 1.5- fold and 1- fold increase respectively, as compared to the wildtype [137]. The *Arabidopsis* ABC transporter of the mitochondrion 3 (*AtATM3*) is involved in the biogenesis of Fe-S clusters and in iron homeostasis. The expression of *AtATM3* into the field-suitable plant *B. juncea* was found to enhance the accumulation of cadmium and the transportation of cadmium to the aerial tissues by 2.4- and 1.7- fold, respectively, when compared to the wildtype plant [138]. The expression of *YCF1* (Yeast Cadmium Factor 1) from *Saccharomyces cerevisiae* was also found to increase the tolerance and accumulation capacities of *B. juncea* to cadmium and lead by 1.5- and 2- fold respectively higher uptake rates than the wildtype [138]. Vital steps towards engineering transporters to tailor specific metal uptake by plants should include

thorough biochemical characterisation of the transporters, to understand the basis of metal specificity, their regulation, their subcellular localisation and their endogenous role.

One of the most promising strategies to detoxify metals is by converting the metal into a less toxic form, or incorporating it into a compound. Sometimes, a combination of different approaches is required; previously, it was shown that detoxification of arsenic in plants could be achieved by expressing genes encoding  $\gamma$ -glutamylcysteine synthetase ( $\gamma$ -ECS) and arsenic reductase (*ArsC*) into *Arabidopsis*. It was observed that the expression of both genes in *Arabidopsis* conferred enhanced tolerance to arsenic, with  $\gamma$ -ECS together with *ArsC*-expressing plants accumulating 2- to 3- fold more arsenic per gram of tissue when compared with the wildtype or to plants expressing either *ArsC* or  $\gamma$ -ECS alone [139].

The ability of bacterial mercuric reductase (MerA) to reduce  $\text{Hg}^{2+}$  to much less toxic  $\text{Hg}^0$  has been demonstrated in plants for the potential phytoremediation of mercury. The expression of modified bacterial MerA in *Arabidopsis* increased tolerance to mercury [135]. When the plants were grown on media containing 50  $\mu\text{M}$  of mercury chloride, the MerA lines exhibited enhanced tolerance compared to the wildtype seedlings [135]. The work was extended to methylmercury toxicity studies, by expressing the bacterial organomercurial lyase MerB in *Arabidopsis*, which conferred tolerance to organomercurials such as methyl mercury by breaking the Hg-C bonds [140]. Amazingly, the expression of both enzymes in *Arabidopsis* increased the tolerance to methyl mercury by 50-times compared to wildtype plants [141]. This work was further extended into phytoremediation-relevant tree species [142]. It was also revealed that the MerA transgenic lines were also tolerant to toxic gold concentrations (150  $\mu\text{M}$ ) suggesting MerA is involved in gold reduction. Earlier work done by Summers and Sugarman [143] also suggested the potential of gold as substrate for MerA activity, based on the formation of dark purple colloidal gold when cells expressing MerA were treated with gold chloride, indicating the reduction of  $\text{Au}^{3+}$  to  $\text{Au}^0$ . However, to date, no subsequent analysis has been carried out to further characterise the involvement of MerA on gold reduction activity.

Chapter 4 and 5 discusses in more detail, the potential of genetic engineering approaches to enhance the resistance of plants towards gold and palladium as well as to increase the formation of metal nanoparticles in plants.

## **1.7 Main objective**

To investigate the potential of plants to uptake palladium and other precious metals from mine wastes, for remediation and re-vegetation purpose.

### **Objectives:**

1. To assess the phytotoxicity of palladium using *Arabidopsis* as the model species.
2. To investigate the potential of willow and miscanthus as field-applicable species for phytomining of palladium and revegetation of mine wastes.
3. To explore the use of genetic engineering to increase palladium and gold uptake, tolerance and nanoparticle formation in *Arabidopsis*.
4. To investigate the potential involvement of *AtHMA5* in the detoxification of palladium and gold in *Arabidopsis*.

## **Chapter 2: Materials and methods**

### **2.1 Materials and suppliers**

All the materials were obtained from: Sigma-Aldrich (Poole, UK), New England Biolabs (NEB) (Hertfordshire, UK), Thermo Fisher Scientific (Loughborough, UK), Invitrogen (Paisley, UK), Promega (Southampton, UK), Qiagen (Crawley, UK), Fermentas (York, UK), Duchefa Biochemie (Haarlem, Netherlands), Melford (Ipswich, UK), Biotline (London, UK) and ClonTech (US). Synthetic ore was supplied by Imerys Minerals Ltd., Cornwall, UK. Purified water was obtained using Milli-Q water filtration system (Merck Millipore, Germany) and sterilised by autoclave if necessary. Primers used throughout this work were synthesised from Sigma-Aldrich (Poole, UK) and Integrated DNA Technologies (Leuven, Belgium).

### **2.2 Plant studies**

Wild-type seeds used throughout this work were the *Arabidopsis thaliana* (*Arabidopsis*) Columbia-0 (Col-0) ecotype.

#### **2.2.1 Seed sterilisation using chlorine gas**

*Arabidopsis* Col-0 seedlings were sterilised by exposing the seeds to chlorine gas in an airtight container for four hours in a fume hood. Chlorine gas was produced by adding 3 ml of concentrated hydrochloric acid with 100 ml of bleach solution.

#### **2.2.2 Murashige and Skoog medium for plant growth**

Murashige and Skoog medium was used as the media for plant growth throughout this work. It contained the following components: 0.025 mg/l  $\text{CoCl}_2 \cdot 6\text{H}_2\text{O}$ , 0.025 mg/l  $\text{CuSO}_4 \cdot 5\text{H}_2\text{O}$ , 36.70 mg/l FeNa EDTA, 6.20 mg/l  $\text{H}_3\text{BO}_3$ , 0.83 mg/l KI, 16.90 mg/l  $\text{MnSO}_4 \cdot \text{H}_2\text{O}$ , 0.25 mg/l  $\text{Na}_2\text{MoO}_4 \cdot 2\text{H}_2\text{O}$ , 8.60 mg/l  $\text{ZnSO}_4 \cdot 7\text{H}_2\text{O}$ , 333.02 mg/l  $\text{CaCl}_2$ , 170 mg/l  $\text{KH}_2\text{PO}_4$ , 1900 mg/l  $\text{KNO}_3$ , 180.54 mg/l  $\text{MgSO}_4$ , 1650 mg/l  $\text{NH}_4\text{NO}_3$  (Murashige T. and Skoog F., 1962). Unless otherwise stated, the pH used throughout this work was altered to pH 5.7 using NaOH.  $\frac{1}{2}$  MS was also supplemented with 20 mM sucrose. Agar was added to prepare solid media. All media were autoclaved prior to be used.

### **2.2.3 Supplements to plant growth media**

To prepare palladium and gold solution, potassium tetrachloropalladate ( $K_2PdCl_4$ ) and potassium tetrachloroaurate ( $KAuCl_4$ ) were prepared freshly by dissolving the metal salt in water to a final concentration of 100 mM and used for the whole experimental studies related to palladium and gold.

## **2.3 Bacterial studies**

### **2.3.1 Growth media used for bacterial growth**

For growing bacteria, Luria Bertani (LB) media was used throughout the whole experiments. LB media contained 10 g/L peptone, 5 g/L yeast extract and 10 g sodium chloride. Agar was added to prepare solid media. All media were autoclaved prior to be used.

## **2.4 Yeast studies**

### **2.4.1 Growth media used for yeast growth**

For growing yeast, yeast extract peptone dextrose (YPD) media was used throughout the whole experiments. YPD media contained 10 g/L yeast extract, 20 g/L peptone and 20 g/L dextrose. Agar was added to prepare solid media. All media were autoclaved prior to be used.

### **2.4.2 Yeast selective media**

For screening of yeast based on selectable marker, Yeast Synthetic Drop-out (YSD) medium without uracil was used throughout this work. It contained the following components: Adenine 18 mg/l, p-Aminobenzoic acid 8 mg/l, Leucine 380 mg/l, Alanine 76 mg/l, Arginine 76 mg/l, Asparagine 76 mg/l, Aspartic acid 76 mg/l, Cysteine 76 mg/l, Glutamic acid 76 mg/l, Glutamine 76 mg/l, Glycine 76 mg/l, Histidine 76 mg/l, myo-Inositol 76 mg/l, Isoleucine 76 mg/l, Lysine 76 mg/l, Methionine 76 mg/l, Phenylalanine 76 mg/l, Proline 76 mg/l, Serine 76 mg/l, Threonine 76 mg/l, Tryptophan 76 mg/l, Tyrosine 76 mg/l & Valine 76 mg/l (Sigma Aldrich). Unless otherwise stated, the pH used throughout this work was altered to pH 6.1 using NaOH. All media were autoclaved prior to be used. For 1 L of media, it contained 1.92 g/L of YSD media, 6.7 g/L of yeast nitrogen base without amino acids and 40 mL/L Glucose or Galactose. Agar was added to prepare solid media. All media were autoclaved prior to be used.

## **2.5 Molecular biology studies**

### **2.5.1 Isolation of genomic DNA from plants (CTAB method)**

Approximately one big leaf was placed in an Eppendorf tube (1.5 mL). 500 µL of 2X CTAB buffer was added into the tube. Pestle was used to grind the leaf inside the tube containing CTAB buffer (2 % CTAB, 1.4 M NaCl, 100 mM Tris-HCl pH 8, 20 mM NaEDTA). The mixture was incubated at 65 °C for 30 to 60 minutes. 300 µL of chloroform:IAA (Iso amyl alcohol) with the ratio of 24:1 was added into the mixture followed by vortex. The mixture was spinned down at high speed for 5 minutes in microcentrifuge. 300 µL of the top aqueous layer was transferred into a clean Eppendorf tube. 960 µL of ethanol and 40 µL of sodium acetate (pH 5.2) were added into the solution. The solution was mixed and left for 40 minute at room temperature or overnight in the fridge to precipitate the DNA. Following a 15 minutes spin down in cold room using microcentrifuge, the supernatant was discarded and the pellet was rinsed with 70 % ethanol. The pallet was dried using speed vac and resuspended with sterile distilled water. DNA was quantified using a Nanodrop ND-1000 Spectrophotometer (Thermo Scientific) at 260 nm.

### **2.5.2 Isolation of plasmid**

Plasmid DNA was isolated using QIAprep Spin Miniprep Kit throughout this study according to manufacturer's protocol. DNA was quantified using a Nanodrop ND-1000 Spectrophotometer (Thermo Scientific) at 260 nm.

### **2.5.3 Purification of DNA / RNA**

Gel and PCR product was purified using Wizard SV Gel and PCR Clean-Up System Kit throughout this study according to manufacturer's protocol. DNA/RNA was quantified using a Nanodrop ND-1000 Spectrophotometer (Thermo Scientific) at 260 nm.

### **2.5.4 DNA sequencing**

The DNA were sequenced by GATC Biotech, and analysed using SeqScanner2.0 (Applied Biosystems) and Clustal Omega [85].

### **2.5.5 Isolation of RNA from plant and yeast**

RNA was isolated from plant and yeast using Isolate II RNA Plant Kit (BIOLINE) throughout this study according to manufacturer's protocol. RNA was quantified using a Nanodrop ND-1000 Spectrophotometer (Thermo Scientific) at 260 nm.

### **2.5.6 Reverse transcription of RNA**

Complementary DNA (cDNA) was synthesised from isolated purified RNA using First strand cDNA Synthesis Using Superscript II Reverse Transcriptase (Invitrogen) according to manufacturer's protocol. DNA was quantified using a Nanodrop ND-1000 Spectrophotometer (Thermo Scientific) at 260 nm.

### **2.5.7 Transformation of *E. coli***

1  $\mu$ L of DNA (10-50 ng) was added into 50  $\mu$ L of competent cells. The cells were left on ice for 5 minutes before heat shocked at 42 °C for 60 seconds and straight away put on ice for another 5 minutes. 500  $\mu$ L of LB media was added into the cells and incubated at 37 °C for another 1 hour. The cells were plated on LB agar and incubated for overnight at 37 °C.

### **2.5.8 Transformation of *Agrobacterium tumefaciens* and *Saccharomyces cerevisiae* (Electroporation)**

80  $\mu$ L of competent *Agrobacterium* cells was transferred and thaw on ice for few minutes. 1  $\mu$ L of DNA was added into the competent cells and briefly incubate on ice for 30 seconds. The cells were transferred into 2 mm micropulsar cuvette. The electroporator was set to 2.5 kV, 400  $\Omega$  resistance and 25  $\mu$ F capacitance. The cells were electric shocked for 5 seconds and transferred into a new Eppendorf tube followed by the addition of 1 mL LB/Sorbitol. The cells were incubated at 30 °C for 1 hour before plated on desired media with appropriate antibiotic.

### **2.5.9 Plant transformation**

The pART27-with insert was used to transform electro-competent *Agrobacterium tumefaciens*. *A. tumefaciens* containing the pART27-insert was used to floral dip *Arabidopsis*. The positive T1 transformants were screened on half-strength MS agar with the presence of 50  $\mu$ g/ml of kanamycin. T2 lines with kanamycin-resistance segregation ratios indicative of single insertional events were selected and homozygous T3 lines (judged by 100 % resistance towards kanamycin) were selected for further analysis. The presence of the insert in these lines was confirmed using PCR and transcript levels were measured using qPCR.

### **2.5.10 Real-Time (quantitative) PCR (qPCR)**

qPCR was performed using cDNA synthesised from RNA as stated previously. Primers for qPCR were designed using Primer Express Version 3 (Applied Biosystems) and were synthesised by Sigma Aldrich (UK). Primers were tested for efficiency prior to use for testing gene expression. Reactions contained 4  $\mu\text{L}$  of cDNA (0.4, 4 or 40 ng), 0.4  $\mu\text{L}$  of primers (10  $\mu\text{M}$ ), 5.2  $\mu\text{L}$  of nuclease free water and 10  $\mu\text{L}$  of Power SYBR green PCR master mix (Applied Biosystems, Warrington, UK) in three technical replicates. Reactions were carried out in a sealed 96 well plate which were centrifuged at 5000 x g for 2 minutes. All qPCR reactions were carried with the following cycle condition ; 2 minutes at 50 °C, 10 minutes at 95 °C followed by 40 cycles of 95 °C for 15 seconds and 60 °C for 1 minute.

## Chapter 3: Palladium uptake in plants

### 3.1 Introduction

#### 3.1.1 Palladium at a glance

Palladium is an element that has a wide application in industry. It is classed as a platinum group metal (PGM), a grouping which also includes platinum, rhodium, osmium, iridium and ruthenium and these metals are often found together in the same ore deposits. William Hyde Wollaston first discovered palladium in 1803 while he was analysing platinum ore obtained from South Africa. Palladium has a very high melting point (Table 3.1), which makes it suitable for use as a catalyst in the production of catalytic converters in the exhaust systems of automobiles. Besides its high demand in many industrial sectors, palladium is also considered as a precious metal, together with gold and other PGMs. Palladium is also commonly used as jewellery and financial investments. As of July 2016, the market price for palladium is around 700 USD/oz.

**Table 3.1:** Properties of palladium

<b>Name</b>	Palladium
<b>Symbol</b>	Pd
<b>Atomic number</b>	46
<b>Atomic mass</b>	106.42
<b>Standard state</b>	Solid
<b>Melting point</b>	1828 K
<b>Boiling point</b>	3236 K
<b>Density</b>	12 000 kg/m <sup>3</sup>

### 3.1.2 Palladium mining activity

Palladium is mined every year to cater for the increasing demand from many sectors, especially from the automotive industry. South Africa, Russia, the United States, Canada and Zimbabwe contain the largest PGM reserves in the world (Figure 3.1) [144]. According to the US geological survey published in 2015, Russia and South Africa each extracted 2,821,920 ounces (80,000 kg) and 2,575,002 ounces (73,000 kg) of palladium respectively in 2015 (Figure 3.2) [145]. These countries are the largest palladium producers, followed by Canada, the United States and Zimbabwe as well as some minor contributions from United Kingdom and Switzerland. Among the most well-known palladium mining companies are Norilsk Nickel (Russia), Impala Platinum (South Africa), Anglo Platinum (Zimbabwe) and Stillwater Mining (Canada), with the Bushveld mining complex in South Africa considered to have the largest PGM reserves in the world.

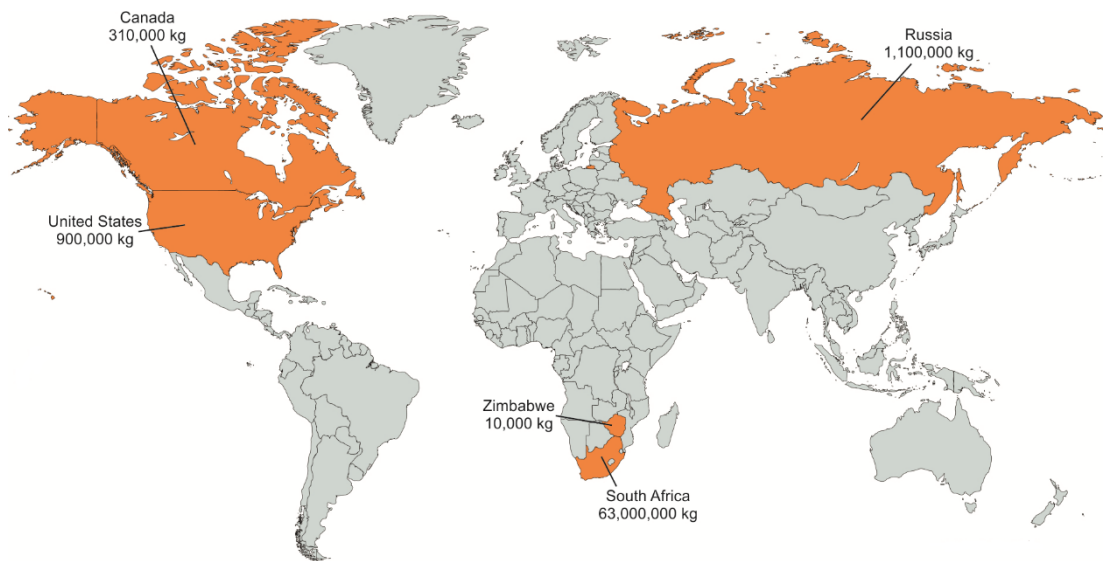


**Figure 3.1:** Distribution of PGM reserves according to countries (in orange colour). Data obtained from the US Geological Survey 2015 [144].

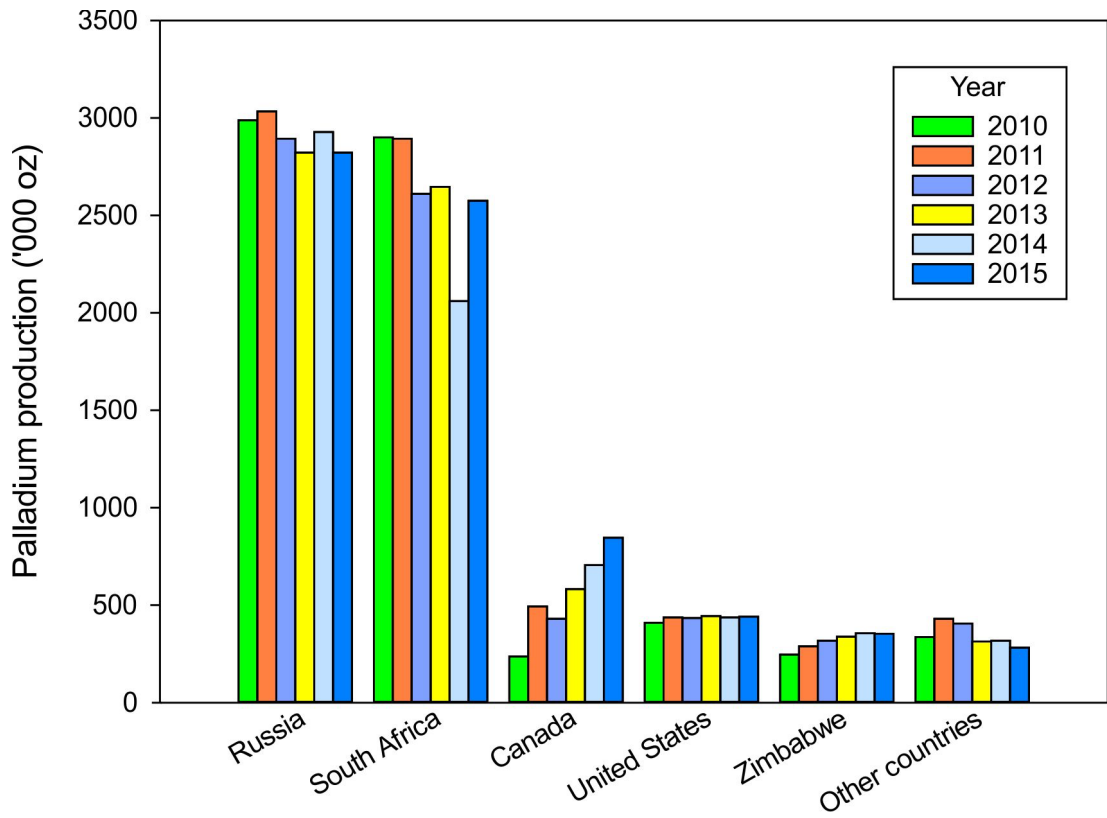


**Figure 3.2:** Palladium production by year according to major producers. Data obtained from US Geological Survey 2016 [145].

### 3.1.3 Uses of palladium

Palladium is mainly used in the automotive industry to make catalytic converters. Data obtained from the PGM Market Report 2015 on palladium production by Johnson Matthey show that the demand for palladium has exceeded supply within the past three years (Figure 3.3). This increase in demand is cited as most probably due to the massive increase in terms of vehicle production year-on-year [146]. The rise of the automotive industry in the early 20<sup>th</sup> century led to an increase in the amount of harmful compounds such as carbon monoxide (CO), hydrocarbon (HC) and nitrogen oxide (NO<sub>x</sub>) emitted into the environment. In 1970, The Clean Air Amendments Act set by the U.S. Environment Protection Agency called for a tighter legislation to reduce emissions of CO, HC and NO<sub>x</sub> by up to 90 % [147]. This legislation led to the development of catalytic converter technology in cars, and was pioneered by Johnson Matthey (UK) [147, 148]. As seen in the schematic diagram in Figure 3.4, gases produced from the internal combustion engine will enter the catalytic converter, which contains catalytically active metals such as platinum, palladium and rhodium coated onto the honeycomb structure of the converter. The CO and HC are oxidised by the platinum or palladium into carbon dioxide and water and released into the environment. Alongside this reaction, rhodium will reduce NO<sub>x</sub> into nitrogen [149]. In terms of application in the production of automobiles, 85 % of the palladium demand is from the production of light duty vehicles followed by light duty diesel vehicle, high duty diesel vehicle and motorcycles with each 10 %, 3 % and 2 % demand respectively (Figure 3.5) [146].

Palladium is also widely used in other industrial applications. According to a report produced by Johnson Matthey [146] (Figure 3.6), aside from the automotive industry, 21 % of palladium goes to other industrial sectors including chemical [150], dental [151] and electronics [152]. In chemical industries, palladium is used as a catalyst in many chemical reactions including the production of hydrogen peroxide, acetaldehyde, vinyl acetate monomer and purified terephthalic acid [153]. In the dental industry, palladium is used as an alloying agent in dental restoration [153]. Palladium is also used in the production of multilayer ceramic capacitors, hybrid integrated circuits, plating connectors and lead-frames [152, 153]. Similar to other precious metals like gold and platinum, palladium is also widely used to produce jewellery, which has a large market in China, the US, the UK and Germany [146].

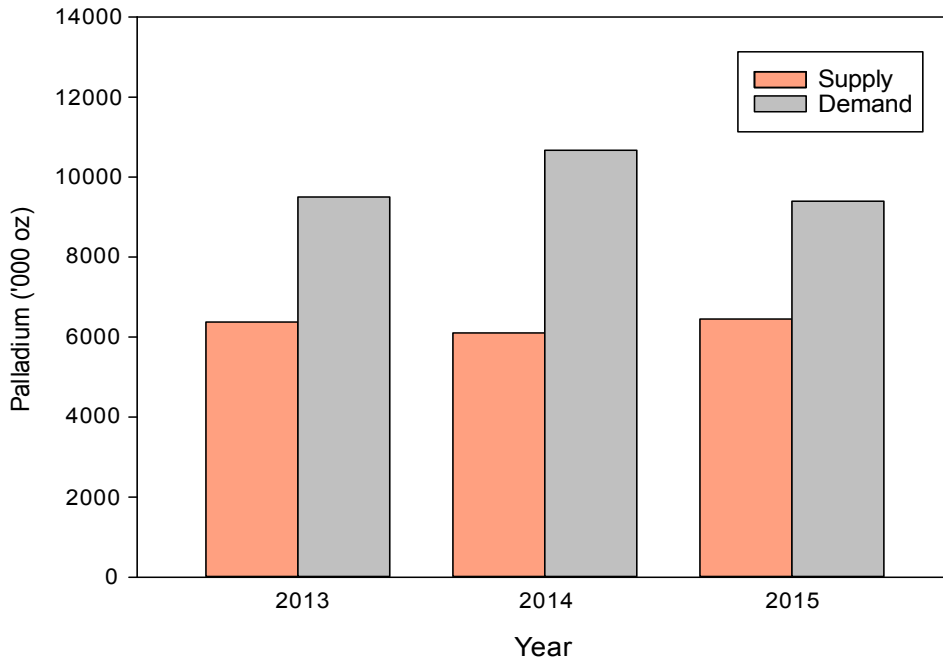


**Figure 3.3:** Palladium supply versus demand by year. Data obtained from the PGM Market Report 2015 (Johnson Matthey) [146].

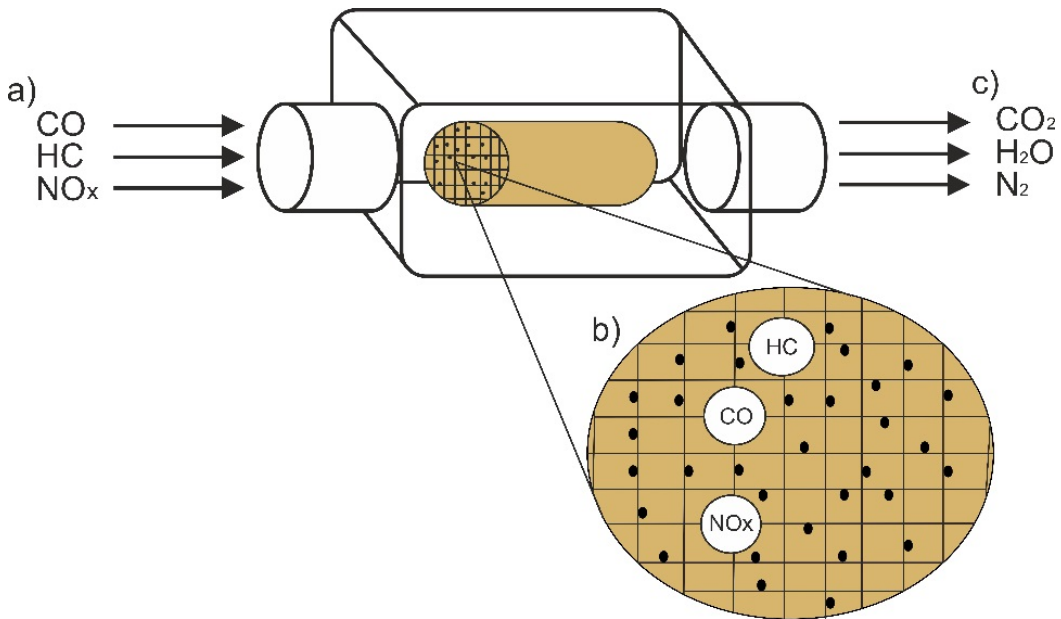


**Figure 3.4:** Schematic diagram of catalytic converter in car exhausts. a) Pollutant molecules CO, HC and NO<sub>x</sub> produced from the engine enter the catalytic converter. b) Pollutants come into contact with the hot metals inside the catalytic converter and undergo chemical reaction to form less harmful molecules. c) The less harmful molecules exit the catalytic converter.

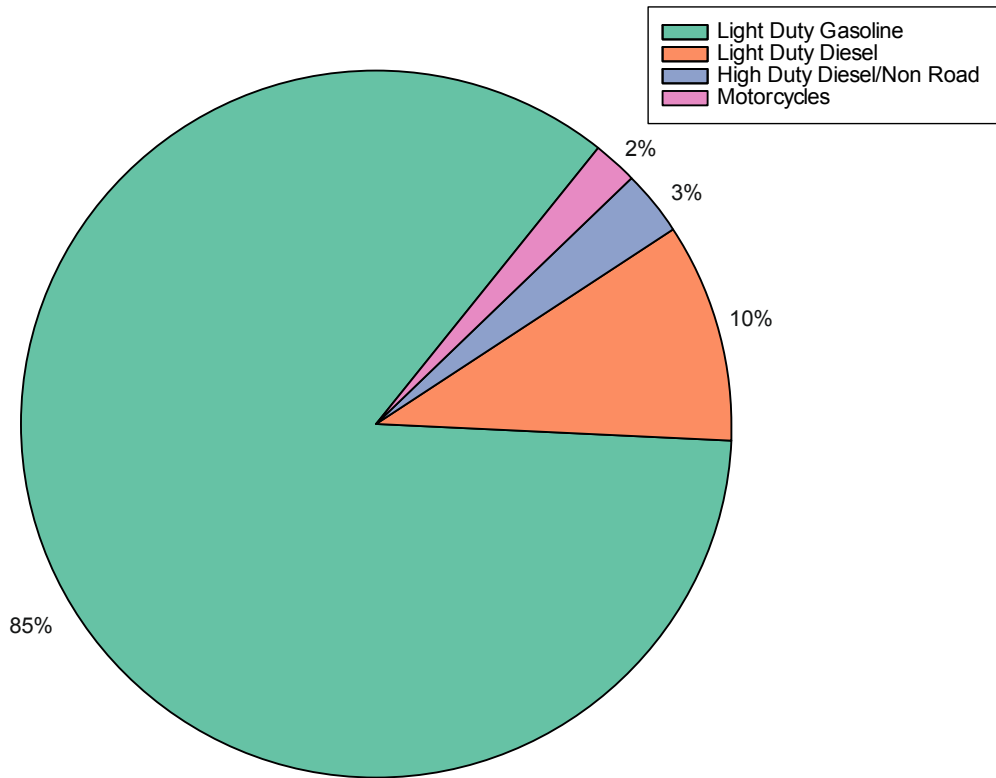


**Figure 3.5:** Palladium demand by automotive sector 2015. Data from the PGM Market Report 2015 (Johnson Matthey) [146].

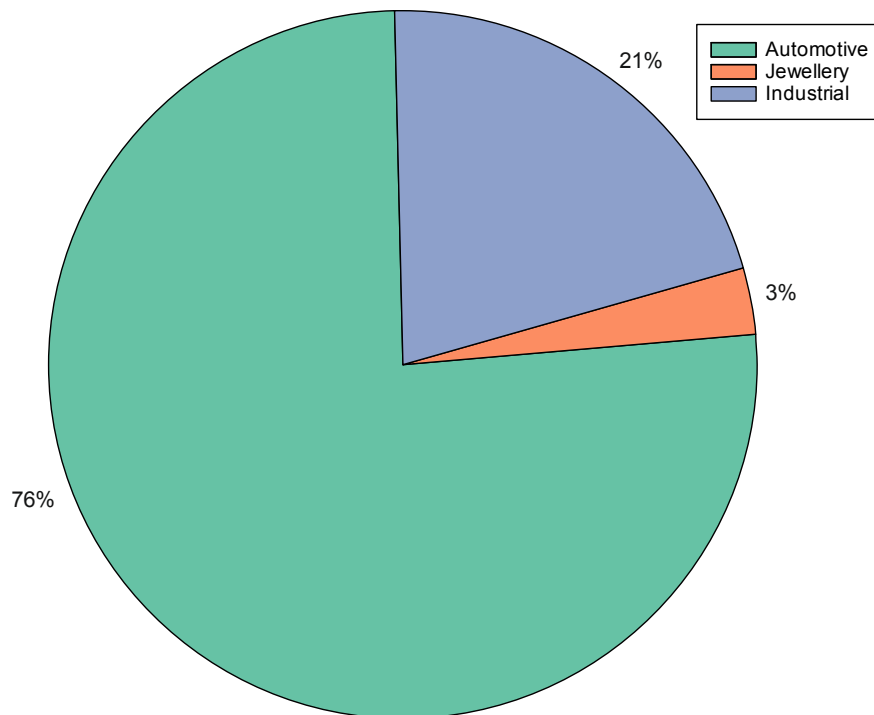


**Figure 3.6:** Palladium demand according to sector in 2015. Data obtained from the PGM Market Report 2015 (Johnson Matthey) [146].

#### 3.1.4 Phytomining of palladium from mine wastes

While demand for palladium is increasing, much of this limited resource is being lost through dispersal and dilution into the environment. Phytomining is an approach whereby specific metals can be extracted and re-concentrated from waste sources. In the case of palladium, waste sources include mine wastes, which contain concentrations of palladium that are currently uneconomic to extract using conventional methods.

The idea of phytomining was first coined by Chaney [154] and has been reviewed by Chaney et al [93] and Anderson et al [92] as a mean of using plants to remove metals from sub-economic ore bodies or contaminated mine sites with the additional aim of recovery of economic amount of metals. Phytomining has been investigated to recover many metals with high commercial value such as gold [126], nickel [92, 118] and silver [106, 125]. In 2009, scientists at the University of Sydney, Australia conducted a technical feasibility and economic viability study on nickel and gold phytomining. They estimated that, at 2009 market values, the profit gain from nickel and gold phytomining, including the biomass energy produced, could generate approximately 11,500 and 26,000 AU\$/ha/harvest using *Brassica juncea* for nickel and *Berkheya coddii* for gold respectively [155].

Phytomining often involves the application of hyperaccumulator species, to grow and concentrate metal into above-ground tissue [92, 93]. Previous work on phytomining of nickel and gold successfully identified several potential hyperaccumulator candidates such as *Brassica* spp. [92, 156], *B. coddii* [95, 97, 157] and *Alyssum* spp. [96, 158, 159]. Significant progress towards the commercialisation of nickel phytoextraction is being made including the use of breeding techniques to produce *Alyssum* sp. cultivars with improved agronomic traits [160, 161]. However, only a limited number of elements are known to be concentrated by hyperaccumulator species, and no suitable species have yet been found for palladium or other PGMs.

### 3.1.5 Use of cyanide to enhance palladium solubilisation

A major hurdle to the application of palladium phytomining is that uptake of palladium and other PGMs from mine waste and soil is often limited by their low bioavailability. These elements generally exist as chemically inert, zero-valent forms, or are bound to minerals. A highly effective recovery method for gold and PGMs is the use of cyanide for solubilisation [124]. The use of cyanide has been found to significantly induce the accumulation of gold into plant aerial tissues [94, 123, 124], and the majority of gold and silver mines use this technology. However, although the application of cyanide is tightly regulated in many countries, improper management has resulted in environmental damage, particularly via spills into waterways [162, 163]. In Canada, it was reported that more than 20,000 steelheads (*Oncorhynchus mykiss*) were killed when mine effluents containing cyanide was accidentally discharged from a mine wastes pond into nearby creek [164]. In 1995, it was also reported that at about 80 km of Essequibo River in Guyana, South America was contaminated with cyanide when a dam nearby collapsed releasing approximately  $3.3 \times 10^9$  L of cyanide-containing waste which killed many fishes and affected the primary water source of the area [165].

Interestingly, many higher plant species are known to produce cyanide naturally for chemical defense [166], as well as by-product in the synthesis of ethylene [167]. Plants also possess an effective cyanide metabolism and detoxification strategy to avoid from any irreversible damage caused by cyanide. The main pathway of cyanide metabolism in plants is mainly catalysed by the action of the enzyme beta-cyanoalanine synthase and cyanoalanine hydrolase which convert free cyanide into asparagine [166, 168, 169]. There are also numbers of willow species which are reported to take up and metabolise cyanide [168-172]. This may present a situation whereby the application of cyanide might enhance plant growth and enable phytoextraction of PGMs [169-171, 173].

### 3.1.6 Field applicable plant species for phytomining of palladium

Mine wastes often contain deleterious traits such as phytotoxic concentrations of heavy metals, sub-optimal pH, low organic matter content and low nutrient content; and these properties may result in suboptimal plant growth and low plant biomass. This has led to the search for plant species which are better suited to the relatively harsh conditions found in metal-rich land and waste material. The search for field applicable plant candidates have also looked on the potential of non hyperaccumulator plant species such as willow (*Salix* sp.) which is reported to be highly tolerant to concentrations of metals (copper, cadmium, nickel and zinc) considered toxic to many other plant species, and able to achieve high biomass in relatively nutrient poor soils [104, 113, 136, 174, 175]. Other species with phytoextraction potential include miscanthus (*Miscanthus giganteus*) [107, 118, 176] and switchgrass (*Panicum virgatum*) [177, 178].

Phytomining can also be seen as an opportunity to clean up environmental pollution [21]. Large areas of land used to dump mine wastes may not just contain PGM metals reserves, but also phytotoxic levels of metals, hydrocarbons, and other wastes as by-products from the mining industry. The use of phytomining to re-vegetate and remediate this contaminated land could be a win-win situation for the environment and industries.

As there is currently little information on plant-palladium interactions, this chapter explores the effect of palladium on the model plant genetics species, Arabidopsis. The main core of this chapter investigates the potential of the field-applicable species willow and miscanthus for palladium uptake from and tolerance to growth on mine wastes. The potential of *Brassica juncea* (mustard) to take up palladium was also examined following the previous success with phytomining gold [92]. This chapter further explores the formation of palladium nanoparticles *in planta* and the use of cyanide to induce palladium uptake and translocation into above ground tissues.

### 3.1.6.1 Willow

Non-hyperaccumulator members of the willow genus have a number of traits that make them suitable candidates for phytomining palladium. They have fast growth rates with high biomass production, are easy to propagate, produce extensive root systems and also have high transpiration rates [104, 105, 114]. Furthermore, compared to many plant species, willow can tolerate relatively high levels of toxic metals, an important trait given that palladium mine wastes often contain levels of metals such as nickel that are phytotoxic to many species. The use of willow in the phytoextraction of metals from contaminated soil has been well documented [104-106, 111-114].

The idea of using willow to extract metals from contaminated soil emerged when ash from willow was found to contain more than 10 times higher levels of cadmium than other forest trees used for bioenergy production [114]. Willow was also previously revealed to accumulate copper [104] cadmium [111], lead [113] and silver [106] in the aerial tissues. Moreover, the advantage of having high biomass production also allows willow to be widely used for bioenergy production [114]. In Sweden, willow is grown on about 15,000 hectares, producing up to 35 tons of stems per hectare per year [114].

There are about 450 different species from the genus *Salix* [104]. Each willow species may have different metal uptake capacity. *Salix nigra*, *S. exigua* and *S. aureo-pendula* were found to accumulate cadmium into the aboveground tissue [104, 111]. *S. miyabeana* was reported to tolerate toxic concentrations of silver [106]. There are also some willow species which are not able to accumulate high amounts of heavy metals [179, 180]. The above properties have made willows excellent candidates for revegetation and remediation of mine wastes. In this chapter, the potential of willow to uptake and tolerate palladium was investigated. Fifteen different willow species were also tested on palladium-containing medium to assess the level of genetic variation in palladium uptake and tolerance capacity.

### 3.1.6.2 Miscanthus

Another potentially field applicable plant species studied in this chapter is miscanthus. This perennial grass is a vigorous, high biomass, non-woody, sterile hybrid that is vegetatively propagated by rhizomes [110, 115, 116]. Structurally, miscanthus straw is composed of approximately 22 % lignin, 36 % cellulose, and 24 % hemicellulose [110, 181].

Miscanthus is able to grow on a range of soil conditions without fertiliser and can grow twice the size of switchgrass. It is estimated that approximately 20 to 35 tons of dry miscanthus straw can be harvested from one-hectare crop per year [118, 182]. The large amounts of biomass produced by miscanthus has made it a suitable feedstock for biofuel and bioenergy production [110], miscanthus biomass can also be used as biomaterial or bioplastic. The idea of using second-generation biofuel plants for phytoextraction of heavy metal and other contaminants is not new [183-185], and its use for palladium phytomining is promising.

Miscanthus is known to be tolerant to a variety of environmental stresses [186]. Previous studies have also demonstrated the ability of miscanthus to be used in remediating soils containing phytotoxic levels of metals such as zinc, copper, nickel, cadmium, arsenic as well as organic pollutants such as polycyclic aromatic hydrocarbons (PAH) [107, 108, 110, 115, 116, 118, 176]. It has been reported that miscanthus can effectively enhance the growth of PAH-degrading bacteria in the root zone, significantly improving the degradation of PAH [187]. Miscanthus has also been used for the phytoextraction of heavy metals from contaminated leachate on landfills [110]. As a perennial crop, it does not have to be replanted every year, which could effectively reduce maintenance costs [110].

In this chapter, the potential of miscanthus for phytomining palladium from mine wastes was investigated.

## **3.2 Materials and methods**

### **3.2.1 Palladium uptake in Arabidopsis**

#### **3.2.1.1 Growth studies of Arabidopsis on solid media containing palladium**

Sterilised Arabidopsis seeds were pipetted onto plates containing  $\frac{1}{2}$  MS (A) with various palladium concentration. Seedlings were then stratified for three days at 4 °C in the dark before being transferred to the growth room. The seedlings were grown under  $20 \text{ mmol.m}^{-2}.\text{s}^{-1}$  light for twelve days with a 16-hour photoperiod, temperatures of 20 °C during the light and 18 °C in the dark and watered as required. Seedling root lengths were photographed on alternate days up to day 12, then total fresh weight determined. Mean root length was measured using ImageJ software and compared using T-test or one-way ANOVA for least significant difference.

#### **3.2.1.2 Growth studies of Arabidopsis on soil containing palladium**

The palladium concentration of soil is reported as mg palladium per kg of soil, which consists of 55 % dry mass and 45 % water. To prepare this soil, a 10 times concentrated palladium stock was prepared by solubilising palladium nitrate ( $\text{PdNO}_3$ ) with nitric acid and mixing it with the gravel-kaolinite mixture in a 1:1 ratio. The concentrated palladium stock was used to prepare the final concentration of 0, 1, 5, 10 and 50 mg/kg of palladium by mixing with soil into a final volume of 18 gram.

Five five-day-old Arabidopsis seedlings were grown in each pot containing 18 grams of palladium-dosed soil. The plants were placed in a growth cabinet (Percival, USA) for another seven weeks. The conditions for the cabinet were set to  $180 \text{ }\mu\text{mol.m}^{-2}.\text{s}^{-1}$  white light, a 16-hour photoperiod, with temperatures of 20 °C during the light and 18 °C in the dark and plants were watered as required.

After seven weeks, half of the pots were treated with 10 mL of 100 mg/kg soil of cyanide (in the form of potassium cyanide), or water and let to grow for another 7 days. The 8 week-old plants were washed free of soils, dried at 60 °C and the dried shoots and roots biomasses recorded. Palladium content was analysed using ICP-MS at the Green Chemistry Centre of Excellence, University of York.

### **3.2.2 Palladium uptake in field applicable plant species**

#### **3.2.2.1 Development of synthetic ore materials**

Synthetic ore material (SOM) was prepared and used for the mustard, willow and miscanthus phytoextraction experiments. The SOM consists of gravel and kaolinite (1:1 w/w) taken from Imery's mining site in Cornwall, UK. Prior to this study, the metal profiles of the gravel and kaolinite were determined using ICP-MS at the Green Chemistry Centre of Excellence, University of York and are shown in Table A1. The SOM did not contain traces of palladium.

To dose the SOM with known concentrations of palladium, a 20 times concentrated palladium-synthetic ore material (Pd-SOM) stock was prepared by solubilising palladium nitrate ( $\text{PdNO}_3$ ) with nitric acid and mixing it with the gravel-kaolinite mixture in a 1:1 ratio. The concentrated Pd-SOM stock was used to prepare the final concentration of palladium by mixing with gravel and kaolinite into a final volume of 1.5 kg. As the concentrated Pd-SOM may cause the media to become acidic, calcium carbonate was also added to neutralise the SOM to pH 7. The final calculated amount of SOM for each pot was 1.5 kg dry weight.

#### **3.2.2.2 Mine waste materials**

To measure the uptake and tolerance of plants in the presence of metals other than palladium, the plants were grown on mine waste materials from the North American Palladium Company and kindly provided by Dr. John Meech at the NBK Institute of Mining, University of Washington, US. The mineral composition of the mine waste materials as well as the elemental profiles are shown in Tables S4, S5 and S6.

#### **3.2.2.3 Mustard**

Plastic P2 trays were used to grow *Brassicca alba* L. (mustard), cultivar Rivona seedlings. 4.2 grams of mustard seedlings were sown onto 1 kg (dry weight) of SOM or mine waste material. The trays were placed in a glasshouse and watered as required.

#### **3.2.2.4 Willow and miscanthus**

Willow rods (Yorkshire Willow Ltd, UK) and miscanthus rhizomes were first rooted in agricultural sand for four weeks. The rooted, in-leaf plants were transferred to 2 L pots containing 1.5 kg of SOM or mining waste materials. General-purpose fertilisers were added weekly according to the manufacturer's instructions. The plants were grown in a glasshouse at the Walled Garden, University of York. The conditions of the glasshouse were set to 20 °C day and 16 °C overnight. Supplemental lighting was provided between 8 am to 12 pm at 55w/m<sup>2</sup>.

After four weeks of growth, the plants were dosed with 150 mL of KCN containing a final concentration of 100 mg cyanide/kg. The plants were left to grow for another 7 days then harvested and dried overnight at 60 °C. The dried biomasses of leaf, stems and roots were measured.

#### **3.2.3 Sample preparation for ICP-MS analysis**

To powder the dried plant materials, metal ball bearings were used by shaking at highest speed for 2 days in an end-over-end mixer. Approximately 0.5 g of the homogenised powder was digested using 5 mL of aqua regia (mixture of 3 parts of concentrated hydrochloric acid and 1 part of concentrated nitric acid) in a glass vial. The samples were heated for 2 hours at 70 °C and then cooled, diluted with 50 mL ultrapure water and filtered using 0.45 µm filters (Millipore Ltd). Metal content was determined using ICP-MS on an Agilent 7700x at the Green Chemistry Centre of Excellence.

### **3.2.4 Testing catalytic activity of the plant derived palladium nanoparticles**

To produce the palladium catalyst, dried plant material was pyrolysed using a Barnstead Thermolyte 6000 Furnace under  $N_2$  ( $1\text{ K m}^{-1}$ ) at 573 K (300 °C) as described by Parker et al (2014) [22]. For the reaction of iodobenzene with methyl acrylate, typical reaction conditions used were: Into a 25 mL round bottom flask the following reagents were measured; iodobenzene (5.00 mmol), methyl acrylate (6.25 mmol), and triethylamine (6.25 mmol) in 1.75 mL of N-methyl-2-pyrrolidone. Once the flask had been heated to the required temperature, 10 mg of palladium catalyst were added. For control experiments no catalyst was added. A reaction with 10 mg of plant material containing no palladium was used as a control. The reaction was allowed to proceed for 2 hours at 393 K and was monitored by GC-FID using diethyl succinate as a standard. After 2 hours the reaction was allowed to cool. The cooled reaction mixture was filtered to remove the catalyst. These experiments were performed by personnel in the Green Chemistry Centre of Excellence.

### **3.2.5 Transmission electron microscopy**

Leaf tissue taken was fixed in 2.5 % (v/v) glutaraldehyde, 4 % (v/v) formaldehyde in 50 mM phosphate buffer pH 7.2 for 3.5 hours. The samples were embedded and sectioned by Meg Stark in the Technology Facility, Department of Biology. To dehydrate the samples, they were treated with a 25-100 % acetone series then infiltrated with Spurr's resin (Agar Scientific) (25, 50 and 75 %) with overnight polymerisation at 343 K. Sections were mounted onto 400 mesh thin-bar Athene grids, and viewed both prior to staining and once stained with saturated uranyl acetate and Reynolds lead citrate using a Technai 12 Bio Twin TEM operating at 120 kV.

### 3.3 Results

#### 3.3.1 Palladium uptake in Arabidopsis

##### 3.3.1.1 Effect of palladium on Arabidopsis growth

The effect of palladium on Arabidopsis germination and seedling growth was investigated using agar plates. At all palladium concentrations tested (ranging from 0 to 30  $\mu\text{M}$ ), 100 % of the seeds germinated. The results in Figure 3.7 showed that with increasing concentration of palladium in the media, the seedling root lengths significantly decreased (ANOVA Tukey's test  $p < 0.001$ ). As shown in Figure 3.8, the roots of 12-day-old seedlings grown on 5, 10, 20 and 30 mM palladium were 4-, 4-, 10- and 13- fold shorter respectively, than the roots of seedlings grown on palladium-free medium (ANOVA Tukey's test  $p < 0.001$ ). It was also observed that increased palladium concentration had significantly decreased the total fresh weight of Arabidopsis plants at 12 days of growth, as compared to the palladium-free plants (ANOVA Tukey's test  $p < 0.001$ ) (Figure 3.9). Root length and total fresh weight analyses showed that Arabidopsis growth was inhibited at the lowest concentration of palladium tested, 5  $\mu\text{M}$  (Figure 3.8, 3.9 & 3.10).

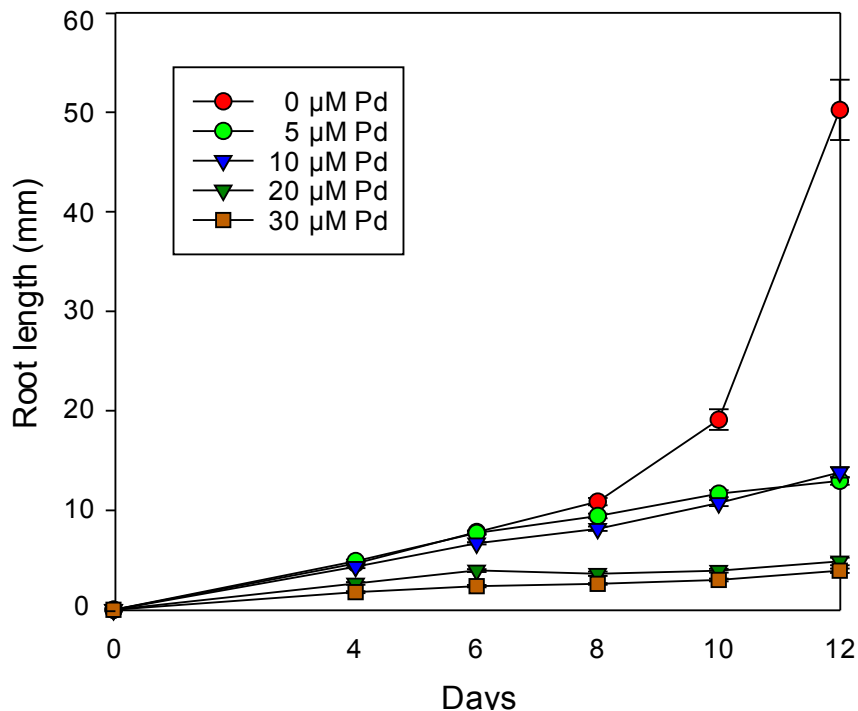


**Figure 3.7:** Germination studies of Arabidopsis seedlings on  $\frac{1}{2}$  MS (A) with different concentration of palladium for twelve days. Results are the mean from 30 biological replicates  $\pm$  SEM.

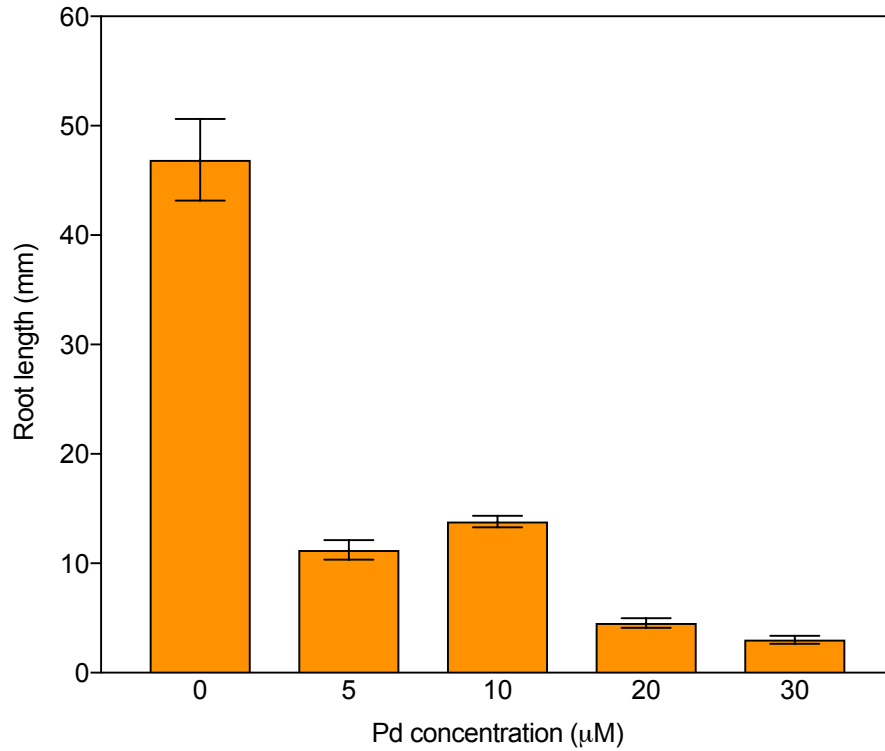


**Figure 3.8:** Root lengths of 12 day-old Arabidopsis Col-0 wildtype seedlings on 1/2 MS (A) media containing increasing palladium concentrations. Results are the mean from 30 biological replicates  $\pm$  SEM. ANOVA Tukey's test.

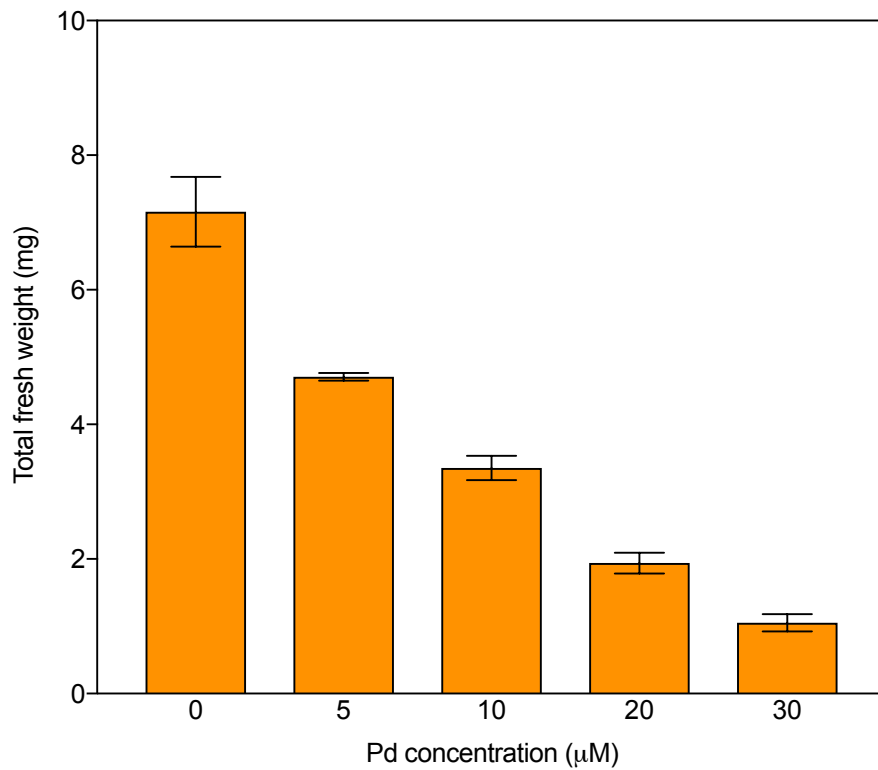


**Figure 3.9:** Total fresh weight of 12 day-old Arabidopsis Col-0 wildtype seedlings on 1/2 MS (A) media containing increasing palladium concentrations. Results are the mean from 30 biological replicates  $\pm$  SEM. ANOVA Tukey's test.

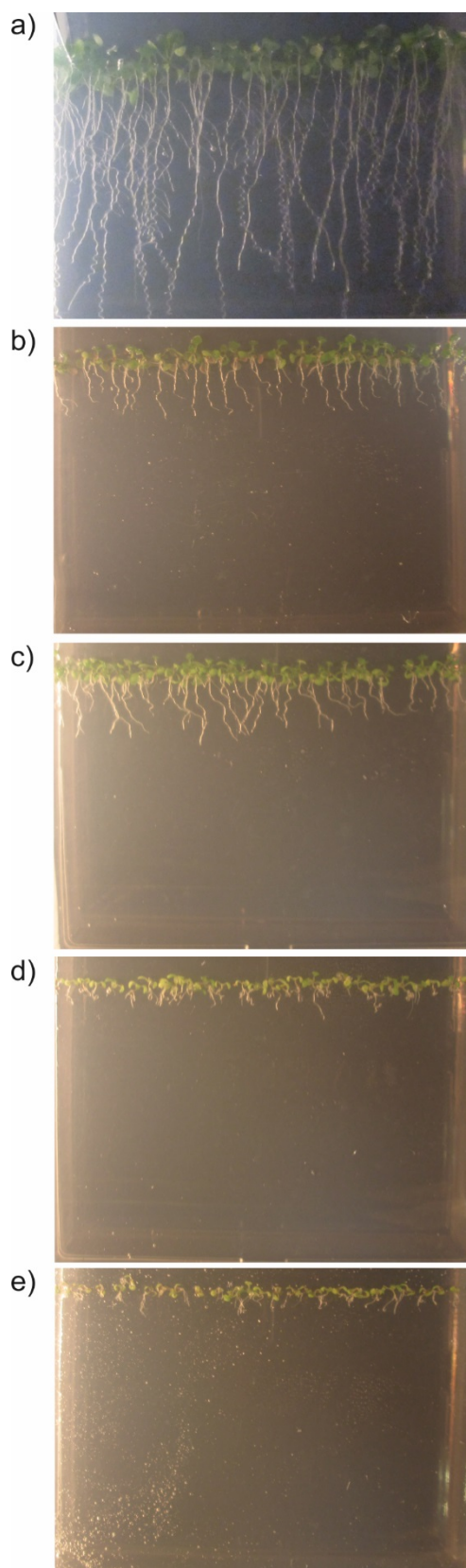


**Figure 3.10:** Appearance of 12 day-old Arabidopsis Col-0 wildtype seedlings on  $\frac{1}{2}$  MS (A) with various concentrations of palladium a) 0  $\mu$ M b) 5  $\mu$ M c) 10  $\mu$ M d) 20  $\mu$ M e) 30  $\mu$ M.

### 3.3.1.2 Growth and palladium uptake studies on Arabidopsis

Previous work published in the Bruce group has revealed that the concentration of palladium accumulated in Arabidopsis should be in the range of 12 – 18 g/kg dry plant for it to make a catalyst with properties comparable to those of a commercially available catalyst [22]. That figure was based on results from experiments conducted in a liquid-based setup; the next step was to investigate the uptake of palladium in Arabidopsis grown in soil containing palladium. To enhance the uptake of palladium, a solubilising treatment of potassium cyanide was applied to half of the plants. As shown in Figure 3.11, the shoot biomass of the non-cyanide treated plants decreased as the concentration of palladium increased to 10 mg/kg (ANOVA Tukey's test  $p < 0.001$ ). No significant difference was found between the biomass of the shoot materials of the cyanide and non-cyanide treated plants except for plants grown on 10 mg/kg of palladium (Student's T-test  $p < 0.001$ ). In Figure 3.12, there was also no difference between the cyanide and non-cyanide treated biomasses of the root material in all palladium concentrations tested, with the exception of the root material for the cyanide and non-cyanide treated plants grown on palladium-free soil and soil containing 5 and 10 mg/kg of palladium.

Subsequent ICP-MS analysis of the shoots and roots revealed that the addition of cyanide increased palladium accumulation in the shoot material by approximately 4-fold as compared to non cyanide treatment (Student's T-test  $p < 0.001$ ) (Figure 3.13 & 3.14). The highest shoot palladium concentration was observed from the plants grown in soil containing the highest concentration of palladium (50 mg/kg) (ANOVA Tukey's test  $p < 0.001$ ). The highest fold uptake was observed within the roots of cyanide treated plants grown in soil containing 10 mg/kg of palladium: an 18- fold increase compared to the roots of the non-cyanide treated plants grown on the same concentration of palladium (ANOVA Tukey's test  $p < 0.001$ ).

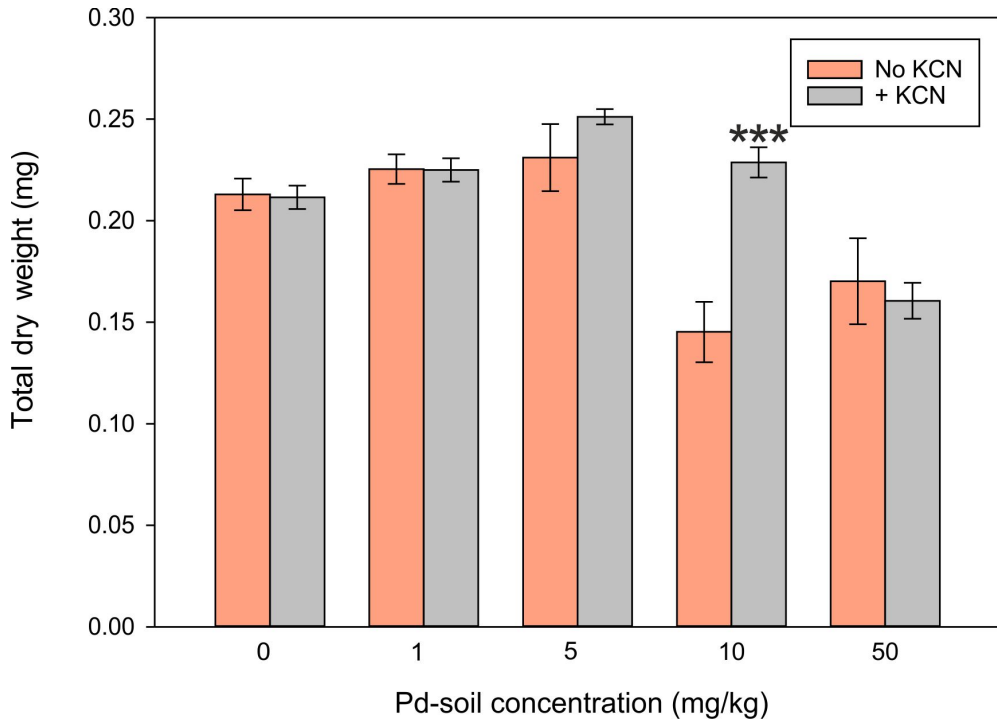


**Figure 3.11:** Total dry weight of shoots of Arabidopsis Col-0 wildtype plants grown in soil containing different concentrations of palladium. Results are the mean from 3 biological replicates  $\pm$  SEM. Student's T-test \*\*\* =  $p < 0.001$  significantly different to non KCN treatment.

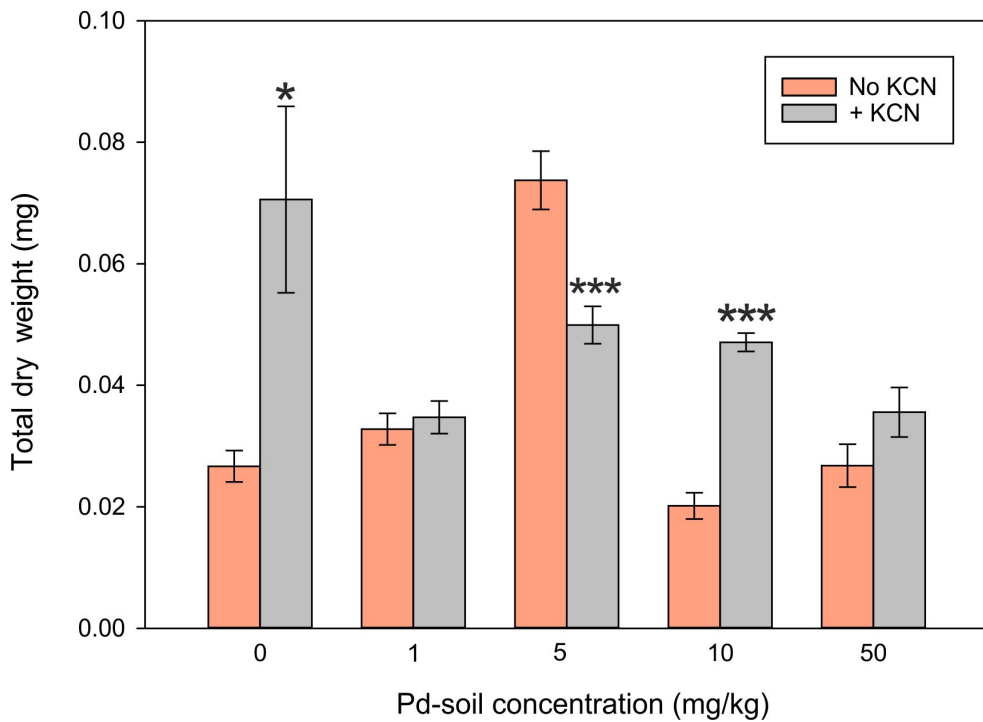


**Figure 3.12:** Total dry weight of roots of Arabidopsis Col-0 wildtype plants grown in soil containing different concentrations of palladium. Results are the mean from 3 biological replicates  $\pm$  SEM. Student's T-test \* =  $p < 0.05$ , \*\*\* =  $p < 0.001$  significantly different to non KCN treatment.

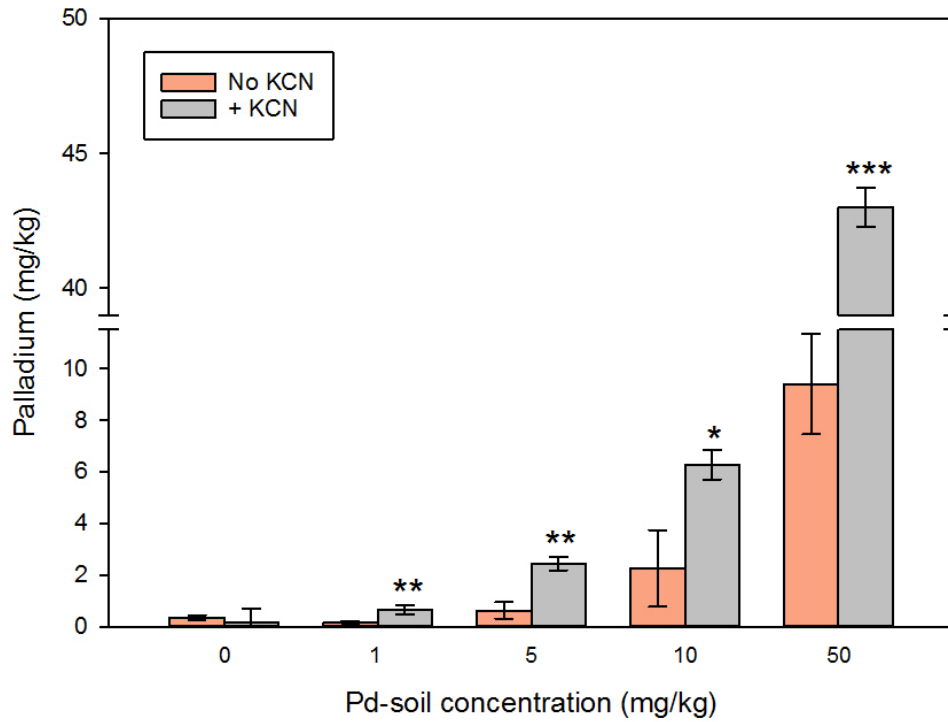


**Figure 3.13:** Palladium levels in shoots of Arabidopsis Col-0 wildtype plants grown in soil containing different concentrations of palladium. Results are the mean from 3 biological replicates  $\pm$  SEM. Student's T-test \*  $p < 0.05$ , \*\*  $p < 0.01$ , \*\*\*  $p < 0.001$  significantly different to non KCN treatment.

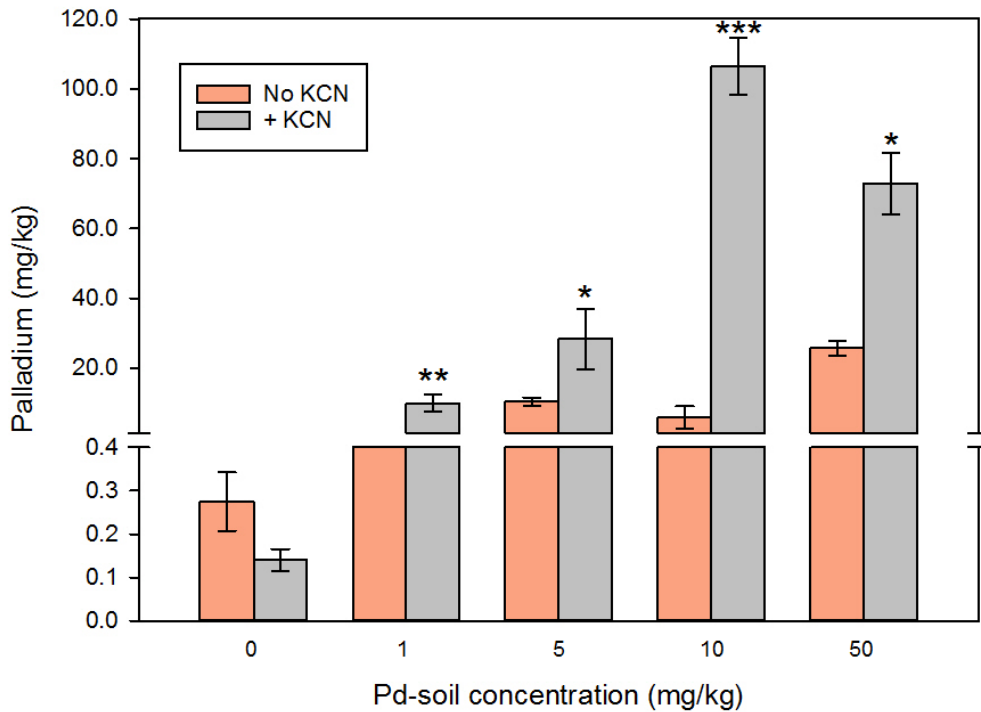


**Figure 3.14:** Palladium levels in roots of Arabidopsis Col-0 wildtype plants grown in soil containing different concentrations of palladium. Results are the mean from 3 biological replicates  $\pm$  SEM. Student's T-test \*  $p < 0.05$ , \*\*  $p < 0.01$ , \*\*\*  $p < 0.001$  significantly different to non KCN treatment.

### **3.3.2 Palladium uptake in mustard**

#### **3.3.2.1 Growth and uptake of palladium in mustard**

As discussed in Section 3.1.4, previous work done by Anderson et al [123] demonstrated that mustard was able to accumulate gold. To test the ability of mustard to take up palladium, a similar experiment to the one described above (Section 3.3.1) for *Arabidopsis* was conducted. Figure 3.16 show that when mustard was grown in SOM containing up to 50 mg/kg palladium, there was no significant effect on the plant growth or biomass in the absence of KCN as compared to cyanide treated plants (Student's T-test  $p > 0.05$ ). However, the biomass of plants grown on 100 mg/kg palladium was a third lower than in the absence of palladium (Figure 3.15). Although the application of cyanide did not significantly affect the subsequent biomasses (Student's T-test  $p > 0.05$ ) (Figure 3.16), it was found to significantly increase palladium levels by 26-, 20-, 30- and 23-fold in plants grown in SOM containing 5, 10, 50 and 100 mg/kg of palladium as compared to the non-cyanide treated plants, respectively (Student's T-test  $p < 0.001$ ) (Figure 3.17). The SOM used throughout this experiment also contained metals other than palladium such as zinc and copper (Table A1) that could be selectively released by the cyanide treatment. As shown in Figure 3.18, in the absence of cyanide, the levels of palladium taken up by the plant increased predominantly at the expense of copper, whereas in the presence of cyanide, levels of copper, which is also solubilised by cyanide, were less affected.

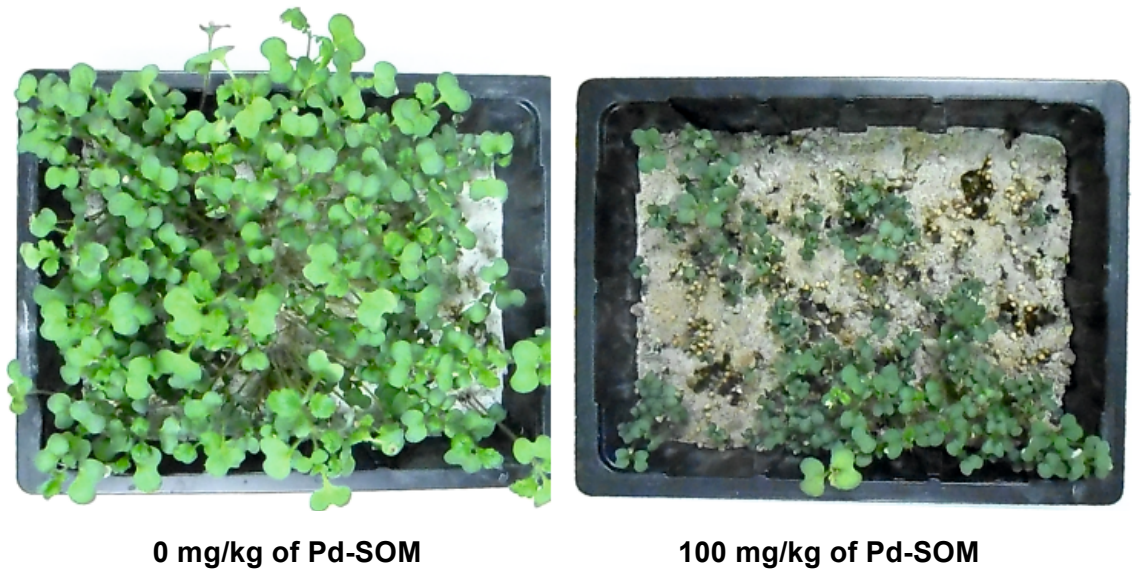


**Figure 3.15:** Appearance of 7-days-old mustard seedlings grown on SOM with and without palladium prior to cyanide treatment.

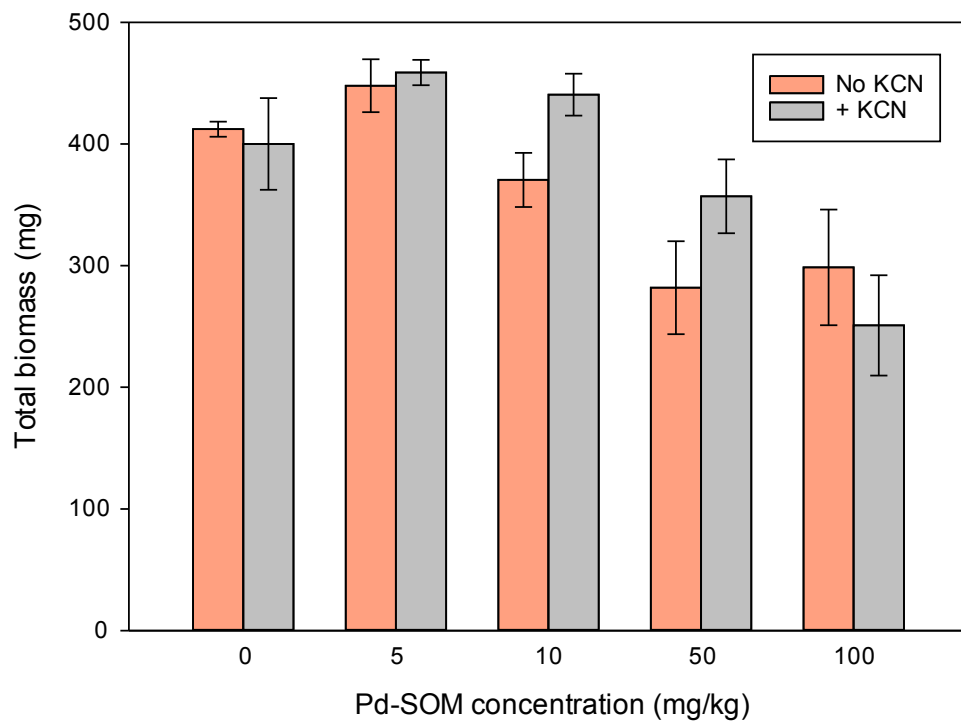


**Figure 3.16:** Total biomass of mustard grown on SOM containing different concentrations of palladium. Results are the mean from 6 biological replicates  $\pm$  SEM. Student's T-test between no KCN and KCN treatment.

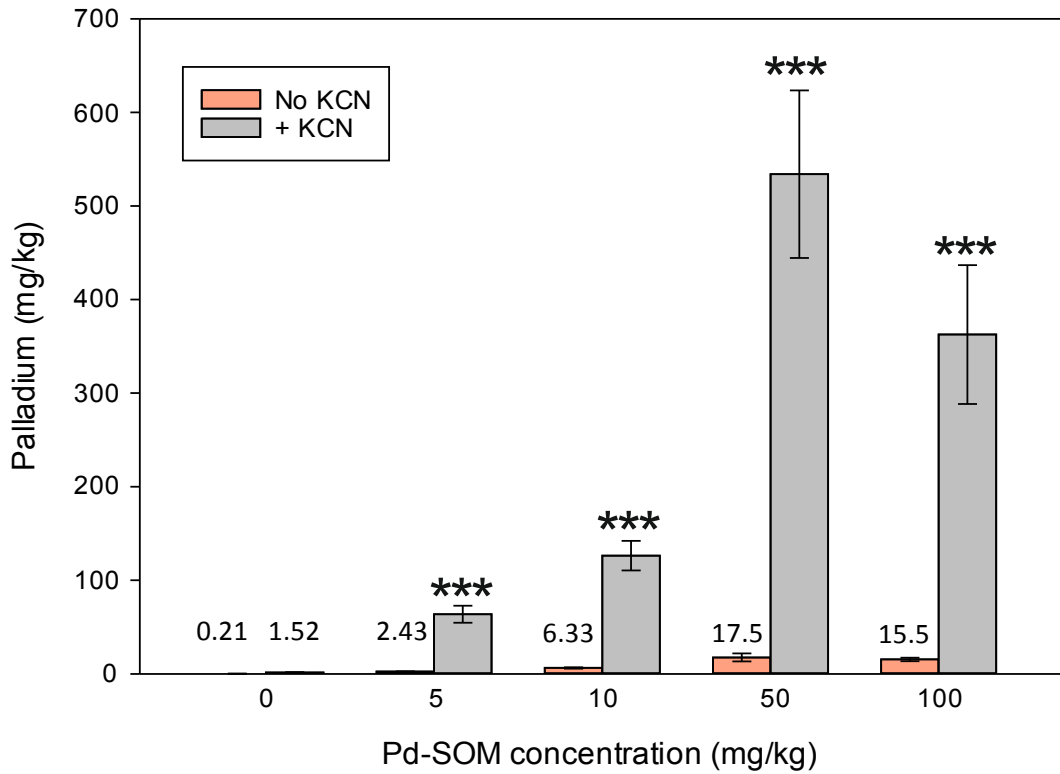


**Figure 3.17:** Palladium levels in aerial tissue of mustard grown on synthetic ore material containing different concentrations of palladium. Results are the mean from 6 biological replicates  $\pm$  SEM. Student's T-test \*\*\* =  $p < 0.001$  significantly different to non KCN treatment.

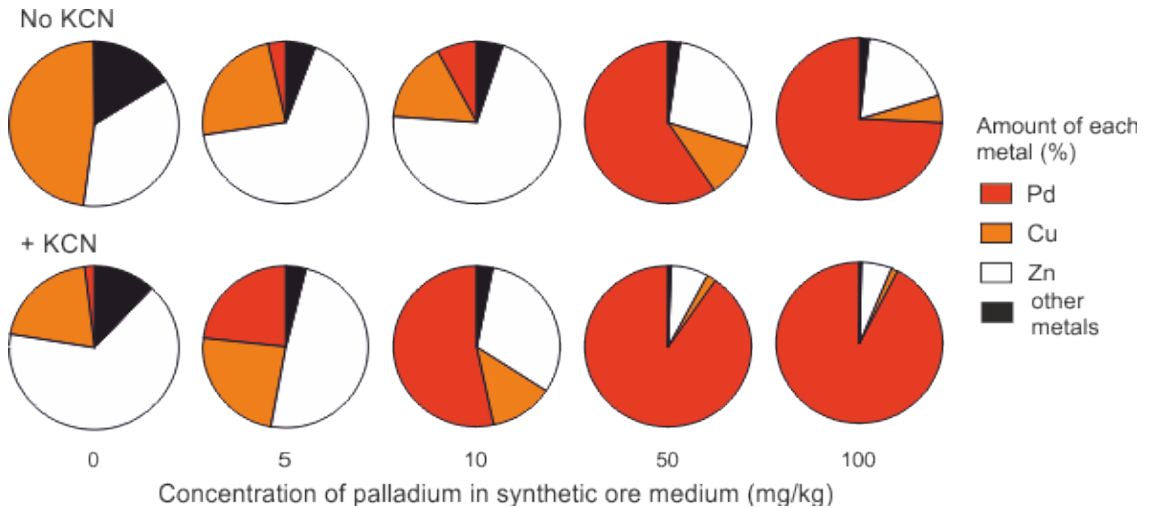


**Figure 3.18:** Pie charts showing relative percentages of metals found in aerial tissue of mustard germinated and grown on SOM dosed with a range of palladium concentrations.

### **3.3.2.2 Uptake of palladium by mustard grown on mine waste materials**

As PGM-rich materials may contain other elements which could inhibit plant growth, the uptake and growth capacity was further investigated on mine waste materials. The chemical composition analysis of the waste materials (Table A2) showed it contained approximately 20 mg/kg of palladium, a concentration below the phytotoxicity levels indicated by previous experiments (Figure 3.16). However, the waste materials did contain high levels of metals known to be phytotoxic, such as nickel. No inhibitory effect could be observed on plants grown on the mine waste materials (Figure 3.19 & 3.20). Based on the ICP-MS results, it was observed that the addition of cyanide significantly increased the uptake of palladium by 89-, 333- and 8.4- fold in plants grown in waste materials containing 5, 10 and 20 mg/kg palladium, respectively as compared to non cyanide treatment (Student's T-test  $p < 0.001$ ) (Figure 3.21).



**0 mg/kg Pd-SOM      Mine waste materials (20 mg/kg of Pd)**

**Figure 3.19:** Appearance of 7-days-old mustard seedlings growing in mine waste materials containing 20 mg/kg of palladium prior to cyanide treatment.

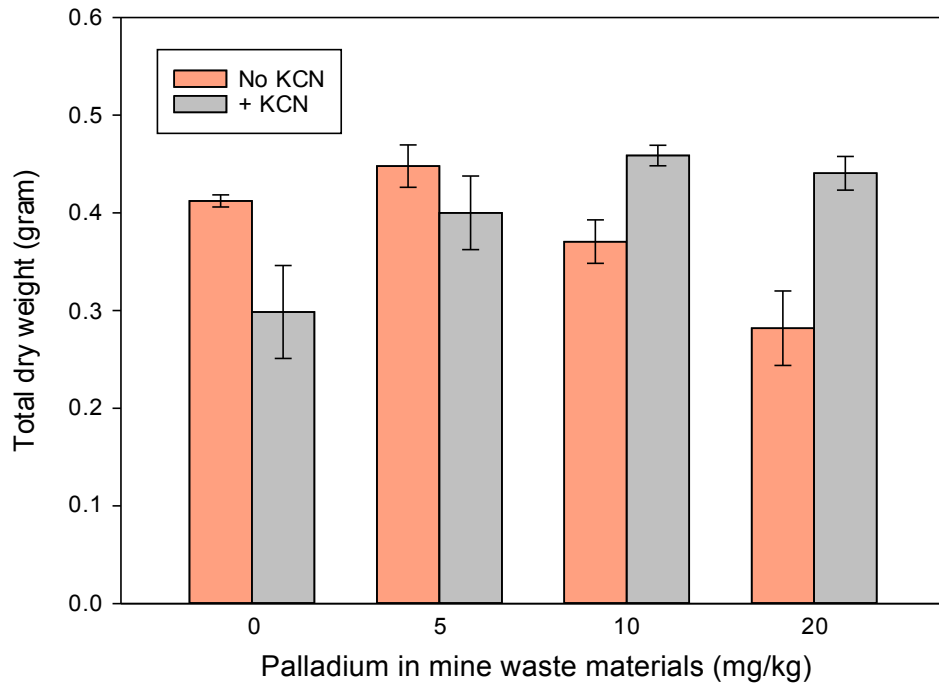


**Figure 3.20:** Biomass of aerial tissue of mustard seedlings germinated on mine waste materials. Results are the mean from 6 biological replicates  $\pm$  SEM. Student's T-test between no KCN and KCN treatment.

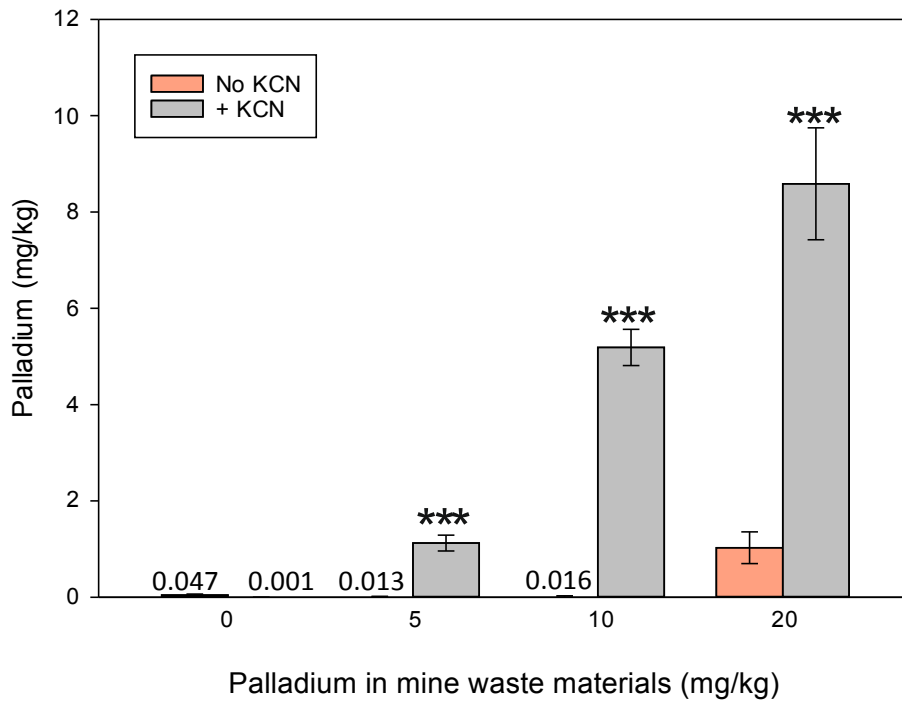


**Figure 3.21:** Palladium levels in the aerial tissue of mustard germinated on mine waste materials. Results are the mean from 6 biological replicates  $\pm$  SEM. Student's T-test \*\*\* =  $p < 0.001$  significantly different to non KCN treatment.

### 3.3.3 Palladium uptake in willow

#### 3.3.3.1 Growth and uptake of palladium by willow

For the willow experiments, a fast-growing, bioenergy hybrid of *S. viminalis*, (Super Willow) was chosen. Rooted Super Willow plants were grown in SOM containing a range of palladium concentrations over a period of four weeks (3.22 to 3.23). After this time, half the plants were treated with cyanide and all plants harvested one week later (Figure 3.24). As shown in Figure 3.25, cyanide treatment did not significantly affect the leaf biomass at the lower concentrations of palladium tested (5 and 10 mg/kg) (Student's T-test  $p > 0.05$ ) as compared to non cyanide treatment except for plants grown on higher concentrations of palladium (50 and 100 mg/kg) (Student's T-test  $p < 0.05$ ). It was also observed that palladium accumulated to significantly higher levels in the leaf material of the cyanide treated plants when compared to the non-treated plants at all concentrations of palladium tested (ANOVA  $p < 0.001$ ) (Figure 3.26). Palladium accumulation in the leaf tissue was increased following cyanide treatment by 126-, 127-, 19- and 23- fold in plants grown on SOM containing 5, 10, 50 and 100 mg/kg palladium, respectively (Figure 3.26).

For the stem material, it was observed that the cyanide treatment did not affect the biomass (Figure 3.27); however, as observed previously with the leaf material, palladium levels were significantly higher in the stems of the cyanide treated plants compared to the non-cyanide treated plants (Student's T-test  $p < 0.05$ ) (Figure 3.28). Palladium uptake in stem tissue was 49-, 114-, 3- and 2- fold higher in stems from cyanide dosed plants than undosed plants grown on SOM containing 5, 10, 50 and 100 mg/kg palladium, respectively (Figure 3.28).

It was also seen that, under cyanide treatment, the accumulation of palladium in the leaf material was significantly higher than in the stem of plants grown in the lowest concentration of palladium (5 mg/kg) (Student's T-test  $p < 0.001$ ) (Figure 3.29).



**Figure 3.22:** Appearance of Super Willow plants prior to transfer to SOM. Super Willow rods were rooted and grown in agricultural sand in Root Trainers for 8-12 weeks.



**Figure 3.23:** Super Willow grown in individual containers containing SOM with various palladium concentrations. The white pots prevented loss of palladium by leaching. The plants were grown for four weeks before dosing with potassium cyanide.

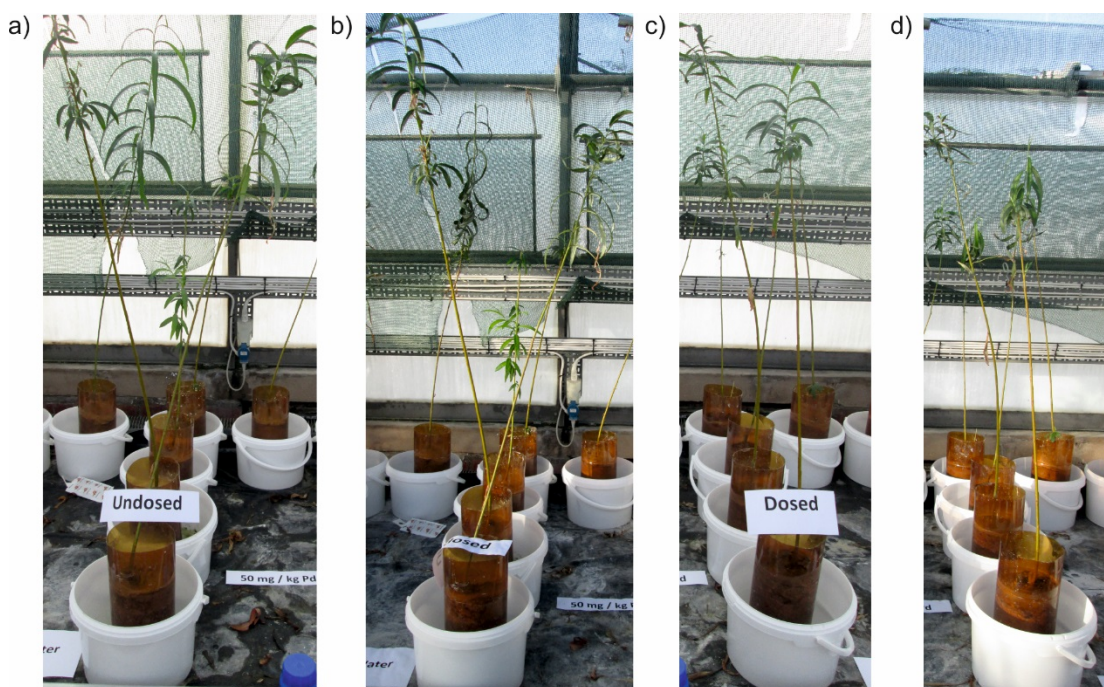


**Figure 3.24:** Super Willow grown on SOM containing 50 mg/kg of palladium before and after seven days of dosing with 100 mg/kg cyanide. a) Undosed Super Willow at day one b) Undosed Super Willow at day seven c) Dosed Super Willow at day one d) Dosed Super Willow at day seven.

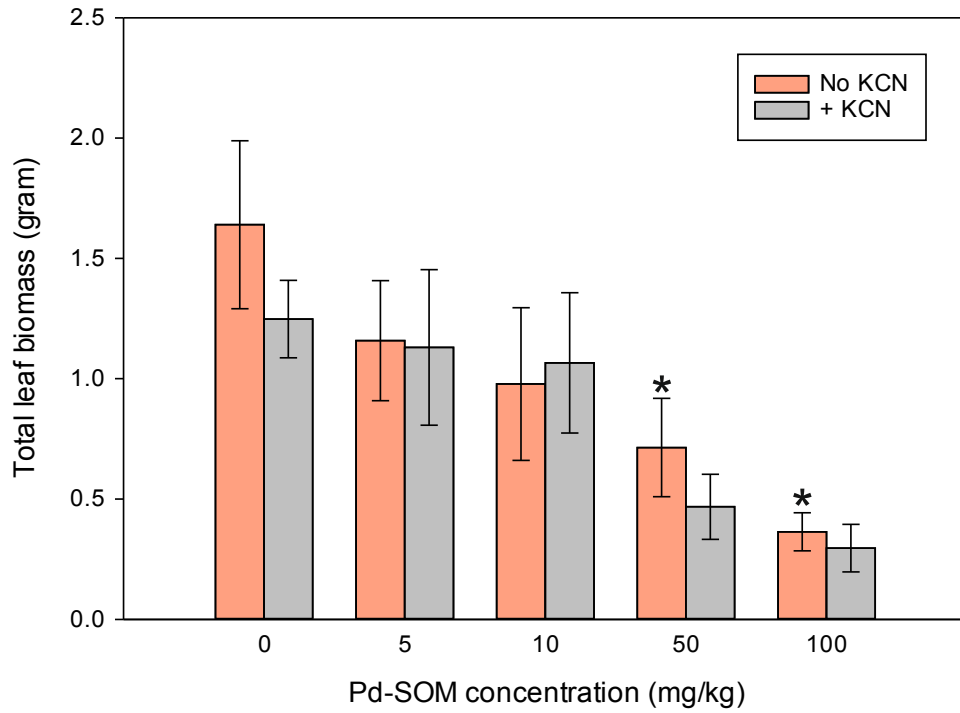


**Figure 3.25:** Total leaf dry biomass of Super Willow grown on SOM containing palladium. Results are the mean from 5 biological replicates  $\pm$  SEM. Student's T-test \* =  $p < 0.05$  significantly different to non KCN treatment.

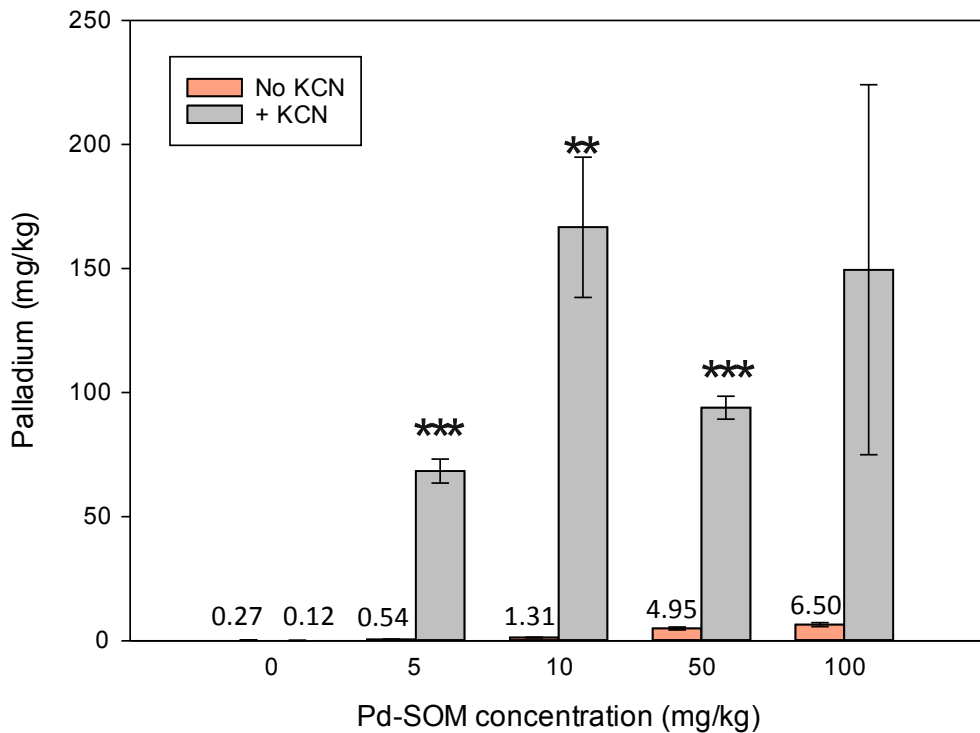


**Figure 3.26:** Palladium levels in the leaf tissues of Super Willow grown on SOM containing palladium. Results are the mean from 5 biological replicates  $\pm$  SEM. Student's T-test \*\* =  $p < 0.01$ , \*\*\* =  $p < 0.001$  significantly different to non KCN treatment.

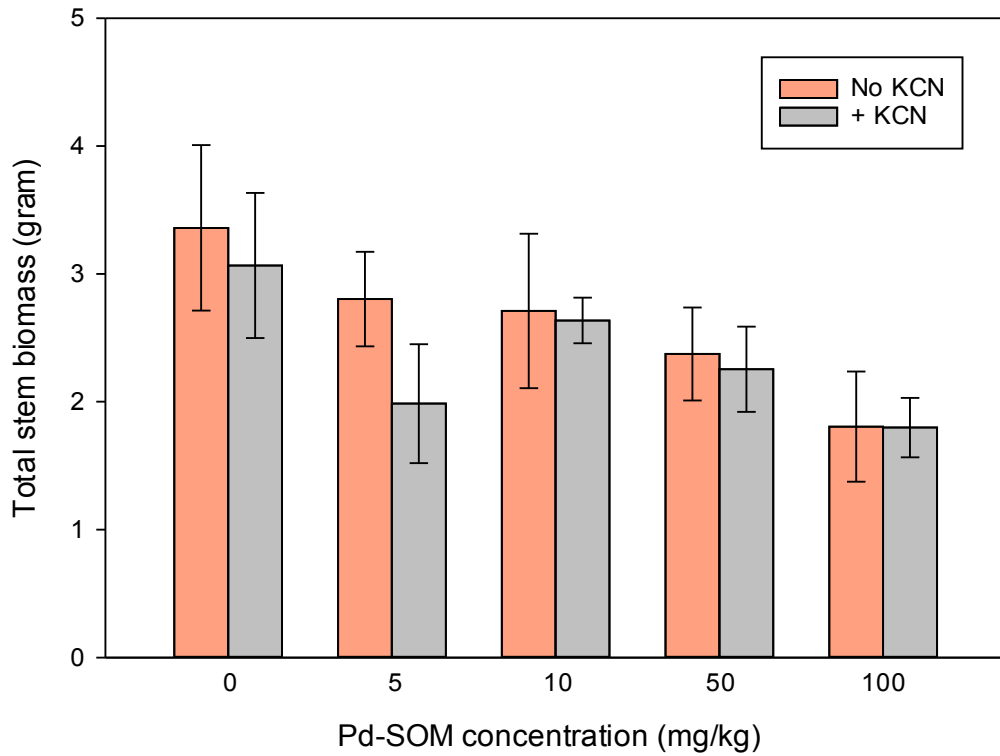


**Figure 3.27:** Total stem dry biomass of Super Willow grown on SOM containing palladium. Results are the mean from 5 biological replicates  $\pm$  SEM. Student's T-test between no KCN and KCN treatment.

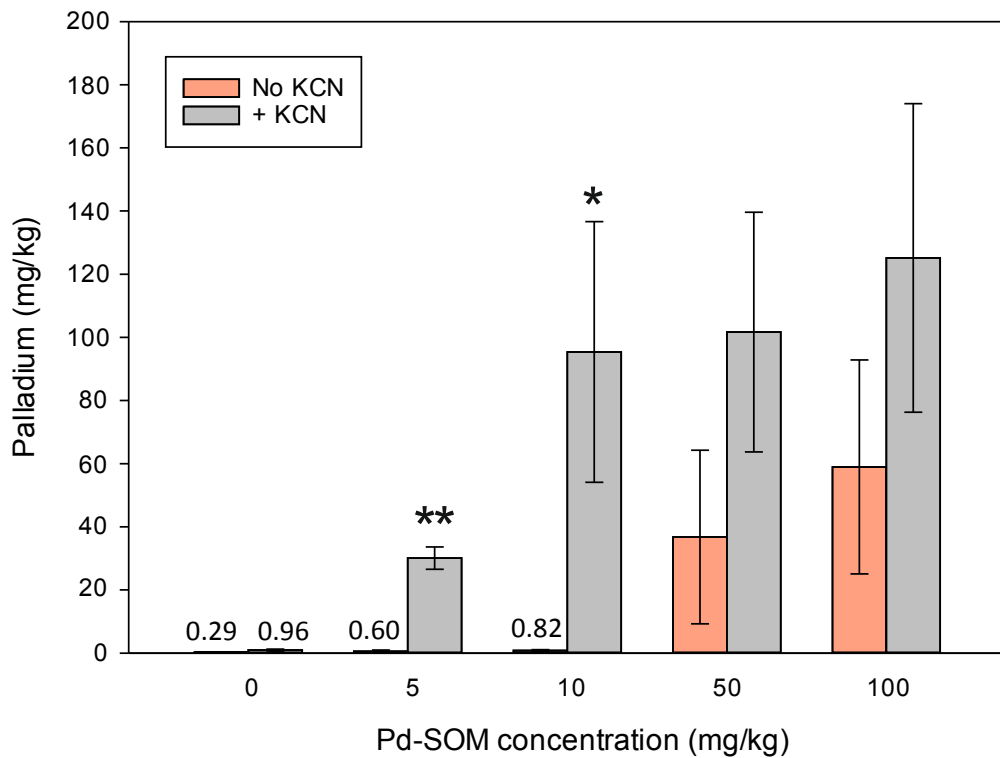


**Figure 3.28:** Palladium levels in the stem tissues of Super Willow grown on SOM containing palladium. Results are the mean from 5 biological replicates  $\pm$  SEM. Student's T-test \* =  $p < 0.05$ , \*\* =  $p < 0.01$  significantly different to non KCN treatment.

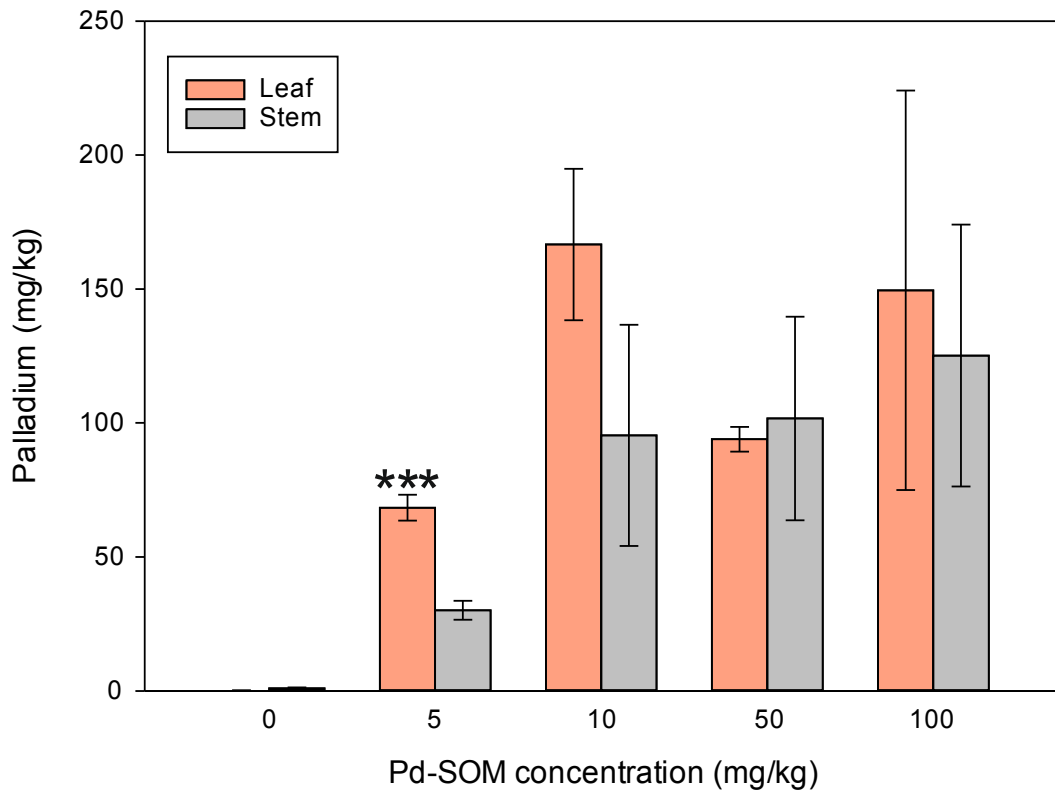


**Figure 3.29:** Palladium levels in the leaf and stem tissues of Super Willow grown on SOM containing different concentration of palladium and dosed with cyanide. Results are the mean from 5 biological replicates  $\pm$  SEM. Student's T-test \*\*\* =  $p < 0.001$  significantly different to stem tissues.

### **3.3.3.2 Growth of willow on mine waste materials**

To assess the uptake of palladium in the presence of other metals found in mine waste materials, Super Willow was grown on mine waste materials. Four-week-old plants grown on mine waste materials containing 20 mg/kg palladium were dosed with 100 mg/kg of cyanide then shoot and root materials were harvested seven days later. As observed in previous experiments on mustard (Section 3.3.2), the addition of cyanide did not affect the leaf or stem biomass of Super Willow (Figure 3.30) but increased the levels of palladium in the leaf and stem tissue by 65- and 45- fold, respectively (Figure 3.31). Cyanide treatment also increased the uptake of other metals present in the mine waste materials such as cobalt, nickel, cadmium, lead and copper into the leaf and stem tissues of the plants (Figure 3.32 & 3.33 and Table A3).

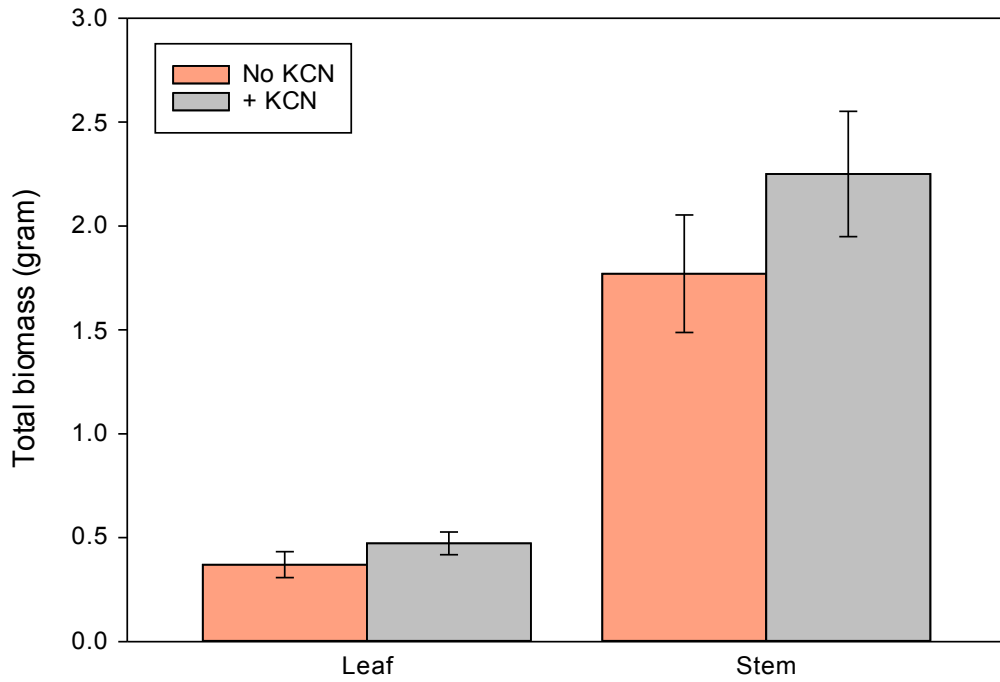


**Figure 3.30:** Total dry biomass of leaf and stem of Super Willow grown on mine waste materials containing 20 mg/kg palladium. Results are the mean from 5 biological replicates  $\pm$  SEM. Student's T-test between no KCN and KCN treatment.

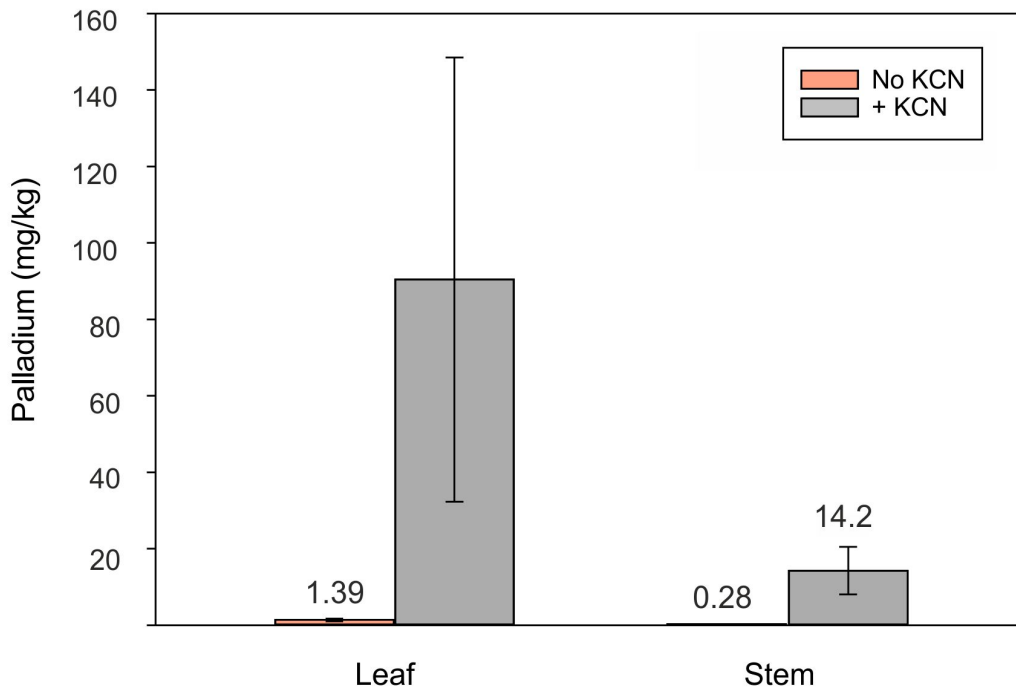


**Figure 3.31:** Palladium levels in the leaf and stem tissues of Super Willow grown on mine waste materials containing 20 mg/kg palladium. Results are the mean from 5 biological replicates  $\pm$  SEM. Student's T-test between no KCN and KCN treatment.

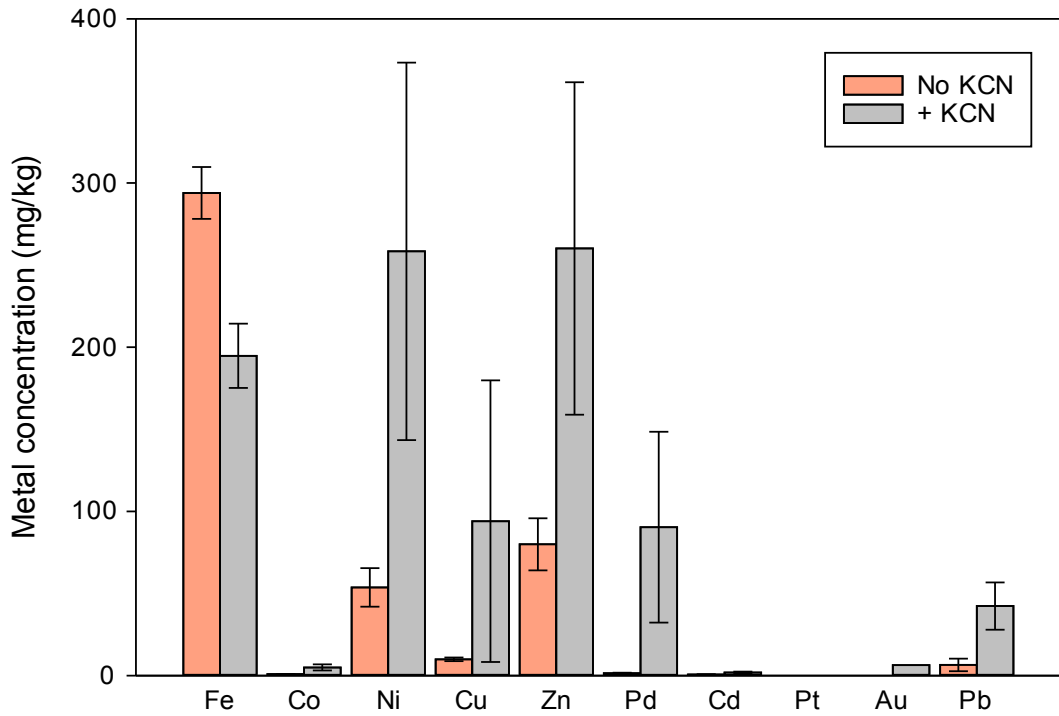


**Figure 3.32:** Levels of metals in Super Willow leaf tissues from plants grown on mine waste materials containing 20 mg/kg of palladium. Results are the mean from 5 biological replicates  $\pm$  SEM. Student's T-test between no KCN and KCN treatment.

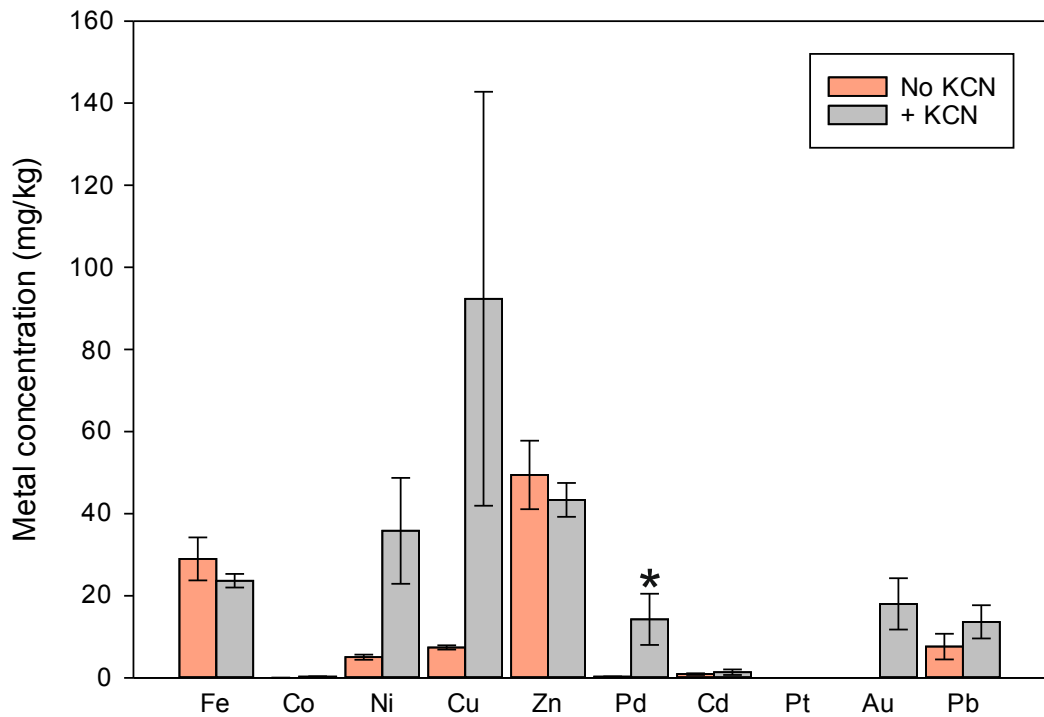


**Figure 3.33:** Levels of metals in Super Willow stem tissues from plants grown on mine waste materials containing 20 mg/kg of palladium. Results are the mean from 5 biological replicates  $\pm$  SEM. Student's T-test \* =  $p < 0.05$  significantly different to non KCN treatment.

### 3.3.3.3 Growth and uptake of palladium by different willow species

Metal uptake capacity varies between species of willow [188]. To test the variability in palladium uptake, 15 different species and cultivars of willow were grown in SOM containing 50 mg/kg palladium and uptake induced with cyanide. Figure 3.34 shows that across all species and cultivars of willow tested, there were 11.5- and 4.7- fold variations in the leaf and stem biomass, respectively. It was found that *S. alba*, *S. candida* and *S. purpurea* (Green Dicks) had consistently high levels of leaf and stem biomass (Figure 3.34). Measuring the content of palladium, revealed that there were 6.7- and 4.5- fold variations, respectively, in the content of palladium in the leaf and stem, with 6- fold more palladium present in the leaves than in the stems (Figure 3.35). The willow cultivar Green Dicks contained significantly higher levels of palladium in the leaves (ANOVA Tukey's test  $p < 0.001$ ) (820 mg/kg) and produced high amounts of leaf and stem biomass (1.23 and 11.8 g) compared to the other species. *S. nigricans* also exhibited a high palladium content in both leaf and stem tissues (525 and 98 mg/kg) but produced lower amounts of total leaf and stem biomass (0.38 and 5.48 g) as compared to Green Dicks. For Super Willow, the concentration of palladium was found to be higher (313 mg/kg) than the previous experiment (Figure 3.26) conducted (94 mg/kg). The difference between the amount of palladium accumulated in the leaf tissue of Super Willow (313 mg/kg) compared to the previous experiment described in Section 3.3.3.1 (94 mg/kg) could be caused by different environmental conditions in the glasshouse during the experiments; warmer, sunnier conditions would increase transpiration rates and could lead to enhanced palladium uptake [189].

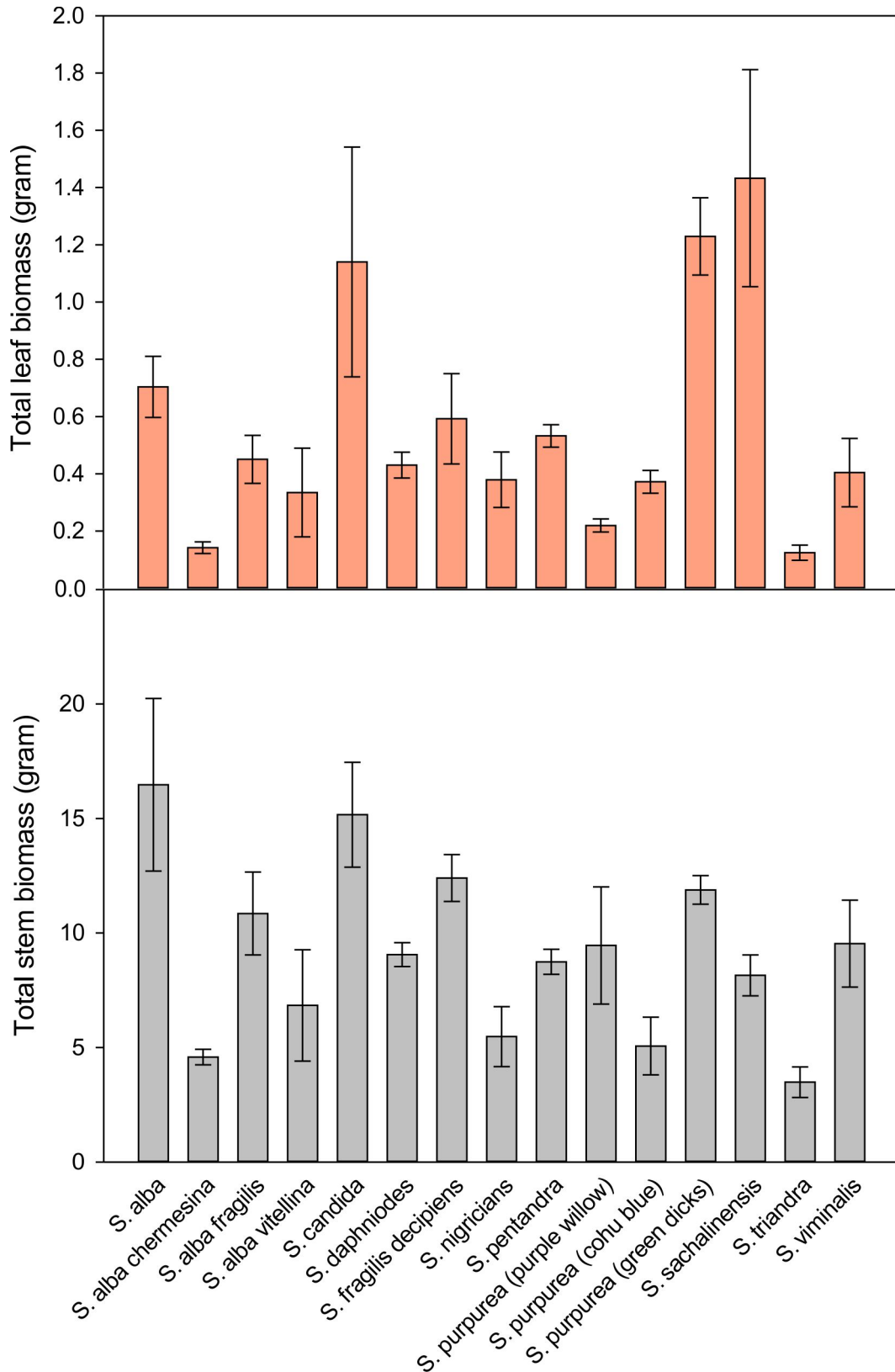


**Figure 3.34:** Total dry weight of leaf (upper bars) and stem (lower bars) tissues from different willow (*Salix* spp) grown on SOM dosed with 50 mg/kg palladium and 100 mg/kg of cyanide. Results are the mean from 5 biological replicates  $\pm$  SEM except for *S. alba*, *S. chermesina* and *S. alba vitellina*) which are mean from 3 biological replicates  $\pm$  SEM. ANOVA Tukey's test.

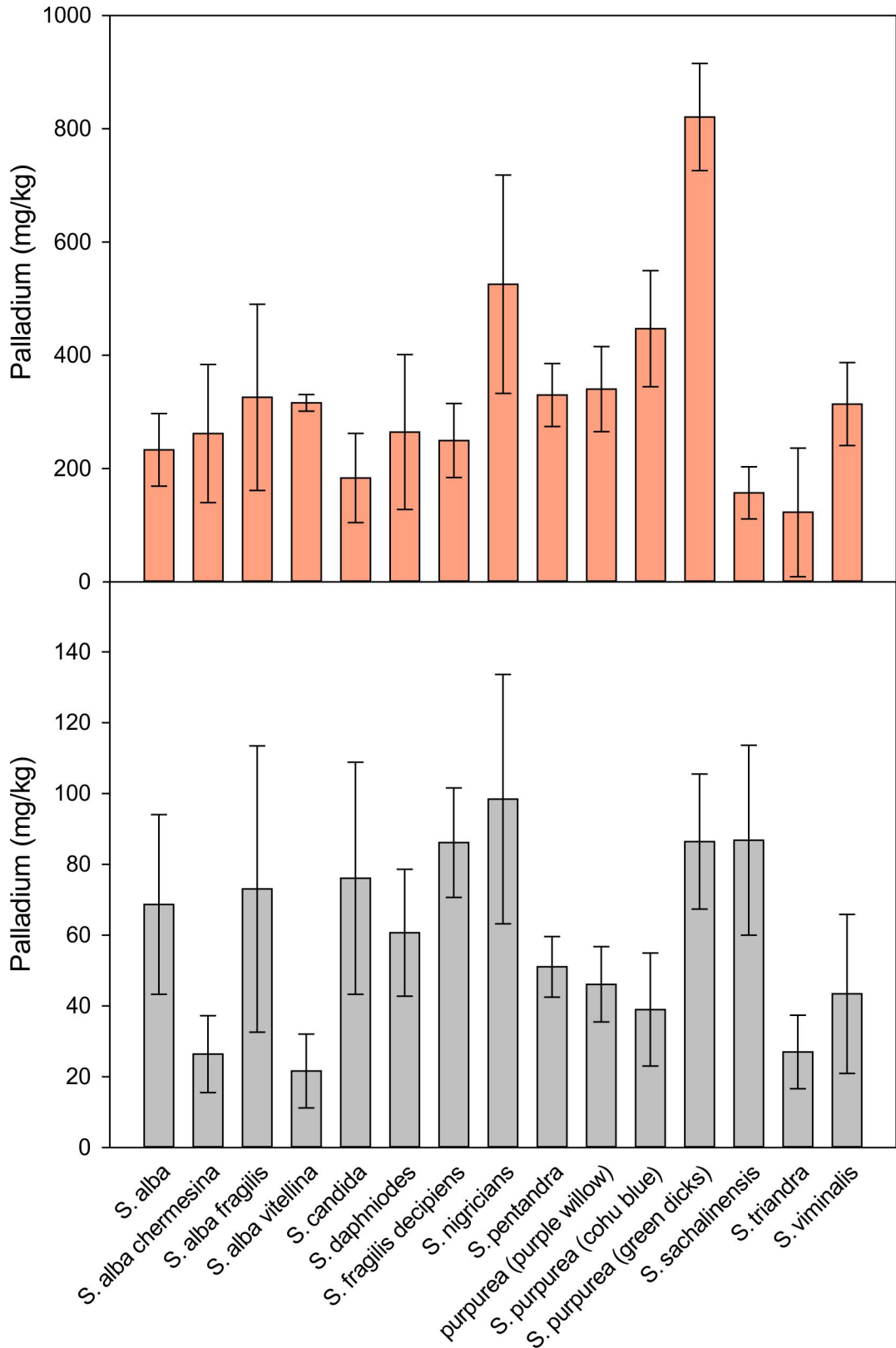


**Figure 3.35:** Palladium levels in the leaf (upper bars) and stem (lower bars) tissues of different willow (*Salix* spp) species grown on SOM dosed with 50 mg/kg palladium and 100 mg/kg of cyanide. Results are from the mean of 5 biological replicates  $\pm$  SEM except for *S. alba*, *S. chermesina* and *S. alba vitellina* which are mean from 3 biological replicates  $\pm$  SEM. ANOVA Tukey's test.

#### **3.3.3.4 Transmission electron microscopy**

To determine if palladium nanoparticles were present in willow grown on SOM containing palladium, the leaf material of willows containing the highest amounts of palladium (Super Willow and Green Dicks grown on SOM containing 50 mg/kg of palladium and treated with 100 mg/kg of cyanide) were fixed, sectioned and analysed using TEM. As a control, a non-cyanide treated sample was also examined using TEM. As previously demonstrated in Section 3.3.3.2, cyanide treatment did not significantly inhibit the growth of Super Willow and Green Dicks when grown on SOM with 50 mg/kg of palladium based on the total biomass of leaf and stem tissues as observed in Figure 3.36.

Small black spots were present in the leaf tissue in both willow species (Figure 3.37). To determine whether these spots were palladium nanoparticles, the samples were sent for microanalysis using Energy-dispersive X-ray spectroscopy (EDX) in the York JEOL nanocentre, University of York.

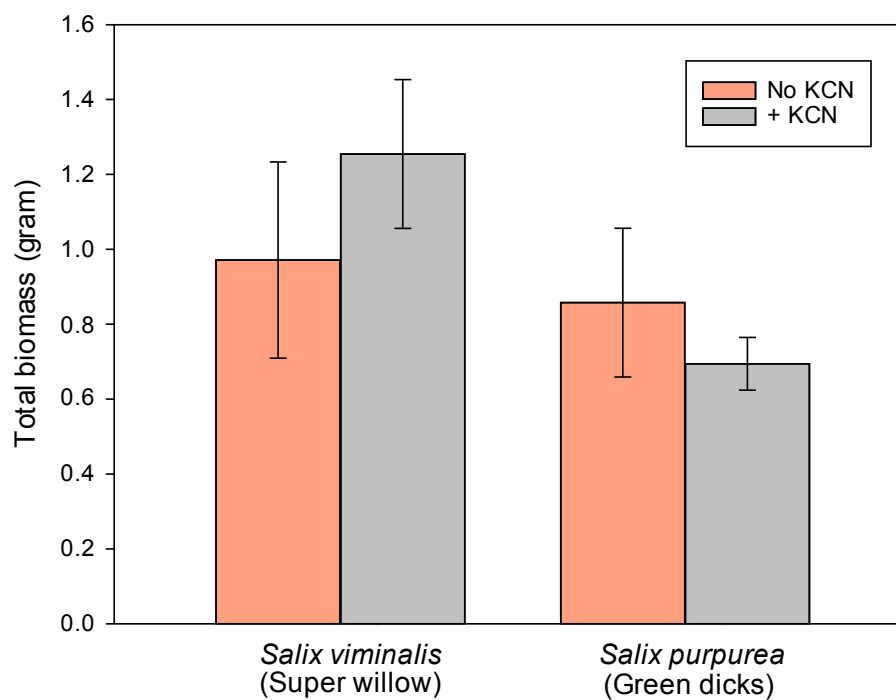


**Figure 3.36:** Total dry weight of leaf tissues from Super Willow and Green Dicks grown on SOM containing 50 mg/kg palladium. Results are the mean from 3 biological replicates  $\pm$  SEM. Student's T-test between no KCN and KCN treatment.

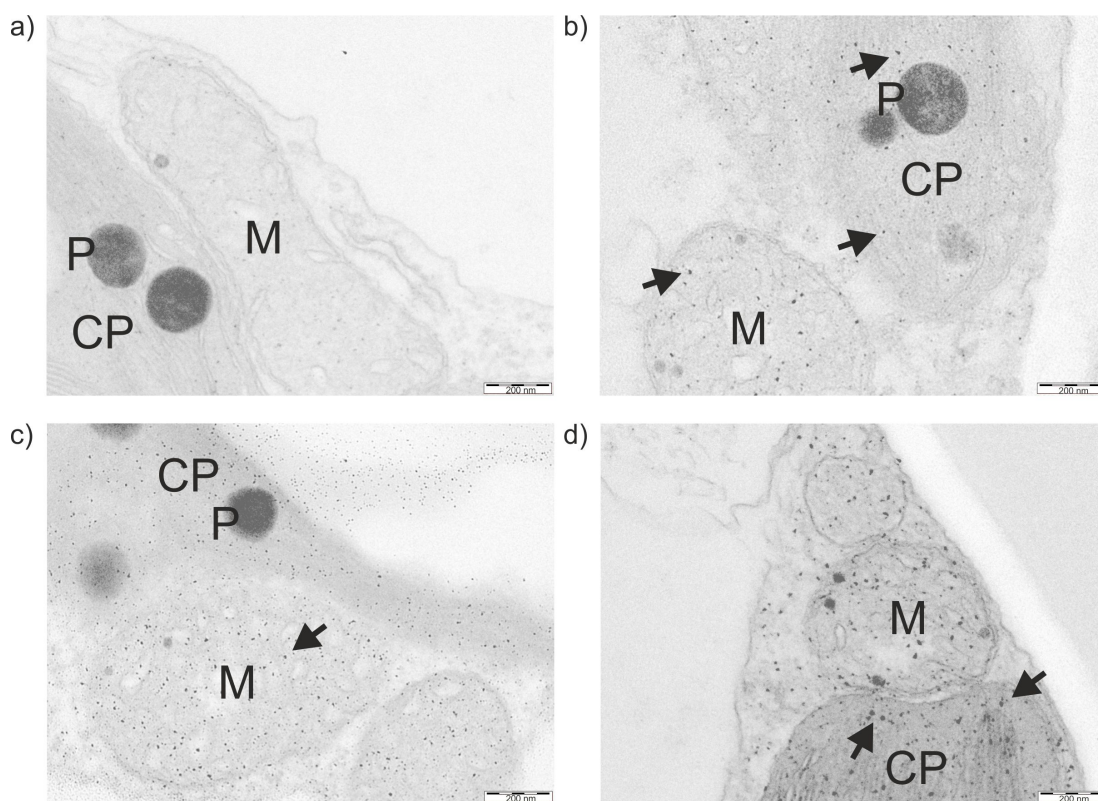


**Figure 3.37:** Electron micrographs of aerial tissue of willows. TEM at 60.5k magnification of leaf tissue from willow plants grown on SOM containing 50 mg/kg of palladium (pH 7) treated with and without cyanide for 7 days. a) Green Dicks without cyanide b) Green Dicks with cyanide c) Super Willow without cyanide d) Super Willow with cyanide. Arrows indicate 'black spots' suspected to be palladium nanoparticles. M; mitochondria, CP; chloroplast, P; plastoglobulins.

This analysis was aided by Dr. Michael Ward at the York JEOL Nanocentre, University of York. Samples taken from the roots of Super Willow grown hydroponically in medium with and without palladium treatment, provided by Andrea Muñoz Garcia from the Green Chemistry, were used as positive controls.

Peaks were identified and assigned by the software running a NORAN System Six (NSS) analysis system. Bombarding the sample with electrons leads to the promotion of different electrons to higher energy states. Electrons from higher states then fall to the level of the promoted electron, emitting an X-ray. Different electrons may be promoted and different electrons fall back into the available energy states emitting X-rays with different energies.

Based on the spectrum generated from the EDX analysis on the TEM images, no peaks could be identified as palladium in any of the samples tested (Figure 3.38 – 3.43). The EDX analysis was able to detect the presence of copper at 8 keV and 9 keV because the sample was embedded on a copper grid to support the sample and X-rays are transmitted as background interference. Time constraints prevented the repeat of this analysis using additional controls containing confirmed palladium nanoparticles.

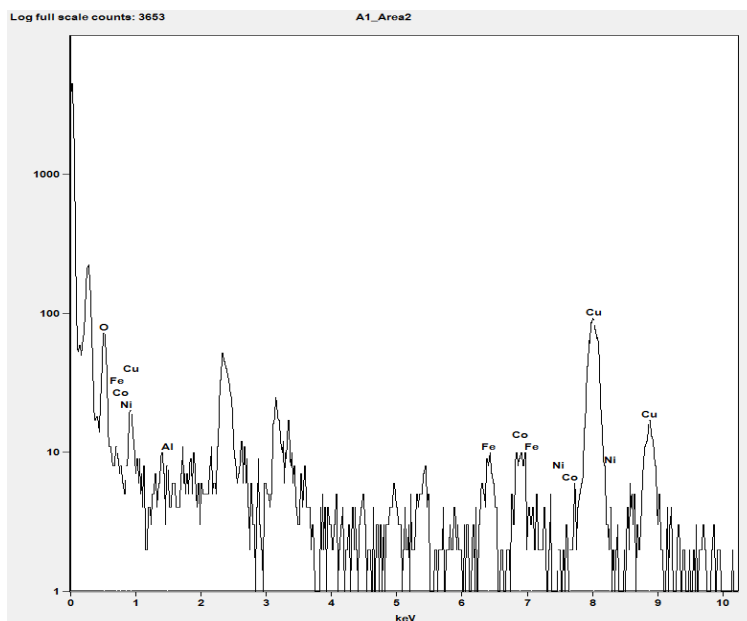


**Figure 3.38:** EDX-derived spectrum from roots of Super Willow plants grown hydroponically in medium with palladium (plants and TEM material kindly supplied by Andrea Muñoz García from the Green Chemistry Centre for Excellence, York).

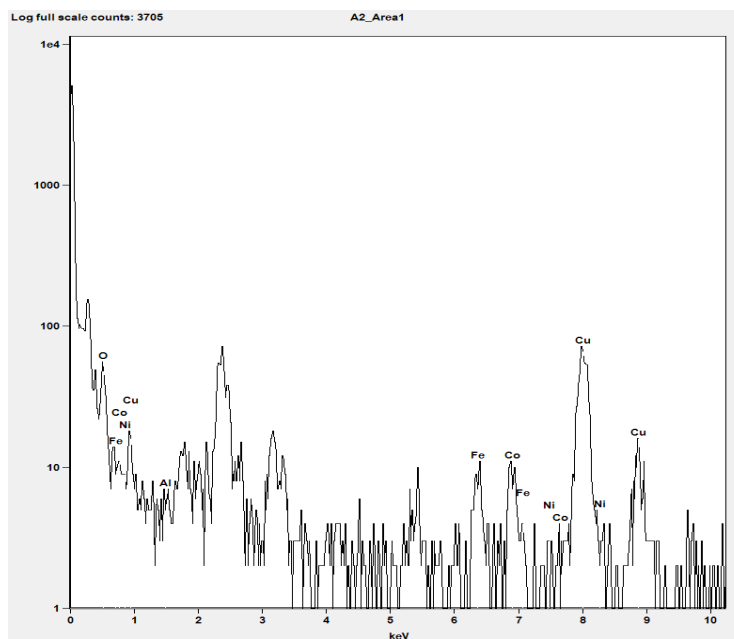


**Figure 3.39:** EDX-derived spectrum from roots of Super Willow plants grown hydroponically in medium without palladium (plants and TEM material kindly supplied by Andrea Muñoz García from the Green Chemistry Centre for Excellence, York).

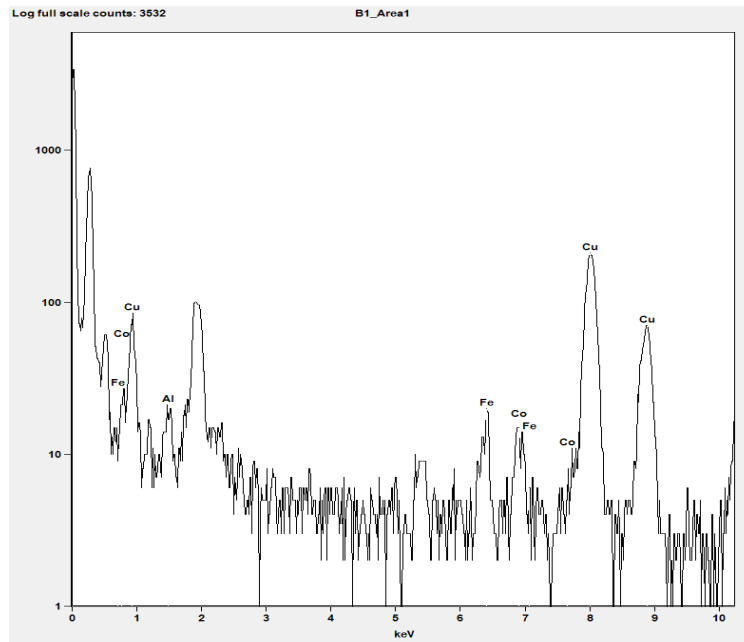


**Figure 3.40:** EDX-derived spectrum from leaf of Super Willow plants grown on SOM containing 50 mg/kg of palladium without cyanide treatment.

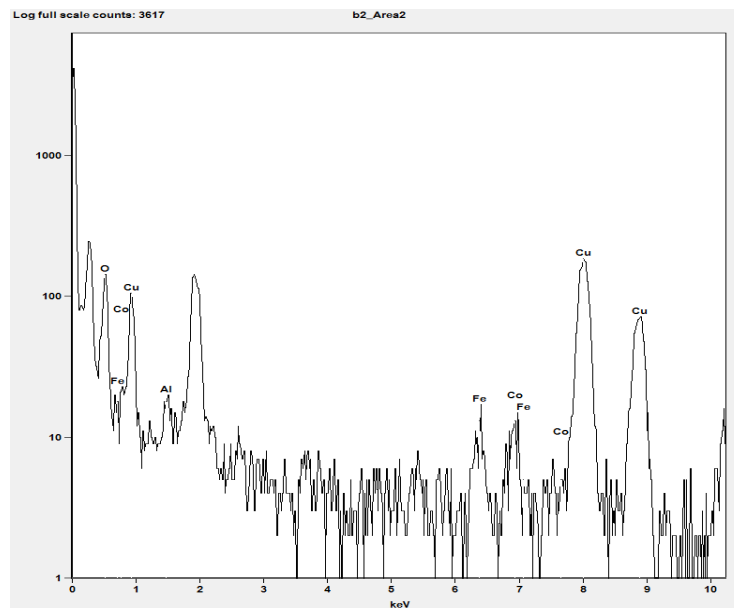


**Figure 3.41:** EDX-derived spectrum from leaf of Super Willow plants grown on SOM containing 50 mg/kg of palladium with cyanide treatment

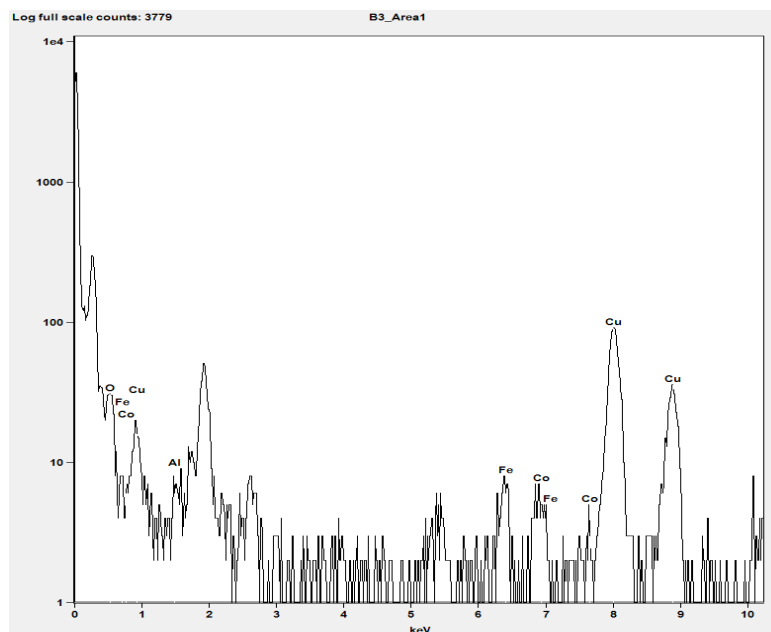


**Figure 3.42:** EDX-derived spectrum from leaf of Green Dicks willow plants grown on SOM containing 50 mg/kg of palladium without cyanide treatment.

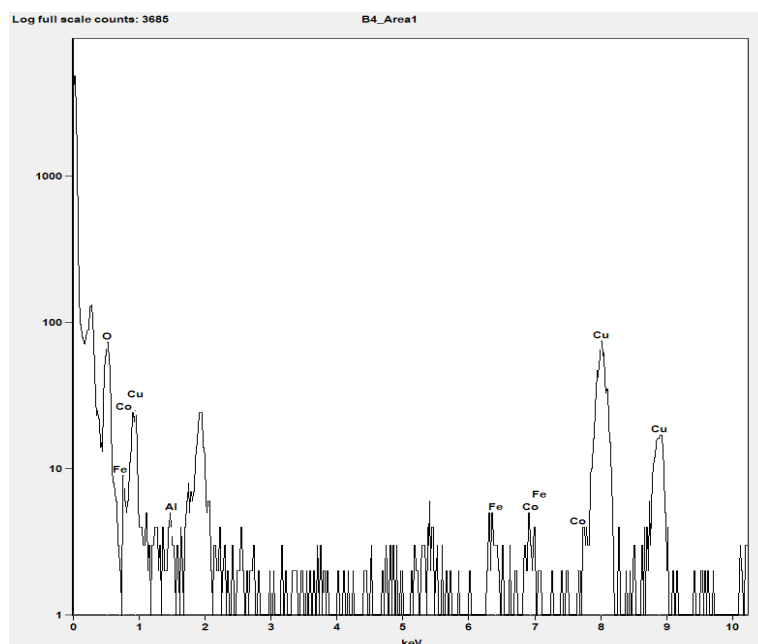


**Figure 3.43:** EDX-derived spectrum from leaf of Green Dicks willow plants grown on SOM containing 50 mg/kg of palladium with cyanide treatment

### **3.3.4 Growth and uptake of palladium by miscanthus**

To investigate the ability of miscanthus to take up palladium, plants were grown on SOM containing 100 mg/kg palladium for four weeks before cyanide was added (Figure 3.44).

Figure 3.45 shows that the addition of cyanide had no effect on the growth of miscanthus based on the biomass of the root and shoot tissue when grown on SOM containing 100 mg/kg of palladium, a concentration in which the biomass of Super Willow was highly reduced (Student's T-test) (Figure 3.25 & 3.27). As expected, cyanide treatment massively and significantly, induced the uptake of palladium into the upper part of the plants with up to 500- fold more palladium than those from non-cyanide treated plants (Student's T-test  $p < 0.01$ ) (Figure 3.46).



**Figure 3.44:** Miscanthus plants grown on SOM containing 100 mg/kg of palladium.

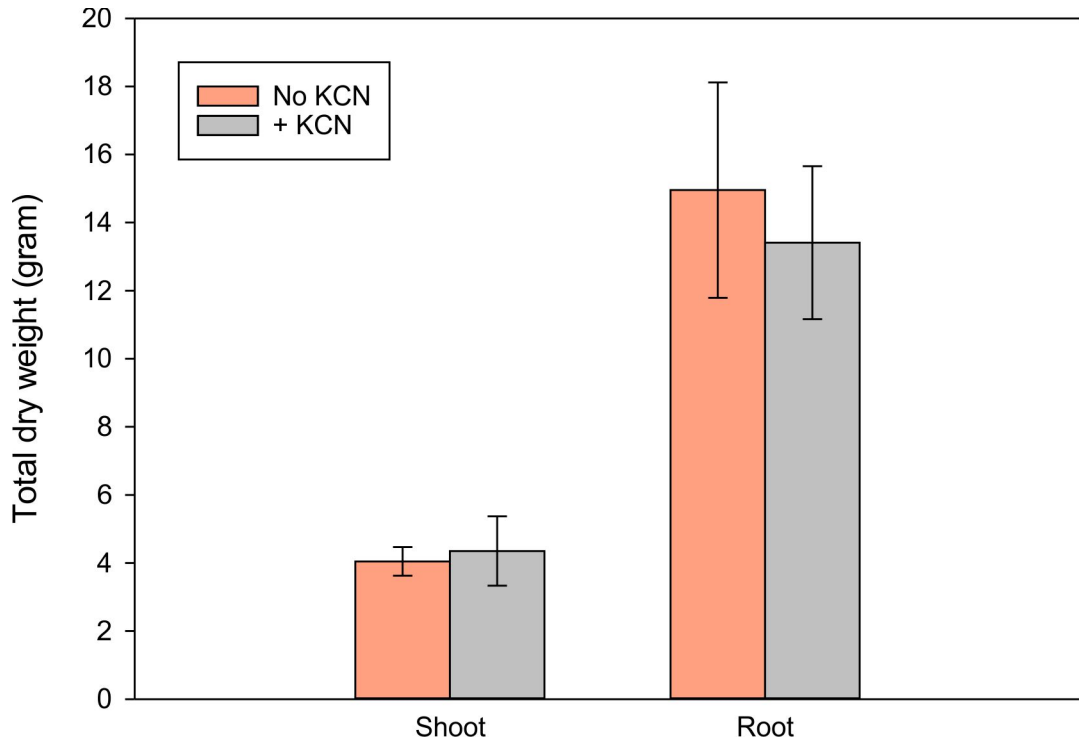


**Figure 3.45:** Total dry weight of shoot and root of miscanthus grown on SOM dosed with 100 mg/kg palladium. Results are from the mean from 7 biological replicates  $\pm$  SEM. Student's T-test between no KCN and KCN treatment.

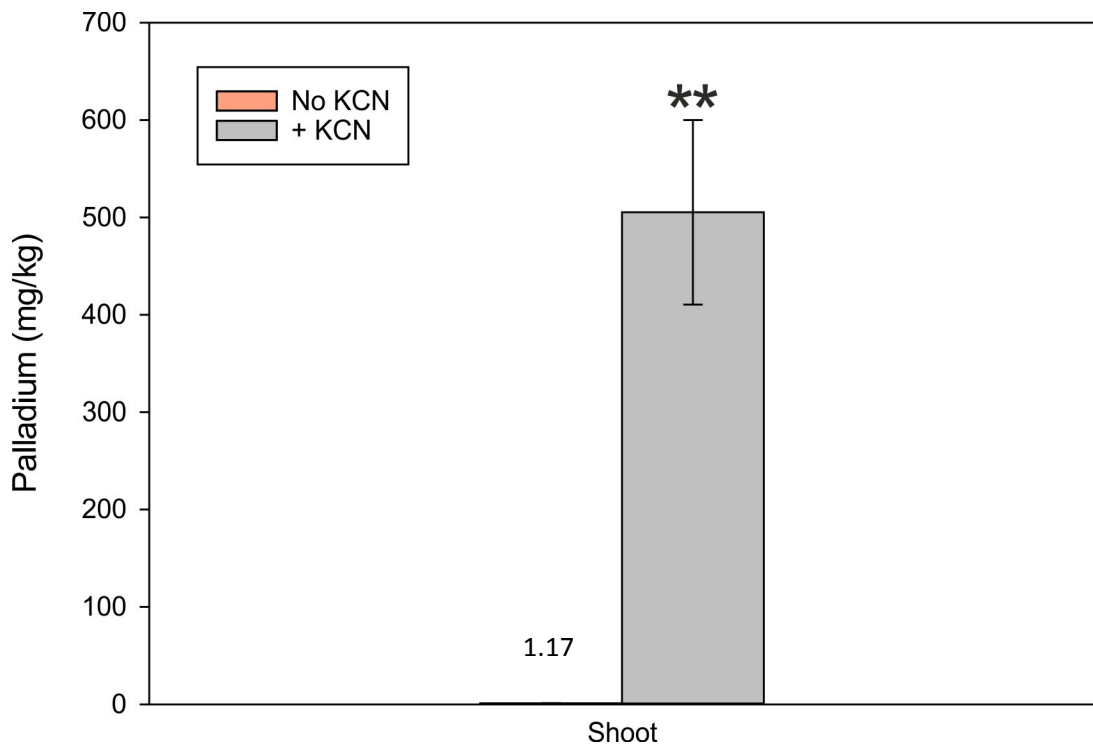


**Figure 3.46:** Palladium levels in the shoots of miscanthus grown on SOM dosed with 100 mg/kg palladium. Results are the mean from 7 biological replicates  $\pm$  SEM. Student's T-test \*\* =  $p < 0.01$  significantly different to non KCN treatment.

### **3.3.5 Testing catalytic activity**

Preliminary testing by collaborators in the Green Chemistry Centre of Excellence on samples of mustard, Green Dicks willow and miscanthus that had the highest concentrations of post-pyrolysis palladium: 0.5, 1.5, and 1.3 g.kg<sup>-1</sup> palladium respectively, resulted in catalytic yields of 5, 7, and 1.2 % respectively (tested in the Heck reaction).

### 3.4 Discussion

#### 3.4.1 Effect of palladium on Arabidopsis

As shown in Section 3.3.1.1, increasing palladium concentration led to a decrease in the root length and total fresh weight of the Arabidopsis plants, with milder effects on germination. As pH was constant, the inhibition was caused by the exposure to palladium. However, compared to palladium, gold inhibition was observed at concentrations 50 times higher than palladium [46] indicating that palladium is more toxic than gold to Arabidopsis.

The exact cause of inhibition by palladium on Arabidopsis growth is unknown and no physiological studies have been conducted to date. It has been reported that palladium can cause growth delay and interfere with stem cell elongation of pea (*Pisum sativum*) [48]. Furthermore, palladium can reduce the leaf length of barley (*Hordeum vulgare*) plants [49]. Palladium is reported to enhance the formation of tissue damaging hydroxyl radicals via the Fenton reaction [190-193], and to increase the formation of reactive oxygen species in other organisms such as zebrafish (*Danio rerio*), which leads to reduced hatching and survival of zebrafish embryos [194]. Therefore, it is possible that the inhibition of Arabidopsis growth by palladium is caused by increased formation of reactive oxygen species within the plant cells. To test this hypothesis, Electron Paramagnetic Resonance (EPR) spectrometry could be used to detect the presence of radicals in response to palladium treatment. The 3,3'-diaminobenzidine (DAB) staining method for reactive oxygen species could also be employed to assess the formation of peroxide in palladium-treated plants. Another point that needs to be considered is the toxicity of palladium nanoparticles in the medium. Agar plates containing palladium turned a distinct brown colour 24 hours after pouring, this is indicative of the formation of palladium nanoparticles. Recent studies have demonstrated an inhibitory effect on Arabidopsis growth caused by metal nanoparticles such as titanium, zinc, silver [195] and copper [196].

### 3.4.2 Field applicable plant species

Willow and miscanthus were chosen and investigated as field applicable plant species with phytomining potential based on favourable agronomic traits, as discussed in Section 3.1. To date, no work has been published on exploiting the ability of these species to take up palladium or any other PGMs from mine wastes. Following the successful application of cyanide to induce the uptake of gold in plants demonstrated by Anderson et al [123], the studies presented here successfully demonstrate the ability of cyanide to improve the accumulation and translocation of palladium in plants.

Fifteen different willow species and cultivars were investigated for their potential to take up palladium. It was observed that leaves of the willow cultivar Green Dicks accumulated the highest levels of palladium (820 mg/kg) (Figure 3.35) and also grew producing one of the highest overall levels of biomass of the fifteen species and cultivars tested, including the fast growing and high biomass species *S. viminalis*. The only recorded data on this cultivar was described by Mirosław et al [189] who showed that when grown on various toxic metals Green Dicks had the lowest copper and chromium uptake compared to eleven other willow species tested. Further uptake tests with Green Dicks could be performed on other PGMs, considering the positive results obtained in the palladium uptake experiments. The 3- to 4-fold levels of variability identified in just fifteen species and cultivars indicate that there is considerable genetic variation for palladium uptake within this genus. The National Willow Collection at Rothamsted Research Centre (<http://www.rothamsted.ac.uk/news/wind-willows>) curates over 300 accessions of willow. To identify the genetic components behind this variation, a genome-wide association study (GWAS) could be used to screen willow accessions for palladium-linked traits. Such a screen would be ambitious: willow is a tree species, and the genetics are not well-studied when compared to *Arabidopsis*. However, using hydroponics to screen rooted willow rods could scale down the amount of glasshouse space required. Subsequent ICP screening to establish palladium metal concentrations in leaves could then be used to identify sub populations with the highest and lowest palladium uptake levels for transcriptome sequencing, and subsequent GWAS. A draft genome for the shrub willow *S. suchowensis* is available, providing a reference sequence suitable for alignment of mRNAseq reads. In addition to GWAS, reads per kilobase per million (RPKM) could be used to examine gene expression in response to the palladium treatment. This approach would also identify willow plant lines that could be used for palladium uptake studies

in mine wastes 'in the field'. Alternatively, GWAS could be conducted in *Arabidopsis* and homologues subsequently identified in willow. This could lead to the identification of the genetic response in *Arabidopsis*, enabling a full functional characterisation in such plant species. Nevertheless, this could be a risky approach, since the genetic pathways related to palladium uptake in willow could be different to the ones in *Arabidopsis*.

Of all the species tested, miscanthus was found to accumulate the highest levels of palladium (505 mg/kg of leaf tissue). Furthermore, this plant also showed a very good tolerance to relatively high concentrations (100 mg/kg) of palladium, even after treatment with cyanide. Compared to the hard wood willow, this non-woody plant could also be a good candidate to harvest palladium from waste materials because of it grow much faster and has more flexible tissues which ease the pyrolysis process.

Although palladium accumulation and translocation was obtained and quantified from the aerial tissues of the willow plants tested, no palladium nanoparticles could be identified based on EDX microanalysis of the leaf material from Green Dicks. The black spots observed by TEM analysis were not found to be palladium nanoparticles. This could be caused by the relatively low concentration of palladium in the biomass compared to previously described work with liquid-culture grown *Arabidopsis* biomass [22]. The lack of observable nanoparticles might also be caused by technical difficulties that arose during the analysis where the membrane was easily ripped during the TEM. Due to time constraints, the analysis could not be repeated. Longer exposure of the plants to palladium and optimised cyanide treatment could lead to enhanced palladium accumulation and, potentially, to the formation of palladium nanoparticles.

Subsequent analysis on harvested, pyrolysed palladium from willow and miscanthus plants showed very low catalytic activity. Post-pyrolysis mustard, miscanthus, and willow (Green Dicks) contained respectively 0.5, 1.5, and 1.3 g/kg palladium, with related catalytic yields (tested in the Heck reaction) of 5, 7, and 1.2 %, respectively. These low yields are almost certainly due to the low palladium concentration accumulated in the plants compared to previous work done with *Arabidopsis* where high catalytic activity was observed. In that work, the amount of palladium accumulated in the post-pyrolysis *Arabidopsis* plants was between 12 - 18 g/kg [22]. However, considering that the plants tested here were able to reach almost 10 % of the total palladium concentration of that in liquid-culture grown *Arabidopsis* after only

a single cyanide treatment and over a few weeks of growth, there is considerable potential to increase palladium uptake in willow and miscanthus to levels that could produce catalytic material comparable with commercially available catalysts. In the field, these plants could be grown on a larger scale and harvested on a three to five-year rotation, possibly in combination with repeated cyanide treatments. Most importantly, this study has shown that willow and miscanthus are able to withstand concentrations of palladium higher than those found in mine waste materials. Willow performed particularly well when grown on waste materials, which contained not just other toxic metals but also limited nutrient supply for plant growth.

Results described here have shown that cyanide treatment improves palladium uptake and translocation from SOM into plant tissues especially into the leaf tissue in all of the plants tested (*Arabidopsis*, mustard, willow & miscanthus).

Similar to gold, palladium and other PGMs also have a high affinity towards cyanide and form complexes. Previous studies have shown that platinum, palladium and rhodium can be extracted from ore using cyanide treatment [197, 198]. Following the Elsner Equation on the dissolution of gold, during the cyanidation process, oxygen will remove one electron from each palladium atom to form a water soluble palladium cyanide complex ( $\text{Pd}(\text{CN})_4^{2-}$ ), improving its bioavailability [199]. Regarding the use of cyanide, there are a number of examples demonstrating the ability of willow to take up and metabolise cyanide and presenting the situation whereby the application of cyanide might enhance plant growth and enable phytoextraction of PGMs [169-171, 173].

However, the use of chemicals such as cyanide poses significant environmental concerns. It has been reported that cyanide can be naturally degraded in the environment [124]. The biodegradation pathway of ammonium thiocyanate into ammonia, bicarbonate and sulfate has been well documented [200, 201]. It has also been shown that plants can degrade cyanide by metabolising it to the amino acid asparagine [202]. Several bacterial strains such as *Bacillus*, *Acinetobacter*, *Pseudomonas* and *Thiobacillus* also transform thiocyanate into sulfate, ammonia and carbon dioxide [203, 204]. Cyanide treatment can also solubilise other non-target metals, such as copper and nickel, possibly affecting the subsequent catalytic activity of the harvested palladium, and further investigations on this matter are needed. Preliminary results in collaboration with the Green Chemistry Centre of Excellence indicate that the presence of nickel in the palladium-containing plant biomass can have additional, beneficial catalytic properties. Recent work by Bakos

et al [205] revealed the combination of low content of palladium with nickel significantly increased the catalytic activity in the hydrogen oxidation reaction as compared to palladium alone.

The application of cyanide directly to mine wastes results in the indiscriminate solubilisation of the target metal throughout the material and possible loss of the metal in the leachate. Targeting solubilisation to the rhizosphere could potentially help to overcome this problem. There are a number of plants that produce cyanogenic compounds as a protection from herbivores. The application of cyanogenic white clover (*Trifolium repens* L.) as a green manure has been reported to release cyanide into soils [173]. With recent advancements in molecular biotechnology, it may be possible that plants could be engineered to release cyanide into the rhizosphere to increase metal solubility and uptake into the plant.

Overall, the results presented here show the potential of willow and miscanthus as phytomining candidates to re-vegetate and take up palladium, and potentially other PGMs, from mine wastes, producing biomass for high-value, plant-based catalysts for industry applications.

## **Chapter 4: Genetic engineering approach to improve gold and palladium tolerance in plants**

### **4.1 Introduction**

While many metals are essential for plant growth, they can be phytotoxic at higher concentrations. To overcome this, plants have evolved a complex, and tightly regulated, system that controls the uptake and distribution of these elements. The studies presented in Chapter 3 and elsewhere [22, 47, 157, 206-208] have shown that, although not essential for growth, platinum group metals (PGMs) and gold are taken up by plants and subsequently deposited as nanoparticles within the plant tissues. These characteristics offer the potential to exploit uptake of these valuable metals by phytomining. Furthermore, in the case of PGMs, studies with palladium have shown that the nanoparticle-containing plant material can be further processed to make a catalyst, adding further commercial value to a phytomining approach [22]. While a promising technology, commercial exploitation is hindered by the relatively poor solubility and low uptake of these metals, and, as shown previously in Chapter 3 and in the work done by Dr. Andy Taylor [46], precious metals such as palladium and gold can cause phytotoxicity. Genetic engineering could present the technology to overcome these problems.

#### **4.1.1 Genetic engineering to enhance precious metals uptake and tolerance**

Anderson et al [123] was the first to demonstrate that plants could be used to harvest gold from ore materials. Gold phytomining, as proposed by Anderson et al [126], can be defined as the ability of plants to accumulate gold greater than 1 mg/kg dry weight. Since gold may share some similar chemical properties with palladium, plants could also be potentially used to uptake palladium from mine waste contaminated area.

However, there are likely to be several limitations inhibiting the rate and accumulation of gold and palladium in plants. The main issue is the relatively low solubility of these elements in soil [209]. Plants take up metals such as nickel, copper and zinc as cations, a form in which these metals are readily found in soil water. On the contrary, gold and palladium exist in the soil either as inert zero-valent ores, or covalently bound in mineral complexes [47]. For effective uptake of gold and palladium in plants, methods currently rely on the use of solubilising agents such as cyanide or thiocyanate to convert the metal to cation form for uptake into plants [123, 126]. Moreover, gold and palladium are likely to inhibit plant growth at concentrations required for viable phytomining [46] (Chapter 3).

Recent work in Prof. Neil Bruce's laboratory has revealed that *Arabidopsis* plants exposed to gold have increased expression of genes involved in plant stress and, decreased expression of metal transporter genes; possibly to reduce gold uptake [47]. Previously, genetic engineering has been demonstrated for the phytoextraction of various metals by plants. For example, bacterial citrate synthase was introduced into *Arabidopsis* to increase citrate production and secretion that resulted in an enhanced aluminium tolerance [70]. Uptake and tolerance of plants to iron was also seen following the expression of the iron regulated transporter *AtIRT1* in *Arabidopsis* [210] and similarly for zinc following the expression of *AtMTP1* [211, 212]. Furthermore, the introduction of the yeast cadmium factor 1 (*ycf1*) gene from yeast into *Arabidopsis* has been reported to enhance lead and cadmium tolerance [213].

#### 4.1.2 Mercuric reductase

Interestingly, as part of a study on mercury phytoremediation Rugh et al [135] observed that when the bacterial mercuric reductase MerA was expressed in Arabidopsis, in addition to an increase in tolerance to mercury, the MerA-expressing plants were also more tolerance to gold. The hypothesis behind expressing MerA in Arabidopsis, is that the presence of MerA in the cytosol will reduce toxic gold and palladium ions to more inert, zero-valent form. This activity will thereby decrease the phytotoxicity, provide zero-valent gold and palladium atoms to seed nanoparticle production, and act as a sink to increase gold and palladium ion uptake.

Mercury, in its organic or inorganic form, is toxic because, in many biological systems it interferes with protein interactions due to its high affinity towards thiols ( $K_{\text{form}}$  for  $\text{Hg}(\text{SR})_2 \geq 10^{40} \text{ M}^{-2}$ ) which increase its capability to undergo rapid exchange between one thiol ligand and another [214]. Previous work by Zhang and Tyerman [215] suggested that inorganic mercury such as  $\text{HgCl}_2$  could inhibit plant growth by affecting the plasma membrane where it damages membrane transporters such as aquaporins, leading to nutrient and water disruption. Inorganic mercury binds strongly to soil components and is less toxic than organomercurials such as methyl mercury, which due to their hydrophobicity, penetrate and accumulate in organelles inhibiting essential oxidative and photosynthetic pathways [216]. In order for bacteria to survive in a toxic mercury environment, they have evolved a mercury resistance operon encoding proteins including MerA and MerB (organomercurial lyase) that are involved in the detoxification of mercury. Together, these proteins are involved in transporting, enzymatic and regulatory functions [217, 218]. As MerB facilitates the protonolysis of organic mercury ( $\text{CH}_3\text{-Hg}^+$ ) to ionic mercury ( $\text{Hg}^{2+}$ ) [216], MerA, which is a flavin oxidoreductase enzyme, will catalyse the reduction of ionic mercury,  $\text{Hg}(\text{II})$  into inert mercury,  $\text{Hg}(0)$  in the cytoplasm of bacterial cells.

MerA was first isolated from *Pseudomonas* K62 [219], then later found in *E. coli* and *Staphylococcus aureus* [143]. The enzyme is a flavoprotein and exhibits similar spectral and biochemical properties to the pyridine nucleotide disulphide oxidoreductase family which includes glutathione reductase [217]. One of the major characteristics of MerA is the homologous cysteine region present in the active site. Similar to other reductases, MerA requires the flavin FAD as a cofactor and utilizes electrons from NADPH for catalytic activity [220]. However, unlike other reductase family members where activity is inhibited upon  $\text{Hg}(\text{II})$  binding, MerA possess unique structural features which enable the catalysis of  $\text{Hg}(\text{II})$  into a volatile, uncharged  $\text{Hg}(0)$ .

The structure of MerA has been well studied over the last three decades. In a key paper, Fox and Walsh [220] investigated the structural similarities between the active sites of MerA and other flavoproteins family members (glutathione reductase and lipoamide dehydrogenase). Fox and Walsh elucidated the role of FAD as the co factor and identified other similarities with glutathione reductase and lipoamide dehydrogenase [221], including significant conservation of residues in the active site of these enzymes.

MerA contains two main components: an N-terminal appendage and a multi domain catalytic core similar to other nicotinamide disulphide oxidoreductase [221-223] (Figure 4.1). MerA binds with Hg(II) at its cysteine pair (C11/C14) in the N-terminal domain before transferring the Hg(II) to another cysteine pair (C558/C559) at the C-terminus of the enzyme [224-226]. A conformational change of the C-terminal leads to the transfer of Hg(II) to the active site cysteine pair (C136/C141) located at the isoalloxazine ring of FAD which is the catalytic core of the enzyme [227]. Lan et al [226] recently described the structural mechanisms by which Hg(II) is transferred from the C-terminal into the MerA core for subsequent reduction. In their work, they demonstrated that Hg(II) is always paired with at least two thiolates before binding to the N-terminal, C-terminal and catalytic core as a neutral complex. NADPH then transfers two electrons to FAD, yielding  $\text{FADH}_2^-$  which subsequently reduces the C136-S-Hg(II)-S-C141 complex to form an inert Hg(0) [226]. The unreactive Hg(0) then exits the cell passively and is volatilized to the environment.

The N-terminal domain (NmerA) of the protein contains the GMTCXXC sequence motif, which is conserved in many soft metal ion trafficking proteins. Ledwidge et al [224] previously described the role and function of NmerA in the reduction of Hg(II) to Hg(0). They showed that NmerA is a stable, soluble, monomeric protein that binds Hg(II) in a 1:1 stoichiometric complex before delivering it to the catalytic core of the MerA. Interestingly, they also demonstrated that NmerA is responsible for protecting the cell against Hg(II) under thiol-depleted conditions by participating in the acquisition and delivery of the bulky  $\text{Hg}(\text{SR})_2$  complex to the catalytic core of the enzyme. This can be an advantage for the survival of cell during thiol-depleted condition as the cysteine thiol in NmerA may also form complex with Hg(II) which further delivered to the catalytic core for reduction process.

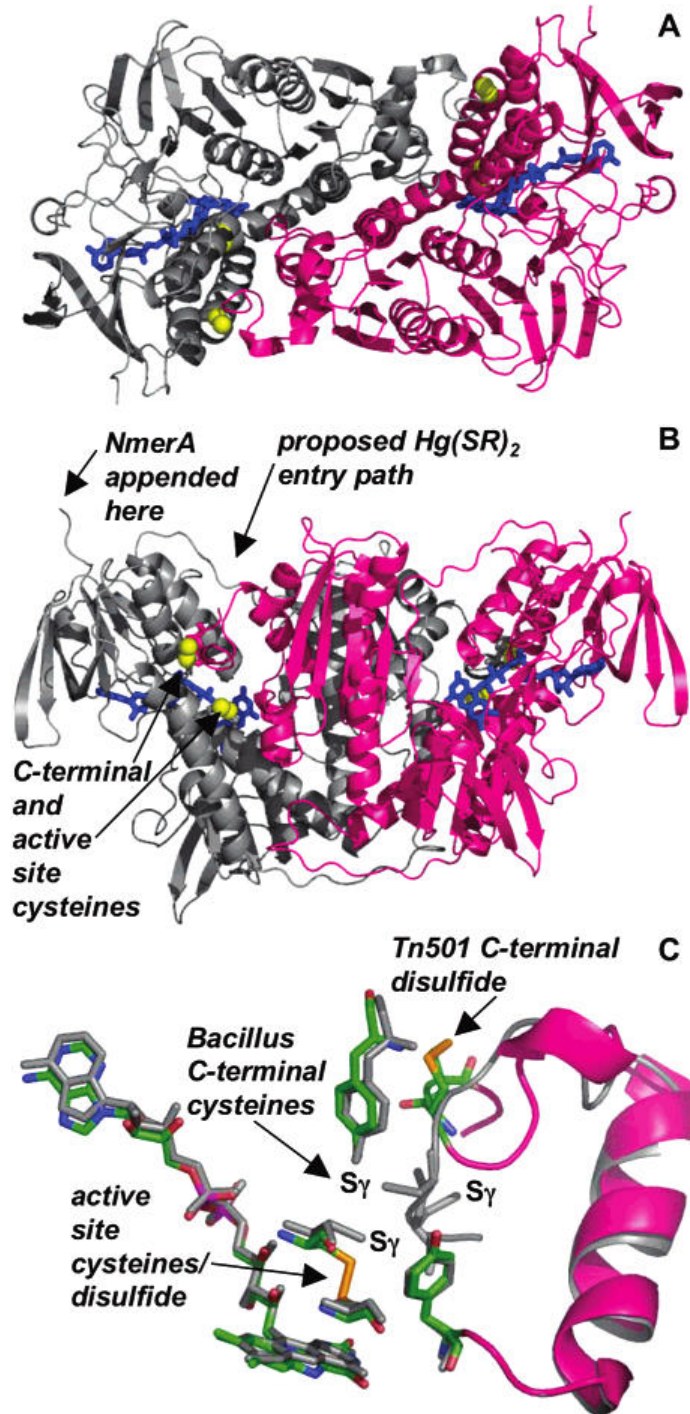


**Figure 4.1:** Catalytic core structure of MerA showing the two MerA subunits coloured in grey and pink, FAD molecules in blue and the sulphur atoms on inner (A)(B) and C-terminal cysteine pairs in yellow (C). Figure re produced from Ledwidge et al [223].

### 4.1.3 Expression of bacterial *merA* in Arabidopsis

The *merA* gene has been introduced into Arabidopsis [135], yellow poplar (*Liriodendron tulipifera*) [142] and rice (*Oryza sativa*) [228] and shown to increase tolerance to mercury up to 100  $\mu\text{M}$   $\text{HgCl}_2$  for the transgenic Arabidopsis and yellow poplar [135, 142] and 250  $\mu\text{M}$   $\text{HgCl}_2$  for the transgenic rice [228]. In the transgenic plants, MerA reduces mercuric ions ( $\text{Hg}^+$ ) into less toxic, inert metallic mercury ( $\text{Hg}^0$ ) which is volatilized out of the plant through the transpiration process in the leaves [135]. Interestingly, MerA-expressing Arabidopsis plants also showed increased tolerance to gold (supplied as  $\text{Au}^{3+}$ ) when compared to wild type plants (Figure 4.2) [135]. This finding indicates that MerA is also able use gold as a substrate, which offers an exciting opportunity to investigate the effect of MerA on the uptake of gold, and possibly palladium, and subsequent metal nanoparticle formation in plants. Compared to mercury, very little is known about the relationship between gold and MerA. The only documented work relating MerA activity with gold was published by Summers and Sugarman [143], where they observed the formation of dark purple colloidal gold, indicating the reduction of Au (III) to Au (0), when *E. coli* cells expressing MerA were treated with gold chloride. As gold shares a number of chemical properties with palladium, it is possible that MerA might also exhibit activity towards palladium. The ability of MerA to increase the resistance of plants towards gold, and possibly palladium, would provide an opportunity to engineer plants with an enhanced ability to take up these precious metals. This chapter uses *E. coli* and Arabidopsis to further investigate the activity of MerA.

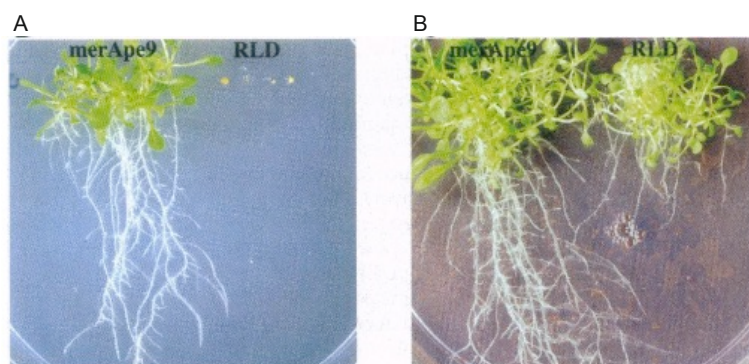


**Figure 4.2:** Arabidopsis plants expressing MerA showing resistance to mercury and gold toxicity. MerA (left hand side, merApe9) and wild type (right hand side RLD) plants growing on  $\frac{1}{2}$  MS containing (A) 50  $\mu\text{M}$  of mercury chloride and (B) 150  $\mu\text{M}$  gold chloride. Picture reproduced from Rugh et al [135].

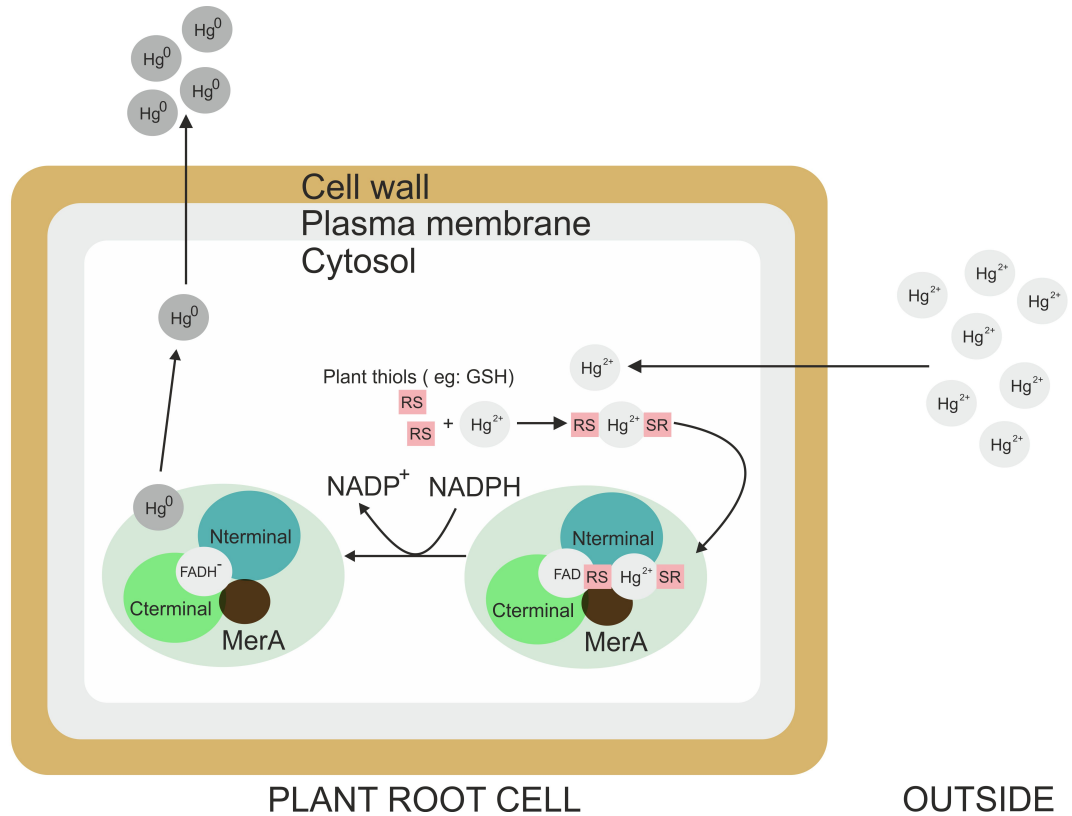


**Figure 4.3:** Diagram outlining mercury detoxification by MerA *in planta*. Ionic mercury in the form of  $Hg^{2+}$  enters the root cell possibly via ionic channels and forming mercury thiolate complexes with random plant thiols such as glutathione (GSH) within the cells. Mercury thiolate complex binds to the binding site located at the N-terminal of MerA [226]. A conformational change of the C-terminal leads to the transfer of Hg(II) to the catalytic core located at the isoalloxazine ring of FAD. NADPH then transfers two electrons to FAD, yielding  $FADH_2$  which subsequently reduce the mercury thiolate complex to form an inert  $Hg^0$ . The unreactive  $Hg^0$  then exits the cell passively and is volatilized to the environment.

## 4.2 Materials and methods

### 4.2.1 Production of Arabidopsis MerA transgenic lines

The codon-optimised mercuric reductase (*merA*) cDNA sequence (Genbank accession number NC\_017659.1) was synthesised by Life Technologies Ltd for expression in Arabidopsis. The *merA* gene was cloned into the intermediary pART7 vector and the subsequent DNA cassette containing *merA*, flanked by CaMV-35S promoter and ocs terminator regions, transferred into the binary pART27 using *NotI* restriction sites [229]. The pART27 vector contains a selectable marker, *nptII*, which confers resistance to kanamycin. The pART27-with insert was used to transform electro-competent *Agrobacterium tumefaciens* as explained in Section 2.5.9.

### 4.2.2 Cloning, expression and purification of MerA recombinant protein in *E. coli*

The codon-optimised *merA* cDNA sequence (Genbank accession number NC\_017659.1) was synthesised by Life Technologies and cloned into the vector pET-16b (Invitrogen) using the In-Fusion Cloning (Clontech Inc.) method and transformed into *E. coli* strain BL21. Colony PCR using T7 primers and internal primers were performed to verify the insert at the *NdeI* and *XhoI* restriction sites in the pET16b. The transformed cells of *E. coli* BL21 harboring pET-16b-*merA* vector were grown and cultured in 500 mL of Luria Bertani (LB) media containing 50 µg/mL of carbenicillin and were incubated in a rotary shaker at 37 °C with 180 rpm. To express the MerA protein, the cultures were induced with 1 mM of isopropyl thio-β-D-galacto-pyranoside (IPTG) at mid-log phase and incubated in the rotary shaker at 20 °C for approximately 8 hours. The cells were then harvested in HIS binding buffer, centrifuged and lysed through a French press cell disruptor. The lysate obtained were clarified by centrifugation at 19,000 x g and filtered at 0.45 µm. The filtered supernatant was loaded onto a HisTrap column (1 mL) (GE Healthcare) and was purified using ÄKTA system with an elution buffer containing 100 mM sodium phosphate (pH 8.0), 0.1 % (v/v) Tween 20, 300 mM NaCl and 500 mM imidazole. The fractions were analysed for the presence of MerA by SDS-PAGE. A thick band of protein was observed with the size of approximately 61.7 kDa, which refers to MerA. The concentration of protein purified was then quantified using absorbance assay at 280 nm using UV spectrophotometer. The protein band obtained was excised from the gel and was sent for protein identification using mass spectrometry at Technology Facility, Department of Biology, University of York.

### **4.2.3 Germination and root length studies**

Sterilised *Arabidopsis* seedlings were pipetted onto ½ MS agar plates containing various concentrations of mercury, gold and palladium at a final pH of 5.7. Plated seedlings were stratified in the dark at 4 °C for three days before transfer to the growth room. Root length and total fresh weight of thirty biological replicates were measured on day twelve of growth. Mean root length and fresh weight were compared using one-way analysis of variance (ANOVA) and student T-test for least significant difference.

### **4.2.4 Kinetic analysis of MerA with mercury, gold and palladium**

MerA assays were carried out by measuring the oxidation rate of NADPH to NADP using a Cary UV Spectrophotometer at 340 nm. The assay was performed at 37 °C in a 1 mL reaction mixture containing a final concentration of 50 mM sodium phosphate buffer, pH 7.4, 100 µM NADPH, 1 mM glutathione and different concentrations of mercury, gold and palladium. Experiments were performed in triplicate. A boiled enzyme control was used to detect any non-enzymatic activity. The initial rate was recorded and Michaelis-Menten curves were constructed using Sigma plot software version 13.0.

### 4.3 Results

#### 4.3.1 Expression of *merA* in Arabidopsis

To verify the *merA* transgene was present in the T3 Arabidopsis lines, PCR was conducted on genomic DNA from rosette leaves using the *merA* internal primers as shown in Figure 4.4.

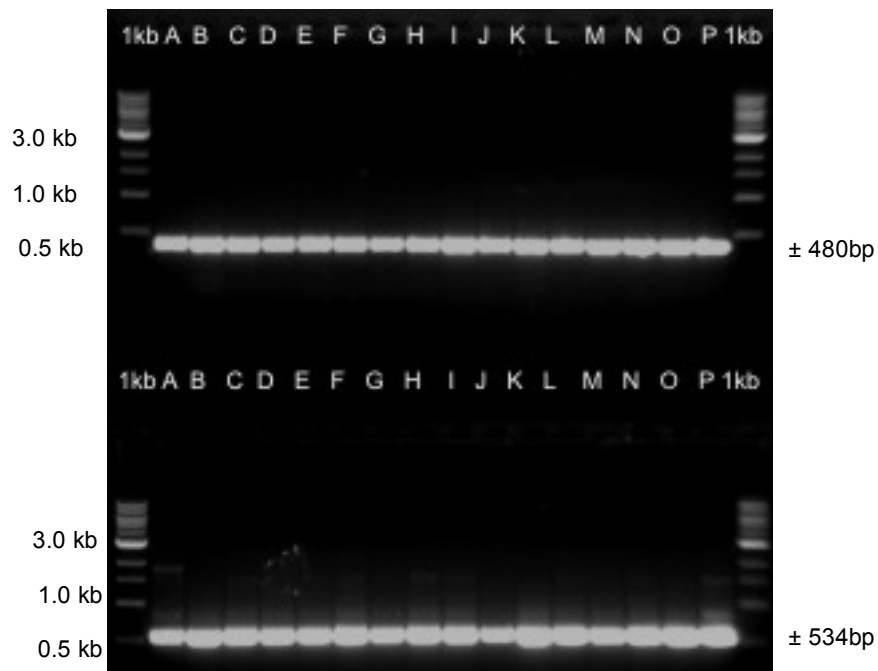


**Figure 4.4:** PCR analysis on DNA isolated from transgenic plants (A-P) using *ACTIN* primers as control (upper gel) and *merA* internal primers (lower gel).

### 4.3.2 Screening of MerA transgenic lines for mercury resistance

To identify the MerA transgenic lines with the highest levels of mercury resistance, the T3 homozygous MerA seedlings were further screened on ½ MS media with 50 µM of HgCl<sub>2</sub>. Based on the root length measurement of 30 seedlings taken at day 12 all of the transgenic lines tested had significantly longer roots than wildtype seedlings (Figure 4.5). Out of the six transgenic lines tested, three lines were observed to be significantly more resistant to mercury when compared to the other MerA transgenic lines (ANOVA Tukey's test  $p < 0.001$ ). This result was further justified by total fresh weight measured on day 12 (ANOVA Tukey's test  $p < 0.01$ ) (Figure 4.6). To quantify the *merA* transcript level, RNA from all the lines were isolated and 2<sup>nd</sup> strand cDNA synthesized using reverse transcriptase. The transcript levels were measured via qPCR using ACTIN as an indigenous control. Based on the result obtained, it was observed that *merA* was expressed in all three lines tested compared to the wildtype plants with MerA transgenic line 22 and 23 showing the highest transcription level (ANOVA Tukey's test  $p < 0.001$ ) (Figure 4.7). Based on the root length studies and qPCR analysis, MerA transgenic line 23 was chosen to be tested for further experiments.

The MerA seedlings were then grown on ½ MS containing different concentrations of mercury to quantify the tolerance to mercury. Based on the initial work done by Rugh et al [135], 100 µM of mercury chloride was used as the maximum concentration, along with 0, 30, 50 and 70 µM.

Root length and total fresh weight analysis on day 12 revealed that the MerA seedlings were more resistant to mercury when compared to the wildtype (Student's T-test  $p < 0.001$ ) (Figure 4.8 and 4.9). It was also observed that the root length and fresh weight decreased as the concentration of mercury increased.

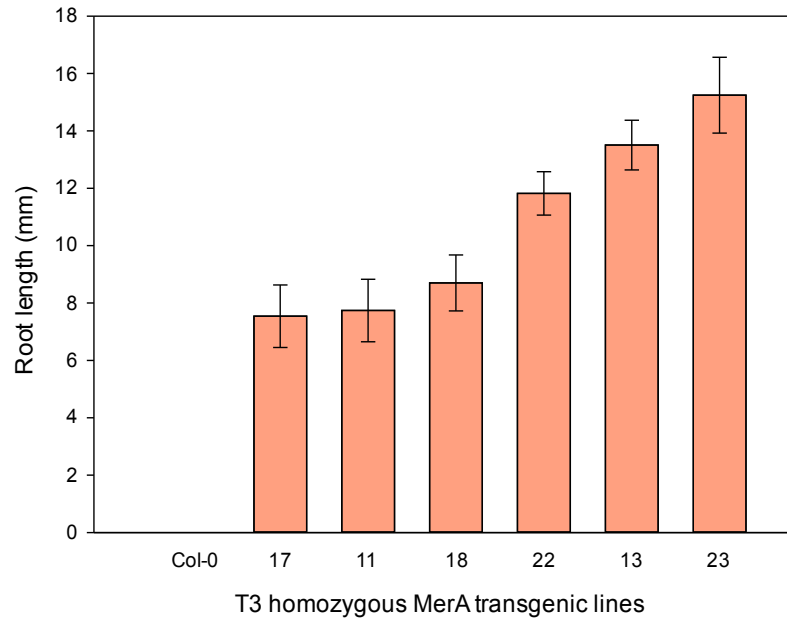


**Figure 4.5:** Root lengths of 12 day-old Arabidopsis Col-0 and MerA seedlings on  $\frac{1}{2}$  MS (A) media containing  $50 \mu\text{M}$  of mercury. Results are the mean from 30 biological replicates  $\pm$  SEM. ANOVA Tukey's test.

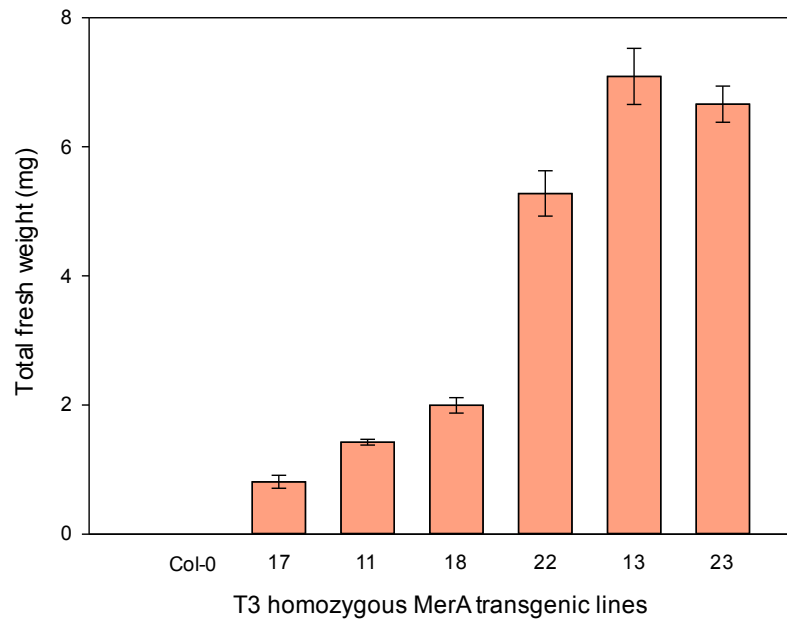


**Figure 4.6:** Total fresh weights 12 day-old Arabidopsis Col-0 and MerA seedlings on  $\frac{1}{2}$  MS (A) media containing  $50 \mu\text{M}$  of mercury. Results are the mean from 30 biological replicates  $\pm$  SEM. ANOVA Tukey's test.

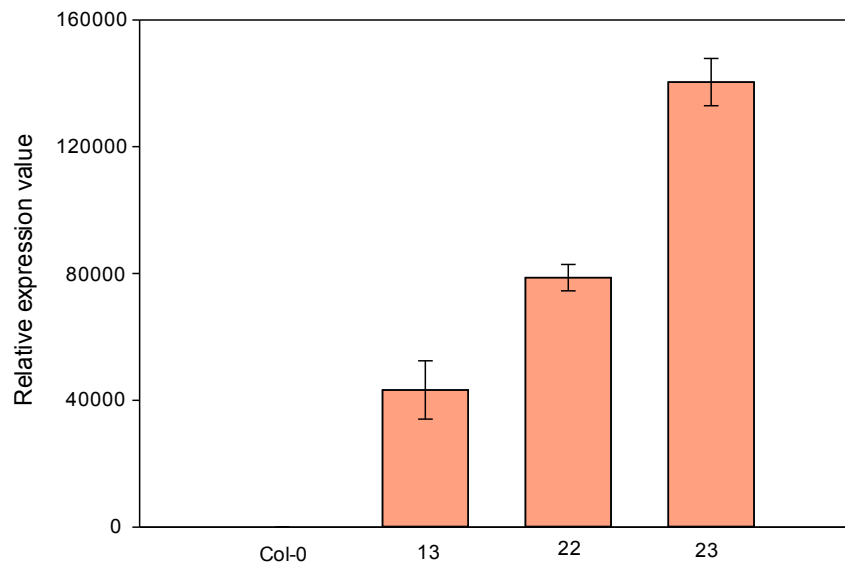


**Figure 4.7:** Relative expression values of *merA* transcript level from the MerA seedlings exhibiting the highest resistance to mercury. The data were normalized to the Arabidopsis *ACTIN* gene and relative fold induction values were calculated using the  $\Delta\Delta C_t$  method [230]. Results are the mean from 3 biological replicates  $\pm$  SEM. ANOVA Tukey's test.

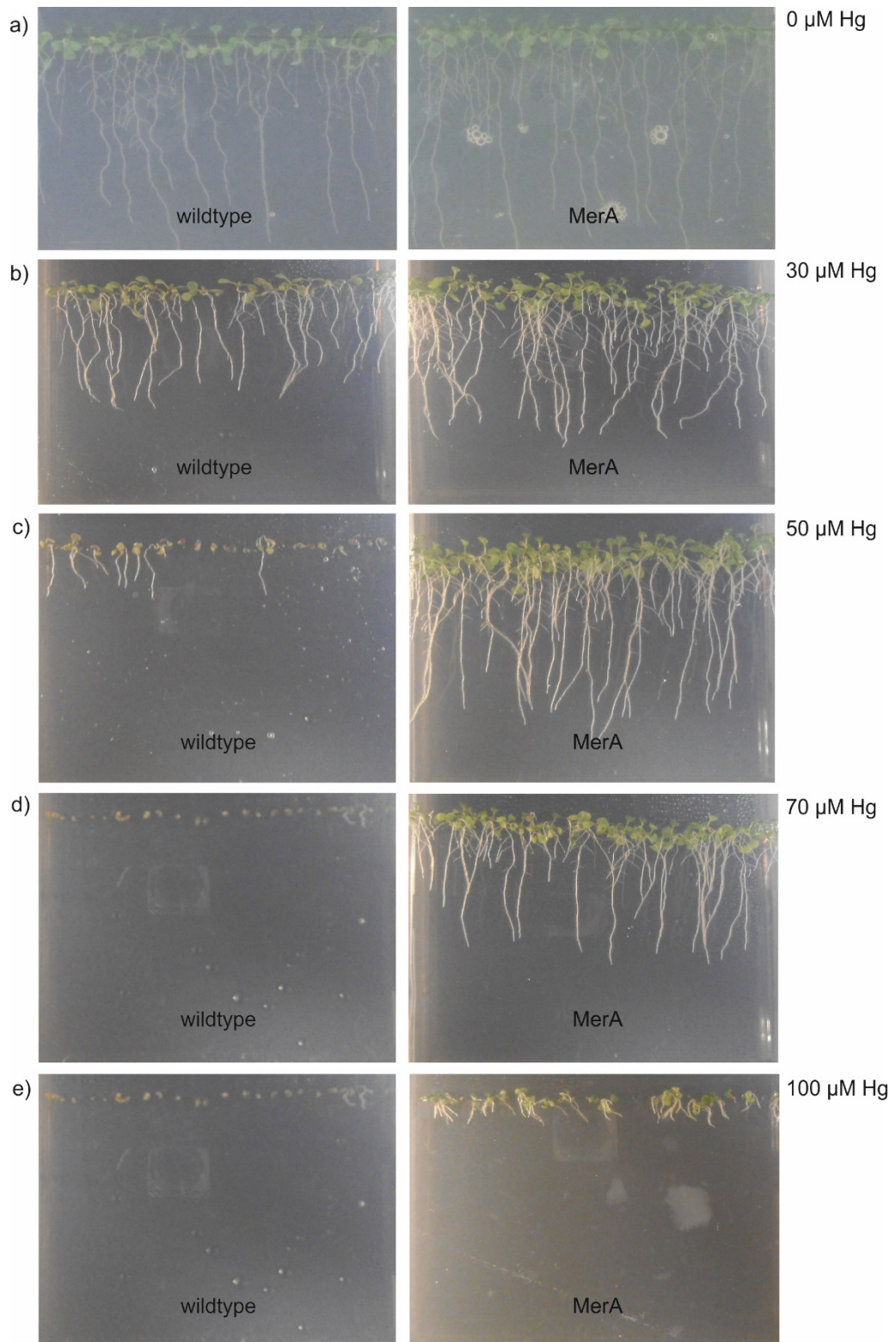


**Figure 4.8:** Appearance of 12 day-old wildtype and MerA seedlings on 1/2 MS (A) plates containing a range of mercury concentrations.

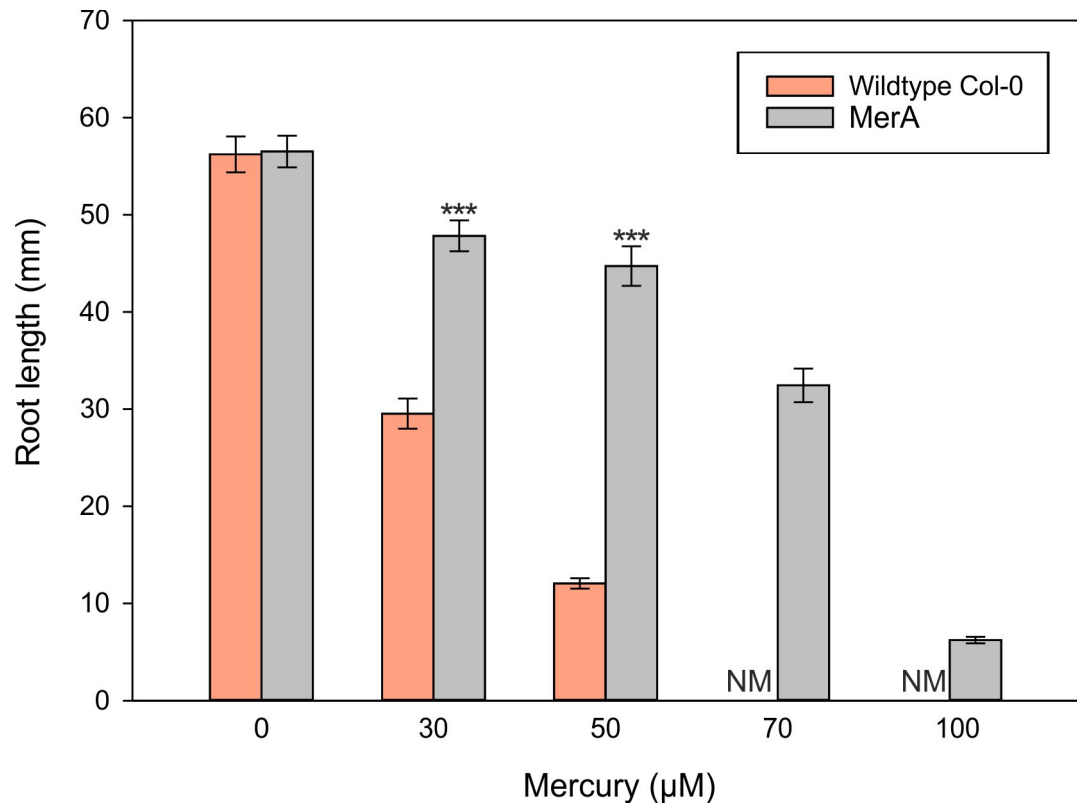


**Figure 4.9:** Root lengths of 12 day-old *Arabidopsis* Col-0 wildtype and MerA seedlings on ½ MS (A) containing increasing concentrations of mercury. NM = not measurable. Results are the mean from 30 biological replicates ± SEM. Student's T-test \*\*\* =  $p < 0.001$  significantly different to wildtype plants.

### **4.3.3 Screening MerA-expressing plants for tolerance to gold**

To investigate the resistance of MerA-expressing *Arabidopsis* plants towards gold, the MerA and wildtype seedlings were grown on solid agar plates containing a range of gold concentrations. The concentrations tested were 0, 50, 100, 150 and 200  $\mu\text{M}$  of potassium gold chloride. It was observed that the root length and fresh weight decreased as the concentration of gold increased for both wildtype and MerA seedlings (Figure 4.10). It was also seen that the colour of the media turned darker purple as the concentration of gold increased suggesting that some of the gold (III) added to the media had been reduced to gold (0).

In the absence of gold, there was no significant difference in root length between the wildtype and MerA seedlings. However, in contrast to the result obtained by Rugh et al [135], the MerA seedlings were no more tolerant to gold than the wildtype plants (Figure 4.14). Furthermore, the root length and fresh weight of 12 day-old MerA-expressing seedlings were significantly lower than the wildtype at all concentrations of gold tested (Student's T-test  $p < 0.001$ ) (Figures 4.11 & 4.12). At 200  $\mu\text{M}$  gold, both wildtype and MerA-expressing seedlings showed a severe inhibition growth effect.

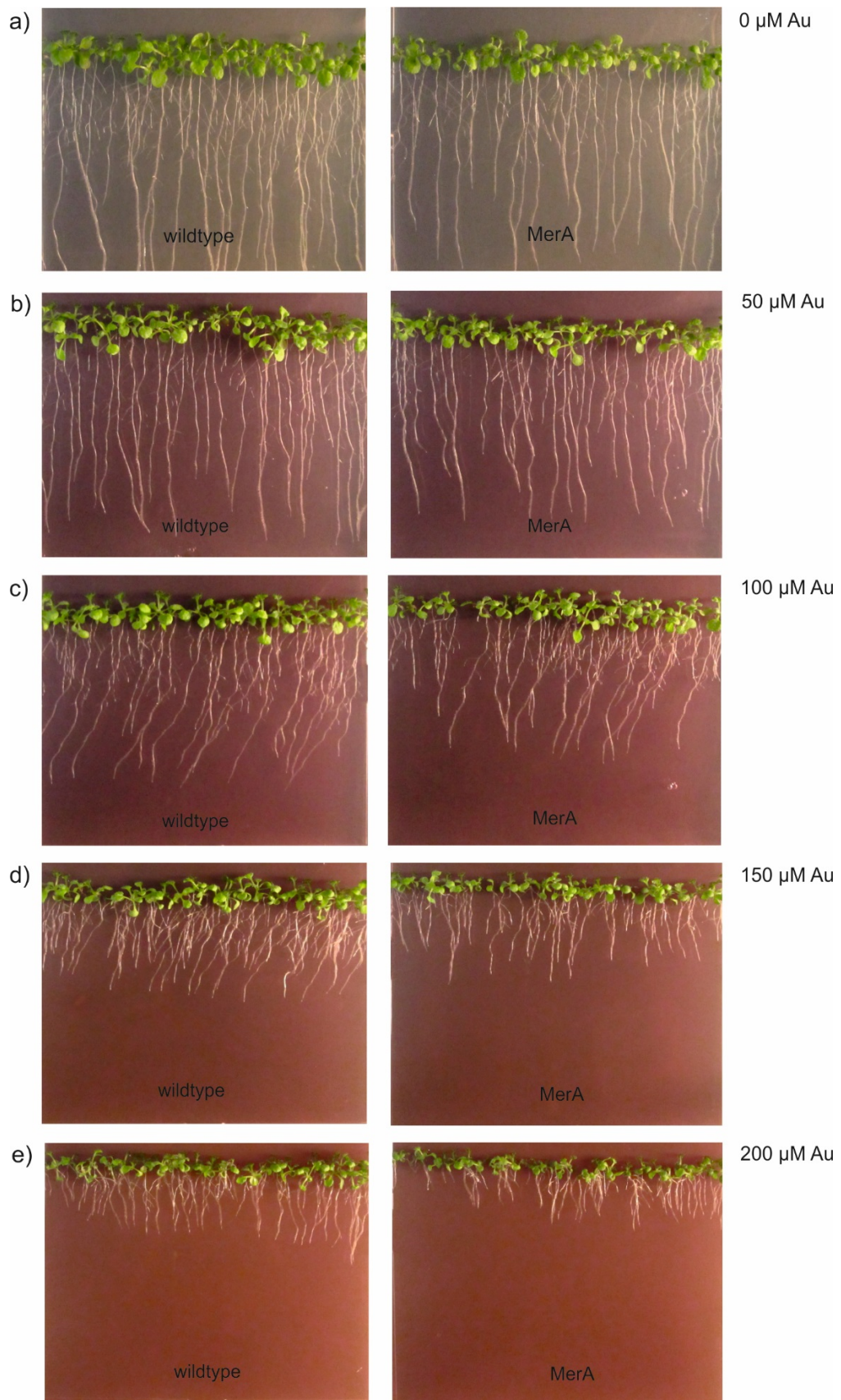


**Figure 4.10:** Appearance of 12 day-old wildtype and MerA-expressing seedlings on 1/2 MS (A) plates containing a range of gold concentrations as indicated in the figure.

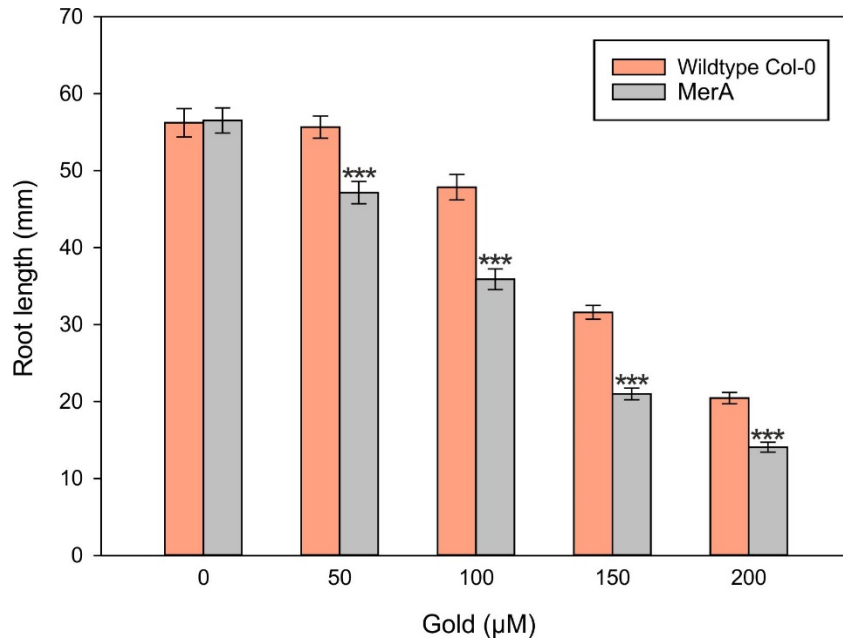


**Figure 4.11:** Root lengths of 12 day-old Arabidopsis Col-0 wildtype and MerA-expressing seedlings on 1/2 MS (A) media containing increasing concentrations of gold. Results are the mean from 30 biological replicates  $\pm$  SEM. Student's T-test \*\*\* =  $p < 0.001$  significantly different to wildtype.

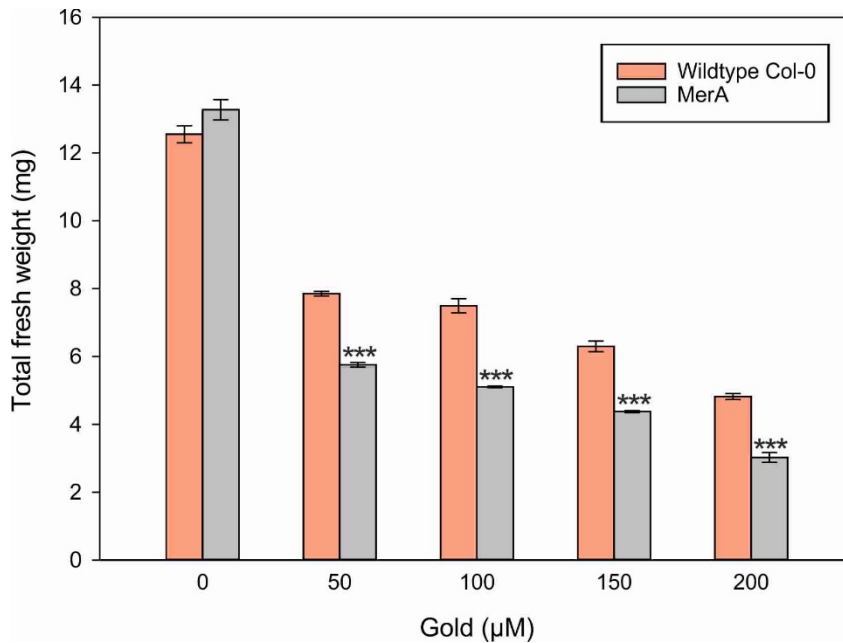


**Figure 4.12:** Total fresh weights 12 day-old Arabidopsis Col-0 wildtype and MerA-expressing seedlings on 1/2 MS (A) media containing increasing concentrations of gold. Results are the mean from 30 biological replicates  $\pm$  SEM. Student's T-test \*\*\* =  $p < 0.001$  significantly different to wildtype.

#### **4.3.4 Screening MerA-expressing plants for tolerance to palladium**

To investigate if the MerA transgenic plants are also tolerance to palladium, both wildtype and MerA-expressing seedlings were germinated and grown on MS media containing a range of palladium concentrations. Figures 4.13, 4.14 and 4.15 show that the root length and fresh weight of both wildtype and MerA-expressing seedlings decreased as the concentration of palladium increased. However, on medium containing 15  $\mu$ M palladium, the wildtype produced significantly longer roots and attained higher fresh weight biomasses than MerA-expressing seedlings (Student's T-test  $p < 0.01$ ).

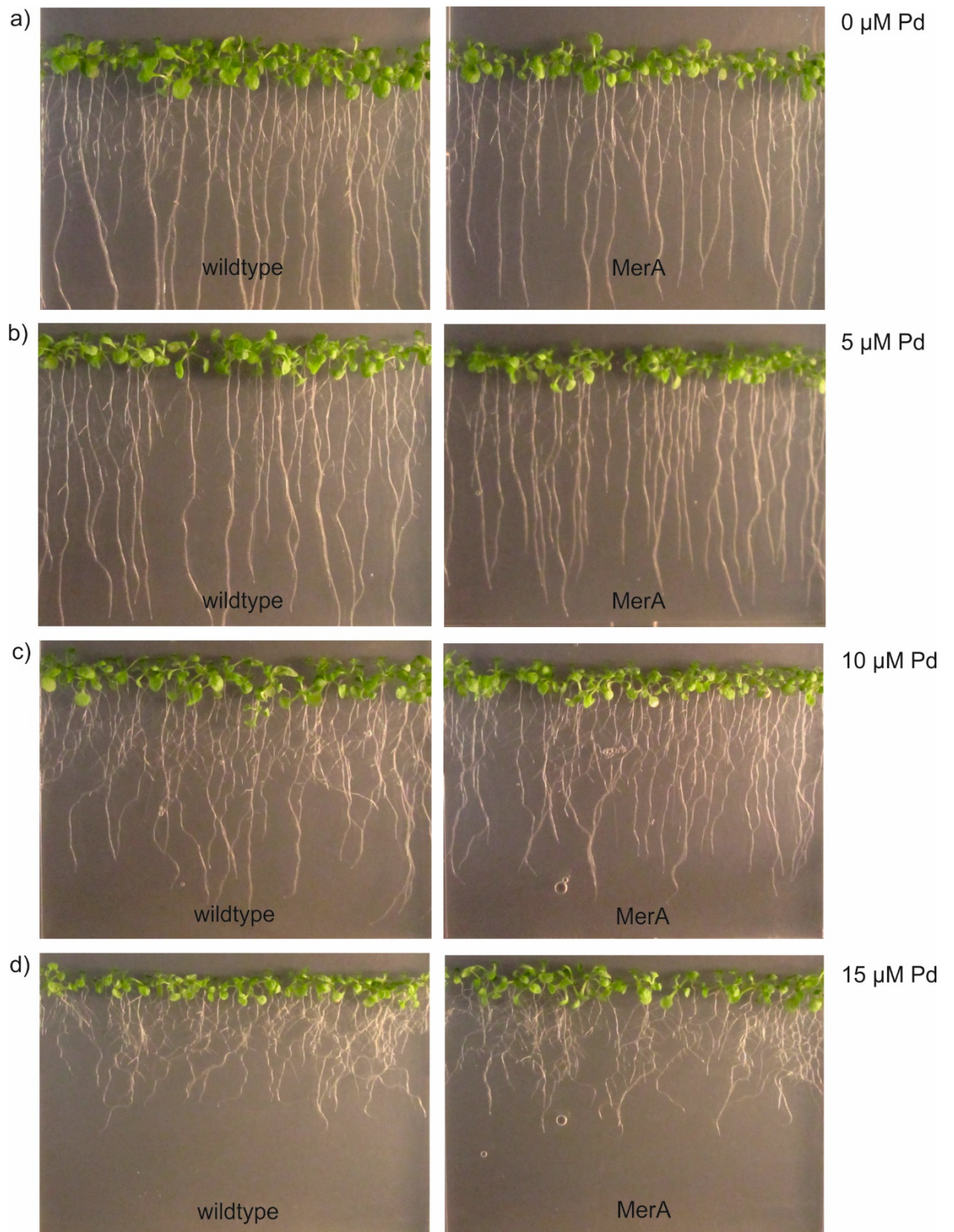


**Figure 4.13:** Appearance of 12 day-old wildtype and MerA-expressing seedlings on  $\frac{1}{2}$  MS (A) plates containing a range of palladium concentrations as indicated in the figure.

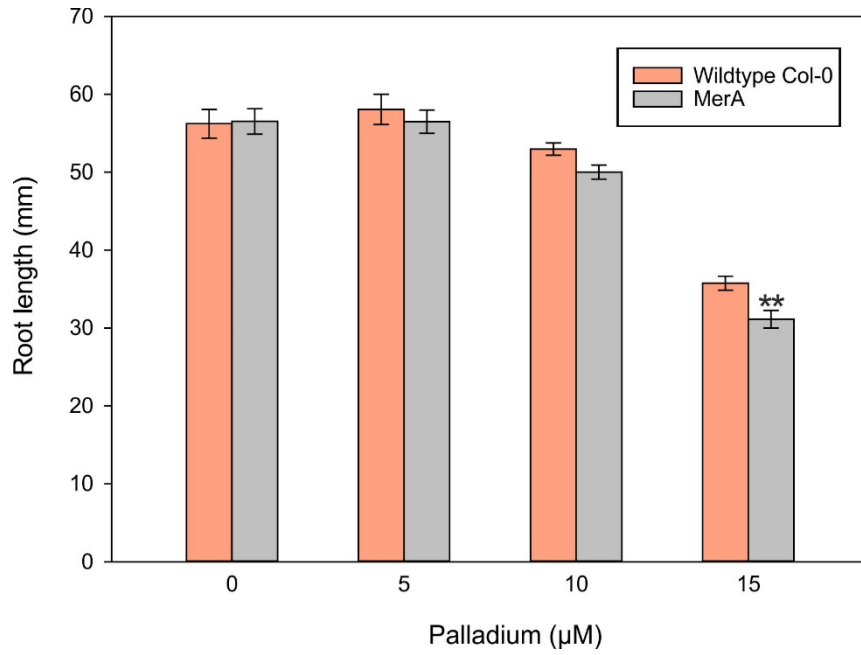


**Figure 4.14:** Root lengths of 12 day-old Arabidopsis Col-0 wildtype and MerA-expressing seedlings on 1/2 MS (A) media containing increasing concentrations of palladium. Results are the mean from 30 biological replicates  $\pm$  SEM. \*\* =  $p < 0.01$  significantly different to wildtype.

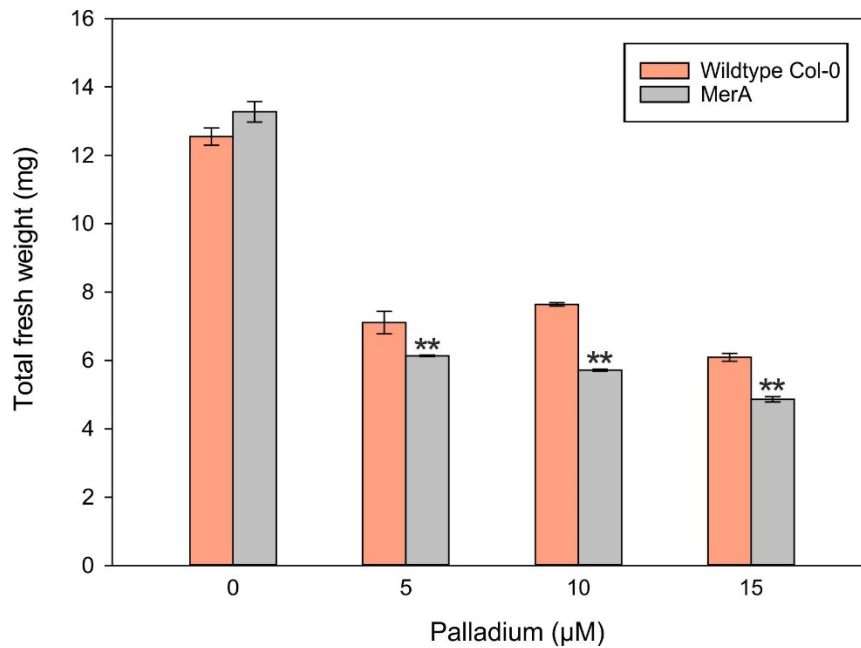


**Figure 4.15:** Total fresh weights 12 day-old Arabidopsis Col-0 wildtype and MerA-expressing seedlings on 1/2 MS (A) media containing increasing concentrations of palladium. Results are the mean from 30 biological replicates  $\pm$  SEM. \*\* =  $p < 0.01$  significantly different to wildtype.

### 4.3.5 Metal uptake studies of MerA-expressing plants from soil containing gold and palladium

Soil-based studies were conducted to investigate the uptake and tolerance of MerA-expressing plants to gold and palladium. The results, shown in Figure 4.16, showed that the application of potassium cyanide increased the levels of gold and palladium taken up by the plants. The effect of potassium cyanide on gold and palladium uptake was significant (Student's T-test  $p < 0.05$ ); the high error bars in the gold study were likely to be the result of different sizes of the plants harvested. However, irrespective of the application of cyanide, there was no difference in the uptake of either gold or palladium by the MerA-expressing plants when compared to the wildtype.

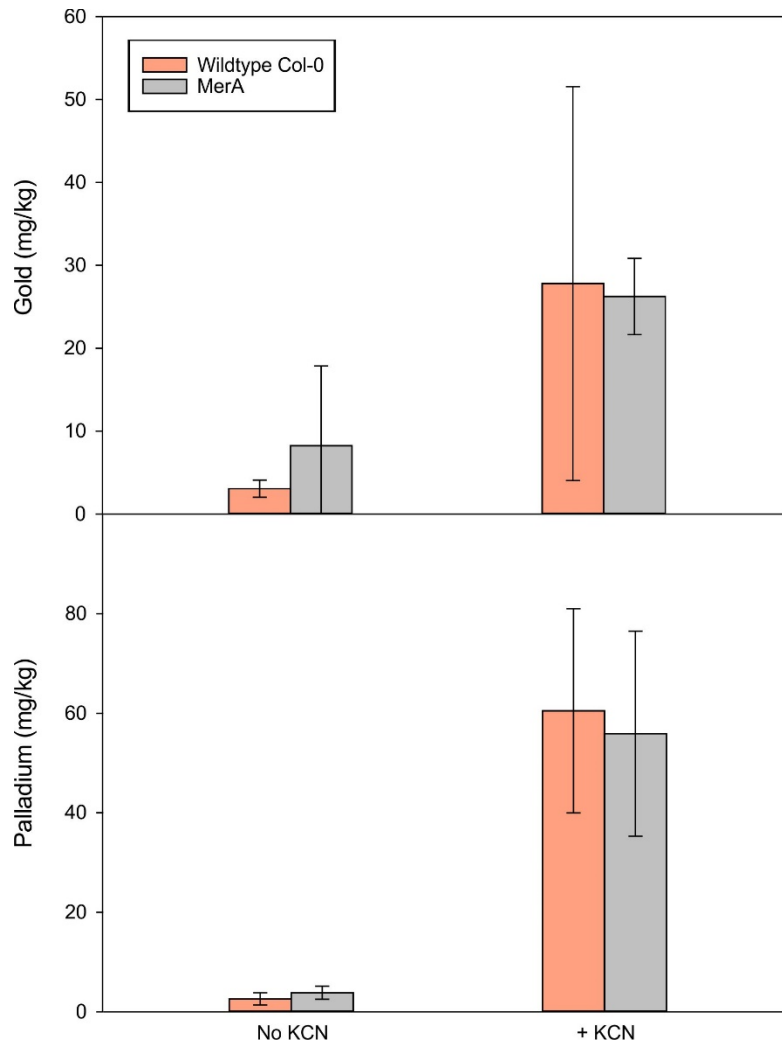


**Figure 4.16:** Levels of gold and palladium in aerial tissues of wild type and MerA-expressing plants. Seedlings were germinated, then grown for 7 weeks in soil containing 50 mg/kg of gold or palladium, then dosed with 100 mg/kg cyanide and grown for another week before harvesting. Metal content was determined using ICP-MS. Results are mean of 8 pots  $\pm$  SEM. Student's T-test between wildtype and MerA-expressing plants.

#### 4.3.6 Cloning, expression and purification of MerA

The MerA-expressing transgenic plants have been reported to be more tolerant to gold compared to wildtype [135]. However, no phenotype could be observed *in planta* for the MerA transgenic lines used in this study. To further investigate the activity of MerA towards gold and palladium MerA was recombinantly expressed and purified from *E. coli*. The codon-optimised *merA* was cloned into pET16b followed by transformation into *E. coli* BL21. The positive transformants were screened on LB media with 50 µg/mL of carbenicillin and the insert was further verified using colony PCR (Figure 4.17 and 4.18). The expression was induced with 1 mM isopropyl thio-β-D-galacto-pyranoside (IPTG) for 8 hours (Figure 4.19). Crude extract was prepared using French press and MerA was purified using a HisTrap column on an AKTA purification system. MerA, which has a molecular weight of 61.7 kDa, was purified to homogeneity and the size and purity verified by SDS PAGE (Figure 4.20), the identity of the purified MerA was then confirmed by mass spectrometry.

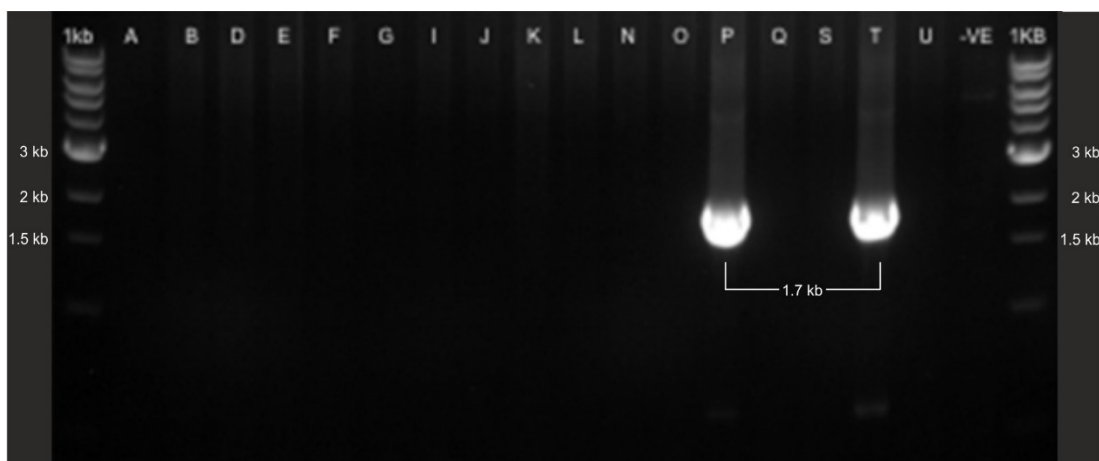


**Figure 4.17:** Agarose gel showing DNA fragments amplified using T7 primers, on bacterial colonies (labelled A to U) transformed with pET16b-merA. Negative control PCR reaction using water as template (-VE).

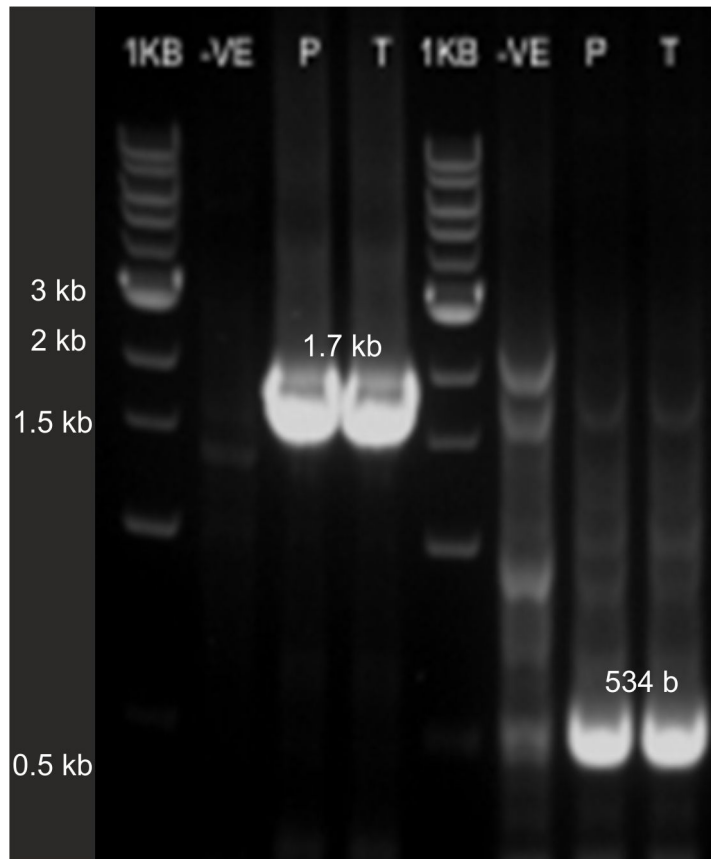


**Figure 4.18:** Colony PCR using T7 primers (expected product size 1.7 kb) and internal primers (expected product size 534 bp) on cloned product to determine *merA* insert.

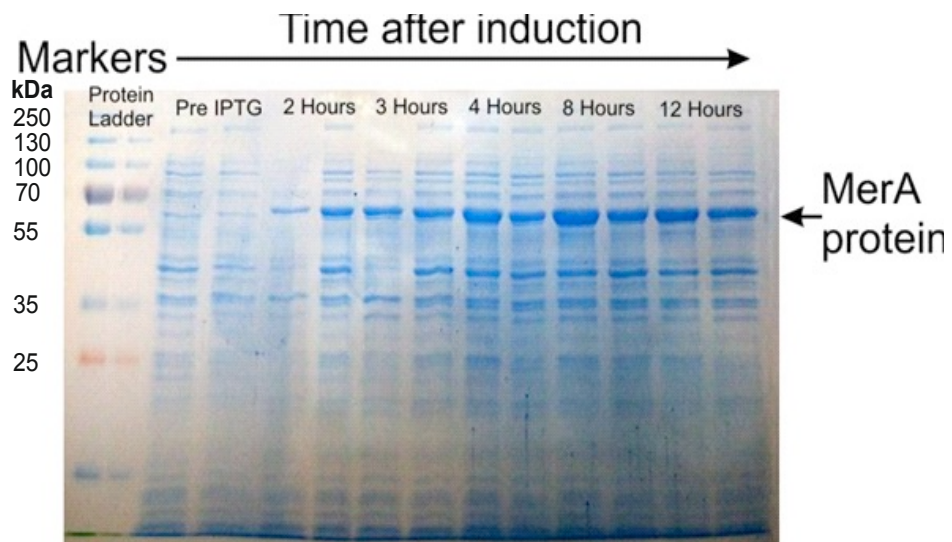


**Figure 4.19:** SDS-PAGE analysis showing expression of MerA by *E. coli* BL21 following induction with 1 mM of isopropyl thio- $\beta$ -D-galacto-pyranoside (IPTG).

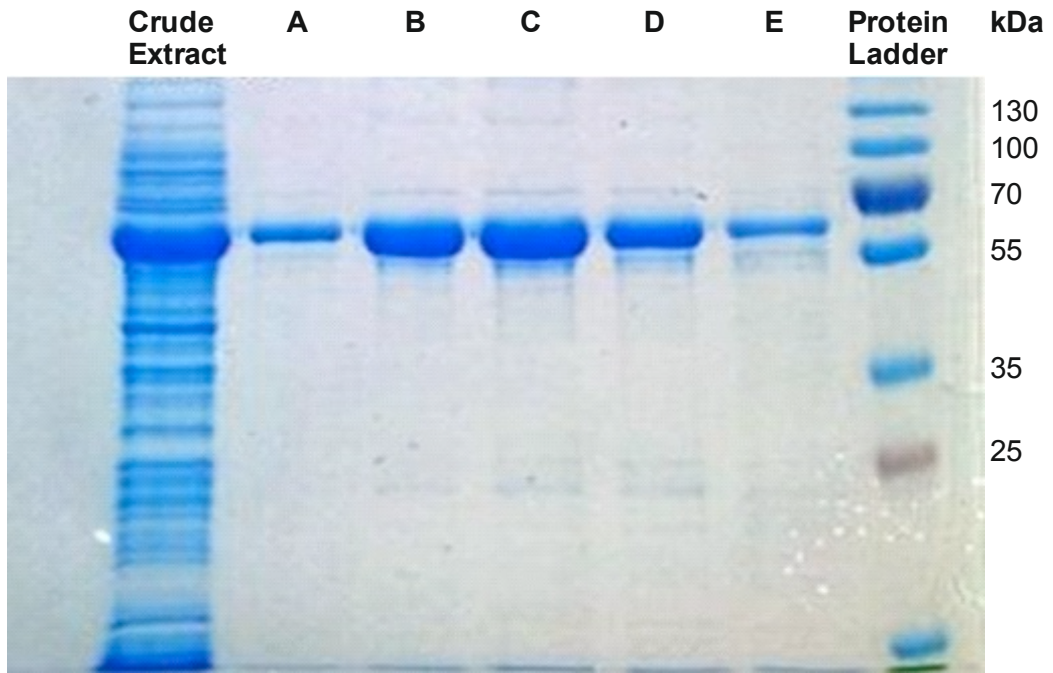


**Figure 4.20:** SDS-PAGE analysis of the expression and purification of MerA. Crude Extract, crude protein extract from *E. coli* BL21 cells after induction and 8 hours of expression; A-E, eluted fraction of the purified proteins; Protein ladder, molecular weight marker (kDa).

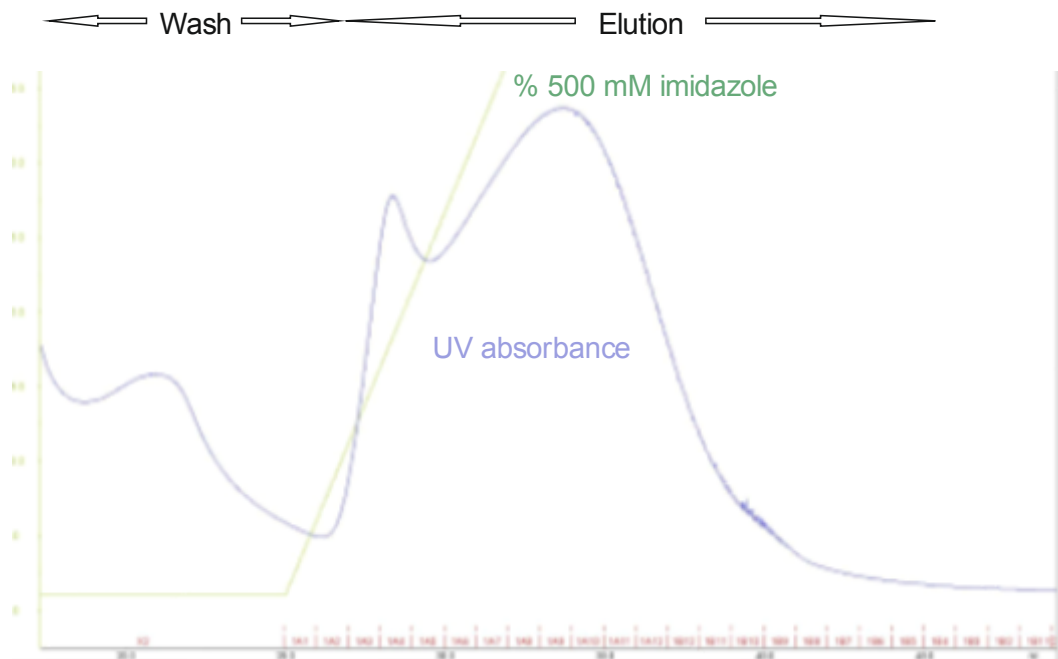


**Figure 4.21:** FPLC Purification profile of HIS-tagged MerA using AKTA Fast Protein Liquid Chromatography (FPLC) purification system. A280 absorbance of liquid from the column flow-through (blue line) and percentage of elution buffer in the column wash buffer (light green line).

### 4.3.7 MerA activity assays with mercury

The tolerance of cells of *E. coli* BL21 expressing MerA to mercury was quantified by measuring the cell growth at OD 600 nm. As shown in Figure 4.22, both the MerA and empty vector containing strains grew rapidly in the absence of mercury. In the presence of 5  $\mu\text{M}$  mercury, the MerA expressing strain grew significantly faster than the cells containing the empty vector. The growth rate of cells of *E. coli* BL21 expressing MerA progressively decreased as the concentration of mercury increased to 10 and 20  $\mu\text{M}$  but reached the same OD with 0 and 5  $\mu\text{M}$  mercury after 24 hours of incubation. The cells containing the empty vector were unable to grow in media containing 10 and 20  $\mu\text{M}$  mercury chloride.

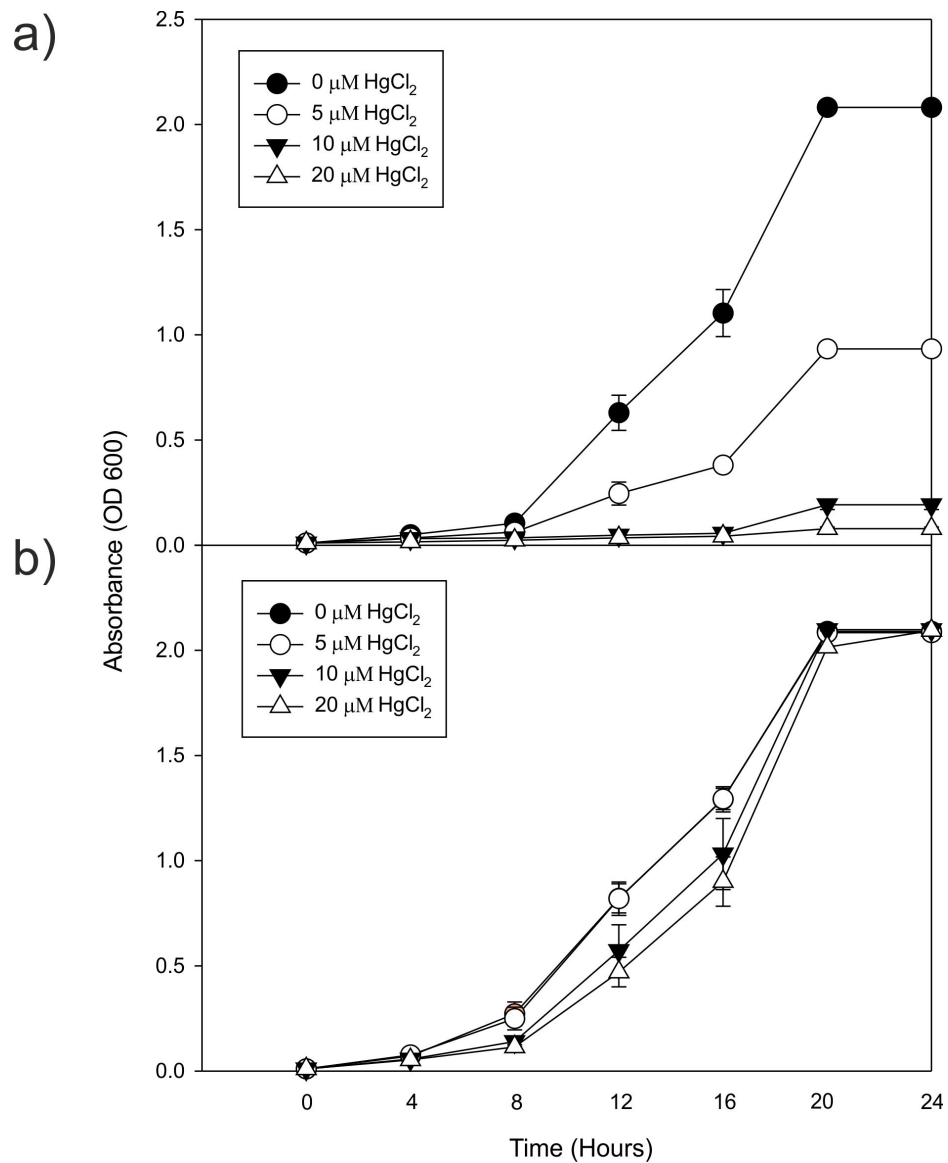


**Figure 4.22:** Growth of cells of *E. coli* BL21 with a) pET16b empty vector and b) pET16b-MerA in LB media with different concentrations of mercury.

To determine the activity of purified, recombinant MerA using mercury as substrate, the oxidation of NADPH was determined by measuring the decrease in absorbance at 340 nm. Figure 4.23 shows the Michaelis-Menten plot obtained for MerA, with a  $V_{\max}$  value of  $0.261 \pm 0.01 \mu\text{mol}\cdot\text{min}^{-1}\cdot\text{mg}^{-1}$  and  $K_m$  value of  $36.50 \pm 3.80 \mu\text{M}$ .

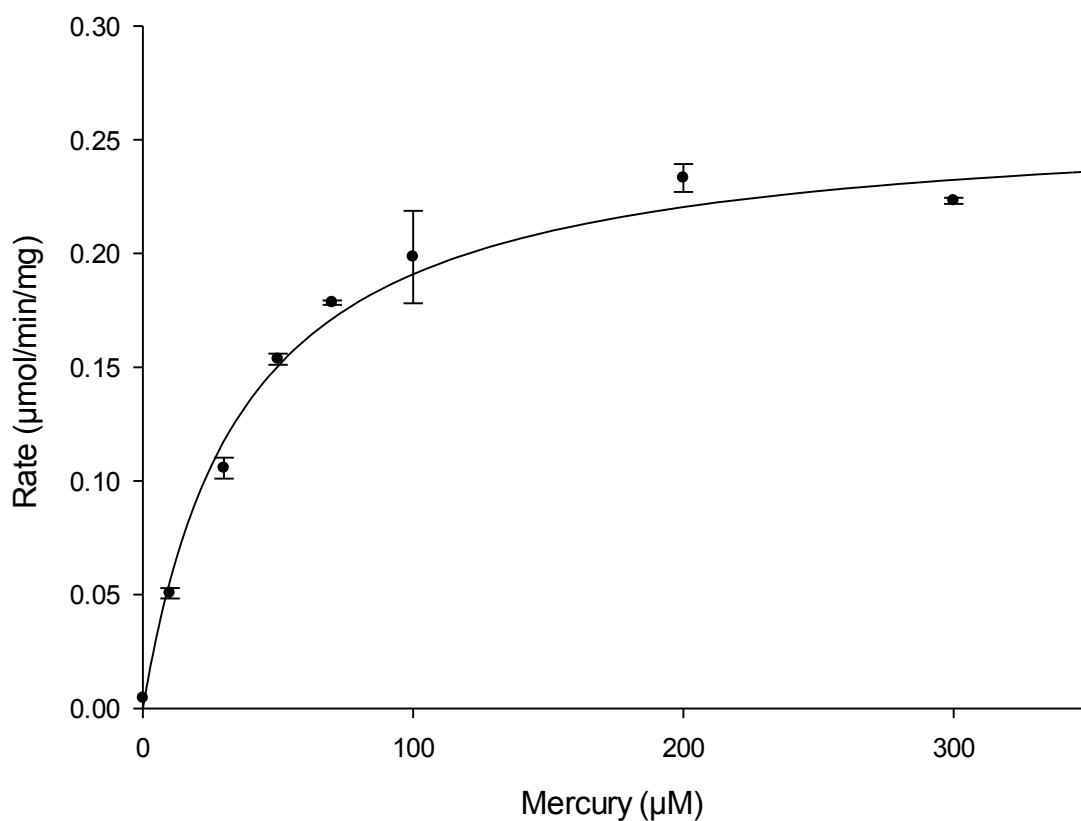


**Figure 4.23:** Michealis-Menten plot showing activity of MerA as measured by the oxidation of NADPH using  $\text{HgCl}_2$  as substrate. Reactions were performed in triplicates  $\pm$  SD.

Different concentrations of purified MerA were tested using 100  $\mu\text{M}$  of Hg. As expected, the rate of activity increased as the concentration of MerA increased (Figure 4.24). No activity was detected with boiled denatured MerA. Exogenous thiol is also required by MerA to prevent the formation of an inhibitory complex between the free Hg ion and the thiolate pair at the N terminal of the enzyme [231]. To confirm that MerA requires the mercury thiolate complex ( $\text{Hg}(\text{SG})_2$ ) instead of free ionic mercury for activity, glutathione was used in the assay. The results in Figure 4.24 show that there was no MerA activity in the absence of glutathione (exogenous thiol).

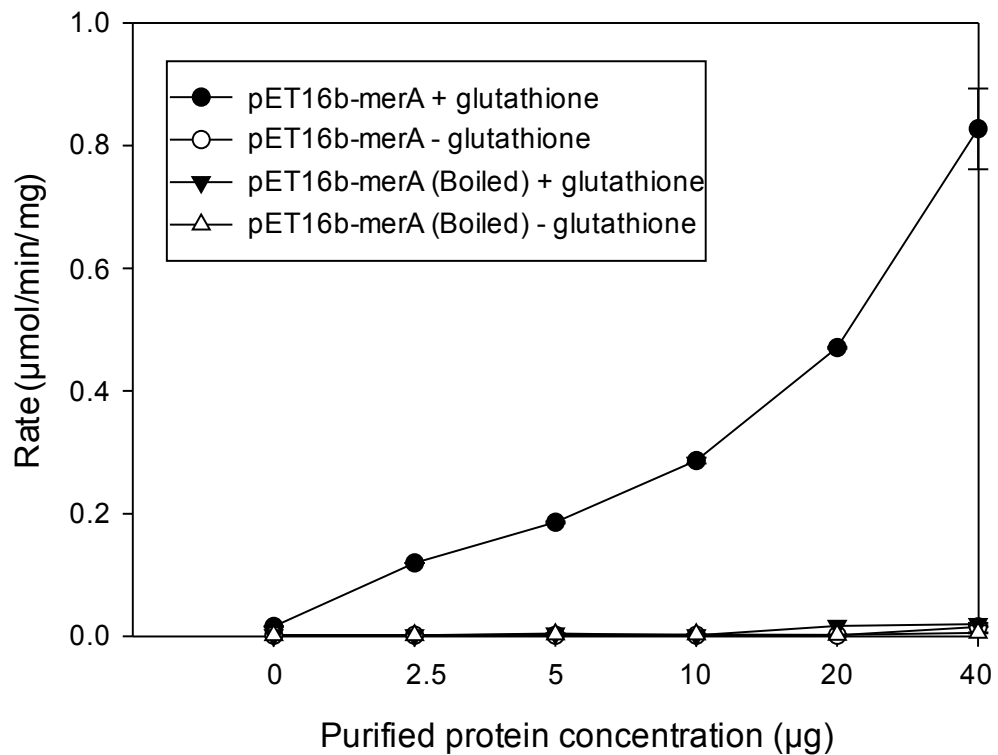


**Figure 4.24:** Activity of purified MerA with 100  $\mu\text{M}$  Hg as substrate. Reactions were performed in triplicates  $\pm$  SD.

#### 4.3.8 Enzymatic assay of MerA activity on gold and palladium

To explore the possibility that MerA has activity towards gold and palladium, similar assays to those conducted using mercury were repeated using gold and palladium as substrates. At the concentration of MerA (10  $\mu\text{g/mL}$ ) that yielded ( $0.261 \pm 0.01 \mu\text{moles/min/mg}$ ) activity towards mercury, there was no decrease in A340 when gold or palladium were supplied as substrate. To investigate if increasing the amount of MerA in the assay would result in detectable NADPH oxidation activity, the amount of MerA was increased by 55- fold to 550  $\mu\text{g/mL}$ , but no activity was detected (Figure 4.25).

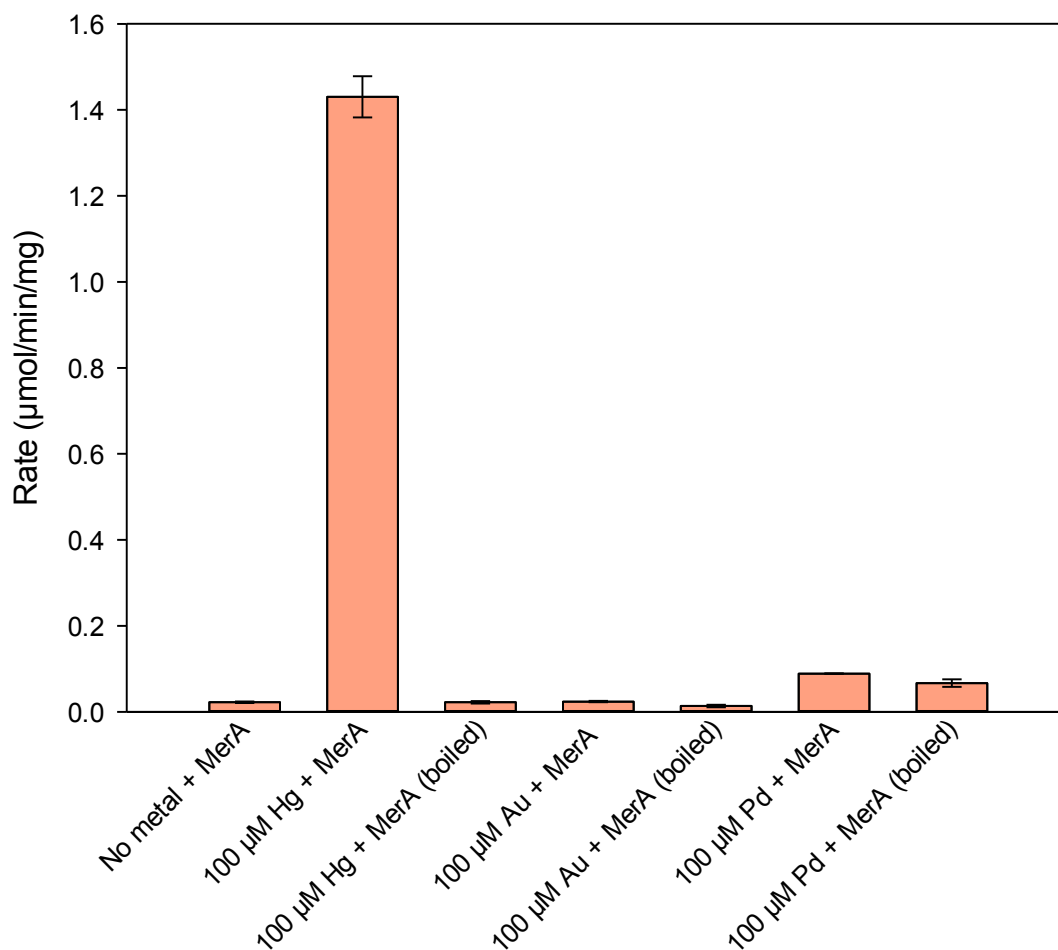


**Figure 4.25:** Activity rate of NADPH oxidation by MerA with 100  $\mu\text{M}$  of mercury, gold and palladium as substrate. Reactions were performed in triplicates  $\pm$  SD.

#### 4.3.9 Enzymatic assay of MerA activity on gold and palladium as inhibitors

Since no activity could be detected when gold or palladium was used as substrate for MerA, the inhibitory activity of these metals in the presence of mercury was investigated. When mercury was used as substrate, as expected, oxidation of NADPH to NADP<sup>+</sup> was detected (Figure 4.26 & 4.27) and when boiled MerA which was assayed, there was no activity in the presence of mercury. However, when gold was added together with the same concentration of mercury the activity rate decreased (Figure 4.26). A similar observation was also seen with palladium (Figure 4.27). The rate detected with boiled MerA and palladium was most likely the result of an increase in absorbance caused by precipitation observed upon palladium addition (Figure 4.27). Using mercury as substrate, the effect of gold or palladium on the activity of a range of MerA concentrations was also tested. Figure 4.28 shows that, with increasing concentration of MerA, activity rates with mercury as substrate, increased, indicating that MerA was not saturating under these conditions. In the presence of gold, MerA activity decreased by approximately 40 %. The presence of palladium was even more inhibitory to MerA, with activity decreased by 70 %. It was also observed that the activity of MerA in the presence of mercury and palladium was significantly lower than in the presence of mercury and gold at 10, 20 and 40  $\mu\text{g}$  of MerA concentrations (ANOVA Tukey's test  $p < 0.001$ ).

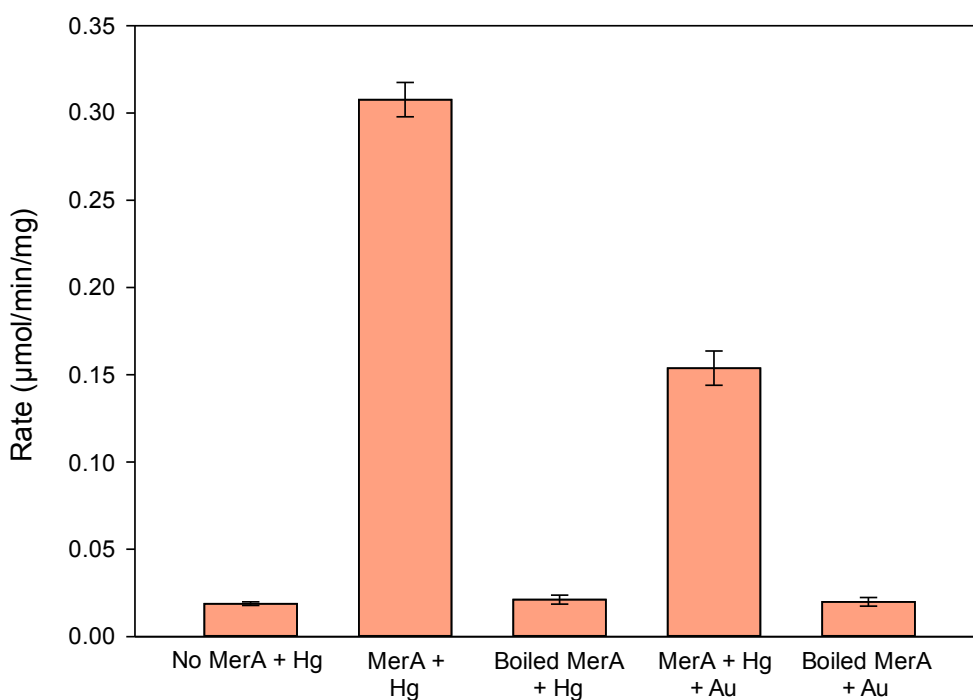


**Figure 4.26:** Activity rate of NADPH oxidation by MerA with 100  $\mu\text{M}$  of mercury and gold as substrate containing a final concentration of 40  $\mu\text{g}/\text{ml}$  purified MerA. Reactions were performed in triplicates  $\pm$  SD.

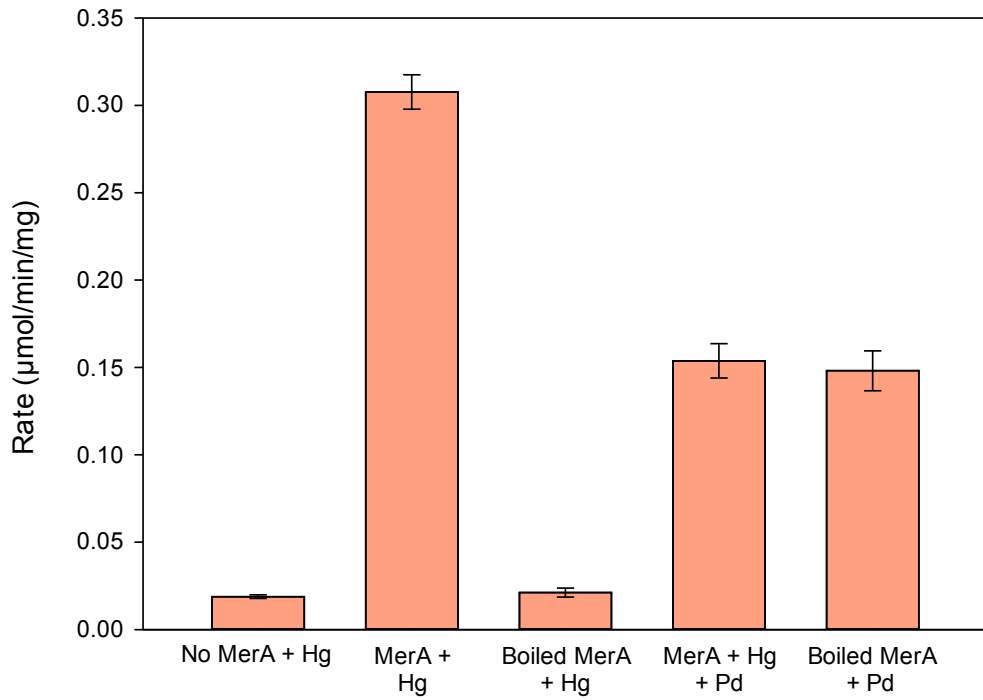


**Figure 4.27:** Activity rate of NADPH oxidation by MerA with 100 μM of mercury and palladium as substrate containing a final concentration of 40 μg/ml purified MerA. Reactions were performed in triplicates ± SD.

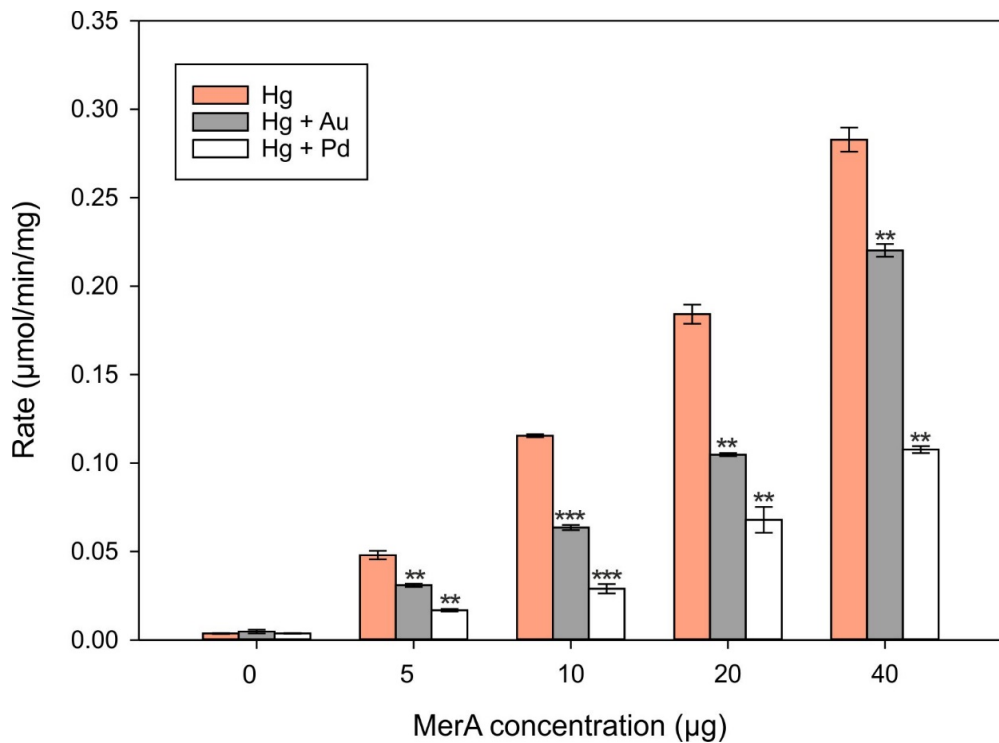


**Figure 4.28:** Activity of MerA with 100 μM Hg, 50 μM Au and 50 μM Palladium as substrate at different concentration of purified MerA. Reactions were performed in triplicates ± SD. Student's T-test \*\* = p<0.01, \*\*\* = p<0.001 significantly different to mercury only as substrate.

#### 4.3.10 Effect of gold and palladium on MerA activity with mercury

The inhibitory effect of gold or palladium to MerA was further investigated by plotting Michaelis-Menten curves to obtain the  $K_m$  and  $V_{max}$  values in the presence of different concentrations of gold or palladium. In this experiment, the rate in the absence of gold was compared to the rate in the presence of 50, 100 and 150  $\mu\text{M}$  of gold. As observed in Figure 4.29 and Table 4.1, the  $V_{max}$  for MerA decreased as the concentrations of gold increased. The  $K_m$  value however varied at different concentrations of gold tested.

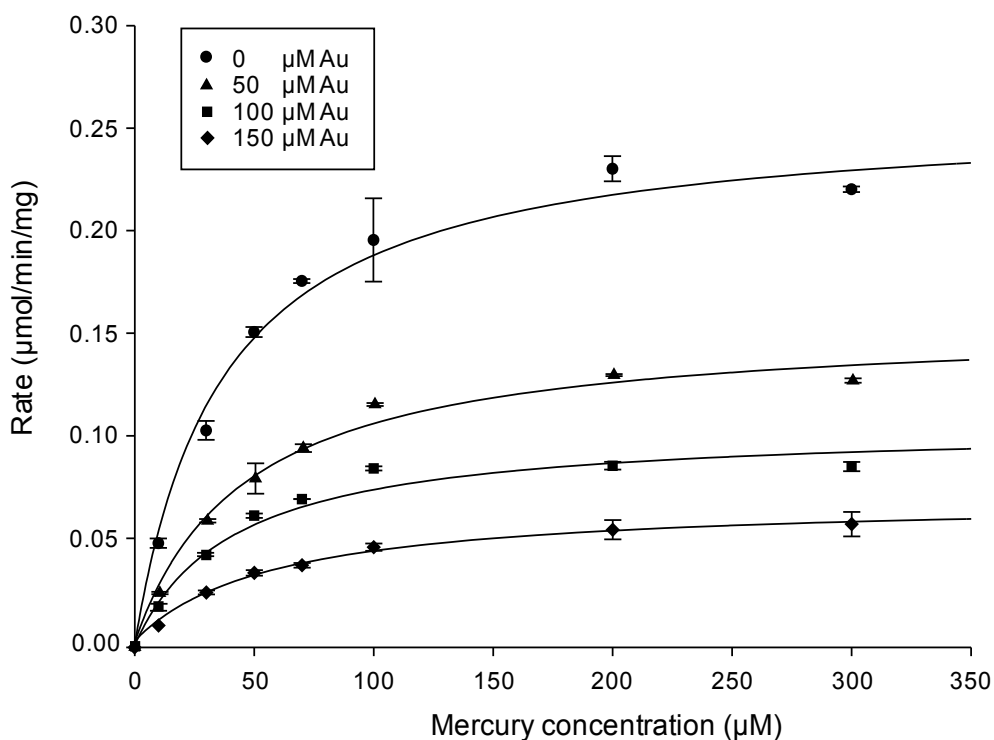


**Figure 4.29:** Michaelis-Menten plots for MerA using mercury as substrate, and a range of gold concentrations. Results are the mean of triplicates  $\pm$  SD.

**Table 4.1:**  $K_m$  and  $V_{max}$  values for MerA using mercury as substrate in the presence of gold.

Au ( $\mu\text{M}$ )	$K_m \pm \text{SD}$	$V_{max} \pm \text{SD}$
0	$49.04 \pm 8.73$	$0.286 \pm 0.02$
50	$46.07 \pm 4.37$	$0.155 \pm 0.01$
100	$41.13 \pm 5.93$	$0.107 \pm 0.01$
150	$58.04 \pm 8.95$	$0.069 \pm 0.01$

Lineweaver-Burk double reciprocal plots of MerA activity are shown in Figure 4.30 and fit the requirements of a mixed inhibition effect for gold.

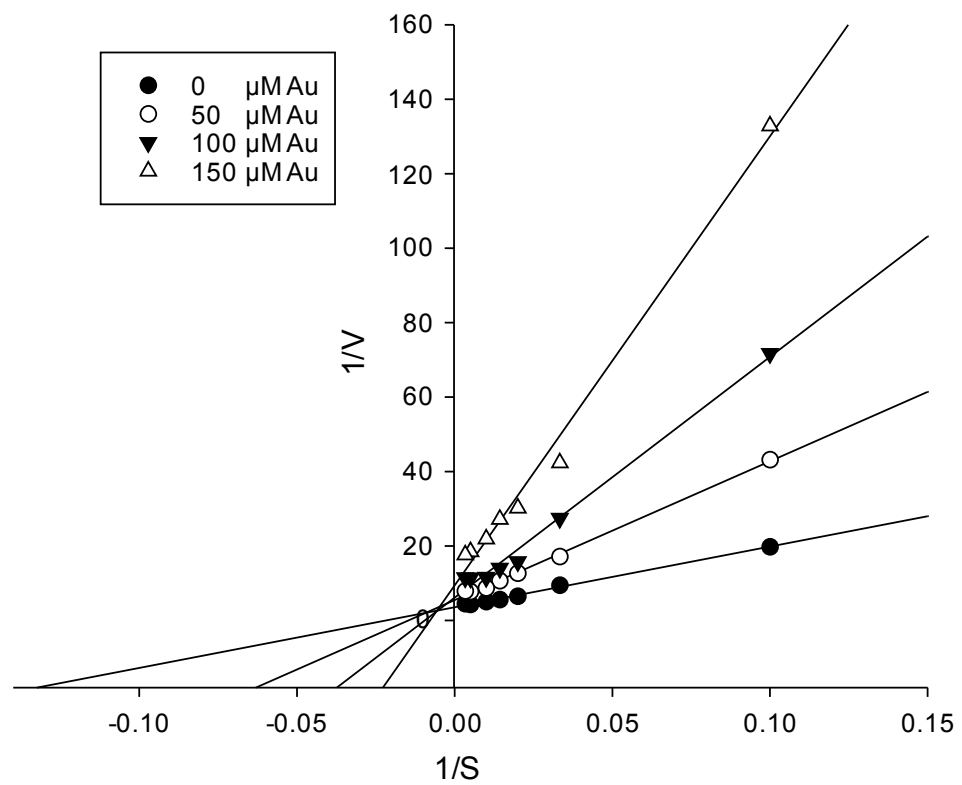


**Figure 4.30:** Lineweaver-Burk double reciprocal plots for MerA with different concentrations of gold.

To determine if there is an inhibitory effect of palladium on the activity of MerA using mercury as substrate, activity of MerA in the absence of palladium was also compared to the rate in the presence of 50, 100 and 150  $\mu\text{M}$  of palladium. As shown in Figure 4.31 and Table 4.2, increasing concentrations of palladium caused inhibition of MerA activity.

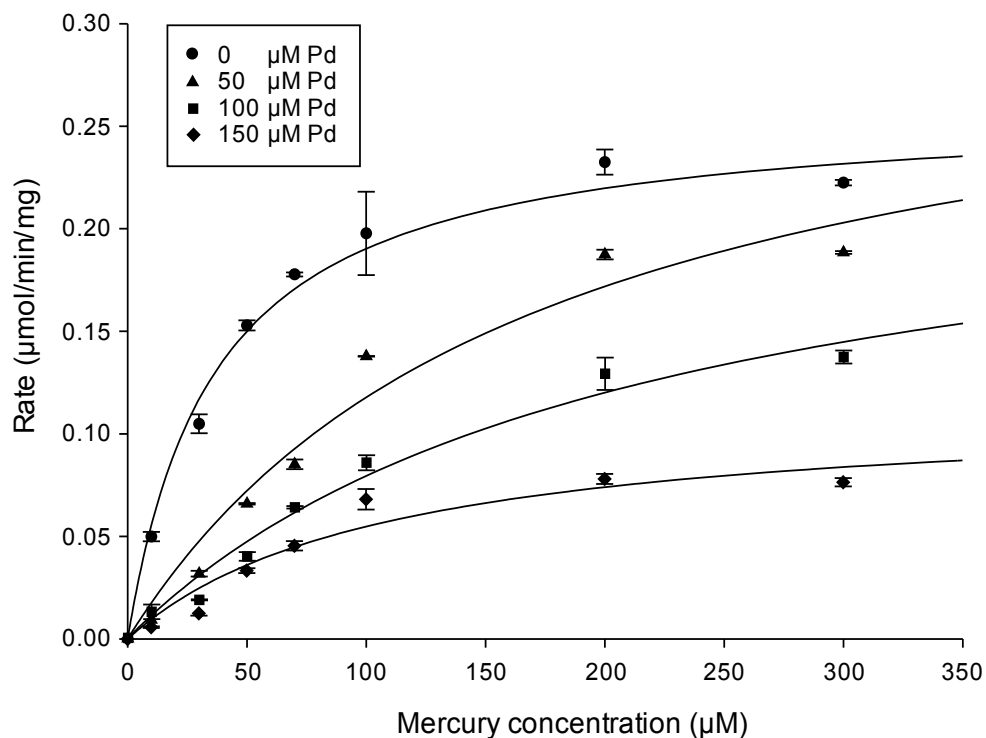


**Figure 4.31:** Michaelis-Menten plots of MerA using mercury as substrate, and a range of palladium concentrations. Results are the mean of triplicates  $\pm$  SD.

**Table 4.2:**  $K_m$  and  $V_{max}$  values for MerA using mercury as substrate in the presence palladium.

Palladium ( $\mu\text{M}$ )	$K_m \pm SD$	$V_{max} \pm SD$
0	$49.04 \pm 8.73$	$0.286 \pm 0.02$
50	$167.01 \pm 36.09$	$0.303 \pm 0.03$
100	$230.63 \pm 59.42$	$0.258 \pm 0.04$
150	$156.65 \pm 52.31$	$0.129 \pm 0.02$

The data were then plotted as a Lineweaver-Burk plot, shown in Figure 4.32. These results also showed that palladium had a mixed inhibitory effect on MerA.

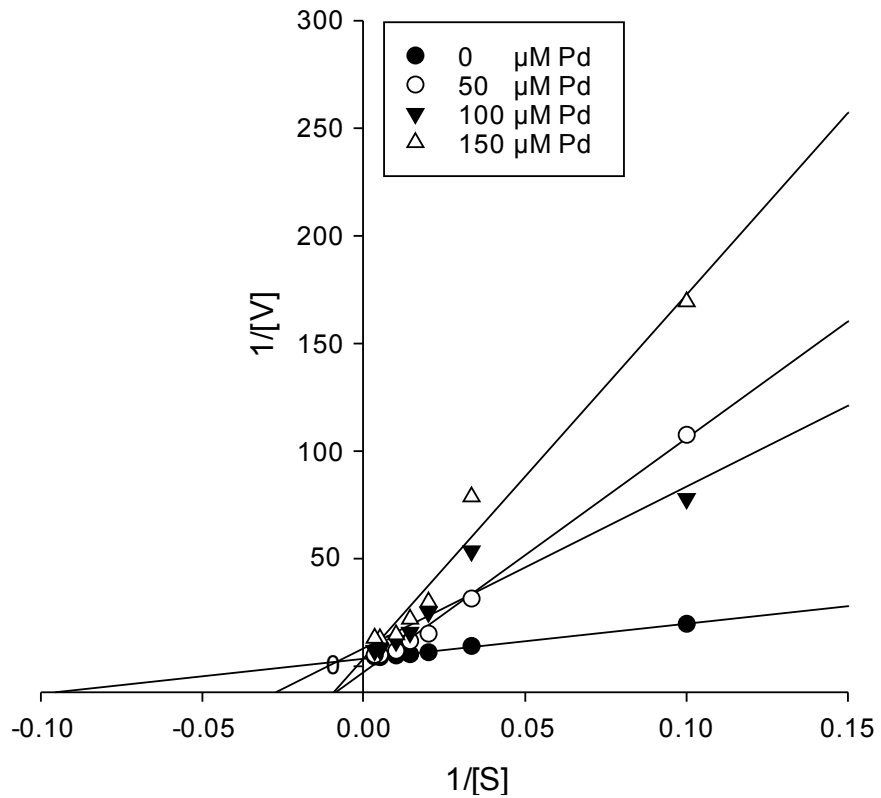


**Figure 4.32:** Lineweaver-Burk double reciprocal plots for MerA with different concentrations of palladium.

#### **4.3.11 Inhibition study of MerA transgenic lines on gold and palladium**

As gold and palladium inhibit the activity of purified, recombinant MerA, the inhibition of gold and palladium on MerA-expressing plants grown in the presence of mercury was investigated.

In this experiment, 50  $\mu\text{M}$  of mercury was chosen because at this concentration, the greatest difference in root length between wildtype and MerA-expressing seedlings was easily distinguished in earlier experiments (Section 4.3.2).

MerA seedlings were grown on  $\frac{1}{2}$  MS (A) containing 50  $\mu\text{M}$  of mercury and a range of gold concentrations (0, 50, 100, 150 and 200  $\mu\text{M}$ ). As a comparison, the transgenic seedlings were also grown on  $\frac{1}{2}$  MS (A) containing gold alone (0, 50, 100, 150 and 200  $\mu\text{M}$ ). After 12 days of growth, both mercury plus gold and gold only treatment had caused a significant reduction on the root lengths of the plants as the concentrations of gold increased (ANOVA Tukey's test  $p < 0.001$ ) (Figure 4.34). It was also observed that the root lengths of the seedlings grown on mercury (50  $\mu\text{M}$ ) in the presence of 50, 100, 150 and 200  $\mu\text{M}$  of gold were reduced up to 16, 32, 72 and 96 % when compared with the seedlings grown on media containing mercury only (50  $\mu\text{M}$ ) suggesting the effect of gold on the activity of MerA to mercury (ANOVA Tukey's test  $p < 0.001$ ) (Figure 4.33 & 4.34).

Similar observation was obtained when the MerA-expressing seedlings were grown on media containing palladium with mercury. The presence of an increased concentration of palladium (5, 10 & 15  $\mu\text{M}$ ) together with 50  $\mu\text{M}$  of mercury or without mercury treatment had significantly reduced the root length of MerA-expressing seedlings (ANOVA Tukey's test  $p < 0.001$ ) (Figure 4.35 & 4.36). The presence of 5, 10 & 15  $\mu\text{M}$  palladium together with 50  $\mu\text{M}$  of mercury had also reduced the root length of the MerA seedlings up to 36, 19 and 48 % reduction respectively when compared to mercury only (50  $\mu\text{M}$ ) treatment suggesting an inhibitory effect on the activity of MerA caused by the presence of palladium.

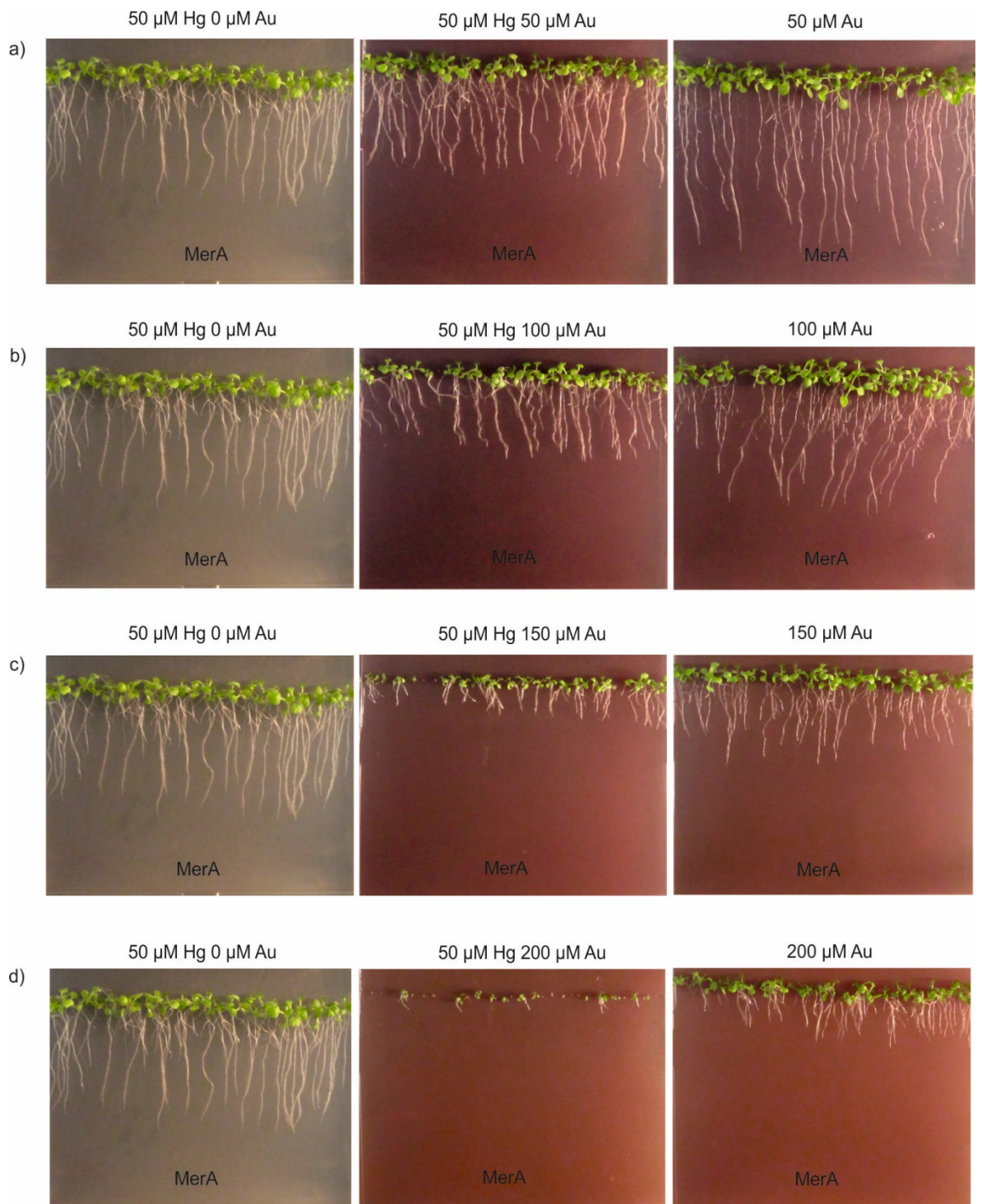


**Figure 4.33:** Appearance of 12 day-old Arabidopsis Col-0 MerA-expressing seedlings on  $\frac{1}{2}$  MS (A) plates containing a range of mercury and gold concentrations.

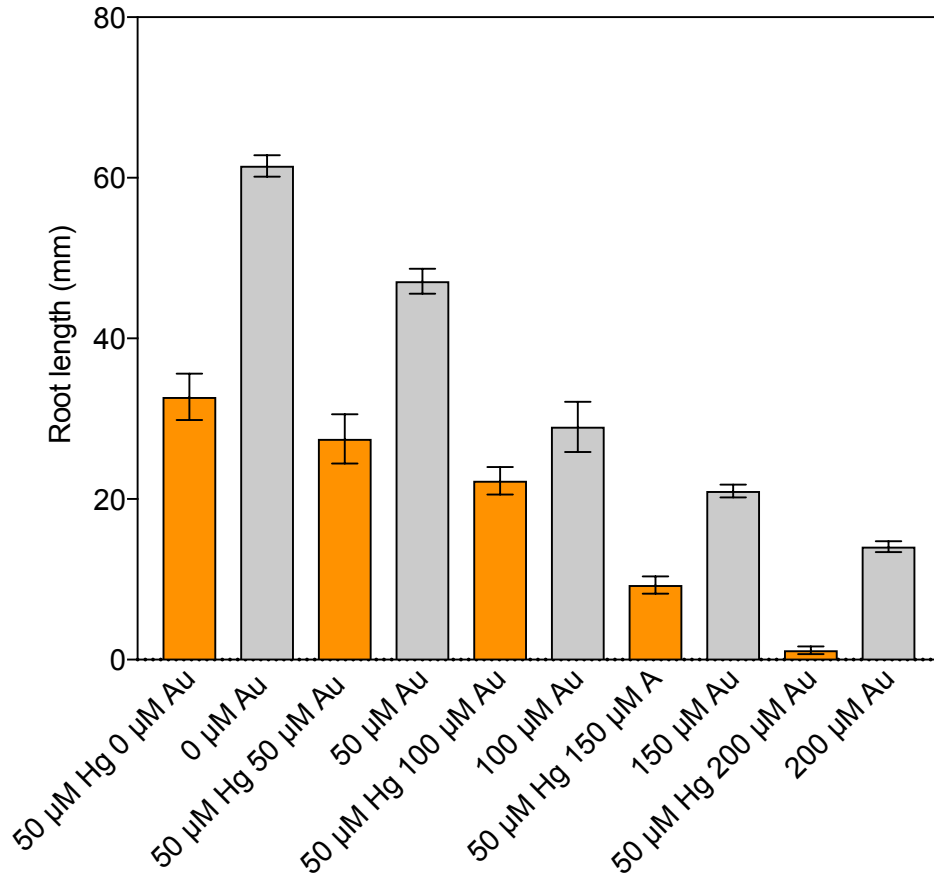


**Figure 4.34:** Root lengths of 12 day-old *Arabidopsis* Col-0 MerA-expressing seedlings on  $\frac{1}{2}$  MS (A) media containing the combination of 50  $\mu$ M of mercury and an increasing concentration of gold and media containing gold only as indicated in the figure. Results are the mean from 30 biological replicates. ANOVA Tukey's test.

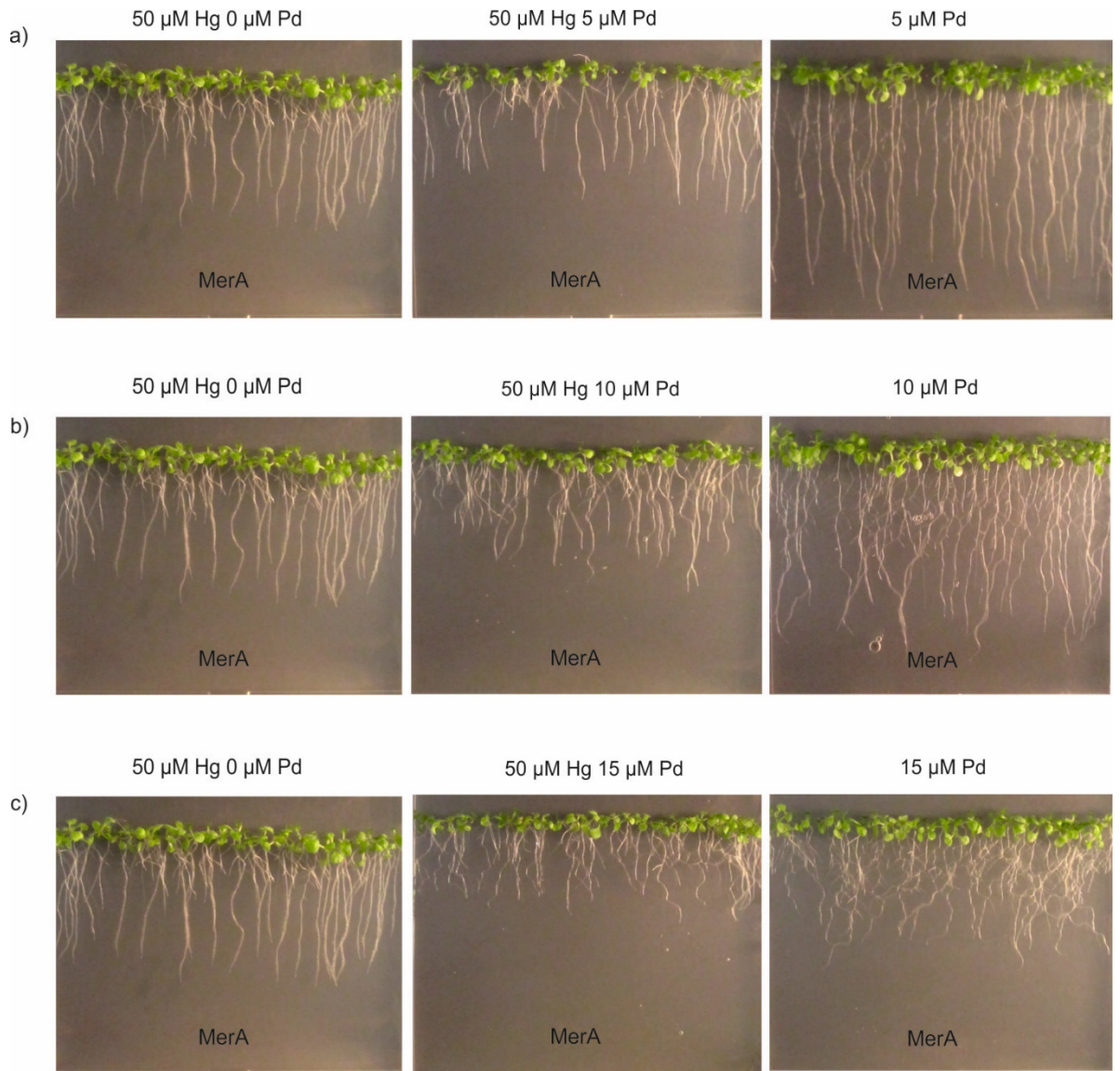


**Figure 4.35:** Appearance of 12 day-old Arabidopsis Col-0 MerA-expressing seedlings on  $\frac{1}{2}$  MS (A) plates containing a range of mercury and palladium concentrations.

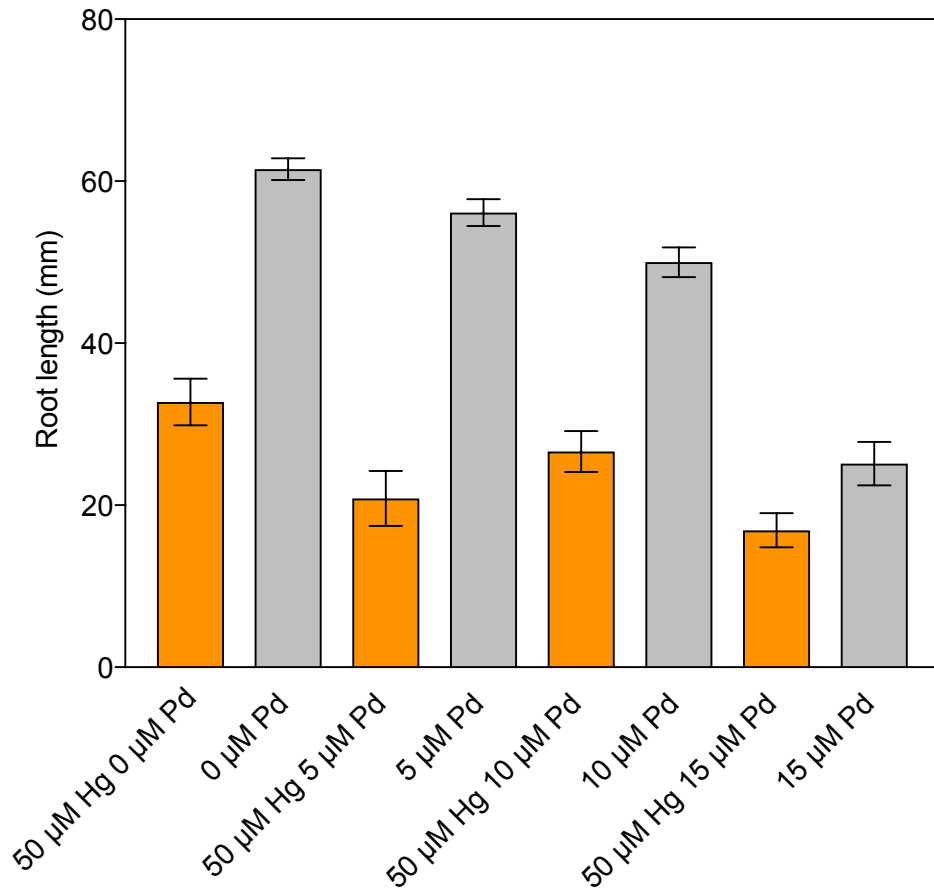


**Figure 4.36:** Root lengths of 12 day-old *Arabidopsis* Col-0 MerA-expressing seedlings on  $\frac{1}{2}$  MS (A) media containing the combination of 50  $\mu$ M of mercury and an increasing concentration of palladium and media containing palladium only as indicated in the figure. Results are the mean from 30 biological replicates. ANOVA Tukey's test.

## **4.4 Discussion**

### **4.4.1 Genetic engineering to increase formation of metal nanoparticles**

Genetic engineering has been shown to be an efficient approach to improve the ability of plants to accumulate and tolerate high concentration of heavy metals [86, 135, 137, 139]. This can be achieved by overexpressing genes that are responsible for metal uptake and also by introducing foreign genes that are able increase tolerance either by metal sequestration, chelation or reduction. Transgenic plants have been shown to increase accumulation, translocation and tolerance to many non-essential heavy metals including lead [213], arsenic [139] and mercury [135]. However, not much focus has been given to improve plants uptake and tolerance to precious metals including gold and palladium.

Gold and palladium are non-essential transition heavy metal, which are normally present in field locations as chemically inert, zero-valent form, or bound to minerals. However, gold and palladium can be accumulated by plant species such as *Berkheya coddii* [157] and *Brassica juncea* [92, 123, 126]. Following recent studies on the formation of gold [46, 47] and palladium [22] nanoparticles in Arabidopsis, it was found that the plant-based palladium nanoparticles could to be used as catalysts in many chemical reactions [22]. Therefore, aside from remediating contaminated mine wastes area, plant could also potentially be used as an alternative to host and produce various sizes of highly valuable precious metal nanoparticles.

In this work, the potential of mercuric reductase expressed in Arabidopsis was investigated for their potential to increase gold and palladium uptake and tolerance in plants.

#### 4.4.2 Mercuric reductase

*Arabidopsis* plants expressing MerA were able to tolerate levels of gold toxic to wildtype plants [135]. This finding was also supported by previous observations by Summers and Sugarman where gold was shown to be a substrate for MerA [143]. However, no further investigations on the activity of MerA to gold have been reported. As gold is chemically similar to palladium, it was hypothesised that palladium might also be a substrate for MerA and increase tolerance to palladium and possibly improve nanoparticle accumulation in plants. This work has investigated the activity of MerA on gold and palladium using purified, recombinant MerA and both *E. coli* and *Arabidopsis* expressing MerA.

As reported previously, the MerA-expressing lines exhibited enhanced resistance to mercury. Interestingly however, MerA-expressing seedlings were significantly shorter than wildtype when grown on gold ( $p < 0.001$ ) (Figure 4.14) or palladium. It is possible that the inhibition is caused by an increased accumulation of gold or palladium in the MerA-expressing lines compared to the wildtype due to the presence of two metal binding domains MXCXXC found in MerA that bind various heavy metals such as copper, cadmium and silver [232]. Further quantification analysis using ICP-MS on the accumulation of gold and palladium between the MerA-expressing plants and wildtype would show whether there is an increase in gold and palladium levels in the MerA-expressing plants.

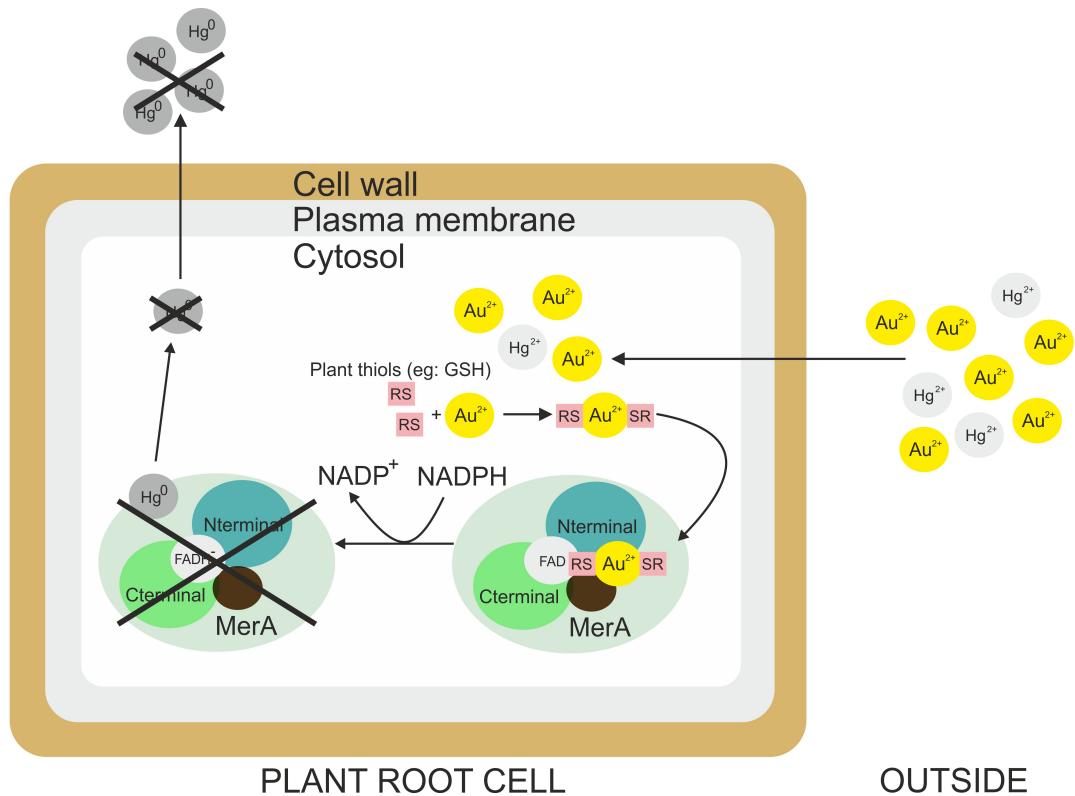


**Figure 4.37:** Putative diagram of expected MerA mechanism in *Arabidopsis* root cell in the presence of gold. Based on the results obtained in Section 4.2.1.11, in the presence of mercury and gold, an increased concentration of gold inhibits the MerA reduction activity on Hg<sup>2+</sup> to Hg<sup>0</sup>. Thus, gold inhibits mercury tolerance in MerA-expressing seedlings. Similar mechanism could be explained in the presence of palladium.

Previous studies have shown that gold is a substrate for MerA and that it confers resistance to gold toxicity when expressed in *Arabidopsis* [135, 143]; however, it was not possible to repeat these earlier findings. In this study the MerA plant lines displayed resistance to mercury but did not show any increased tolerance to gold or palladium. It is difficult to explain this discrepancy, as the full-length *merA* sequence used by Rugh was not published; there might have been a mutation in the Rugh sequence that conferred activity of MerA tolerance to gold.

The activity of MerA to gold was further investigated using purified recombinant protein. As expected, there was no activity when glutathione as the thiol was not used, confirming that exogenous thiol is needed in the reaction in order to prevent the formation of an abortive complex of Hg (II) with the thiolate pair of reduced MerA [50]. Free ionic mercury was also reported to form a covalent 1:1 complex with NADPH, which may also limit the activity of MerA [233].

The assay was repeated with gold and palladium but no activity could be detected even with higher concentrations of MerA (Figure 4.29). Rinderle et al [234] had suggested that gold could act as a non-competitive inhibitor to MerA. Based on this evidence, inhibition assays were conducted. Kinetic analysis using Michaelis-Menten and Lineweaver-burk plots (Figure 4.29- 4.32 & Table 4.3 & 4.4) indicate that gold and palladium are acting as mixed inhibitors of MerA. In mixed inhibition, an increase in  $K_m$  values shows that the inhibitor favours binding the free enzyme, while a decrease in  $K_m$  values indicates that the inhibitor binds preferentially to the enzyme-substrate complex. When gold was added into the reaction at the concentrations of 50 and 100  $\mu\text{M}$ , there was a decrease in the  $K_m$  value, indicating that gold inhibits MerA activity at these concentrations by binding to the MerA-Hg complex. But at 150  $\mu\text{M}$ , gold the affinity of the enzyme for the substrate by binding to the free enzyme complex was lower. In the addition of palladium, it was found that palladium had favoured binding to the free enzyme, causing a decreased affinity of the enzyme for substrate. It was also found that the presence of both metals decreased the maximum enzyme reaction rate. Previous studies have shown that transition metals were also able to inhibit the activity of MerA. It was reported that copper, gold, silver and zinc are also inhibitors of MerA [232, 234, 235]; however, this is the first report that demonstrates palladium as an inhibitor of MerA. The inhibition caused by these metals suggests that the activity of MerA could be affected if MerA transgenic plants were used to remediate mercury-contaminated land that was also contaminated with heavy metals. In agreement with this hypothesis, it was observed that the root length growth of MerA transgenic plants grown on media containing both gold (or palladium) and mercury were significantly inhibited when compared to transgenic plants grown on mercury alone. Overall, based on the results obtained in this work, it is concluded that gold and palladium are not substrates for MerA.

## **Chapter 5: The use of peptides to increase formation of gold and palladium nanoparticles in plants**

### **5.1 Introduction**

#### **5.1.1 Use of peptides for the formation of gold and palladium nanoparticles**

Biomining is the process of synthesizing nanomaterials using biological molecules [236]. One of the most recent biomining approaches, and considered as the future of 'green' synthesis, is using peptides isolated from biomining organisms for the development of catalysts [237-242]. These short (c.10-15 amino acid) peptides can be used to seed the production of metal nanoparticles. Selectively altering the amino acid sequence changes the reductive capabilities and binding strengths of the peptides enabling nanoparticles of different sizes and shapes to be produced.

To identify or isolate potential peptide candidates a 'top down' approach is used. This approach is based on screening peptides with diverse functional groups, and high affinities towards metal binding, as well as specific amino acids, which are able to reduce metal ions. It involves multistep processing including isolation, purification and cloning of specific proteins which can be very complex and time consuming [242]. Moreover, the active proteins identified from this method are always a minor component embedded in the myriad of proteins recovered, and can also vary widely in composition; features which may cause problems later when analysing and identifying the active proteins involved [242].

Researchers have also investigated the prospect of combinatorial screening approaches such as the phage display method to select peptide sequences that bind specially to inorganic surfaces such as metal (Figure 5.1) [237, 240]. Phage display is a powerful screening method whereby large peptide libraries are expressed as fusions with phage coat proteins resulting in the display of the fused peptide on the outer surface of the phage particle. The selection of desired peptides is achieved after multiple rounds of biopanning which is based on the affinity of the peptides towards specific targets. This technology offers an alternative 'green' approach for the use of non-natural peptides to control the fabrication of nanomaterials [240, 241]. Peptides identified via phage display method were also able to synthesize various shapes of silver [240], gold [243], platinum [244] and barium titanate [245] nanoparticles without any exogenous reducing agent [240].

Once candidate peptides have been isolated, a more focused methodology can be employed by constructing further peptides sequences based on known specific binding and reduction abilities towards metal. This 'bottom up' approach is aimed at identifying peptides capable of not just producing nanoparticles, but also allowing the manipulation of the size and shape of the nanoparticles. Tan et al [242] investigated the binding and reduction potential of 20 natural  $\alpha$ -amino acids with gold. Tryptophan (W) was found to be the fastest gold reducing amino acid while tyrosine (Y) had the strongest binding to gold. The potential of peptides to enhance the formation gold nanoparticles was further exploited by designing a combination of short, multifunctional peptides combining amino acids with various reduction and binding strengths [242] with the shape-directing peptide sequence SEKL-GASL [237]. Previous work by Brown et al [237] demonstrated that a peptide containing SEKL-GASL repeats, and isolated from *E. coli*, was able to direct the shape and formation of gold nanoparticles. However, due to its complex and relatively long sequence (>100-mer), the reduction rates were slow and the gold nanoparticles formed were relatively large in size (500-1000 nm diameter). By designing short multifunctional peptides which combined the shape-directing peptide sequence and different amino acids residues with various binding and reduction potential, Tan et al [18] demonstrated that these combinations were able to influence the size of gold nanoparticles formed *in vitro* as follows: SEKLGASL (control) > SEKLYYGASL > SEKLFFGASL > SEKLWWGASL > GASLWWSEKL [242] (Figure 5.2), with these peptides producing mean nanoparticle (termed 'plates' in the study) diameters of 20, 40, 80, 180 and 200 nm respectively (Figure 5.3). As nanoparticle size and shape can affect catalytic activity, this finding may offer another greener approach for industrial applications.

The ability of specific peptides to increase metal nanoparticle formation is not only limited to gold; peptides producing a range of palladium nanoparticles have also been reported [238, 241, 246]. Previously, palladium nanoparticles of varying size were shown to be formed by the use of strong reducing agents such as sodium borohydride ( $\text{NaBH}_4$ ) [238] and L-ascorbic acid [247]. However, the formation *in vitro* of smaller, more uniform palladium nanoparticles ( $2.9 \pm 0.4$  nm) were obtained using the peptide, QQSWPIS (Q7), which was isolated from a phage display library [238]. In the same study, tryptophan (W) was also found to be important in both the reduction and binding of palladium. Another peptide which was found to enhance the *in vitro* formation of various sizes of palladium nanoparticles is TSNAVHPTLRHL (Pd4) [241]. Pd4, also isolated via the phage display method, produces palladium

nanoparticles *in vitro* with a diameter of  $1.9 \pm 0.3$  nm [241]. These nanoparticles were further found to be catalytically active for Stille coupling reactions [241].

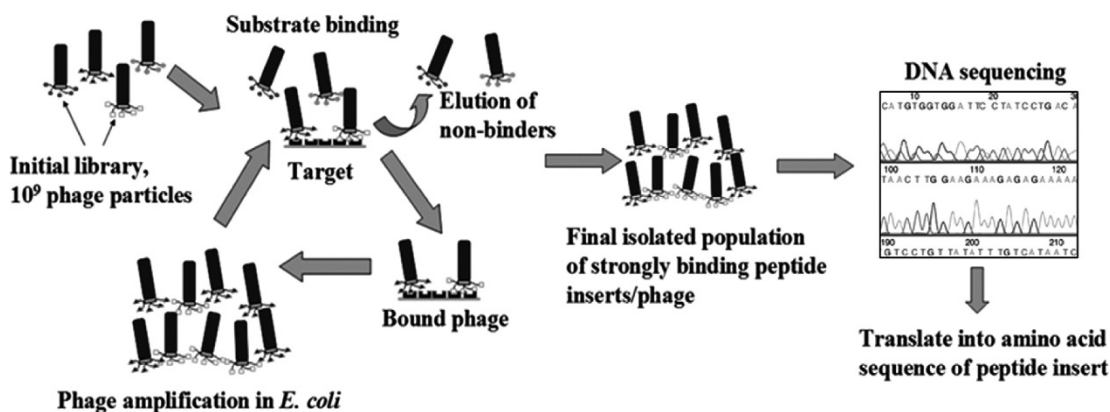


**Figure 5.1:** An illustration of the bio-panning process to isolate peptides possessing high affinity towards inorganic material through phage display. Figure reproduced from Dickerson et al [239].

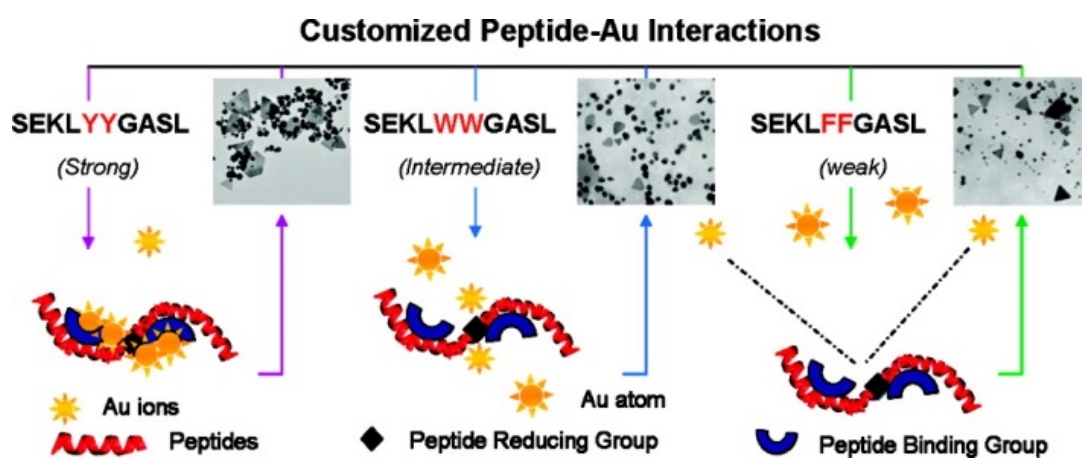


**Figure 5.2:** The use of peptides for gold nanoparticle formation showing different sizes and shapes of nanoparticles as a result of strong, intermediate and weak metal binding peptides. Figure reproduced from Tan et al [242].

**Table 5.1:** Peptide sequences involved in formation of metal nanoparticles.

Peptide	Metal	Nanoparticle Diameter Formed (nm)	Reference
SEKLGASL	Au	~180	[248]
SEKLFFGASL	Au	~80	
SEKLWWGASL	Au	~40	
GASLWWSEKL	Au	~20	
QQSWPIS	Pd	2.9 ± 0.4	[238]
TSNAVHPTLRHL	Pd	2.0 ± 0.4	[249]

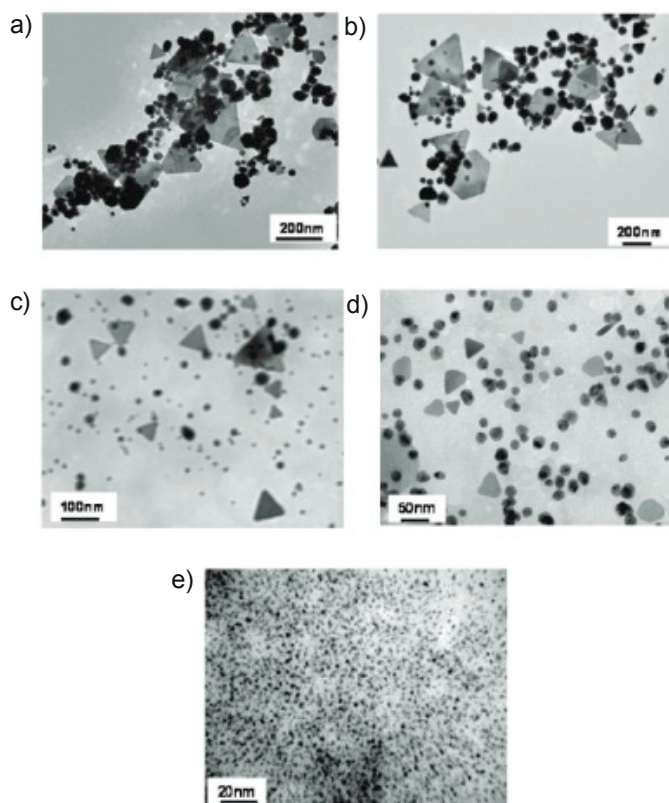


**Figure 5.3:** TEM images of peptide synthesis of gold nanoparticles using multifunctional peptides a) SEKLGASL b) SEKLYYGASL c) SEKLFFGASL d) SEKLWWGASL e) GASLWWSEKL. Picture re produced from Tan et al [248].

### 5.1.2 Metal nanoparticle formation in plants

Following uptake in Arabidopsis, both gold [46, 47] and palladium [22] appear to be rapidly reduced, and accumulate as nanoparticles within plant tissues. Previous work has shown that metal nanoparticles are formed by living organism such as plants, algae and bacteria [250-253]. Bio-based metal nanoparticles have also shown promising catalytic ability in a variety reactions such as Stille, Suzuki and Heck coupling reactions [241]. However, metal nanoparticles produced from bacteria may have some limitations in terms of their application. Strong reducing agents such as sodium borohydride  $\text{NaBH}_4$  [238] and sodium hypophosphite ( $\text{NaPH}_2\text{O}_2$ ) [254] are always required for nanoparticle formation in bacteria. Sulphur, can also be released when bacterial cells disintegrate at high ( $>60\text{ }^\circ\text{C}$ ) temperature. Sulphur will integrate into the reactions and could reduce performance of catalyst used [253].

Plants have been proposed as a viable alternative for metal nanoparticles synthesis [22]. Unlike commercially grown bacterial cultures, plants are autotrophic, and well known for their ability to uptake metals, and they are also capable of reducing metal ions to form crystalline nanostructures [125]. It is also known that plants can deposit gold and palladium as metal nanoparticles [22, 47]. Thus, plant biomass containing metal nanoparticles could be used to make efficient catalysts. The production of the plant-based catalyst also requires fewer processing steps compared with current catalyst production.

Prof Neil Bruce's group, along with colleagues from the Green Chemistry Centre of Excellence at York have shown that Arabidopsis containing palladium nanoparticles can be used to produce supported palladium catalysts, without using any toxic chemicals or energy intensive processes [22]. They also observed that the supported catalysts had activity compared to commercially available palladium catalysts. While studies have demonstrated the ability of specific peptides to reduce ionic gold and palladium into metal nanoparticles *in vitro* [238, 240, 242, 246, 248, 255, 256], no one has yet published studies transferring this technology into plants. This chapter explores the potential of six peptides (SEKLWWGASL, SEKLFFGASL, SEKLGASL, GASLWWSEKL, Q7 and Pd4) (Table 5.1) to seed the formation of gold and palladium nanoparticles *in planta*.

## 5.2 Materials and methods

### 5.2.1 Production of transgenic *Arabidopsis* expressing short synthetic peptides

Six DNA sequences encoding short peptides were purchased as single-stranded short oligonucleotides (primers) (Table 5.2). The DNA sequences were first codon optimized to improve protein expression in *Arabidopsis*. This work was done by an undergraduate project student, Ivan Gyulev, using software obtained from <http://www.kazusa.or.jp/codon/>. The oligonucleotides were re-suspended and mixed in order to allow double-stranded DNA to form. Each peptide-encoding DNA was synthesized with flanking regions homologous to the desired insertion site into the pART7 vector. In-Fusion Cloning (Clontech inc.) was used to introduce the peptide DNA sequence into this plasmid. The subsequent DNA cassette containing the peptide-encoding DNA, flanked by CaMV-35S promoter and ocs terminator regions, was transferred into the binary pART27 using *NotI* restriction sites [229]. The pART27 vector contains a selectable marker, *nptII*, which confers resistance to kanamycin. The pART27-with insert was used to transform electro-competent *Agrobacterium tumefaciens* as explained in Section 2.5.9. Genotyping of the T3 generation of homozygous transgenic lines and qPCR analysis for expression profiling to measure the transcript level of inserted peptides sequences were successfully conducted by Dr. Emily Johnston.

**Table 5.2:** Primers used to synthesise peptides

Peptides	Ordered primers (5'-3')
SEKLGASL (Delta)	TTTGGAGAGGACACGCTCGAGTGTGCTATGTCTGAAAAGTTGGGAGCTTCTCTTTAATGACGATCATATGAAGCTTTCGAGGAATTCGGTA
	TACCGAATTCCTCGAAAGCTTCATATGATCGTCATTAAGAGAAGCTCCCAACTTTTCAGACATAGCGACACTCGAGCGTGTCTCTCCAAA
SEKLFFGASL (Beta)	TTTGGAGAGGACACGCTCGAGTGTGCTATGTCTGAAAAGTTGTTTTTGGAGCTTCTCTTTAATGACGATCATATGAAGCTTTCGAGGAATTCGGTA
	TACCGAATTCCTCGAAAGCTTCATATGATCGTCATTAAGAGAAGCTCCAAAAACAACCTTTTCAGACATAGCGACACTCGAGCGTGTCTCTCCAAA
SEKLWWGASL (Alpha)	TTTGGAGAGGACACGCTCGAGTGTGCTATGTCTGAAAAGTTGTGGTGGGGAGCTTCTCTTTAATGACGATCATATGAAGCTTTCGAGGAATTCGGTA
	TACCGAATTCCTCGAAAGCTTCATATGATCGTCATTACAACCTTTTCAGACCACCAAAGAGAAGCTCCCATAGCGACACTCGAGCGTGTCTCTCCAAA
GASLWWSEKL (Epsilon)	TTTGGAGAGGACACGCTCGAGTGTGCTATGGGAGCTTCTCTTTGGTGGTCTGAAAAGTTGTAATGACGATCATATGAAGCTTTCGAGGAATTCGGTA
	TACCGAATTCCTCGAAAGCTTCATATGATCGTCATTACAACCTTTTCAGACCACCAAAGAGAAGCTCCCATAGCGACACTCGAGCGTGTCTCTCCAAA
QQSWPIS (Zeta)	TTTGGAGAGGACACGCTCGAGTGTGCTATGCAACAATCTTGGCCTATTTCTTAATGACGATCATATGAAGCTTTCGAGGAATTCGGTA
	TACCGAATTCCTCGAAAGCTTCATATGATCGTCATTAAGAAATAGGCCAAGATTGTTGCATAGCGACACTCGAGCGTGTCTCTCCAAA
TSNAVHPTLRHL (Eta)	TTTGGAGAGGACACGCTCGAGTGTGCTATGACTTCTAATGCTGTTTCATCCTACTCTTAGACATCTTTAATGACGATCATATGAAGCTTTCGAGGAATTC
	TACCGAATTCCTCGAAAGCTTCATATGATCGTCATTAAGATGTCTAAGAGTAGGATGAACAGCATTAGAAGTCATAGCGACACTCGAGCGTGTCTCTCTC
pART7 Forward	ACGTTCCAACCACGTCTT
pART7 Reverse	GAATGAACCGAAACCGGCG

### 5.2.2 Whole-plant liquid culture experiments

To measure the formation of metal nanoparticles in the peptide-expressing transgenic lines, whole-plant liquid culture experiments were conducted (Figure 5.4). Sterilised seedlings were sprinkled on to  $\frac{1}{2}$  MS agar plates and stratified (cold room, in dark) for 3 days. The seedlings were transferred to the growth room and grown vertically for 7 days. Eight seedlings of the 7-day-old plants were then transferred into 100 mL conical flasks containing 20 mL of  $\frac{1}{2}$  MS media. The plants were grown in the liquid culture on a shaker in growth room (130 rpm) for a further 2 weeks. The media was then replaced with 20 mL of 0.75 mM potassium (III) tetrachloroaurate in water and returned to the growth room at 130 rpm for another 24 hours. Seven biological replicates from three plant lines of each peptide were analysed in this experiment. After 24 hours of treatment, the 22 day-old plants were washed three times in distilled water directly into conical flask for rinsing.

For TEM analysis, one leaf was removed from one gold-treated and one control-treated flask for each genotype. Sections cut out in fixative, prepared for TEM analysis, and images taken by Liz Rylott and Meg Stark, detailed protocols are in Section 3.2.5.

Nanoparticle cross-sectional diameter was measured from TEM images of the plant using ImageJ software (version 1.5). A minimum of 100 (but often >250) nanoparticles were measured for each material. All of the images analysed were taken at 105K magnifications.

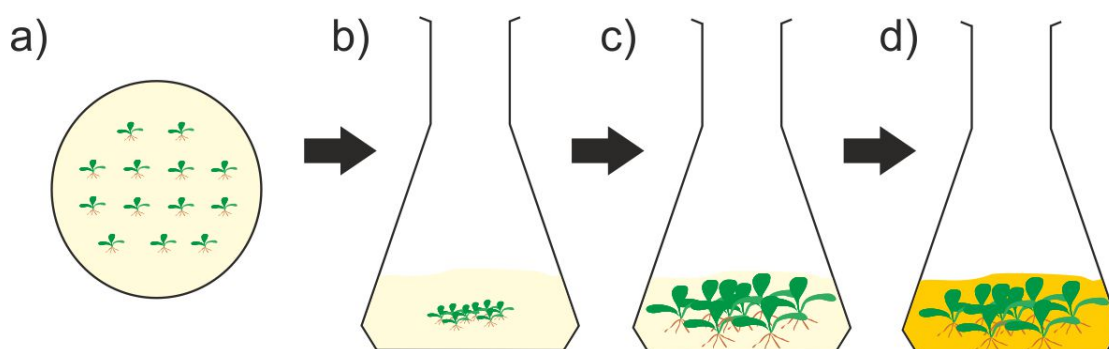


**Figure 5.4:** Whole-plant liquid culture experimental settings. a) Seedlings were grown on  $\frac{1}{2}$  MS agar for 7 days. b) 7 day-old seedlings were transferred into 100 mL flask containing 20 mL  $\frac{1}{2}$  MS media. c) Plants were grown for another 2 weeks d) Media was replaced with 20 mL metal solution and grown for another 24 hours before harvesting.

## 5.3 Results

### 5.3.1 Peptide expressing Arabidopsis lines

Figure 5.5 explains the cloning strategy involved on introducing the peptide DNA sequences into pART27. The constructs with the insert were sent for sequence for verification. Analytical digestion was used to verify the insert. Genotyping conducted by Dr. Emily Johnston showed that all plant lines tested contained the gene of interest (results not shown). Subsequent qPCR analysis, also done by Dr. Emily Johnston, showed transcript levels of epsilon, alpha, beta and delta (Figure 5.6). Expression analysis on the eta and zeta lines were yet to be conducted due to time limitation.

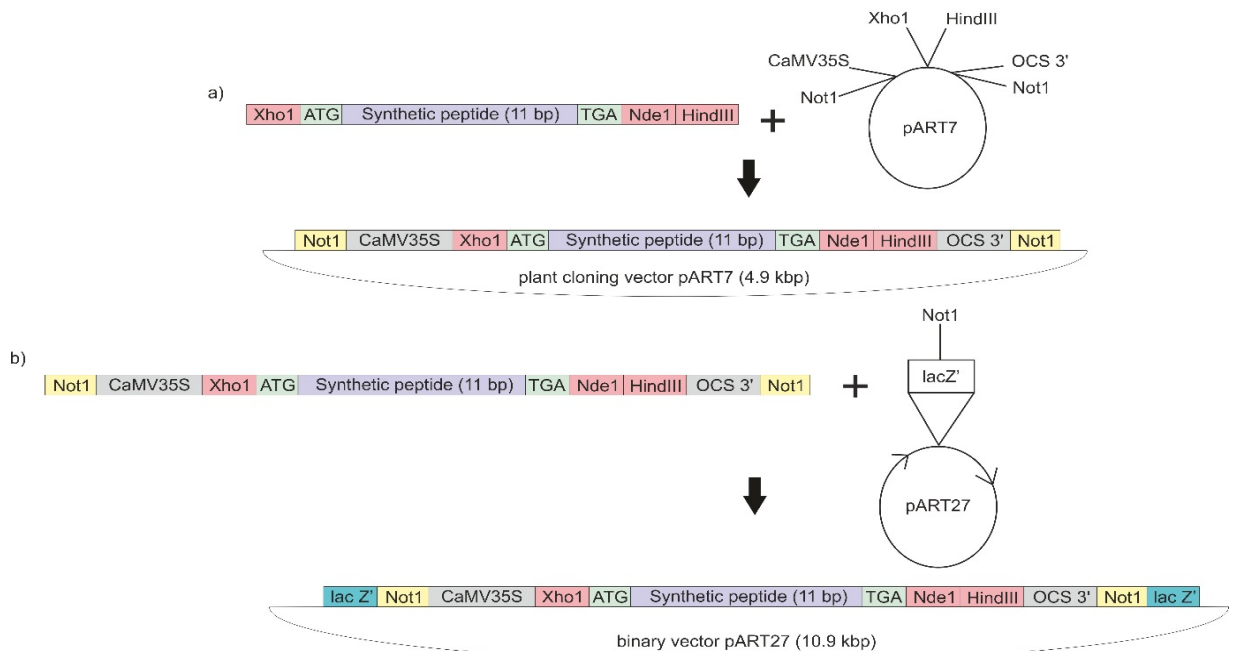


**Figure 5.5:** Cloning strategy of synthetic peptides. a) Peptide-coding sequences with flanking digest sites constructed and ordered as primer sequences, PCR, and then *XhoI* and *HindIII* digest for ligation into pART7. b) *NotI* used to digest peptide with flanking CaMV35S and ocs 3' sequences from pART7, into pART27.

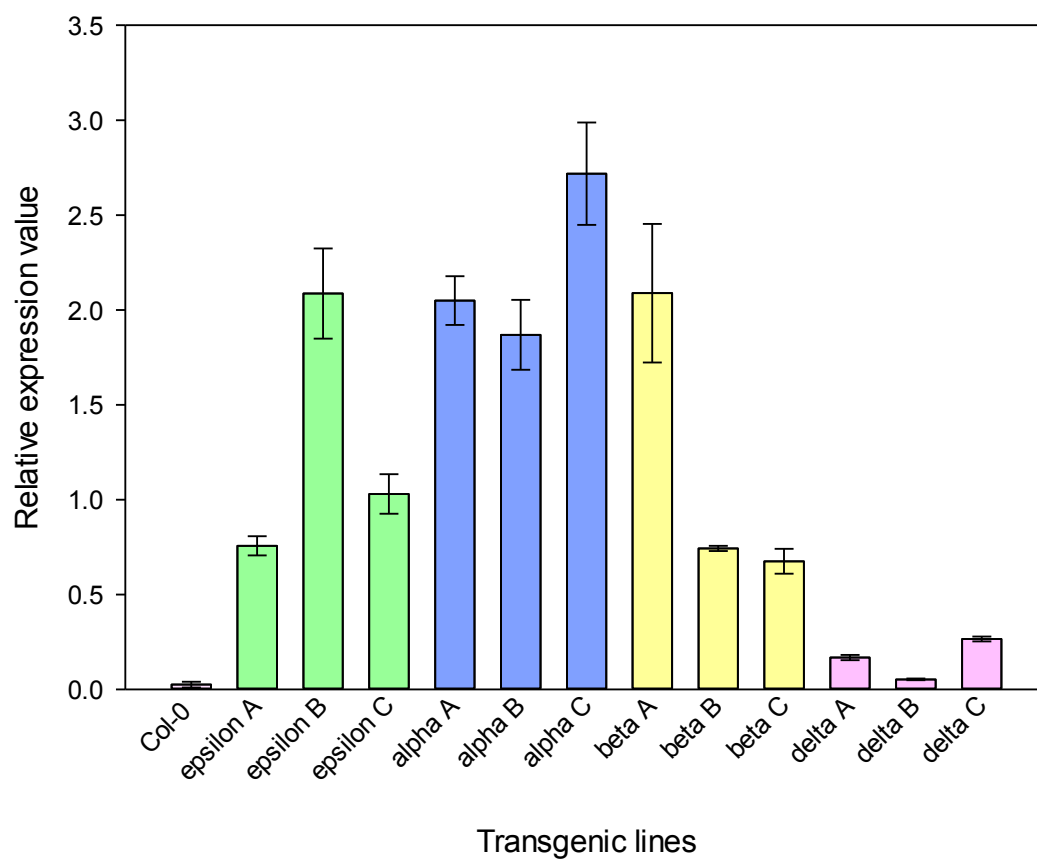


**Figure 5.6:** Relative expression of *epsilon*, *alpha*, *beta* and *delta* transcript levels of transgenic plants relative to delta B. The data were normalized to the Arabidopsis *ACTIN* gene and relative fold induction were calculated using the  $\Delta\Delta Ct$  method [230]. Results are the mean from seven biological replicates of three plant lines  $\pm$  SD. Results obtained from Dr. Emily Johnston.

### 5.3.2 Formation of gold nanoparticles from peptide-expressing transgenic plants

Whole-plant liquid culture experiments were conducted to investigate the potential of the synthetic peptides to seed the formation of various sizes of metal nanoparticles *in planta*. Results shown here are from the epsilon, alpha, beta and delta lines which yield gold nanoparticles formation [242]. Due to time constraints, the eta and zeta lines were not investigated further in this study.

The TEM images and histograms from the leaves of all plants tested are shown in Figure 5.7 to 5.10. These results revealed that after 24 hours of dosing with 0.75 mM gold solution, the plants had formed various sizes of well-dispersed gold nanoparticles. Epsilon lines had the highest (23 %) distribution of small (< 10 nm) gold nanoparticles followed by alpha, wildtype, beta and delta with 20, 20, 16 and 8 % respectively (Figure 5.11). No significant different could be observed between each lines except for delta which stated the lowest percentage distribution of small gold nanoparticles (<10 nm) (ANOVA Tukey's test  $p < 0.001$ ). Interestingly, the opposite was observed for large (> 30 nm) nanoparticles with the epsilon lines exhibiting 2 % as compared to alpha, wildtype, beta and delta with each stated 4, 6, 4 and 8 % distribution respectively (Figure 5.12).

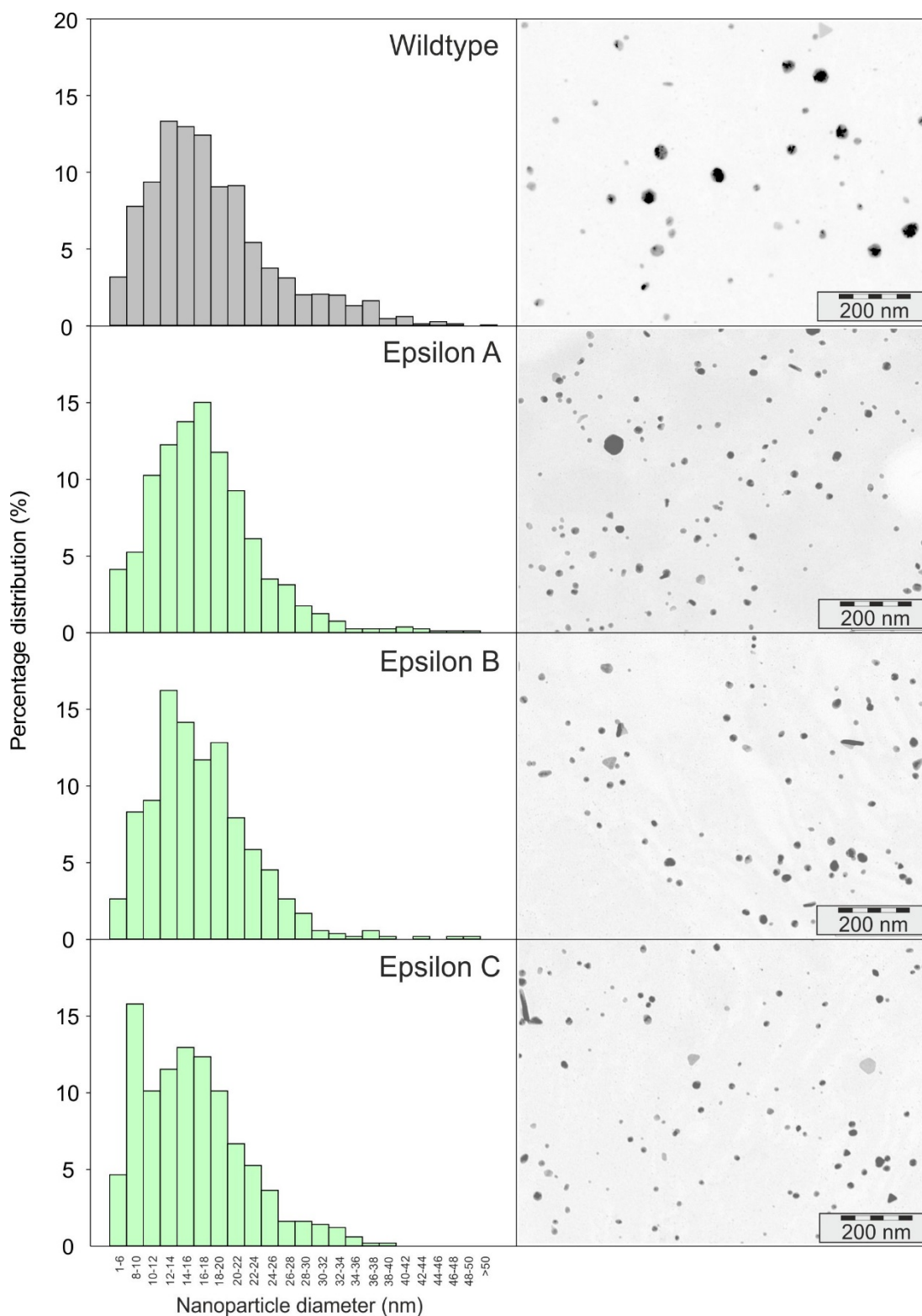


**Figure 5.7:** Histogram of percentage distribution of gold nanoparticles and TEM images at 105k magnification obtained from Arabidopsis Col-0 wildtype and three, independently-transformed epsilon lines after treatment with gold for 24 hours. Percentage distributions are constructed based on the TEM images taken from a single leaf from seven biological replicates of three epsilon lines.

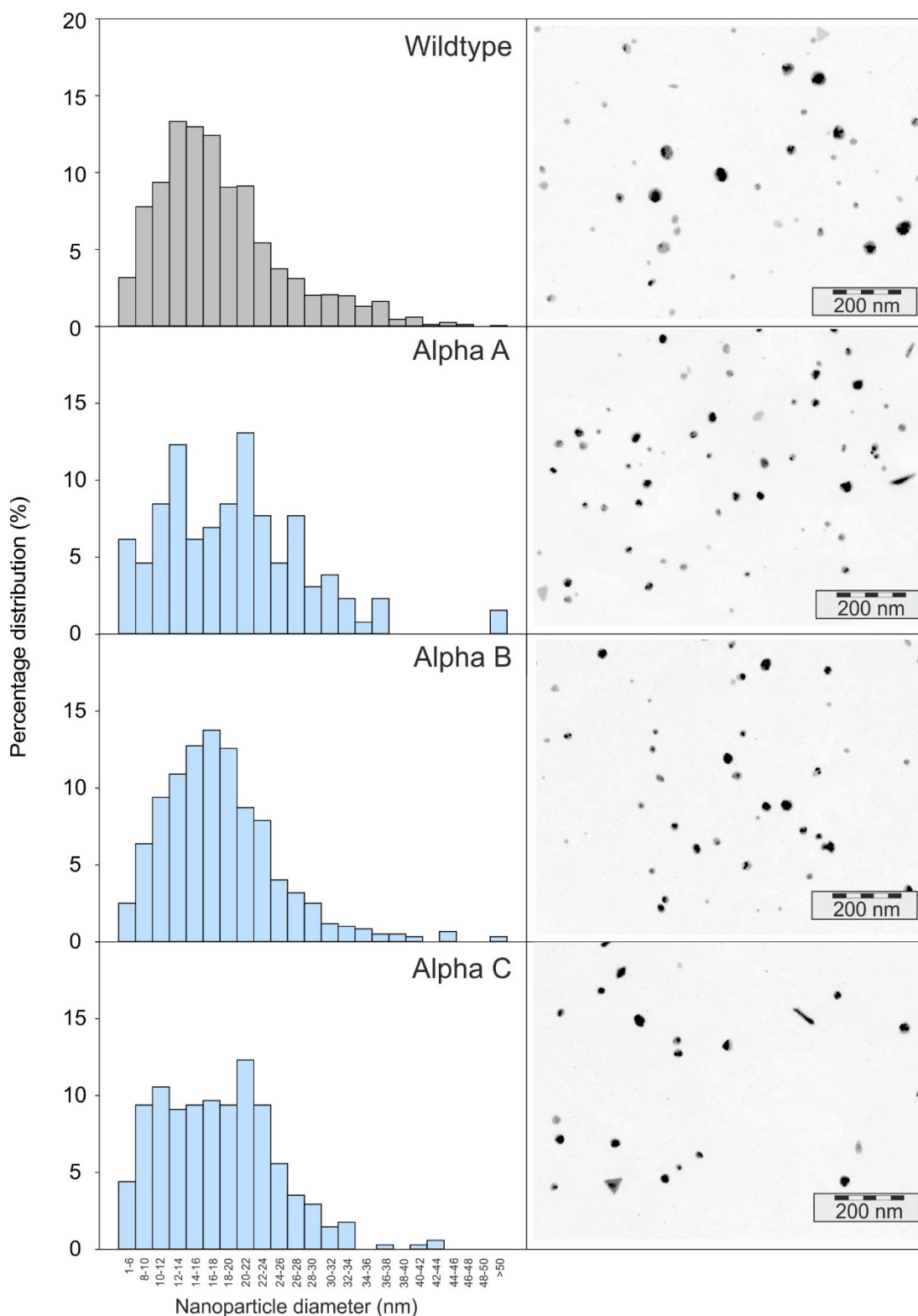


**Figure 5.8:** Histogram of percentage distribution of gold nanoparticles and TEM images at 105k magnification obtained from Arabidopsis Col-0 wildtype and three, independently-transformed alpha lines after treatment with gold for 24 hours. Percentage distributions are constructed based on the TEM images taken from a single leaf from seven biological replicates of three alpha lines.

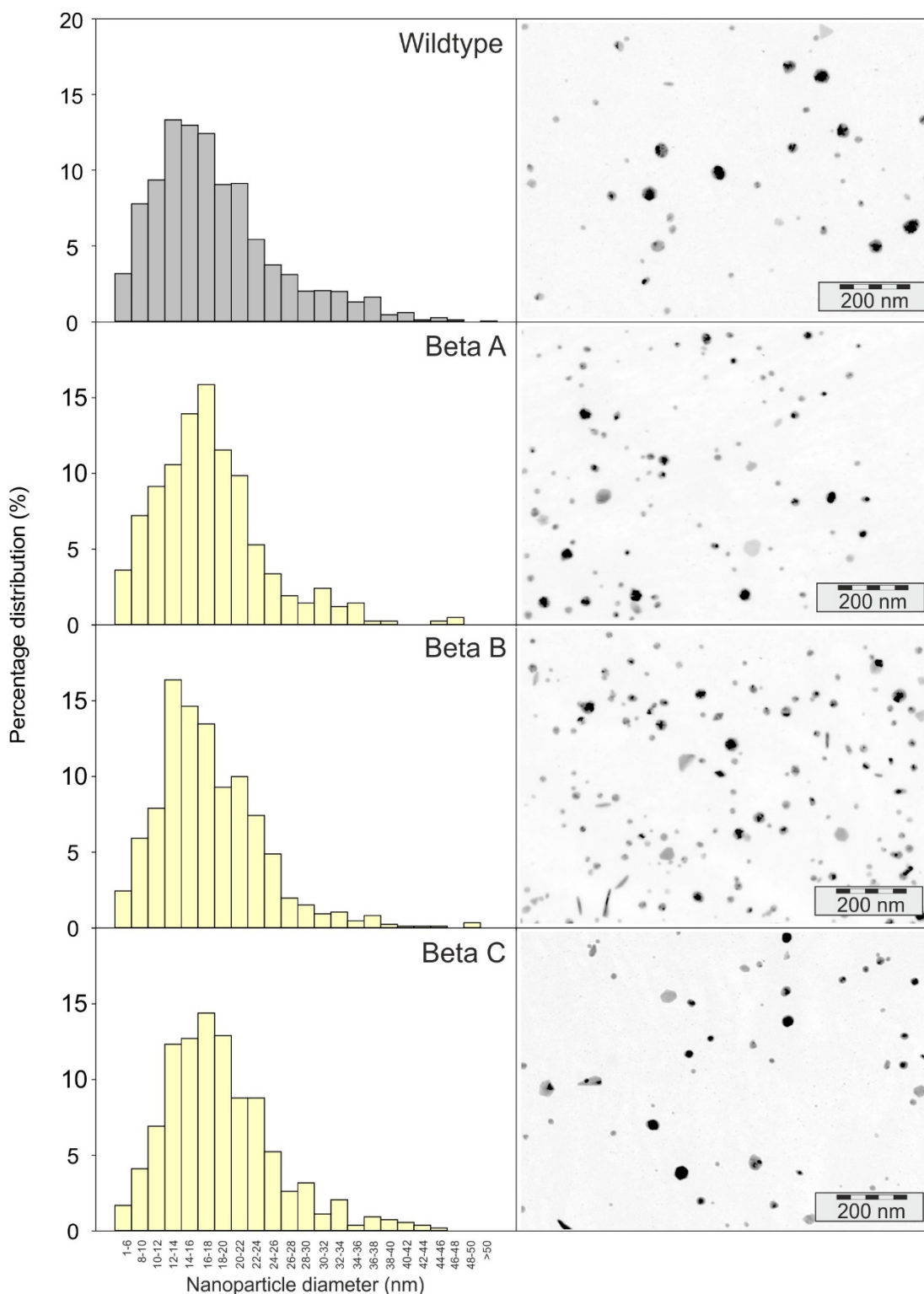


**Figure 5.9:** Histogram of percentage distribution of gold nanoparticles and TEM images at 105k magnification obtained from Arabidopsis Col-0 wildtype and three, independently-transformed beta lines after treatment with gold for 24 hours. Percentage distributions are constructed based on the TEM images taken from a single leaf from seven biological replicates of three beta lines.

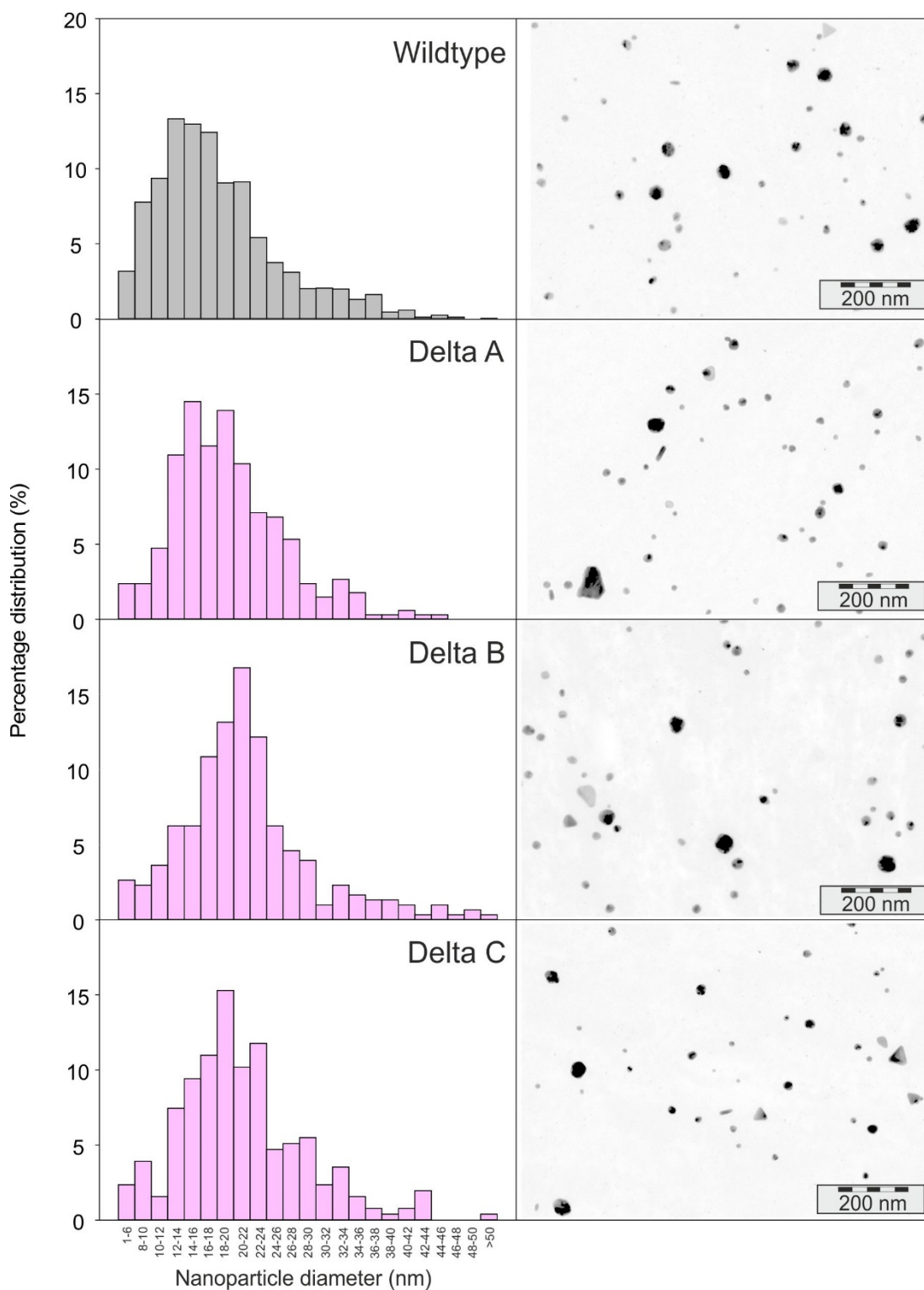


**Figure 5.10:** Histogram of percentage distribution of gold nanoparticles and TEM images at 105k magnification obtained from *Arabidopsis Col-0* wildtype and three, independently-transformed delta lines after treatment with gold for 24 hours. Percentage distributions are constructed based on the TEM images taken from a single leaf from seven biological replicates of three delta lines.

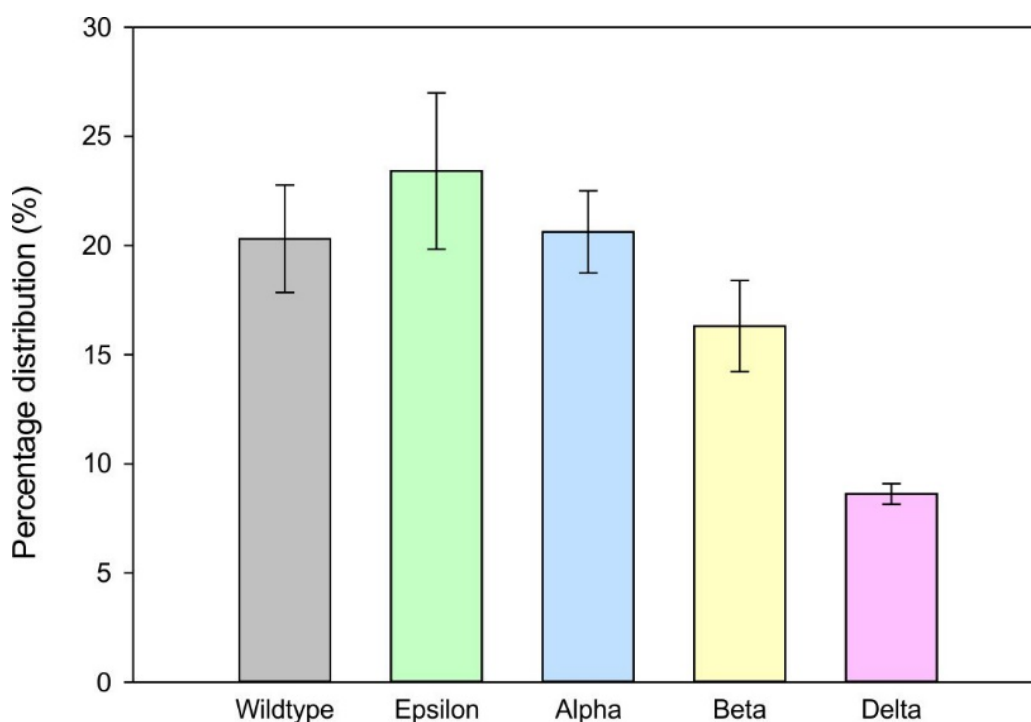


**Figure 5.11:** Percentage distribution of gold nanoparticle with diameter size less than 10 nm obtained from Arabidopsis Col-0 wildtype and transgenic plants expressing different peptide sequences as stated. Results are mean from three independently-transformed line  $\pm$  SEM. ANOVA Tukey's test.

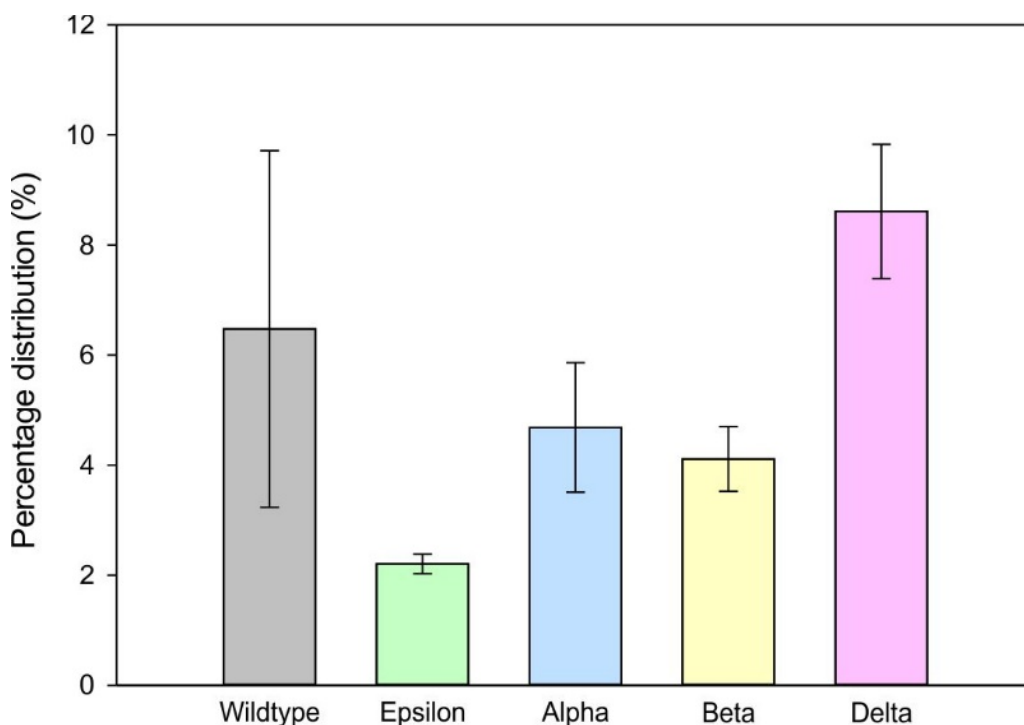


**Figure 5.12:** Percentage distribution of gold nanoparticle with diameter size larger than 30 nm obtained from Arabidopsis Col-0 wildtype and transgenic plants expressing different peptide sequences as stated. Results are mean from three independently-transformed line  $\pm$  SEM. ANOVA Tukey's test.

## 5.4 Discussion

This study investigates the potential of expressing synthetic peptides *in planta* to seed the formation of gold or palladium nanoparticles. Six, codon-optimised DNA sequences encoding short peptides were used in this study, all previously shown to seed the formation of gold (epsilon, alpha, beta and delta) or palladium (eta and zeta) nanoparticles of various sizes *in vitro* [238, 242, 246]. The qPCR analysis showed low transcript levels of delta as compared to the other DNA-encoding-peptides. Interestingly, the size of delta (SEKLGASL) is 2 amino acids shorter than the other SEKLxxGASL peptides, which contain 10 amino acids. Perhaps, the shorter, delta-encoding RNA transcripts have reduced stability and are degraded more quickly than transcripts expressing the other peptides. Further analysis would be needed to verify this hypothesis. The TEM analyses shown here demonstrate that all of the transgenic lines (epsilon, alpha, beta and delta) and wildtype were able to form gold nanoparticles *in planta*, and the nanoparticle size correlated with that produced *in vitro* (Figure 5.3). Many successful catalytic reactions are achieved when metal nanoparticles used are within the size range of 1 – 10 nm [241, 242, 246, 257, 258]. It has been shown previously that the catalytic properties of metal nanoparticles can be dramatically influenced by the shape and size of particle formed [238, 256]. Smaller size particles increases the ratio of surface area to bulk atoms which allows more surface atoms to be available for catalytic reactions [259]. The formation of large nanoparticles might potentially interfere with the catalytic activity of other nanoparticle present. The difference in terms of size of nanoparticle formed can be related to the structural design of the peptides. The peptide sequences were designed by combining two shape-directing sequences (SEKL and GASL) which were identified in the gold-binding polypeptides from *E. coli* [237] together with amino acids with different reduction ( $W > Y > F$ ) and binding ( $Y > W > F$ ) capabilities. Changing the order of the amino acid sequence could result in different metal reduction capability [242]. In agreement with the results obtained by Tan et al [242], it was observed that the high percentage of small nanoparticle (1-10 nm) was obtained when highest reduction capability amino acids (WW) is sandwiched together with two reduction rate up-regulators (L,S) (Figure 5.11). The presence of strong binding residue (G) next to the strong reduction residues (WW) would lower the reduction capability, as observed between the epsilon and alpha lines, due to the high tendency of the strong binder (G) to bind gold to the surface, resulting in the loss of energy (entropy penalty) for reduction activity [242]. Ultimately, the presence of strong binding and the absence of strong reduction

residues (WW) in the delta lines (SEKLGASL) resulted in high percentage distribution of large nanoparticles ( $> 30$  nm), a similar phenomena observed previously in the work done by Brown et al [237] (Figure 5.12).

Further work is now on-going at the Green Chemistry Centre of Excellence to test the catalytic activity of the processed nanoparticle-containing plant biomass in catalytic. These studies will first compare the performance of catalytic activity of metal nanoparticle from the epsilon lines, which produce the highest percentage of small ( $< 10$ nm) nanoparticles with wildtype. The absence of target protein in the peptide sequence for antibodies prevented the western blot analysis to be conducted. Alternatively, protein identification analysis using the Matrix-Assisted Laser Desorption Ionization Time-of-Flight (MALDI TOF) mass spectrometer is currently being carried out to identify the presence of peptides based on the peptide mass fingerprint database obtained from the molecular mass of the peptides. Overall, results presented in this section demonstrate the ability to finely tune the size of desired metal nanoparticle within plant tissues, which can be used in many catalytic reactions.

## **Chapter 6: Potential involvement of *AtHMA5* in gold and palladium detoxification**

### **6.1 Introduction**

The effect of precious metals on plant growth has not yet been extensively studied. However, untreated mine waste areas can contain significant amounts of precious metals which are uneconomical to extract using conventional methods. Phytomining could be a suitable, and cost efficient, approach to solve the problems of mine waste revegetation and stabilisation and offer the added incentive of a potentially high valuable by-product which could be generated from the treatment. To develop an efficient phytomining process, the uptake, tolerance and detoxification mechanisms in plants in response to the exposure to precious metals need to be understood.

Microarray gene expression analysis on gold-treated *Arabidopsis* roots published by the Bruce group revealed that genes encoding enzymes involved in ameliorating plant stress were upregulated in response to gold treatment [46, 47]. Interestingly, the study also identified a discrete number of genes encoding metal transporters, which were down regulated in response to gold, suggesting a direct involvement of these transporters towards gold uptake and tolerance in *Arabidopsis*. Gold treatment was also found to induce the up regulation of the heavy metal ATPase *AtHMA5* which is involved in copper detoxification [79]. This chapter highlights the potential involvement of *AtHMA5* in the detoxification of gold and palladium in plants.

### 6.1.1 Microarray analysis of Arabidopsis in response to gold

Previous microarray analysis performed by Dr. Andrew Taylor revealed the genetic response of Arabidopsis roots to gold exposure [46]. Following additional qPCR expression studies, the following genes were confirmed to be up or down regulated in response to gold.

The Iron Regulated Transporters (IRT), *IRT1* and *IRT2*; Metal Tolerance Protein 2 (*MTPA2*); and the Tonoplast Intrinsic Proteins (*TIP2;2* and *TIP2;3*) were found to be downregulated in response to gold by 132.37, 38.4, 17.93, 16.84 and 10.79-fold change respectively (Figure 6.1). The *IRT1* and *IRT2* membrane transporters have high affinity towards iron, but can also interact with manganese, zinc and cobalt [210, 211]. The *MTPA2* gene which encodes metal tolerance protein 3 is a vacuolar transporter conferring zinc tolerance in Arabidopsis by mediating the subcellular sequestration of excess zinc into the vacuole [260]. Both *TIP2;2* and *TIP2;3* encode aquaporins which are involved in transporting methylammonium and ammonium across the tonoplast membrane into the vacuole [261].

In addition to the transporter genes listed above, genes traditionally involved in ameliorating stress were also identified, such as *ATGSTU12*, *CYP71A12*, *AT1G14550* and *UGT73B4* (Figure 6.1). The *AtGSTU12* gene encodes a tau-class glutathione transferase (GST), and was the most highly up regulated gene in the microarray dataset (220 fold) followed by the cytochrome P450, *CYP71A12* (127 fold). Glutathione transferases and cytochromes P450 are known to be up regulated in response to stress and increased peroxide production [262, 263]. This result shows that although considered relatively inert and harmless, gold can cause phytotoxicity.

In the same work, *AtHMA5* was also found to be up regulated (Figure 6.2). A previous microarray study on the bacterium *Cupriavidus metallidurans* exposed to gold revealed that *Rmet\_3524*, which encodes a copper transporting P-type ATPase CopA homologous to HMA5 (40 % identity), was also up regulated in response to gold [264].

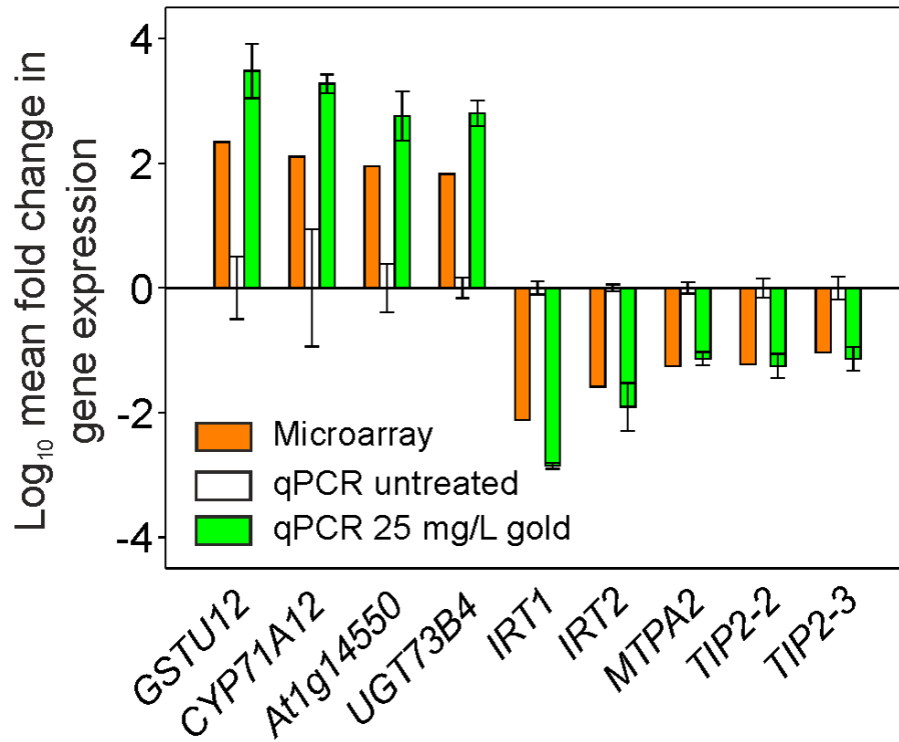


**Figure 6.1:** Comparison of qPCR and microarray gene expression levels in gold-treated *Arabidopsis* root tissue. The data were normalized to the *Arabidopsis ACTIN2* gene and relative fold induction calculated using the  $\Delta\Delta Ct$  method [230]. Results are the mean from three biological replicates  $\pm$  SD. *GSTU12* (Glutathione transferase), *CYP71A12* (Cytochrome P450), *At1g14550* (Anionic peroxidase), *UGT73B4* (UTP-glucosyltransferase), *IRT1* (Fe(II) transport protein), *IRT2* (Fe(II) transport protein), *MTPA2* (Zinc transport protein), *TIP2;2* and *TIP2;3* (Membrane channel like protein) Figure reproduced from Taylor et al [47].

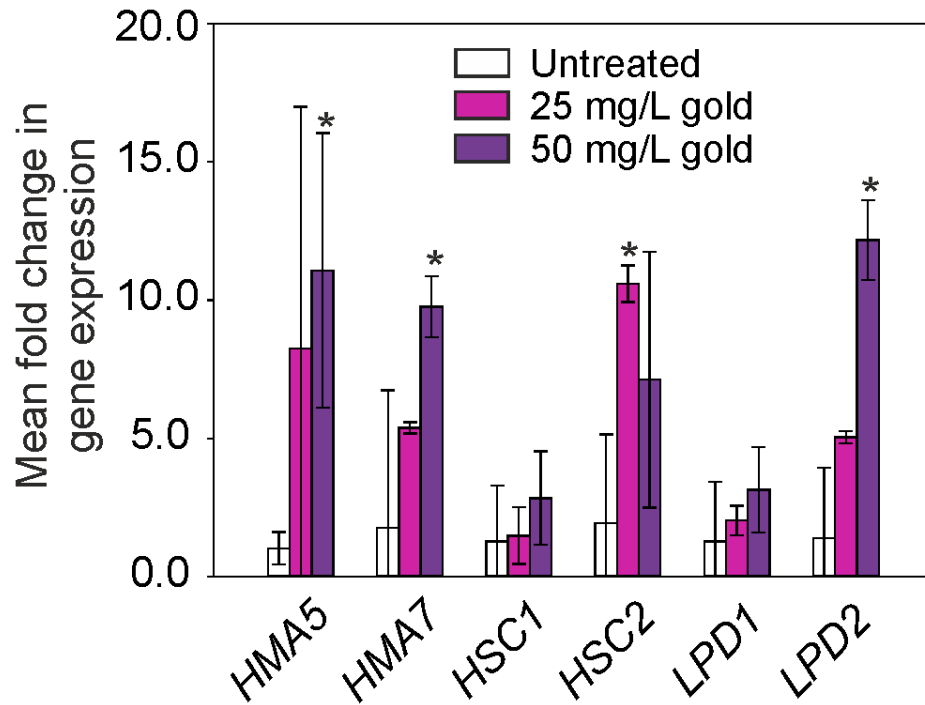


**Figure 6.2:** Gene expression levels in gold treated *Arabidopsis* root tissue. The data were normalized to the *Arabidopsis ACTIN2* gene and relative fold induction calculated using the  $\Delta\Delta C_t$  method [230]. Results are the mean from four biological replicates  $\pm$  SD. \* denotes significantly (Student's T-test  $p < 0.05$ ) more upregulated than untreated samples. *HMA5* (Heavy metal ATPase 5), *HMA7* (Heavy metal ATPase 7), *HSC1* (Heat shock cognate 1), *HSC2* (Heat shock cognate 2), *LPD1* (Lipoamide dehydrogenase 1), *LPD2* (Lipoamide dehydrogenase 2). Figure reproduced from Taylor et al [47].

### 6.1.2 Heavy metal ATPase 5

An efflux membrane transporter, HMA5 is involved in copper detoxification and regulation in plants [30, 52, 79, 89]. Similar to many other HMAs described in Chapter 1, microarray data available through Genevestigator [265] indicate that *AtHMA5* is highly expressed in the root pericycle cells and in the pollen of the Arabidopsis plant (Figure 6.3). A P-type ATPase transporter, HMA5 is, possesses the general characteristics therein, such as eight transmembrane domains (TMD), two MxCxxC amino terminal metal-binding domains (MBDs), a DKTGTG aspartate phosphorylation site, an ion transduction motif (CPC), a TGEA phosphatase domain, a GDG ATP binding domain and an HP motif (Figure 6.4) [79]. Like all other P-type ATPases, HMA5 hydrolyses ATP and uses the phosphate to form an acyl-phosphorylated intermediate which is subsequently dephosphorylated by phosphatase activity. The energy generated from the phosphorylation and dephosphorylation cycle is used to translocate cations across lipid bilayers [266]. HMA5, 6, 7 and 8, form a subgroup which share identity and are categorised as monovalent transporters due to their function in transporting monovalent cations, such as  $\text{Cu}^+$ , in many plant species (Figure 6.5). HMA7, which is highly homologous (48 % identity) to HMA5, is reported to be involved in  $\text{Cu}^+$  delivery to create functional ethylene receptors in plants, as well as for copper homeostasis in seedlings [267, 268].



**Figure 6.3:** Heat map generated from DNA microarray data showing percentage of *AtHMA5* gene expression potential in different parts of plant tissues. Data obtained from Genevestigator [265], accessed 15<sup>th</sup> September 2016.

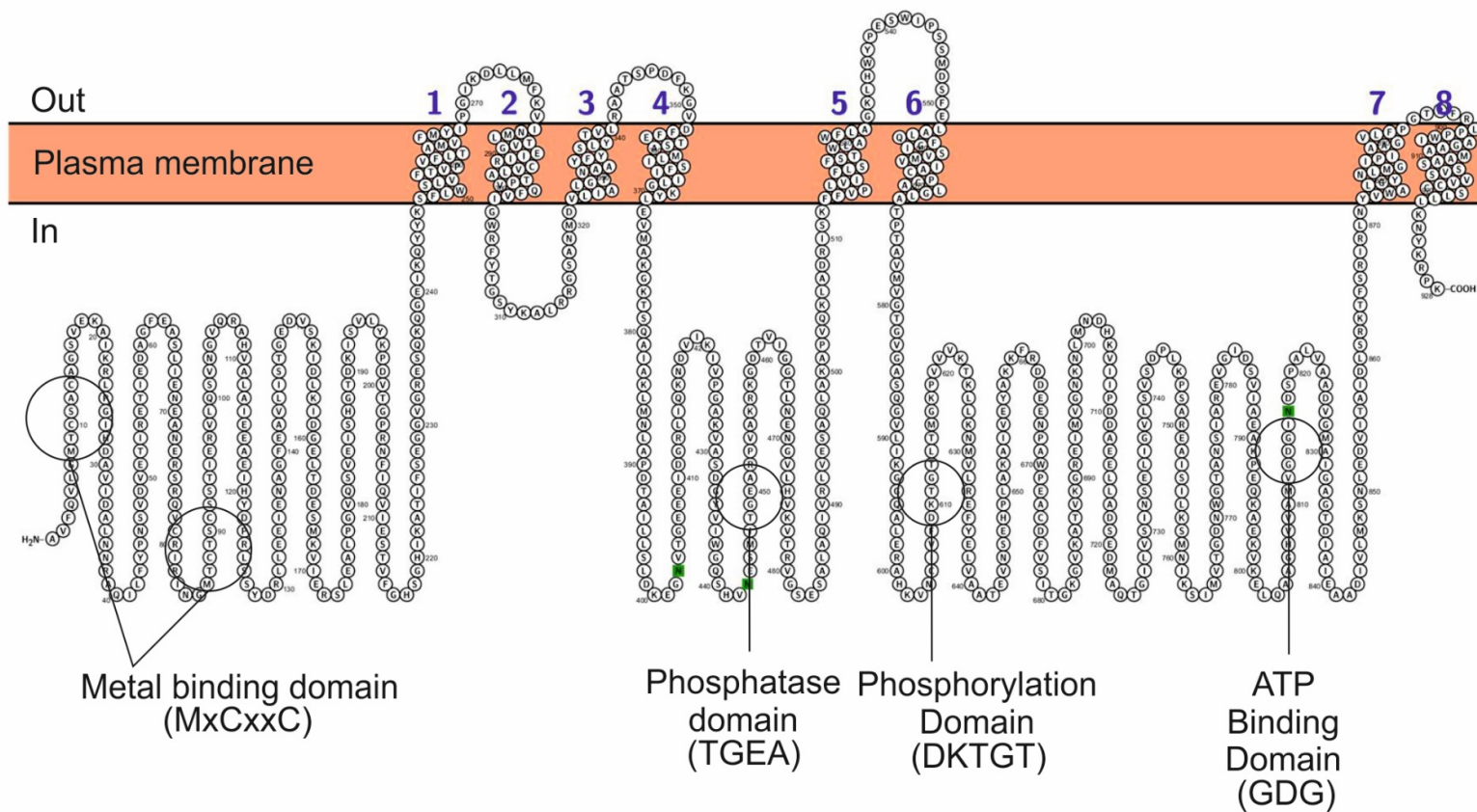


**Figure 6.4:** Schematic view of the predicted topology of *AtHMA5*. Transmembrane domains are numbered from 1 – 8. The sequences of putative functional domains are shown and the conserved residues at the transmembrane Cu-binding site are indicated.

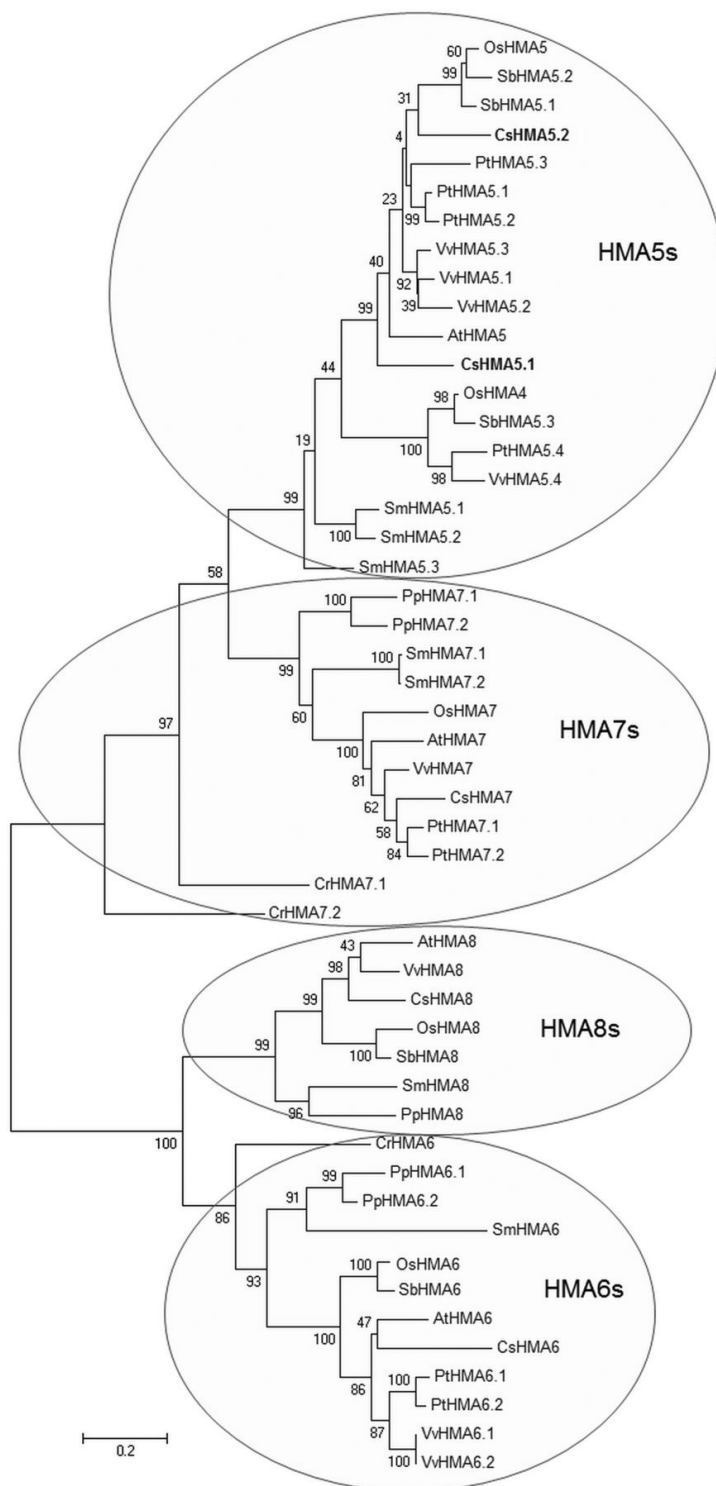


**Figure 6.5:** Phylogenetic tree analysis of heavy metal ATPase 5, 6, 7 and 8 from different plant species. The sequences were aligned using Clustal W and the tree was generated using Mega 6.0. Figure reproduced from Migocka et al [52].

To date, only three HMA5 orthologues have been functionally characterised: from Arabidopsis, AtHMA5 [79, 89]; from rice (*Oryza sativa*), OsHMA5 [30] and from cucumber (*Cucumis sativus*), CsHMA5.2 [52]. OsHMA5 and CsHMA5.2 share 72 and 70 % identity, respectively, with AtHMA5. As shown in Table 6.1, AtHMA5 is more closely related to OsHMA5 than to CsHMA5.2. All of the studies agree that HMA5 transmembrane transporters function by effluxing copper ions ( $\text{Cu}^+$ ) from the cytosol out of the cell (AtHMA5 and OsHMA5) [30, 79] or from the cytosol into the vacuole (CsHMA5.2) [52].

The amino acid sequence analysis from Arabidopsis (Accession number 1009106656), cucumber (Accession number KJ818255) and rice (accession number AB840272) obtained from the TAIR (The Arabidopsis Information Resource) database and from the GenBank Data Library [269] and aligned using the Clustal O software [270] revealed that all three HMA5s, possess the same typical features of a P-type ATPase pump (Figure 6.6). The alignment shows high levels of conservation within parts of the protein including two MXCXXC metal binding motifs, a DKTGT phosphorylation site, CPC amino acid motif, TGEA phosphatase domain, GDG ATP binding domain and eight transmembrane domains.

**Table 6.1: Percentage identities of the AtHMA5 proteins.** CsHMA5.2, *Cucumis sativus*; AtHMA5 *Arabidopsis thaliana*; and OsHMA5, *Oryza sativa*. Values were obtained using the amino acids sequences from TAIR and GenBank [269] and alignments using Clustal O [270].

	<b>CsHMA5.2</b>	<b>AtHMA5</b>	<b>OsHMA5</b>	<b>Location</b>
<b>CsHMA5.2</b>	100.00	-	-	Vacuole membrane [52]
<b>AtHMA5</b>	69.88	100.00	-	Plasma membrane [79]
<b>OsHMA5</b>	64.82	71.91	100.00	Plasma membrane [30]

Chapter 6: Potential involvement of AtHMA5 in gold and palladium detoxification



**Figure 6.6:** Clustal O alignment of amino acid sequences of CsHMA5.2, AtHMA5 and OsHMA5. Consensus amino acid residues are marked with asterisk. Signature sequences of ATPase are boxed (2 MXCXXC binding domain, 8 transmembrane domains, 1 TGE phosphatase domain, 1 CPC amino acid motif, 1 DKTGT phosphorylation site and 1 GDG ATP binding domain). Transmembrane domains are highlighted in yellow.

The first characterisation study of *AtHMA5* demonstrated that a *hma5* mutant exhibited root hypersensitivity, including stunted root growth, in the presence of excess copper [79]. The mutant plants also showed higher copper accumulation in the roots, as compared to wildtype plants when grown on excess copper [79] (Figure 6.7). As *AtHMA5* expression was mostly observed in root tissues, it was hypothesised that the transporter is located at the plasma membrane of the root cells (Figure 6.8). Due to some difficulties during the cloning procedure, the authors of the study were unable to perform the subcellular localisation analysis to confirm this hypothesis. However, a microarray study conducted by Birnbaum et al [271] previously showed that *AtHMA5* is mostly expressed in the pericycle of the root cells. Andres-Colas et al [79] conducted a yeast two-hybrid analysis that indicated that *AtHMA5* interacts with Arabidopsis ATX1-like copper chaperones, as a potential regulatory pathway for copper ions into the metal-binding domains of *AtHMA5*.

Kobayashi et al [89] performed quantitative trait locus (QTL) analyses to determine the basis of the natural variation of copper tolerance in Arabidopsis. The authors concluded that amino acid polymorphisms at selected, conserved domains controlling the copper translocation capacity from roots to shoots, play a major role in copper tolerance in Arabidopsis.

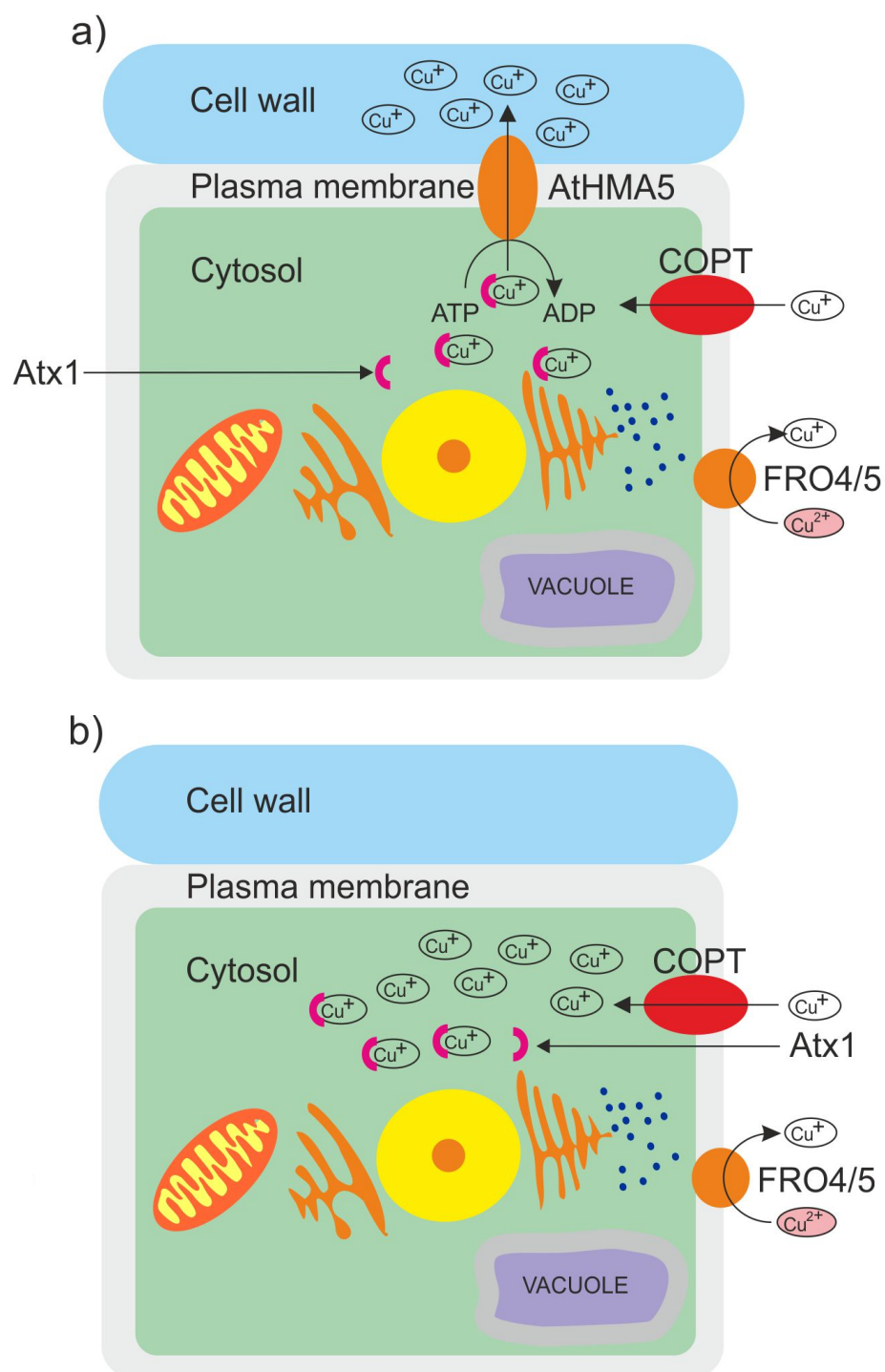


**Figure 6.7:** Mechanism of copper detoxification in Arabidopsis plant root cells. a)  $\text{Cu}^{2+}$  is reduced to  $\text{Cu}^+$  by FRO4/5 (Ferric Reduction Oxidase 4/5). Plants take up  $\text{Cu}^+$  via the COPT transporter.  $\text{Cu}^+$  is pumped out into the cell wall and translocated to the shoot via xylem. b) In the absence of AtHMA5, high concentrations of  $\text{Cu}^+$  cannot be pumped out, causing root growth inhibition.

Deng et al [30] observed that *OsHMA5* in rice did not participate in copper detoxification mechanisms but was only involved in the translocation of copper from roots to shoots. They observed that an *Oshma5* mutant plant line accumulated lower levels of copper in the shoots and higher levels of copper in the roots compared to wildtype plants. As the xylem is the main pathway for copper translocation to the shoots, the authors also measured the concentration of copper in the xylem sap and found that copper levels in the xylem sap of the mutant decreased with continued exposure time to copper, when compared to wildtype plants. Dose-response experiments showed that the copper concentration was also lower in the xylem sap of the mutant, compared to wildtype, when grown on increased copper concentrations. In contrast to *Athma5*, it was observed that *Oshma5* roots were not hypersensitive to did not exhibit root hypersensitivity. This observation suggests that *OsHMA5* is not involved in copper detoxification in rice. However, tissue specificity and subcellular localisation analysis using *OsHMA5* fused with GFP revealed that the fluorescence signal was only detected in the pericycle of the roots and observed at the peripheral region of the cells outside the nuclei when co stained with 4',6-diamidino-2-phenylindole (DAPI), suggesting its location in the plasma membrane, as suggested for *AthMA5* previously (Figure 6.8).

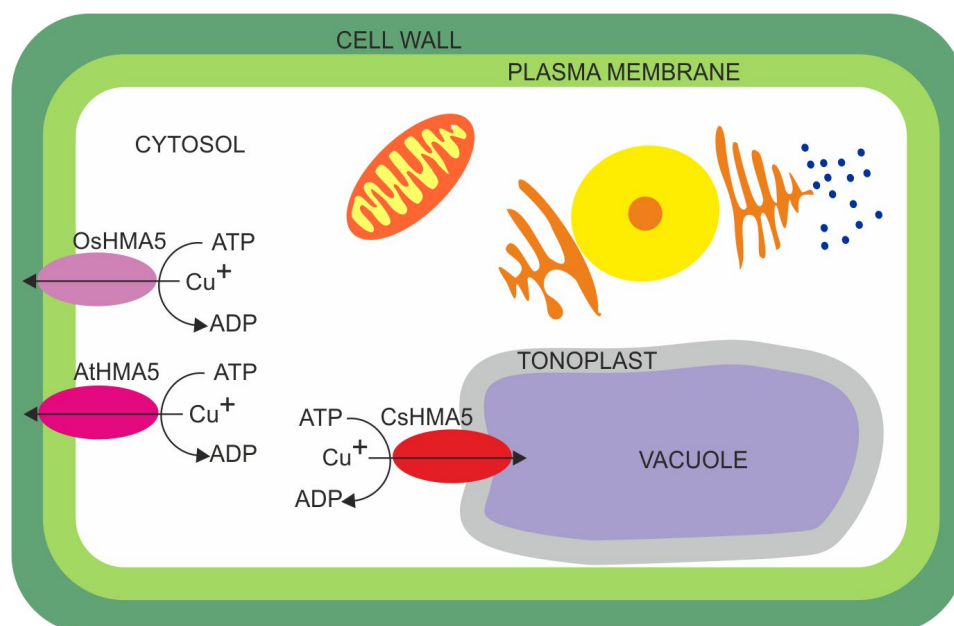


**Figure 6.8:** Diagram showing different subcellular locations of HMA5s from different plant species in a root cell. *OsHMA5* from rice (*Oryza sativa*), *AtHMA5* from Arabidopsis (*Arabidopsis thaliana*), *CshMA5.2* from cucumber (*Cucumis sativus*).

Recent functional characterisation studies on *CsHMA5.2*, demonstrated its involvement in copper detoxification mechanism, by increasing copper sequestration into the vacuole of the cucumber root cells (Figure 6.8) [52]. This was demonstrated by expressing *CsHMA5.2* in the yeast mutant strain  $\Delta ace1$ , which is unable to grow in high concentrations of copper due to the loss of function of Ace1. Ace1 encodes a transcription factor that regulates the expression of proteins involved in copper detoxification such as CUP1 and CRS5, which are small cysteine-rich metallothioneins that sequester Cu ions.

Organ expression profiling using qPCR indicated that *CsHMA5.2* was highly expressed in the roots similar to *AtHMA5* and *OsHMA5*. However, subcellular localisation analysis on *CsHMA5.2*, by western blot analysis of membranes isolated from cucumber roots, showed that *CsHMA5.2* co-localised with vacuolar PPase, a marker protein for the vacuolar membrane rather than the plasma membrane marker protein, H<sup>+</sup>-ATPase. Subcellular localisation studies of *CsHMA5.2*-GFP fusions in yeast using fluorescence microscopy revealed that the protein was present in the vacuolar membrane of the mutant strain.

Following the successful expression of *CsHMA5.2* in the yeast mutant strain  $\Delta ace1$ , it was observed that expression of *CsHMA5.2* complemented Ace1 by restoring the growth of the yeast mutant strain on media containing 50  $\mu$ M of copper and, surprisingly, also on silver. Metal content analysis using ICP-MS revealed that  $\Delta ace1$  expressing *CsHMA5.2* contained more copper than  $\Delta ace1$  transformed with the empty vector.

Taking together this result with the vacuolar localisation, as observed previously, it can be hypothesised that *CsHMA5.2* mediates copper tolerance by enhancing intracellular sequestration of copper ions into the vacuole instead of effluxing it out of the cell, as previously observed for *AtHMA5* [3].

Andres-Colas et al [79] observed that *AtHMA5* was partially expressed when the plant was treated with silver (Ag<sup>+</sup>). Furthermore, expression of *CsHMA5.2*, in the yeast mutant strain  $\Delta ace1$  conferred enhanced tolerance to silver [52]. Subsequent ATPase activity assays revealed that, as with copper, *CsHMA5.2* was also activated by silver, although at 2 to 3 fold less than for copper, signifying that copper is a more favourable substrate [52]. Other metals, such as Fe<sup>+</sup>, Cd<sup>+</sup> and Zn<sup>+</sup>, were also tested for changes in gene expression or activity of *AtHMA5* or *CsHMA5.2* but activity was only observed with copper and to a lower level, with silver [52, 79]. There are a number of chemical similarities between copper and silver: they are adjacent

elements in Group 11 of the periodic table and activity towards both these elements is not confined to the HMA5 transporters. For example, silver also activated the bacterial copper transporter CopA from *Archaeoglobus fulgidus* [272].

While undeniably there are many chemical differences separating gold and palladium from silver and copper, these elements share a number of chemical properties, and the question as to whether HMA5 is involved in the uptake and/or regulation of gold, and possibly even palladium in the plant makes it an interesting candidate worthy of further investigation. This chapter explores the potential of gold and palladium as substrates for AtHMA5 and the potential for this as a route for the detoxification of these metals in plants.

## 6.2 Materials and methods

### 6.2.1 Hydroponic based experiment settings

Arabidopsis seedlings, ecotype Col-0, were grown hydroponically on rafts, using a modified system similar to that described by Kumari et al [273], with the roots submerged. The 5 mm diameter holes of Foamex rafts (dimensions: 5 mm thickness, 8 cm diameter, 2 cm diameter hole for raft removal and 84 x 5 mm diameter holes) was produced by the Workshop in the Department of Biology, University of York. The rafts were autoclaved, then the 5 mm holes were plugged with sterile  $\frac{1}{2}$  MS (A) and floated on 100 mL of autoclaved  $\frac{1}{2}$  MS within 560 mL Weck jars. Ten seeds, which had already been stratified in sterilised water, were transferred onto each Foamex raft and the jars closed with micropore tape and metal clamps. The jars were transferred to a growth room at low light conditions ( $20 \mu\text{mol}\cdot\text{m}^{-2}\cdot\text{s}^{-1}$ , 16 h light, 8 h dark cycle) and the plants grown for 3 weeks.



**Figure 6.9:** Hydroponic growth of Arabidopsis seedlings. Three-week-old plants growing on a Foamex raft floating on 100 mL of  $\frac{1}{2}$  MS (A) in a Weck jar.

### **6.2.2 Metal treatment on plants**

After 3 weeks of growth, the medium was replaced with medium containing copper sulphate ( $\text{CuSO}_4$ ), potassium tetrachloroaurate ( $\text{KAuCl}_4$ ) or potassium tetrachloropalladate ( $\text{K}_2\text{PdCl}_4$ ), according to the specific concentration required by the experiment. The plants were returned to the growth chamber, prior to harvesting as described by Kumari et al [273].

### **6.2.3 RNA extraction from Arabidopsis**

After 6 hours of treatment with the metal solution, root plant tissues were harvested and snap frozen in liquid nitrogen then homogenised using a pestle and mortar. Isolate RNA (ii) kits (Bioline) were used to extract RNA from homogenised root plant tissue (approximately 100 mg per sample) according to the manufacturer's instructions. The quality of RNA was verified and quantified using a Nanodrop ND-1000 Spectrophotometer (Thermo Scientific) at 260 nm.

### **6.2.4 Reverse transcription of plant RNA**

Plant cDNA was synthesised from total RNA using Superscript (ii) Reverse Transcriptase (Invitrogen): 0.5  $\mu\text{g}$  of total RNA was mixed with 1  $\mu\text{L}$  of oligo (dT) 12-18 (500  $\mu\text{g}/\text{mL}$ ), 1  $\mu\text{L}$  dNTP mix (10 mM) in a final volume of 12  $\mu\text{L}$ . The mixture was heated at 65 °C for 5 minutes and then chilled on ice. 5X first-strand buffer with 0.1 M DTT and 40 units/ $\mu\text{L}$  of RNaseOUT were added gently into the mixture followed by incubation at 42 °C for 2 minutes. A 1  $\mu\text{L}$  sample containing 200 units SuperScript (ii) Reverse Transcriptase was added by pipetting, followed by incubation at 42 °C for 50 minutes. The reaction was inactivated by heating at 70 °C for 15 minutes.

### **6.2.5 qPCR analysis**

The template used for qPCR analysis throughout this work was the cDNA synthesised from RNA isolated from the roots of 3-weeks-old Arabidopsis treated with metals for 6 hours. The primers used were based on previous microarray work done by Taylor et al [47] and are listed in Table 6.2 and 6.3. Data were normalised using *ACTIN2* as an endogenously expressed control. For yeast studies, the data was normalised to the *Saccharomyces cerevisiae TAF10* gene. Relative fold induction was calculated using the  $\Delta\Delta\text{Ct}$  method [230].

**Table 6.2:** Primers for qPCR analysis in response to palladium. F and R at the end of the primer names represent the forward and reverse primers respectively.

<b>Gene</b>	<b>Primer Name</b>	<b>Sequence (5' – 3')</b>
<i>ATGSTU12</i>	ATGSTU12F	GATCTTTCCATCCTCCCAACAC
	ATGSTU12R	CAACGAAGTGAGCCCAAAAAC
<i>CYP71A12</i>	CYP71A12F	TGGTAACCTCCACCAGCTTAGC
	CYP71A12R	TGGTCCGTACCGAAGGCTTA
<i>At1g14550</i>	At1g14550F	CTATTC AGGAGCACACACCATAGG
	At1g14550R	TGTCGCTTGAGTTCTCGTAAAGC
<i>AtHMA5</i>	HMA5F	TCTCAAGCGATCGCAAAGC
	HMA5R	ATTCCCTTCCTTGTCCAAACTCA
<i>AtHMA7</i>	HMA7F	TCAGCCTGGTGATACATTAAGTTC
	HMA7R	CCCCACACCACAACACCAT
<i>IRT1</i>	IRT1F	CTTTGATCACGGTTGGACTTCTAA
	IRT1R	AGATCCACGAGTGCCATGTAAA
<i>IRT2</i>	IRT2F	TCTTTTCAGCCGTTACATTTTCG
	IRT2R	AGAAGAAAAACATTTGACGATCATGA
<i>MTPA2</i>	MTPA2F	CATAGTTGTAGAAGTCGTTGGAGGAA
	MTPA2R	GCAAAGGCTGCAACATCAGA
<i>TIP2;2</i>	TIP2;2F	TGACCTTTGCTCTGGTCTACACA
	TIP2;2R	TGGTCCCGAGTGAACCTTTC
<i>TIP2;3</i>	TIP2;3F	CCCAGCTGGTCTTGTAGCAATT
	TIP2;3R	TGTTAGCCGCAATGGAAACTC
<i>ACTIN2</i>	ACTINF	TACAGTGTCTGGATCGGTGGTT
	ACTINR	CGGCCTTGGAGATCCACAT

**Table 6.3:** Primers for qPCR analysis to measure expression analysis of Heavy Metal ATPases in response to palladium. All the primers were taken from Taylor et al [47] and Del Pozo et al [274] except for HMA2, 3 and 4, which were constructed using Primer Express v3.0. F and R at the end of the primer names represent the forward and reverse primers respectively.

Gene	Primer Name	Sequence (5' – 3')
<i>AtHMA1</i>	HMA1F	GAGATTGTGCCTGTAGATTGCG
	HMA1R	TCATTCCATGCCTTTGTAGCC
<i>AtHMA2</i>	HMA2F	TACTCTCCCTTCCGTTGGCT
	HMA2R	TGCTCCCACGGTTACAACAA
<i>AtHMA3</i>	HMA3F	GCCACGTCAGGGTTTCTGAT
	HMA3R	CACTCAATGCTTGAGACCCAGT
<i>AtHMA4</i>	HMA4F	CCCTTCCAAATTGCTAAGGCAC
	HMA4R	GAGCCAACGTAAAGGCGAGT
<i>AtHMA5</i>	HMA5F	TCTCAAGCGATCGCAAAGC
	HMA5R	ATTCCCTTCCTTGTCCAAACTCA
<i>AtHMA6</i>	HMA6F	AAGATACTGGAAAGCCAACCTCA
	HMA6R	GCAAGCGTCTCGCCTAAACT
<i>AtHMA7</i>	HMA7F	TCAGCCTGGTGATACATTAAGTTC
	HMA7R	CCCCACACCACAACACCAT
<i>AtHMA8</i>	HMA8F	GCTTTGTGCTCCTTGGTCGT
	HMA8R	CAGAATCCACTGGGGTGTATTG

### 6.2.6 Procurement and verification of the *hma5-1* knockout mutant

The previously characterised *hma5-1* line [79] was obtained from the European Arabidopsis Stock Centre (NASC). To corroborate the presence of the T-DNA insert in *hma5-1*, PCR reactions were designed using the combination of primers specific to the left border of the T-DNA with either the gene-specific primers flanking the *AtHMA5* open reading frame as stated by Andres-Colas et al [79].

**Table 6.4:** Primers for identification of T-DNA insertion in *hma5-1* lines

Primer name	Sequence (5' – 3')
Primers specific to T-DNA	GGCAATCAGCTGTTGCCCGTCTCACTGGTG
Primers <i>HMA5</i> Flanking A	CAAGATTTCGCGCACAAAGACGATCGATTAC
Primers <i>HMA5</i> Flanking B	CTCGCTCCACCTGAAATCTCCCGAATCTCC

### 6.2.7 Cloning of *AtHMA5* into pYES2 yeast expression vector

The yeast expression vector pYES2 was provided by Dr. Frans Maathuis (York). As the pYES2 vector does not contain the ATG initiation codon, the ATG sequence together with the addition of TCT yeast consensus sequence were added to the start of the *AtHMA5* cDNA sequence. The full length (2988 bps) *AtHMA5* cDNA (TAIR accession number 1009026218) was then codon-optimised for expression in yeast. The *SacI*, *NotI* and *SphI*, *XbaI* restriction sites were introduced on the left and right flanks of *AtHMA5* respectively and the sequence was then synthesised by GeneArt (ThermoFisher).

The Infusion cloning kit (Clontech) was used to clone *AtHMA5* into the pYES2 yeast expression vector (Invitrogen), which placed the gene under the control of the *GAL* promoter. Infusion primers were designed by combining 15 bases, which are homologous to pYES2 vector with 18-25 bases, which are specific to the targeted gene (*AtHMA5*) as follows:

Forward            5'AGAGCTCAACACAATGTCTACGAAGCTTTTGTGCTTACATG  
Reverse            5' AGCGGCCGCTTAAACTCGCTCCACCTGAATCTC

The pYES2-*AtHMA5* construct was transformed into XL10-Gold Ultracompetent *E. coli* cells (Agilent) via heat shock. Positive transformants were identified following screening on LB media containing 50 µg/mL of carbenicillin. Successful insertion of the *AtHMA5* gene into pYES2 was verified using restriction enzymes, colony PCR and sequencing.

### 6.2.8 Transformation of pYES2-*AthMA5* into *Saccharomyces cerevisiae*

Three *S. cerevisiae* strains were used in this work: the parental strain BY4741 (*MAT $\alpha$* ;his3D1; leu2D0 met15D0; ura3D0; YDR205w::kanMX4), a copper-sensitive yeast mutant strain BY4741  $\Delta ace1$  (*MAT $\alpha$*  his3 $\Delta$ 1 leu2 $\Delta$ 0 ura3 $\Delta$ 0 met15 $\Delta$ 0 *ACE1*::kanMX4) and a Ccc2 transporter mutant strain BY4741  $\Delta ccc2$  (*MAT $\alpha$*  his3 $\Delta$ 1 leu2 $\Delta$ 0 ura3 $\Delta$ 0 met15 $\Delta$ 0 *CCC2*::kanMX4). All strains were purchased from Euroscarf (Frankfurt, Germany).

For the yeast transformation protocol, competent yeast cells were prepared by overnight growth in 5 mL Yeast Peptone Dextrose (YPD) media at 30 °C on a shaker (180 rpm) until cell density reached an OD600 = 0.6. The cells were chilled for 20 minutes on ice, harvested by centrifugation at 3,000 rpm for 5 minutes at 4 °C and washed twice with sterilised ice-cold distilled water. The cells were then resuspended with 150  $\mu$ L of 1 M sorbitol on ice, 40  $\mu$ L of cells were then transferred into a clean Eppendorf tube and carefully mixed with 5  $\mu$ L of plasmid (around 5  $\mu$ g) by gently flicking the tube. The mixture was transferred into 0.2 cm pre chilled cuvette and charged at 1.5 kV, 200 mA and 25  $\mu$ F for 5 seconds. One mL of 1 M sorbitol was immediately added into the reaction. Positive transformants were screened on yeast synthetic drop-out (YSD) medium (Sigma) containing minimal media without uracil. Successful transformants were further verified using colony PCR.

### 6.2.9 Transmembrane protein extraction analysis

Membrane preparation from yeast cells was performed as described by Forbes and Cox [275], with minor modifications. Yeast cells were grown on YSD medium and the expression of *AthMA5* was induced with 2 % (w/v) of galactose overnight. Cells were suspended in 25 mM HEPES-NaOH, pH 7.4 containing 150 mM NaCl and 1 mM EDTA and phenylmethylsulfonyl fluoride (PMSF) [52]. Cells were disrupted with acid-washed glass beads (425-600  $\mu$ m; Sigma), vortexed for 5 minutes. Unbroken cells and heavy organelles were separated by centrifugation twice at 10,000 g for 30 seconds. Supernatants were further centrifuged at 20,000 g for 30 minutes to collect the membrane fractions. The final membrane pellet was solubilised with 100  $\mu$ L of buffer containing 1 % (v/v) Triton X-100. Insoluble materials were removed by centrifugation at 20,000 g for another 30 minutes. Solubilised membrane proteins were loaded onto a 10% acrylamide gel, and proteins separated by SDS-PAGE.

### **6.2.10 Spot analysis experiment**

For all of the experiments involving the drop test technique, yeast cell cultures were grown overnight in YSD media containing 2 % (w/v) glucose (Glu) and 6.7 g/L yeast nitrogen base without amino acids, unless stated. The cultures were incubated at 30 °C. The overnight cultures were centrifuged at 3,000 rpm for 5 minutes, washed twice with sterilised water and serially diluted with YSD media containing 2 % (w/v) galactose (Gal), replacing Glu, to OD600 = 0.3. Then 3 µL of the culture was spotted on YSD (agar) media with 2 % (w/v) Gal, supplemented with different concentrations of metals (copper in the form of CuSO<sub>4</sub>, gold in the form of KAuCl<sub>4</sub> and palladium in the form of K<sub>2</sub>PdCl<sub>4</sub>). Plates were incubated at 30 °C and pictures were taken and analysed after 5 days of growth.

#### **6.2.10.1 Ace1 functional complementation assay**

For Ace1 functional complementation assays, yeast cells were grown on YSD media containing different concentrations of copper, as described by Migocka et al [52] and grown as indicated in section 6.2.10.

For growth analysis, yeast cells were grown on YSD media containing 0 and 1000 µM of copper and incubated at 30 °C. The cell density (OD600) was measured using the UV spectrophotometer after 24 hours of growth.

#### **6.2.10.2 Ccc2 functional complementation assay**

For Ccc2 functional complementation assays, yeast nitrogen base without copper and iron (Bio-101) were used for the preparation of the YSD media, as suggested by Forbes and Cox [275]. The iron-limited medium was prepared by adding 1 mM EDTA (as an iron chelator), 50 µM FeSO<sub>4</sub> and 1 µM CuSO<sub>4</sub>. The iron copper sufficient media was prepared by supplementing the iron-limited medium with 500 µM CuSO<sub>4</sub> or 350 µM FeSO<sub>4</sub> and the cells were grown as indicated in section 6.2.10.

#### **6.2.10.3 Activity of AtHMA5**

The yeast parental strain BY4741 and the  $\Delta ace1$  mutant, transformed with either the pYES2-AtHMA5 construct or the pYES2-empty vector, were spotted on YSD plates containing different metals (copper, gold and palladium) at concentrations described in section 6.2.10.

#### **6.2.10.4 Activity of AtHMA5 on excess copper in the presence of gold or palladium**

The yeast parental strain BY4741 and the  $\Delta ace1$  mutant, transformed with the pYES2-AtHMA5 or the pYES2-empty vector, were spotted on YSD plates with 1000  $\mu\text{M}$  of copper as a positive control and on YSD plates containing 1000  $\mu\text{M}$  of copper with 100, 200, 300, 400 and 500  $\mu\text{M}$  of gold each. For palladium analysis, the culture was spotted on YSD plates containing 1000  $\mu\text{M}$  of copper as a positive control, and on plates containing 1000  $\mu\text{M}$  of copper with 700, 800 and 900  $\mu\text{M}$  of palladium each. As controls, the yeast cells were spotted on plates containing the same concentration of gold or palladium as indicated previously. The yeast cells were grown as indicated in section 6.2.10.

## 6.3 Results

### 6.3.1 Arabidopsis gene expression in response to palladium

To check whether the genes strongly regulated by gold were also regulated in the presence of palladium, Arabidopsis roots were exposed to palladium (same concentration used for gold), and qPCR analysis conducted. The results, presented in Figure 6.10, show that the expression patterns of the ten targeted genes in response to palladium were similar to those observed for gold by Dr Taylor (Figure 6.3) [46, 47].

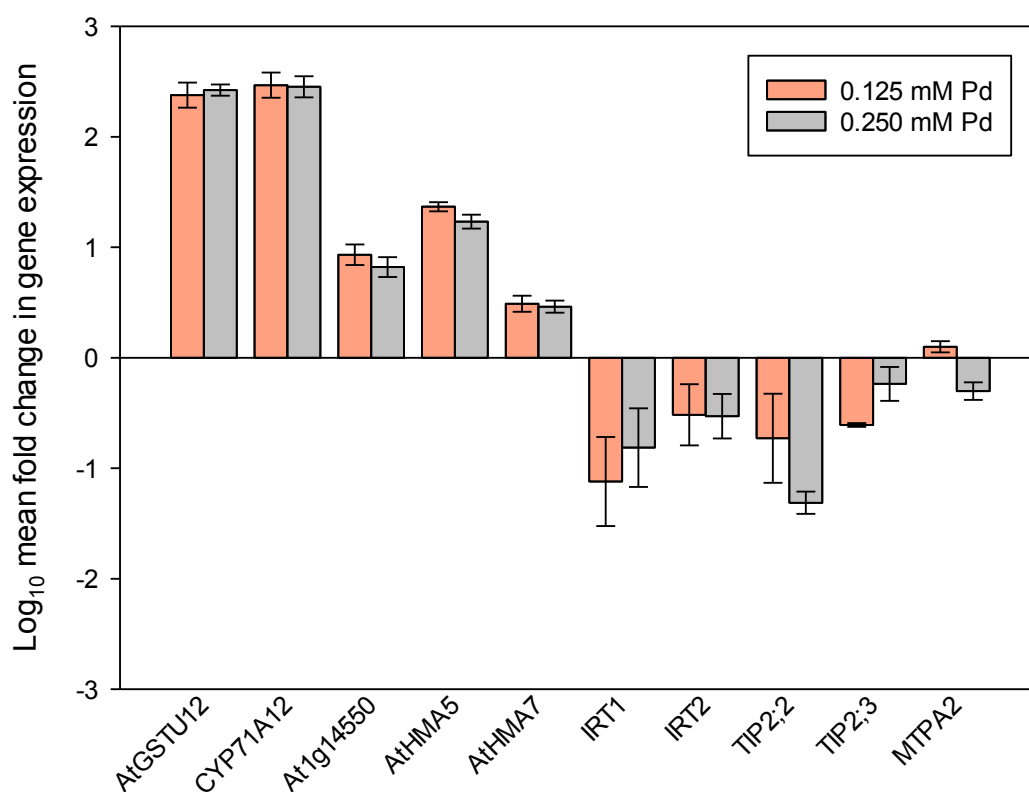


**Figure 6.10:** Relative expression of ten genes in Arabidopsis roots in response to palladium. The data were normalised to the Arabidopsis *ACTIN2* gene and relative fold induction was calculated using the  $\Delta\Delta C_t$  method [230]. Results are the mean from four biological replicates  $\pm$  SEM.

The results in Figure 6.10 clearly show that *AtHMA5* and *AtHMA7* were upregulated in response to palladium. To investigate the expression profiles of all eight *AtHMAs* present in *Arabidopsis*, further qPCR analyses were performed. As shown in Figure 6.11, all of the *AtHMAs* were upregulated except for *AtHMA2* and 3. As predicted, *AtHMA5* was the most highly upregulated gene, as compared to other *HMA* genes (ANOVA  $p < 0.001$ ). As *AtHMA5*, 6, 7 and 8 were previously reported to be involved in copper detoxification [78], the expression of these genes in response to excess copper or palladium was also compared.

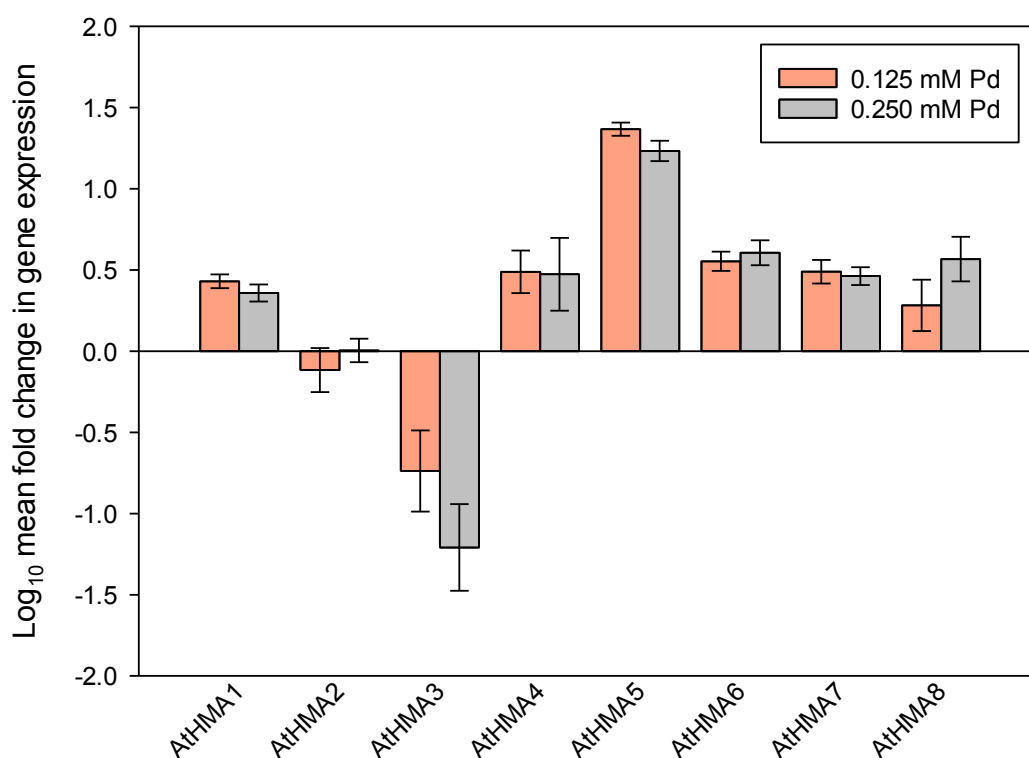


**Figure 6.11:** Relative expression of heavy metal ATPase genes in *Arabidopsis* in response to palladium. The data were normalised to the *Arabidopsis ACTIN2* gene and relative fold inductions were calculated using the  $\Delta\Delta C_t$  method [230]. Results are the mean from four biological replicates  $\pm$  SEM. ANOVA Tukey's test.

Quantitative PCR analysis was performed on cDNA samples derived from *Arabidopsis* roots treated with either 0.125 mM of copper or palladium. As a result, *AtHMA5* (12.5- fold), *AtHMA6* (1.5- fold), *AtHMA7* (6.2- fold) and *AtHMA8* (3.4- fold) were all up regulated in response to copper. *AtHMA5* and *AtHMA7* were also significantly upregulated compared to *AtHMA6* and *AtHMA8* when the plants were treated with copper (ANOVA  $p < 0.001$ ). The *AtHMA5* gene was significantly upregulated (5.2- fold) (Student's T-test  $p < 0.01$ ) when compared to *AtHMA7* when the plants were treated with palladium but was significantly lower than copper treated samples (Student's T-test  $p < 0.05$ ) (Figure 6.12). To determine whether *AtHMA5* has activity towards these metals, the gene was cloned and expressed in yeast for yeast functional complementation analysis on copper and palladium. The *Arabidopsis hma5-1* mutant was also obtained to investigate the response of this mutant to the presence of palladium.

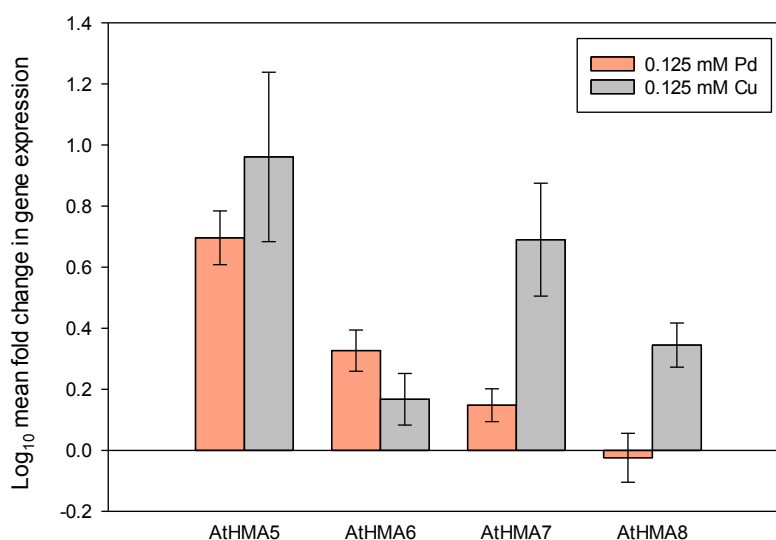


**Figure 6.12:** Relative expression of heavy metal ATPase genes (*AtHMA5*, 6, 7, 8) in *Arabidopsis* in response to palladium and copper. The data were normalised to the *Arabidopsis ACTIN2* gene and relative fold induction values were calculated using the  $\Delta\Delta C_t$  method [230]. Results are the mean from four biological replicates  $\pm$  SEM. ANOVA Tukey's test.

### 6.3.2 Characterisation of the *Arabidopsis hma5-1* mutant

Sequence analysis confirmed the presence of a T-DNA insert 1419 basepairs from the ATG start codon, and in the second exon of *AtHMA5*, as described by Andres-Colas et al [79] (Figure 6.13). Three primers were used in the PCR reaction to confirm the insert. The first combination of primers is that of the *AtHMA5* right flank primer with the specific T-DNA primer and the second combination of primers is made of the *AtHMA5* left flank primer with the specific T-DNA primer. The 18S primers were used for positive control reactions. On the acrylamide gel analysis, two bands around 1.5 kb and 2.0 kb based on the combination of the primers (Figure 6.14) could be observed, corresponding to the inserted T-DNA. No bands were observed in the wildtype lines, thus confirming the T-DNA insertion only in the mutant line. Given the PCR results, in combination with the copper hypersensitive phenotype reported below, the mutant was not further verified by sequencing.

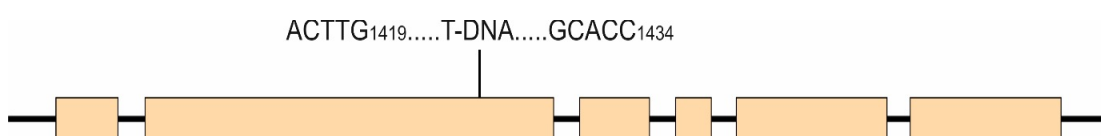


**Figure 6.13:** Schematic diagram of the location of T-DNA insertion sites in the HMA5 gene. Exons are boxed and connecting lines indicate introns. T-DNA boundary *AtHMA5* sequences at the insertion sites are shown.



**Figure 6.14:** T-DNA inserts within the *hma5-1* line. A DNA electrophoresis gel showing that the insert was present in the *hma5-1* plants tested, compared to the Col-0 wildtype plants. 18S primers were used for the control reactions. Primer combinations includes primers specific for the left border of T-DNA with gene-specific primers flanking *AtHMA5* open reading frame.

### 6.3.3 Growth studies of the *hma5-1* mutants on copper

The *hma5-1* mutants are hypersensitive to copper [79]. To verify this phenotype, *hma5-1* seedlings, together with Col-0 wildtype seedlings, were grown on ½ MS(A) supplemented with various concentrations of copper (0, 10, 20, 30 and 40 µM). Based on the measurements taken on the 12<sup>th</sup> day of growth, it was observed that, as the concentration of copper increased, the average root length of *hma5-1* seedlings became significantly shorter and the seedling fresh weights were reduced, when compared to the wildtype, (Student's T-test  $p < 0.001$ ) (Figure 6.15 and 6.16). As also observed in previous work by Andres-Colas et al [79], increasing copper concentration almost completely inhibited the growth of *hma5-1*, with more than an 80 % reduction in both root length and total fresh weight of *hma5-1* plants when grown on ½ MS containing 20, 30 or 40 µM of copper (Figure 6.17).

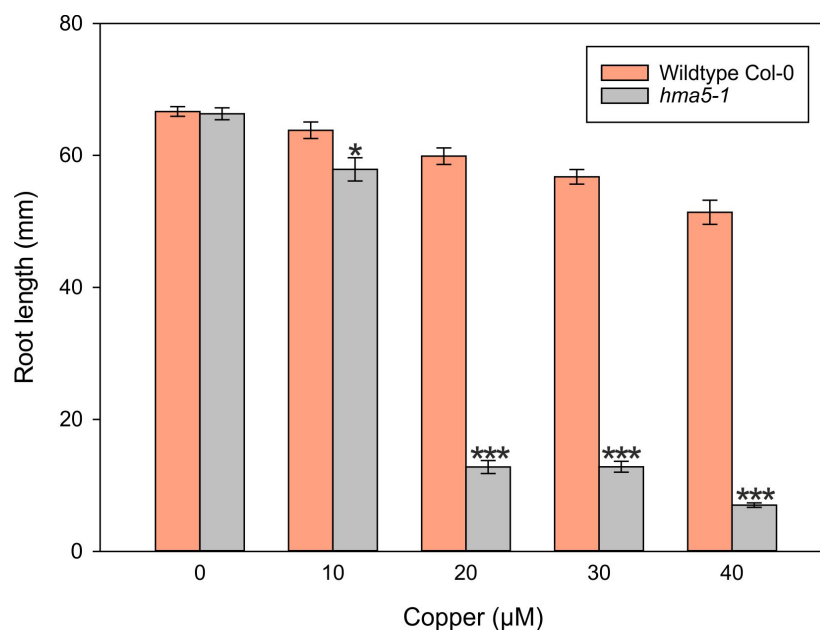


**Figure 6.15:** Root lengths of 12 day-old Arabidopsis Col-0 wildtype and *hma5-1* mutant seedlings on 1/2 MS (A) media containing increasing copper concentrations. Results are the mean from 30 biological replicates  $\pm$  SEM. Student's T-test \* =  $p < 0.05$ , \*\*\* =  $p < 0.001$  significantly different to wildtype.

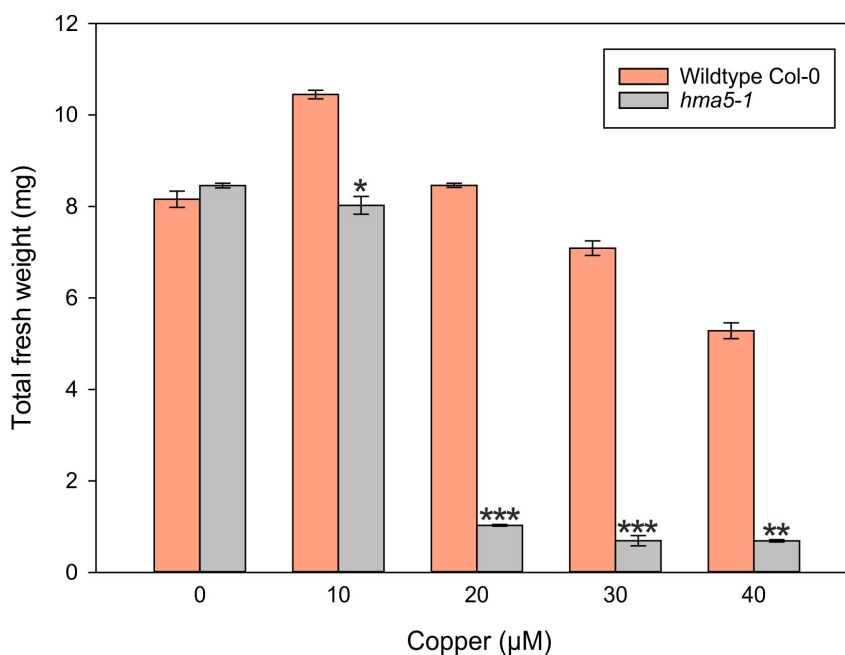


**Figure 6.16:** Total fresh weights 12 day-old Arabidopsis Col-0 wildtype and *hma5-1* mutant seedlings on 1/2 MS (A) media containing increasing copper concentrations. Results are the mean from 30 biological replicates  $\pm$  SEM. Student's T-test \*\* =  $p < 0.01$ , \*\*\* =  $p < 0.001$  significantly different to wildtype.

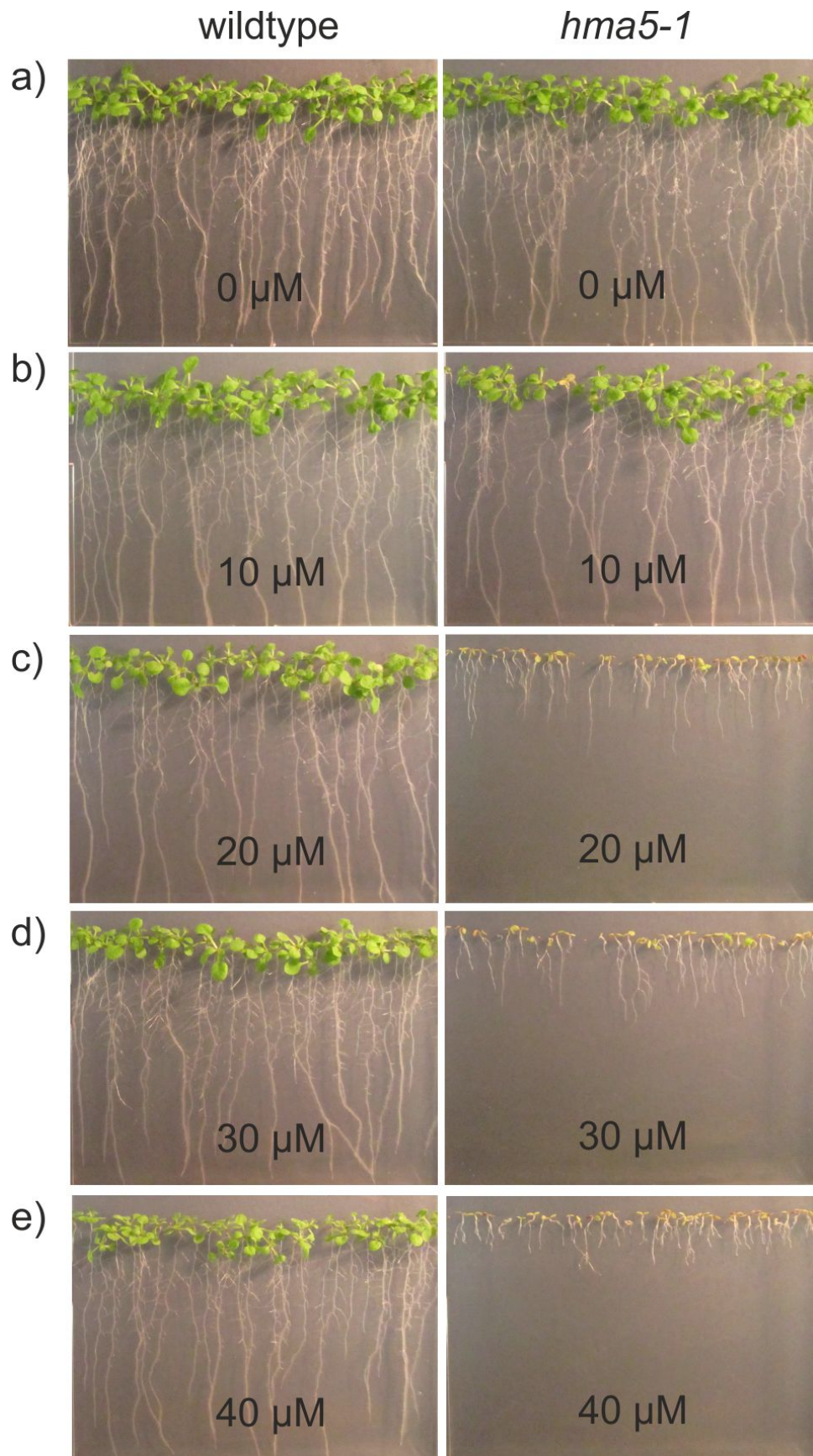


**Figure 6.17:** Appearance of 12 day-old Arabidopsis Col-0 wildtype and *hma5-1* seedlings on  $\frac{1}{2}$  MS (A) with various concentrations of copper as indicated in the picture.

#### **6.3.4 Growth studies of *hma5-1* mutants on gold**

Wild type and *hma5-1* seedlings were grown on ½ MS (A) containing a range of gold concentrations to establish whether the *hma5-1* seedlings were more sensitive than wildtype to gold. As shown in Figure 6.18 & 6.19, there was no significant difference between the root length and total fresh weight of *hma5-1* mutant and wildtype line on all concentrations of gold tested (Student's T-test). It was also observed that the growth of both mutant and wildtype seedlings decreased with increasing gold concentration (0, 50, 100, 150 & 200 µM) (ANOVA Tukey's test  $p < 0.001$ ) (Figure 6.18, 6.19 & 6.20).

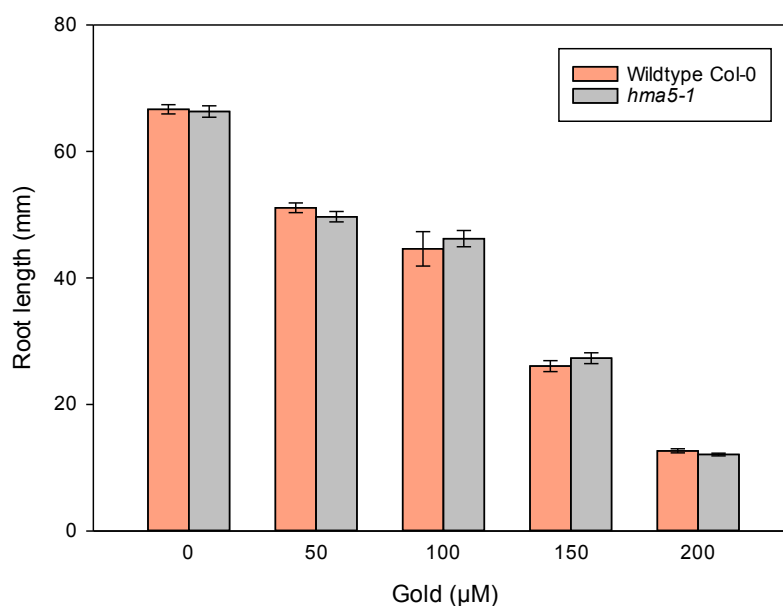


**Figure 6.18:** Root lengths of 12 day-old Arabidopsis Col-0 wildtype and *hma5-1* mutant seedlings on 1/2 MS (A) media containing increasing gold concentrations. Results are the mean from 30 biological replicates  $\pm$  SEM. ANOVA Tukey's test.

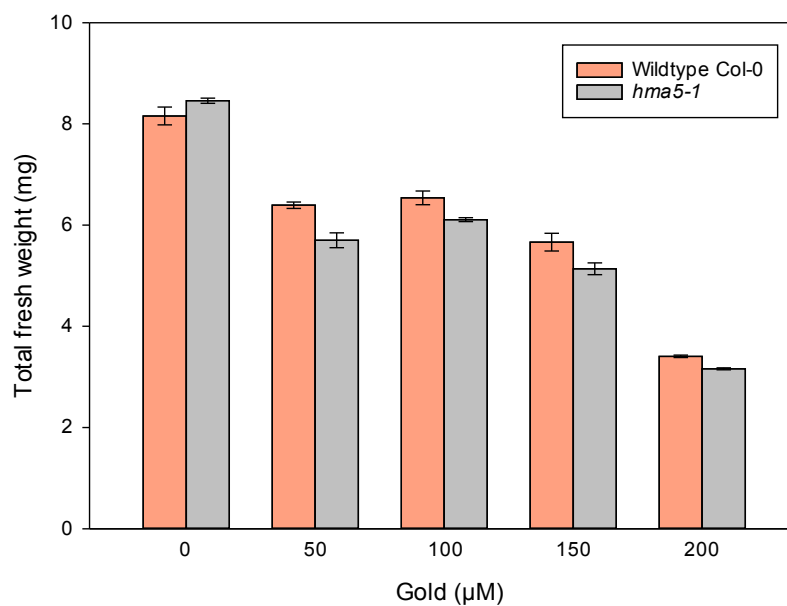


**Figure 6.19:** Total fresh weights 12 day-old Arabidopsis Col-0 wildtype and *hma5-1* mutant seedlings on 1/2 MS (A) media containing increasing gold concentrations. Results are the mean from 30 biological replicates  $\pm$  SEM. ANOVA Tukey's test.

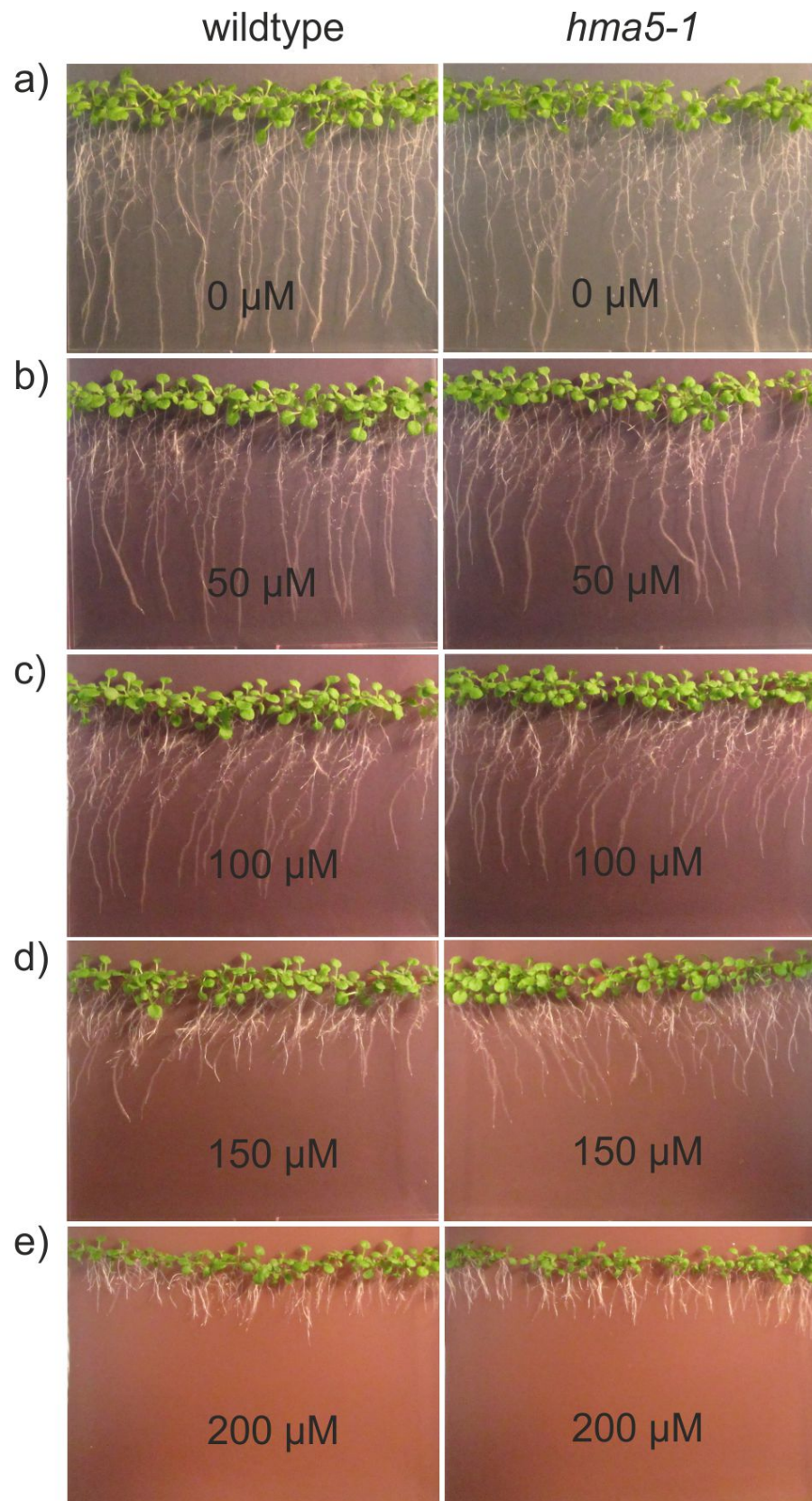


**Figure 6.20:** Appearance of 12 day-old *Arabidopsis* Col-0 wildtype and *hma5-1* seedlings on  $\frac{1}{2}$ MS (A) with various concentrations of gold.

### 6.3.5 Growth studies of *hma5-1* mutants on palladium

To investigate the potential involvement of *AtHMA5* in the detoxification of palladium, *Arabidopsis Col-0* wildtype and *hma5-1* mutant seedlings were grown on ½ MS (A), supplemented with a range of palladium concentrations. As discussed in the previous chapter (Chapter 3, Section 3.3.2), palladium caused inhibitory effects to *Arabidopsis* seedlings when grown on agar plates containing concentrations as low as 10 µM. Therefore, in this experiment, the *hma5-1* and wildtype seedlings were grown on ½ MS (A) with 0, 5, 10, 15 and 20 µM. Root length and total fresh weight measurements of 12 day-old plants are shown in Figures 6.21 & 6.22, respectively. In agreement with the observations on gold (Section 6.3.5), there were no significant differences between *hma5-1* and the wildtype plants on all palladium concentrations (Student's T-test) (Figure 6.18 & 6.19). As expected, it was observed that the growth of both type of plants decreased as concentration of palladium increased (0, 5, 10, 15 & 20 µM) (ANOVA Tukey's test  $p < 0.001$ ) (Figure 6.23). This result further suggests that *AtHMA5* is not involved with any palladium detoxification mechanism in *Arabidopsis*.

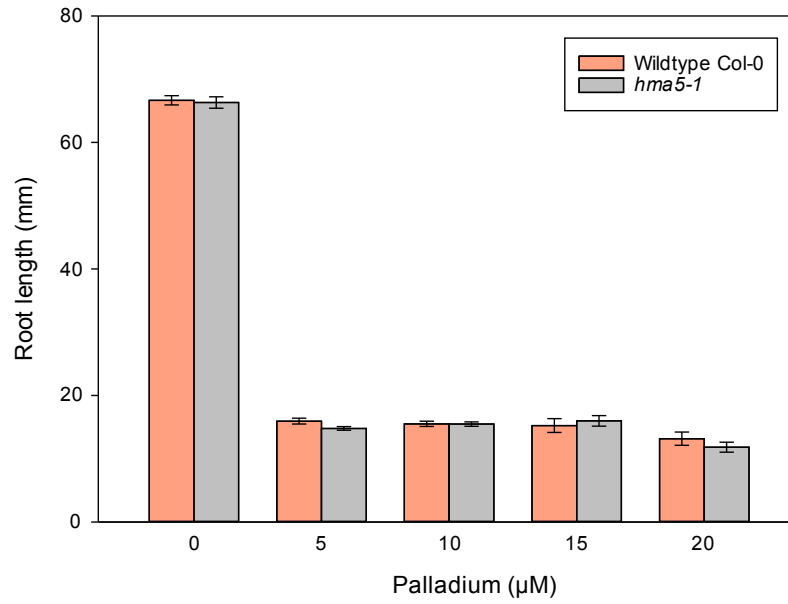


**Figure 6.21:** Root lengths of 12 day-old *Arabidopsis* Col-0 wildtype and *hma5-1* mutant seedlings on  $\frac{1}{2}$  MS (A) media containing increasing palladium concentrations. Results are the mean from 30 biological replicates  $\pm$  SEM. ANOVA Tukey's test.

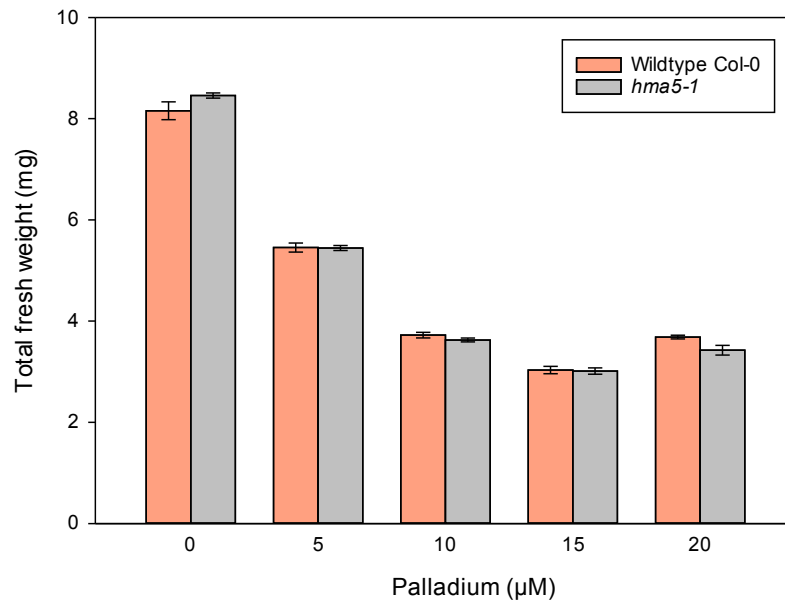


**Figure 6.22:** Total fresh weights 12 day-old *Arabidopsis* Col-0 wildtype and *hma5-1* mutant seedlings on  $\frac{1}{2}$  MS (A) media containing increasing palladium concentrations. Results are the mean from 30 biological replicates  $\pm$  SEM. ANOVA Tukey's test.

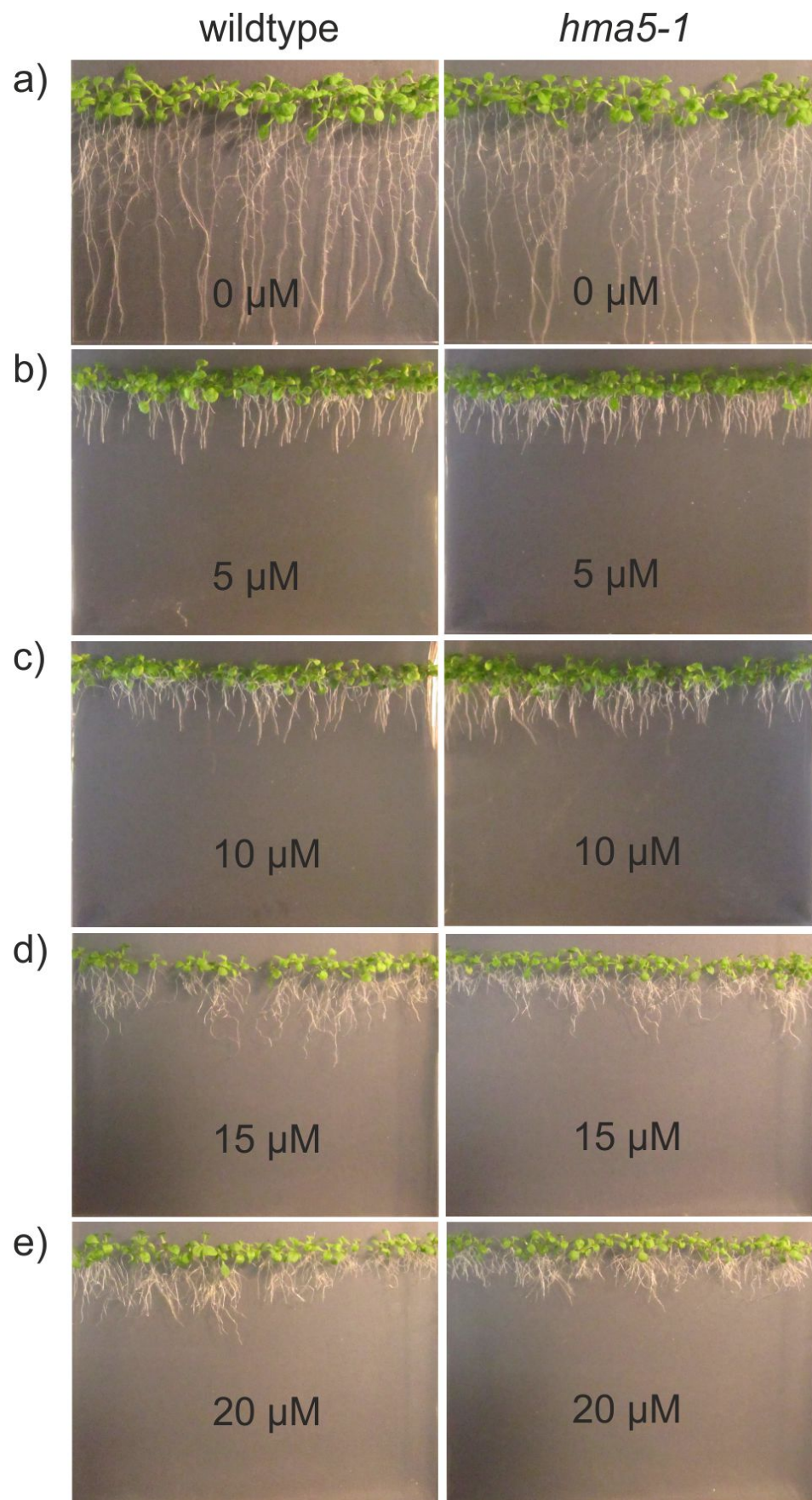


**Figure 6.23:** Appearance of 12 day-old Arabidopsis Col-0 wildtype and *hma5-1* seedlings on  $\frac{1}{2}$ MS (A) with various concentrations of palladium.

### 6.3.6 Cloning and expression of *AtHMA5* in yeast

Codon-optimised *AtHMA5* was cloned into the pYES2 vector and cloning was verified via enzymatic restriction, as shown in Figure 6.24, and DNA sequencing. The purified plasmid bearing *AtHMA5* was then transformed into yeast. Positive transformants were verified using colony PCR (Figure 6.25).

No specific protein tag (eg; His/ Strep) was introduced in the cDNA sequence to avoid any functional inhibition or background activity in the transformed yeast. However, without an affinity tag subcellular localisation of the expressed HMA5 by western blotting could not be performed. Quantitative PCR analysis showed that *AtHMA5* was transcribed in the yeast strain; however, following SDS-PAGE, there were no bands at the predicted size for *AtHMA5* in the lane containing the extracted transmembrane fraction of yeast transformed with pYES2-HMA5, when compared to empty vector control lane (Results not shown). Growth density across increasing time points have shown that yeast cells expressing pYES2-*AtHMA5* grew more slowly than the empty vector, suggesting that the yeast was utilising additional energy to express the *AtHMA5* gene in its system, compared to the strain transformed with the empty vector (Figure 6.26).

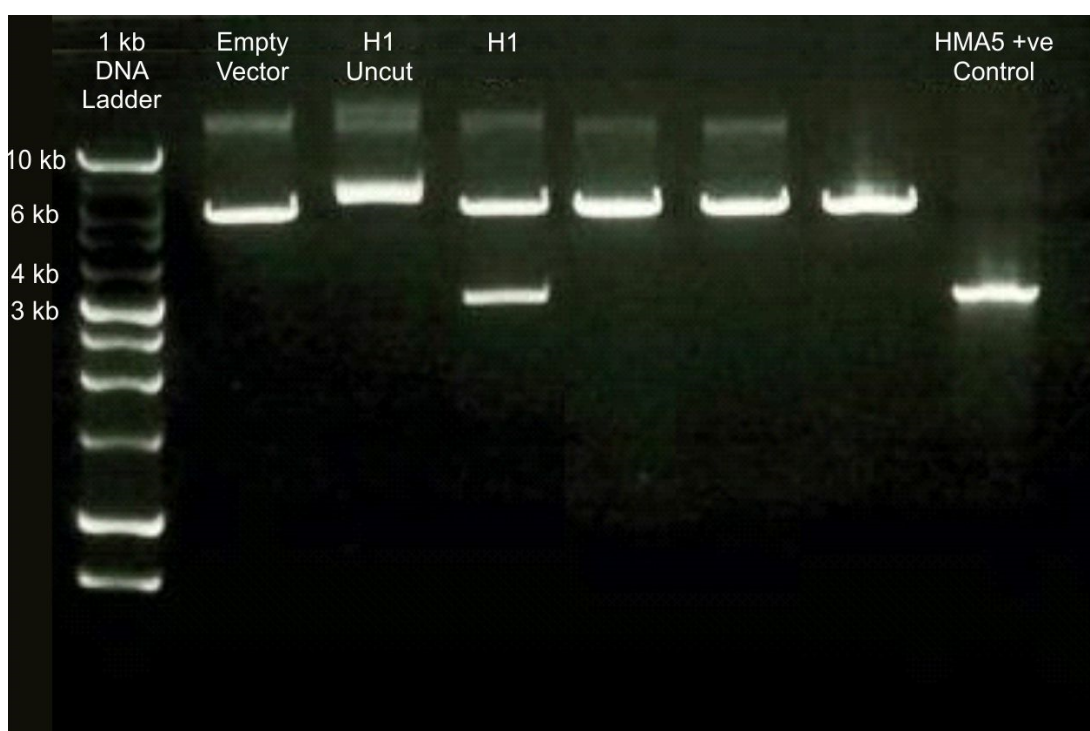


**Figure 6.24:** Verification of *AtHMA5* insert via digestion at Xho1 and Nde1 restriction site of pYES2 vector. Sample H1 was further verified by sequencing.

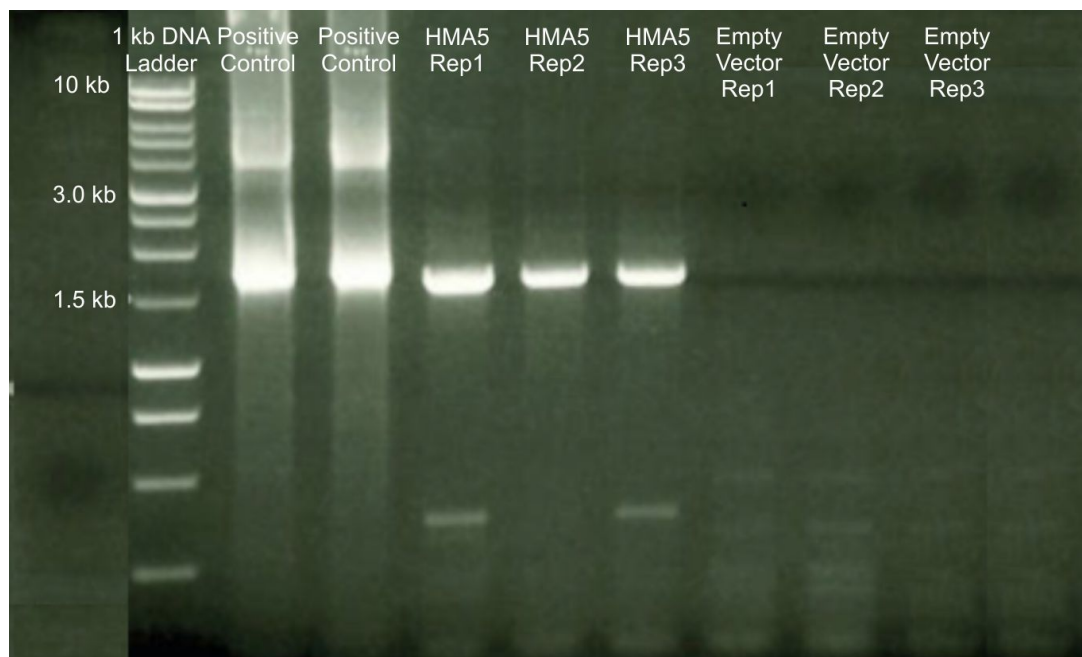


**Figure 6.25:** Colony PCR of yeast strains BY4741 expressing pYES2-*AthHMA5* and empty vector.

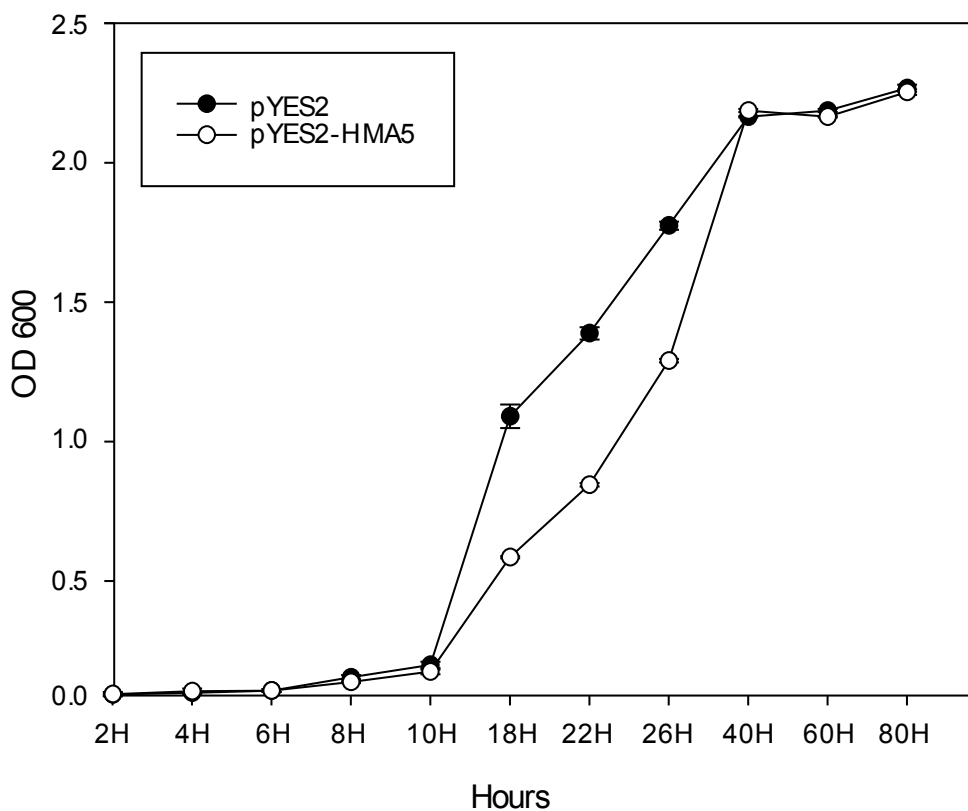


**Figure 6.26:** Growth of yeast BY4741 transformed with pYES2-*AthHMA5* or pYES2 empty vector after 80 hours of incubation at 30 °C. Results are the mean from three biological replicates  $\pm$  SEM.

### 6.3.7 Activity of *AtHMA5* on copper

To measure the activity of *AtHMA5* in yeast, spot analysis assays were conducted on YSD plates containing different concentrations of copper. As shown in Figure 6.27, there was no difference between pYES2-*AtHMA5* and pYES2-empty vector of both parental and mutant  $\Delta ace1$  yeast strain grown on plates containing 0, 100 or 500  $\mu\text{M}$  of copper. As the concentration was increased to 1000  $\mu\text{M}$ , no growth was observed for the mutant strain  $\Delta ace1$  with empty pYES2 vector, whereas the expression of *AtHMA5* had complemented the  $\Delta ace1$  strain. Growth density analysis further showed that the expression of *AtHMA5* also significantly increased tolerance of  $\Delta ace1$  to excess copper (1 mM) when compared to the strain transformed with the empty vector (Student's T-test  $p < 0.01$ ) (Figure 6.28).

The expression of *AtHMA5* was also verified by cloning and expressing the *AtHMA5* gene into the yeast mutant strain  $\Delta ccc2$ . Based on the spot analysis, no difference could be observed on iron and copper sufficient media. However, it was observed that the expression of *AtHMA5* complemented the function of *Ccc2*, which regulates copper delivery from cytosol to multicopper oxidase Fet3P, by restoring the growth of yeast mutant strain  $\Delta ccc2$  on copper deficient media (Figure 6.29).

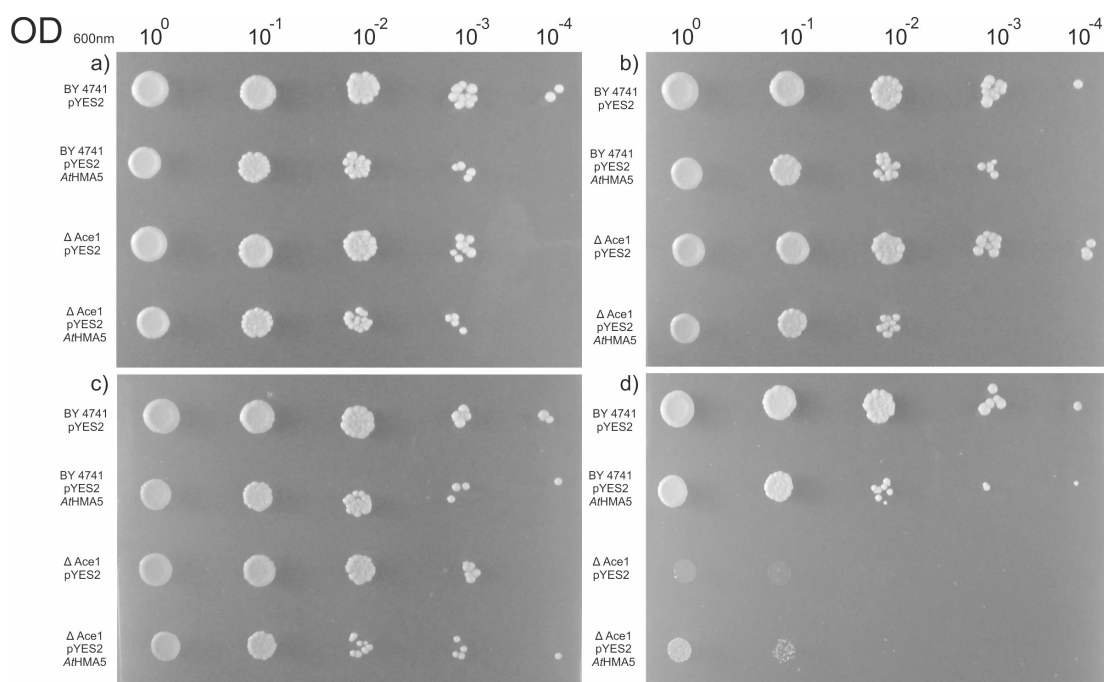


**Figure 6.27:** *Ace1* functional complementation assay on YSD medium containing various copper concentrations. Three microliters of cell suspension with an OD<sub>600</sub> of 0.3 and four serial 1:10 dilutions were spotted and incubated at 30 °C for 5 days on YSD media containing a) 0 b) 100 c) 500 and d) 1000 µM of copper.

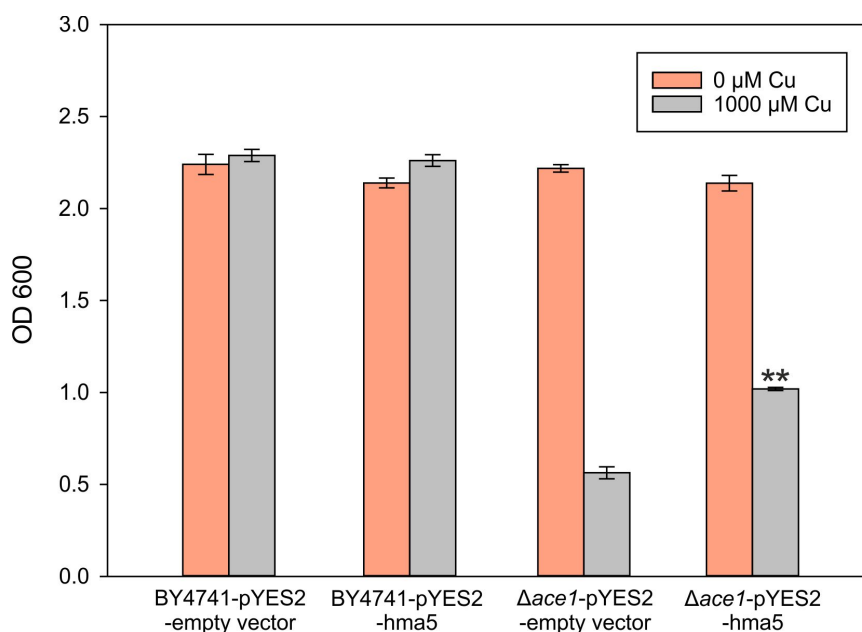


**Figure 6.28:** Growth density of yeast strains on excess copper. Results are the mean from three biological replicates  $\pm$  SEM. Student's T-test \*\* =  $p < 0.01$  significantly different to mutant strain  $\Delta ace1$  with empty vector of pYES2.

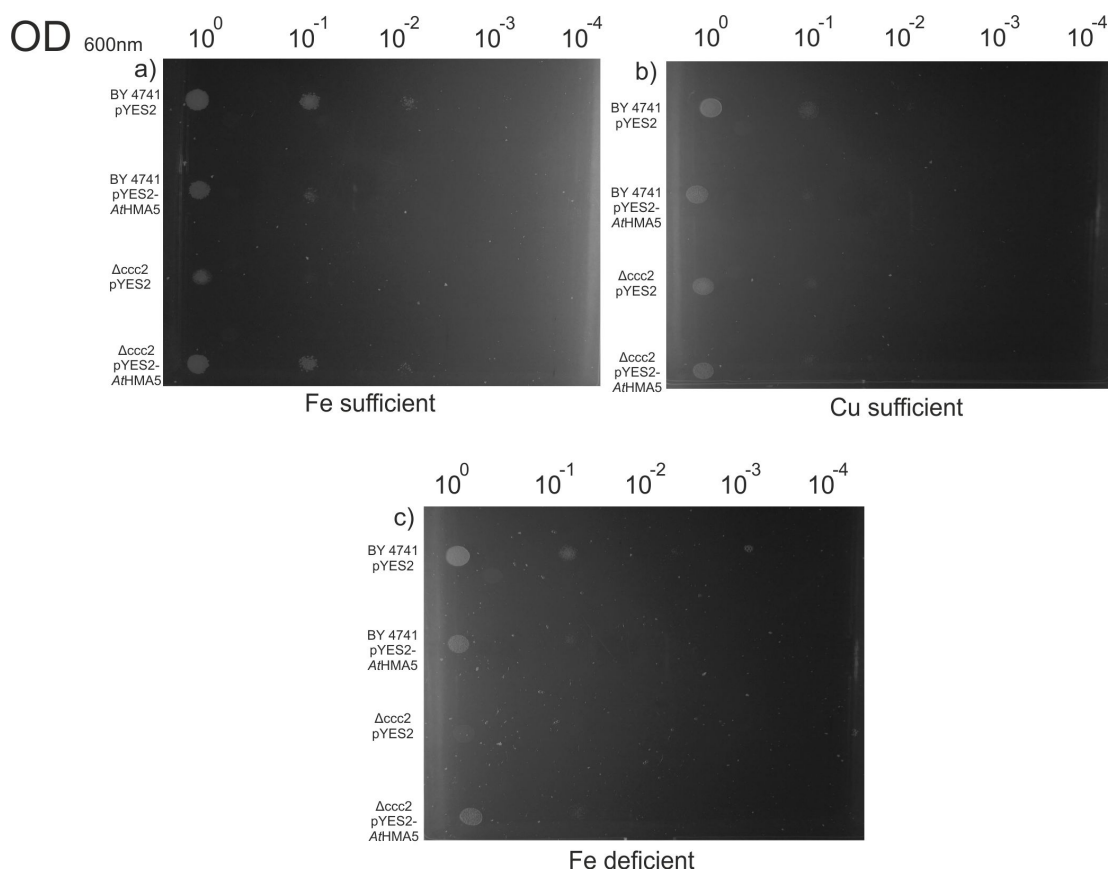


**Figure 6.29:** *Ccc2* functional complementation assay on YSD medium containing various media. Three microliters of cell suspension with an OD<sub>600</sub> of 0.3 and four serial 1:10 dilutions were spotted and incubated at 30 °C for 5 days on YSD media with a) Fe sufficient b) Cu sufficient and c) Fe deficient condition.

### **6.3.8 Activity of *AthMA5* on gold or palladium**

The potential activity of *AthMA5* towards gold or palladium was further investigated by conducting spot analysis assays on media with various concentrations of gold or palladium. As observed in Figure 6.30, the growth of all strains tested decreased with increasing concentrations of gold. The growths of all strains were inhibited as the concentration of gold reached 500  $\mu\text{M}$ .

Similar results to gold were also observed when the yeast strains were spotted on selective media containing palladium. The growth of all strains tested decreased with increasing concentrations of palladium (Figure 6.31). None of the strains grew on plates containing 1 mM of palladium.

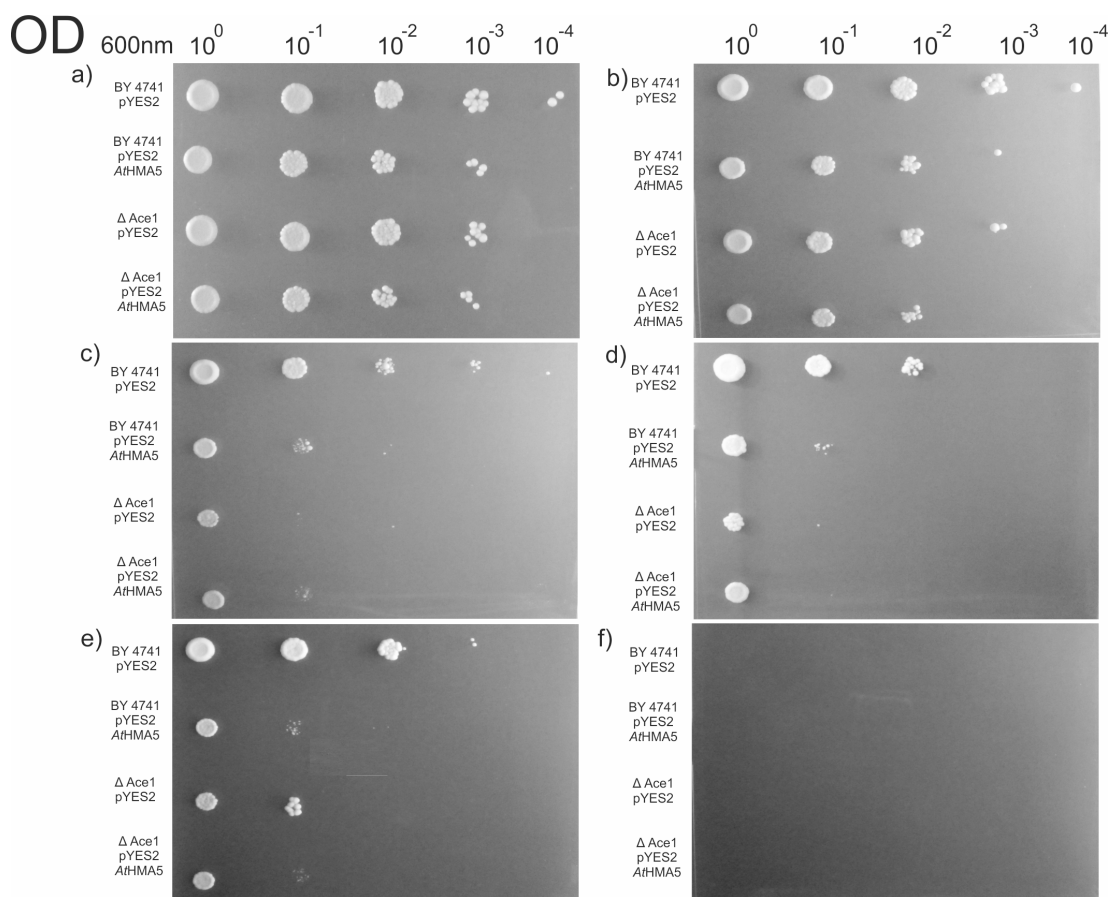


**Figure 6.30:** Spot assay analysis on YSD medium containing gold. Three microliters of cell suspension with an OD<sub>600</sub> of 0.3 and four serial 1:10 dilutions were spotted and incubated at 30 °C for 5 days on YSD media with a) 0 b) 100 c) 200 d) 300 e) 400 and f) 500  $\mu$ M of gold.

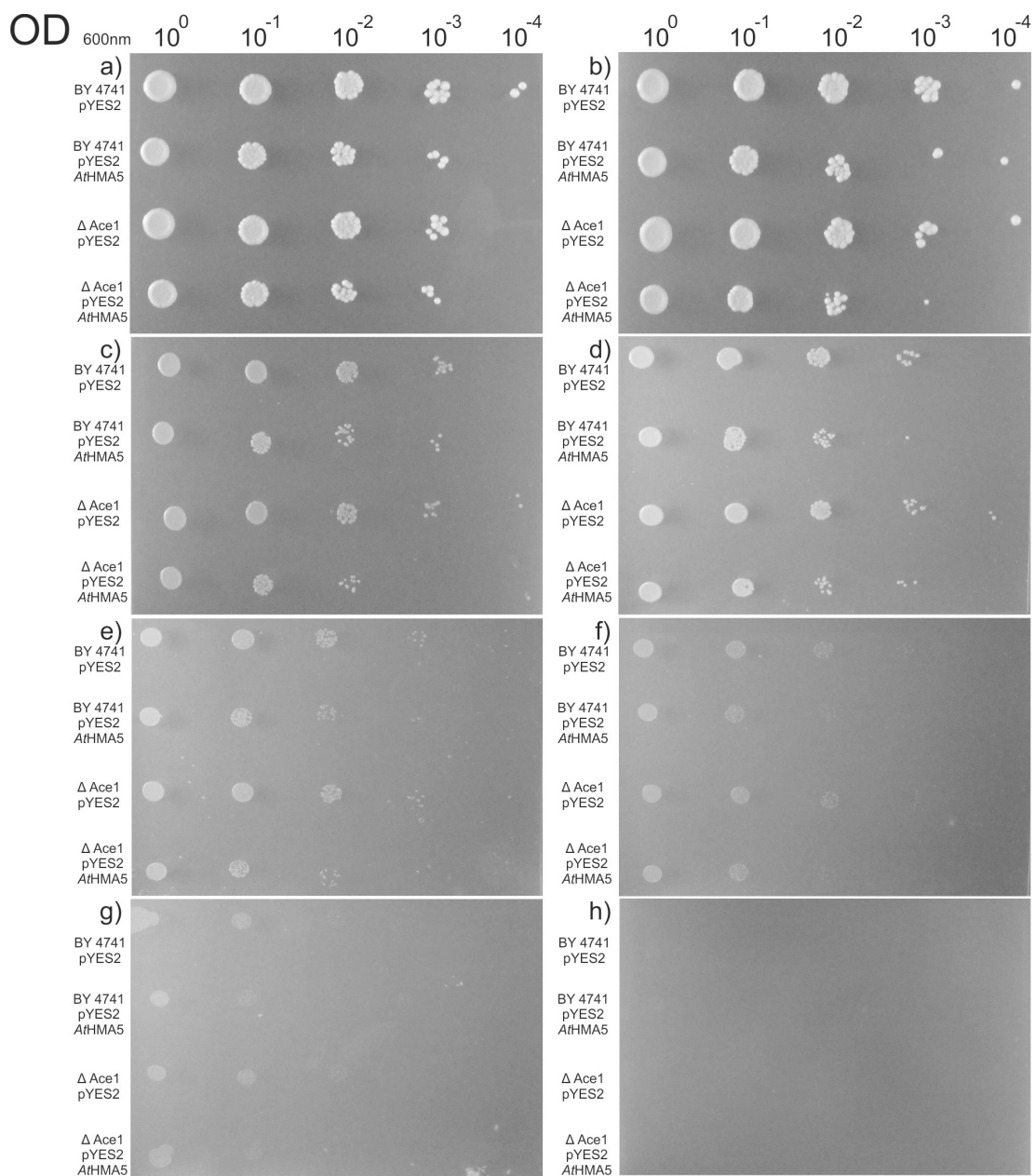


**Figure 6.31:** Spot assay analysis on YSD medium containing palladium. Three microliters of cell suspension with an OD<sub>600</sub> of 0.3 and four serial 1:10 dilutions were spotted and incubated at 30 °C for 5 days on YSD media with a) 0 b) 100 c) 500 d) 600 e) 700 f) 800 g) 900 and h) 1000 μM of palladium.

### **6.3.9 Activity of *AtHMA5* on excess copper in the presence of gold or palladium**

To establish if gold or palladium interfere with the ability of *AtHMA5* to transport copper, growth of the yeast strains in the presence of copper was measured in the presence and absence of gold or palladium.

As shown in Figure 6.32 and 6.33, the growth of  $\Delta ace1$  expressing *AtHMA5* in media containing excess copper (1 mM), was inhibited in the presence of either gold or palladium. Plates containing gold or palladium alone did not show any difference in terms of growth on all strains tested, as observed previously in Section 6.3.8.

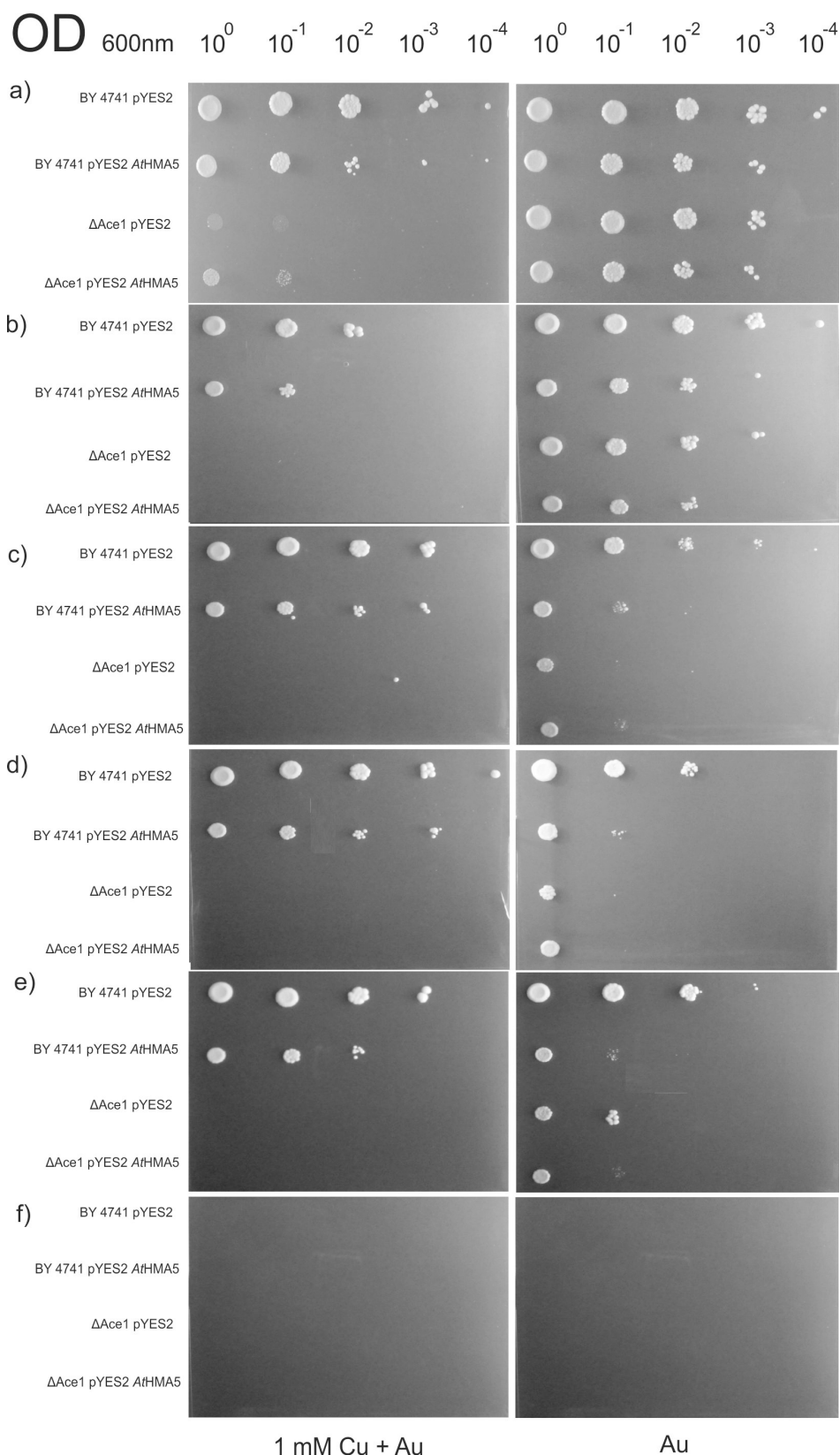


**Figure 6.32:** Spot assay analysis on YSD medium containing 1 mM copper plus various concentrations of gold and gold only. Three microliters of cell suspension with an OD<sub>600</sub> of 0.3 and four serial 1:10 dilutions were spotted and incubated at 30 °C for 5 days on YSD media with 1 mM copper plus or only a) 0 b) 100 c) 200 d) 300 e) 400 and f) 500 μM of gold.

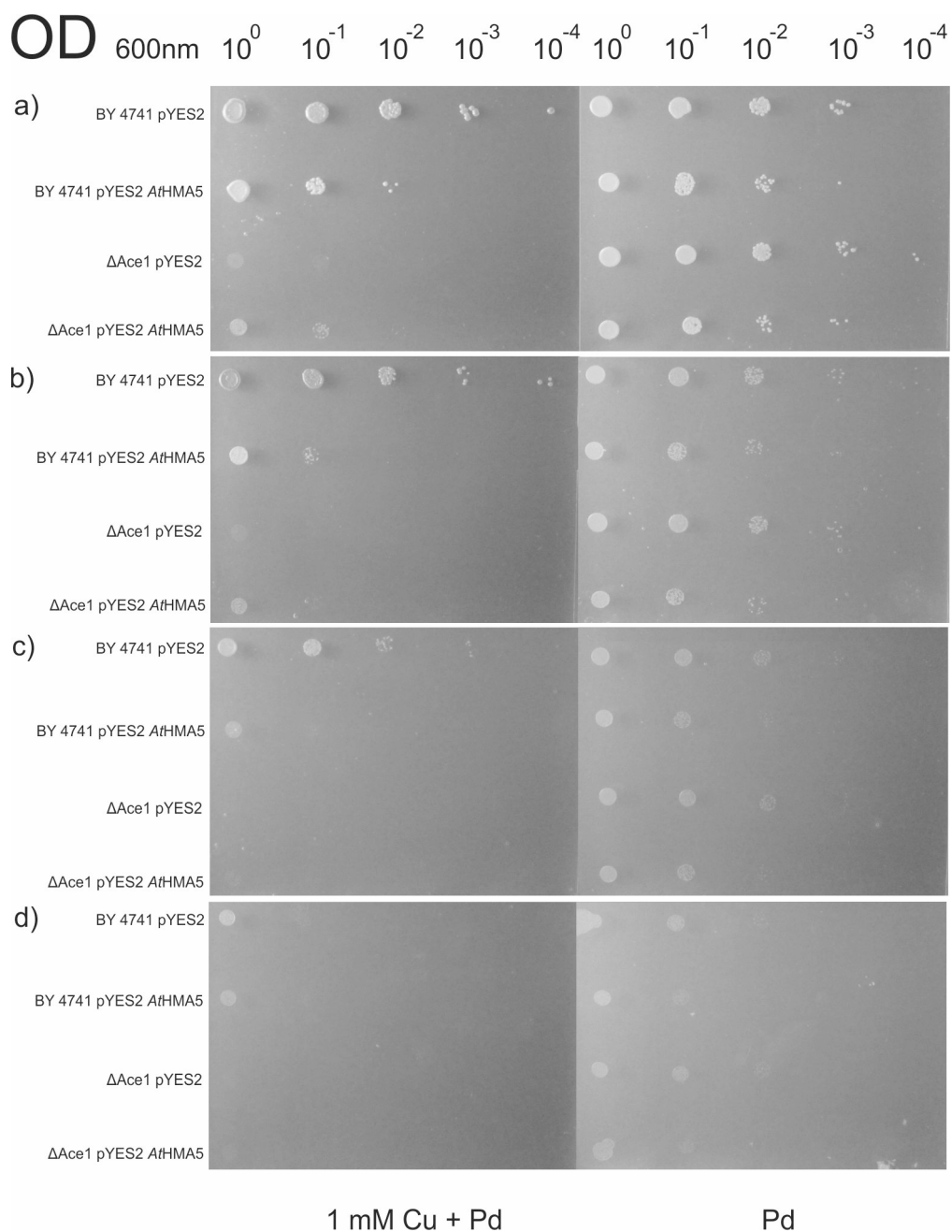


**Figure 6.33:** Spot assay analysis on YSD medium containing 1 mM copper plus various concentrations of palladium and palladium only. Three microliters of cell suspension with an OD<sub>600</sub> of 0.3 and four serial 1:10 dilutions were spotted and incubated at 30 °C for 5 days on YSD media with 1 mM copper plus or only a) 0 b) 700 c) 800 d) and 900 μM of palladium.

## 6.4 Discussion

In agreement with the results obtained by Taylor et al [46, 47] with gold, treatment of *Arabidopsis* plants with palladium strongly downregulated the expression of *IRT* and *TIPs* and *MTPA* in the roots. The *IRT* genes (*IRT1* and *IRT2*) are reported to transport a broad range of metals including essential and non-essential metals such as iron, cadmium, cobalt, manganese and zinc [210, 211, 276, 277]. Previous microarray analysis showed that the expression of *IRT1*, which encodes an iron uptake transporter, was strongly down regulated in response to exposure to cadmium, indicating that the plant is avoiding accumulating the metal to toxic levels [278]. Cadmium, which has no function in plant growth, was also found to decrease the level of *IRT1* expression in *Arabidopsis* [279]. The growth of *irt1* *Arabidopsis* mutants was also inhibited completely when the plants were grown on iron-deficient medium supplemented with cadmium, suggesting a direct involvement of *IRT1* in the uptake of cadmium in *Arabidopsis* [279]. Therefore, it could be hypothesised that precious metals such as gold and palladium could also affect the expression of these genes.

This study is the first to show the expression of the whole *AtHMAs* family in response to palladium, and to compare expression levels of *AtHMA5* to 8 in response to copper and palladium exposure. The chemistry of gold and palladium shows that these metals can exist in monovalent forms, which would be compatible with *AtHMA5* activity, but they can also exist in di- and trivalent forms. However, given the relatively unreactive nature of these elements, the form that is most likely to be taken up, may depend more on the chemistry of the surrounding soil or medium, rather than the preference of the transporter.

Comparison between the expression values of *AtHMA5*, 6, 7 and 8 in response to excess copper or palladium showed that the upregulation of the genes was enhanced when plants were treated with copper (Figure 6.12). It has been well documented that *AtHMA5*, 6, 7 and 8 are all involved in copper regulation and detoxification in *Arabidopsis* [79, 84, 89]. *AtHMA7*, which is closely related to *AtHMA5*, is reported to transport copper from the cytosol into the Golgi apparatus in the cells, where copper serves as a cofactor for post-translational modification of proteins [267, 280]. *AtHMA7* delivers copper to Ethylene Response1 (ETR1), located at the Golgi apparatus, which is responsible for ethylene-binding mechanism [280]. Similar to *AtHMA5*, the expression of *AtHMA7* in the yeast  $\Delta ccc2$  mutant cells also complement its function when grown on iron deficient media, suggesting a

direct role of *AtHMA7* in copper delivery. *AtHMA6* and 8 are responsible for the delivery of copper to plastocyanin, an important component of the chloroplast photosynthetic electron transfer chain activity [281]. Recently, it has been shown that *AtHMA8* has higher affinity than *AtHMA6*, for copper [84]. This was observed by comparing the concentration of copper in the yeast membranes expressing either *AtHMA6* or *AtHMA8* using ICP-MS. It was found that the copper concentration in the membrane containing *AtHMA8* was about one-third of the value obtained from *AtHMA6* even when the yeast strains were treated at lower copper condition. This tight regulation might explain why *AtHMA8* is upregulated in response to copper but unaffected by palladium treatment.

It was previously reported that no metal other than copper or silver could induce the expression of *AtHMA5* [52, 79]. Together with the results obtained in Dr. Andrew Taylor's work [46], this is the first evidence showing that palladium and gold can also be added to the list.

Despite the transcriptional and circumstantial evidence pointing towards *AtHMA5* having activity towards gold and/or palladium, no phenotypes were observed when the *hma5-1* mutant was exposed to these metals. It is possible that this is because there is redundancy with other transporters. A likely candidate could be *AtHMA7*, which is closely related to *AtHMA5*. Generating a *hma5hma7* double mutant could perhaps enable the study of growth sensitivity on media containing gold or palladium, assuming such a double mutant was viable.

It still remains that palladium and gold are taken up by plants, and given the wealth of evidence for metal cation transport, transporters facilitate this uptake. To broaden the search for palladium and gold transporters, additional mutants in transporters with altered copper profiles could be identified by screening mutants from the Salt and Schroder Arabidopsis Ionomics Database [282-284]. This database, available at PlantsT (<http://www.ionomicshub.org/>) contains shoot elemental profiles for "10,600 fast neutron mutagenized Arabidopsis plants comprising 5847 M2 plants (representing 2373 M1 parental lines Salt lab and 1100 parental lines Schroeder lab) and 420 M3 families selected in the M2 generation for their modified elemental-profiles". Initially, the mutants could be screened for altered root length on media containing gold or palladium, with subsequent studies to measure total biomass and tissue content using ICP-MS.

The yeast functional complementation assays demonstrated that *AtHMA5* can complement the copper sensitive  $\Delta ace1$  mutant. This is in agreement with previous work by Migocka et al [52], which showed that expression of *CsHMA5.2* in the copper-sensitive  $\Delta ace1$  yeast mutant strain increased tolerance to excess copper. *Ace1* is a transcription activator protein that contains a copper-cysteine-rich DNA binding domain at its N-terminal region [285] and is responsible for the activation of the metallothionein-encoding genes *Cup1* [286] and *Crs5* [287], as well as superoxide dismutase *SOD1* in response to excess copper in yeast. *Cup1* and *Crs5* are involved in copper detoxification mechanisms in yeast by encoding small cysteine-rich metallothioneins that bind to excess  $Cu^+$  [286] while *SOD1* which encodes a Cu-Zn superoxide dismutase enzyme, may also function as a metallothionein, by directly binding and then sequestering excess  $Cu^+$ , to prevent dysfunctional copper binding to biological metal ligands [288]. Therefore, the mutated *Ace1* gene results in the inability of the  $\Delta ace1$  mutant to grow in excess copper conditions. However, *CsHMA5.2* is localised in the root tonoplast [52] and in the vacuolar membrane of yeast [52], whereas *AtHMA5* is likely to be expressed in the root plasma membrane [79]; no subcellular localisation of *AtHMA5* in the yeast has yet been conducted. Since both proteins are able to complement the function of *Ace1* in excess copper condition, investigating the location of *AtHMA5* in yeast could further explain its involvement in copper detoxification in yeast.

The functional expression of *AtHMA5* in yeast was also verified by successfully complementing the function of *Ccc2* in the  $\Delta ccc2$  mutant when grown on iron deficient media (Figure 6.29). *Ccc2* is a P-type ATPase pump localised in the Golgi compartment in the secretory pathway [289], which regulates copper delivery from the cytosol to multicopper oxidase *Fet3P*. *Fet3P*, located in the Golgi, is involved in the high affinity uptake of iron in yeast [290]. Thus, yeast lacking the *Ccc2* protein are unable to transport copper from the cytosol to the Golgi and are not able to grow on iron-deficient media. However *AtHMA5* is an efflux transporter, and putatively located in the plasma membrane [79]. It is unclear how increasing the efflux of copper in the  $\Delta ccc2$  cells and lowering cytosolic copper levels complements  $\Delta ccc2$  phenotype. A previous study by Kobayashi et al [89] had also shown the ability of *AtHMA5* to complement the function of *Ccc2* in iron deficient media. Other  $Cu^+$  plasma membrane transporters, such as *OsHMA5* [30] and *BnRAN1* [289] (which are highly homologous to *AtHMA5*) are also able to complement the function of *Ccc2*. It might be possible that *AtHMA5* could also be colocalised in another part of the intracellular membrane. This has been observed for the closest *AtHMA5*

homologue (45 % identity), the Menkes disease transporter (ATP7A) [79]. Previous work on ATP7A has shown that this P-type ATPase pump, which is primarily located at the *trans*-Golgi network for intracellular copper homeostasis, is also able to be relocated to the plasma membrane to extrude excess copper out of the cell [79, 266, 291, 292]. Further investigation by mutations on several conserved regions of ATP7A, such as at the phosphorylation (DKTGT) and the phosphatase domain (TGE), which are also present in *AtHMA5*, suggests that the key aspect of the translocation of the transporter is associated with the formation of the phosphorylated intermediate during the catalysis [266]. It could be that when *AtHMA5* is expressed in the  $\Delta ccc2$  cells and grown on iron-deficient conditions, the phosphorylated intermediate formed in the presence of  $\text{Cu}^+$  in the media induces translocation of *AtHMA5* to the Golgi network to deliver  $\text{Cu}^+$  to the Fet3P for iron uptake in yeast. Further experimental work is required to test this hypothesis.

From the functional expression studies on *AtHMA5*, as well as from the results obtained with the *hma5-1* mutant plant line, it can be clearly concluded that gold and palladium are not substrates for *AtHMA5*.

Interestingly though, additional analysis on the activity of the  $\Delta ace1$  mutant yeast strains expressing *AtHMA5* towards excess copper in the presence of gold or palladium, indicated that copper transport by *AtHMA5* was inhibited by the presence of gold or palladium. This observation suggests that gold and palladium are able to bind to *AtHMA5*. A hypothesis is that gold and palladium may act as non-competitive inhibitors, binding to the two MXCXXC metal binding sites present on *AtHMA5*. To investigate this, recombinantly expressed and purified *AtHMA5* would be required, ATPase assays could then also be carried out to investigate whether gold or palladium can activate *AtHMA5*.

If gold and palladium bind to the MXCXXC sites, it would be interesting to discover if this binding regulates *HMA* transcription. Broad ranges of metals are able to increase the expression of genes encoding specific metal transporters [52, 77]. Silver, for example, has been shown to induce the expression of *HMA5* and also shown to have a good binding affinity and transport activity with *HMA5* in Arabidopsis [79] and cucumber [52]. However, it is also well-established that increased transcription does not necessarily result in an increase in subsequent protein activity. Recent work by Shin et al [293] revealed that the increased expression of *AtHMA5* transcript in the mutant *atx1* in response to excess copper did not result in a corresponding increase in copper tolerance or root to shoot

translocation, compared to the wildtype. Thus, while gold and palladium are able to trigger the expression of the *AtHMA5* transcript, the inability of *AtHMA5* to detoxify gold or palladium could be further compounded by the lack of ATX1 expression, or ability of these metals to form complexes with ATX1, or other chaperones. While ATPase, phosphorylation and transport activity assays, in the presence and absence of metal chaperones such as ATX1 or CCH could be used to investigate the requirement of specific metal-chaperone complexes, in the case of HMA5, the yeast functional studies presented here demonstrate that gold and palladium are not substrates for transport.

The exact subcellular localisation of *AtHMA5* when expressed in yeast is unknown and could be determined by tagging *AtHMA5* with GFP. If *AtHMA5* is highly expressed in the vacuole membrane, then it could be that growth inhibition might be caused by an increased concentration of gold or palladium in the vacuole. Excess copper would be kept in vacuole and then be pumped back into the cytoplasm when needed. Unlike copper, gold and palladium might not be recycled back as they have no known function in yeast growth. Metal quantification analysis using ICP-MS could be used to further investigate this hypothesis.

Overall, the results obtained from this work show that *AtHMA5* is not directly involved in the detoxification mechanism of gold and palladium but could be highly expressed in response to the metals due to a general heavy metal binding mechanism towards metal transporters.

## Chapter 7: Final discussion

### 7.1 Research in context

In this study, the main aim was to investigate the potential of plants to take up palladium and other precious metals from mine wastes, for remediation and re-vegetation purpose. Chapter 3 explores the phytotoxicity of palladium and presents different plant species as candidates for use in phytomining. Chapter 4 investigates the potential of bacterial *merA* gene expressed in plants as a genetic engineering approach to improve palladium and gold tolerance in plants. Chapter 5 explores the ability of short synthetic peptides expressed in plants to increase the formation and manipulate the deposition of metal nanoparticles within plants. Chapter 6 investigates the biochemistry behind uptake and detoxification of palladium and gold in plants, including the potential involvement of the transporter *AtHMA5*.

This research,

1. Reveals that willow (*Salix viminalis* & *S. purpurea*) and miscanthus (*Miscanthus giganteus*) are potential candidates for revegetating, phytomining and remediating palladium-containing mine wastes.
2. Demonstrates that the application of cyanide to mine wastes significantly increases palladium uptake and subsequent translocation from roots to the aerial tissues of plants.
3. Explains and defines that high (> 12 g/kg) levels of palladium accumulation are required to yield commercially-equivalent catalytic activity.
4. Demonstrates that gold nanoparticle size *in planta* can be manipulated by the expression of specific peptide sequences.
5. Concludes that expression of the bacterial mercury reductase (MerA) does not increase Arabidopsis tolerance to palladium or gold.
6. Identifies that palladium or gold inhibit the activity of MerA towards mercury.
7. Rules out the involvement of the copper transporter *AtHMA5* in the detoxification of palladium and gold in Arabidopsis.

## **7.2 Willow and miscanthus could be used in phytomining of palladium from mine wastes**

As discussed in Chapter 3, phytomining could be an efficient approach to re-vegetate and remediate mine wastes. In addition to cleaning up highly contaminated land, a phytomining approach could also add value via the production of bioenergy and from the metal harvested. To my knowledge, no prior research has been carried out to explore the potential of plants to extract palladium from mine wastes. Palladium, which undoubtedly has application in many industrial sectors, can be reclaimed back from mine wastes using conventional methods to obtain the bulk metal, or, an avenue that has the potential to add further value, the use of the metal-containing plant biomass to make catalysts.

It was found that cyanide treatment significantly increases the translocation of palladium into the aerial tissues of both willow and miscanthus. When willow was grown on mine wastes, it was observed that the cyanide-induced treatment also increased the uptake of copper, iron, nickel and zinc. When different varieties of willow species were tested, it was found that *S. purpurea* (Green Dicks) had the highest palladium accumulation in the leaf materials (0.8 g/kg) and also showed good growth tolerance when compared with other willow species grown on synthetic media containing 50 mg/kg of palladium.

Miscanthus, which is a non-woody grass species, produced over a 500-fold increase in shoot palladium content when the plants were dosed with cyanide as compared to the non-treated plants. In this project, miscanthus plants were grown on synthetic ore medium containing 100 mg/kg of palladium. As 127-fold higher fold uptake was observed when willow plants were grown on lower (< 10 mg/kg) palladium concentration, it would be interesting to investigate the uptake level of miscanthus plants grown on lower palladium concentrations. Based on the results obtained on willow grown on lower (10 mg/kg) palladium concentration, it is expected that more palladium accumulation in the shoot materials would be observed on miscanthus plants grown on lower palladium concentration.

In subsequent catalytic studies on the plant biomass yielded poor catalytic activity. This was expected, as the highest palladium concentration obtained from plant biomass was low (0.8 g/kg) when compared to previous published work on plant-based palladium nanoparticles (12-18 g/kg). TEM and EDX analysis performed on the aerial tissues indicated that palladium nanoparticles were absent. This is most likely due to the low palladium concentration accumulated in the shoot biomasses of

willow and miscanthus (0.8 & 0.5 g/kg respectively). However, these experiments were conducted in very different conditions to the original hydroponics studies using Arabidopsis. The experiments using Arabidopsis were carried out as part of a proof-of-concept study, to explore whether plant-derived palladium nanoparticles could confer commercially-comparable catalytic activity, and the experimental setup favoured high levels palladium uptake by Arabidopsis. In contrast, this work aimed to reproduce a phytomining scenario, with plants grown on synthetic ore media containing palladium to mimic the real conditions of mine wastes. Considering the ability of willow and miscanthus to tolerate and accumulate significant concentrations of palladium in the presence of other toxic metals, it can be proposed that these plants could be suitable field-applicable candidates for phytomining of mine wastes. Furthermore, another point that needs to be considered is the length of cyanide treatment time; cyanide was only applied for seven days, in a single dose in all experiments in this study. As only the solubilised palladium ions need to be within the rhizosphere to be taken up, the indiscriminate application of saturating doses of cyanide can result in the leaching, and loss, of potentially extractable metal. Further optimisation of cyanide treatment would need to be carried out, to tailor the solubilisation and boost the uptake of palladium into the upper parts of the plants. Although the use of cyanide raises some environmental concerns, the concentration used throughout this work (0.01 %) is the cyanide concentration currently used by mining industries to extract gold [294]. As explained in Chapter 3, cyanide will decompose into less toxic chemicals when exposed to sunlight, air and other oxidants and studies show that the presence of willow massively enhanced cyanide degradation [168-172]. This work has also shown that the addition of cyanide did not significantly affect the growth of willow and miscanthus.

Overall, considering the beneficial impact towards the environment and low cost of operation and maintenance, this plant-based technology can be considered to be more beneficial to the environment than using chemical-based approaches for metal extraction from mine wastes.

### 7.3 Expression of bacterial *merA* gene to improve precious metals uptake and tolerance in plants

Many researchers have shown that genetic engineering can be an efficient tool to improve plant performance, including increasing uptake, translocation and tolerance to various heavy metals. This may be by manipulating endogenous genes or by the introduction of foreign genes such as from bacteria or yeast, to introduce improved traits for metal uptake and sequestration. Examples of successful plant genetic engineering approaches have been detailed in Chapter 4.

In this study, the potential of genetic engineering to improve the ability of plants to take up and tolerate palladium and gold were investigated. In the literature, there are many papers describing how genetic engineering can enhance metal tolerance in plants and increase accumulation of non-essential metals such as arsenic [139], mercury [135, 140-142], lead [213] and cadmium [82]. However, no work has been published on the use of transgenic plants for palladium and gold.

Previous work has reported that the expression of MerA confers on Arabidopsis plants enhanced tolerance to mercury and gold, by reducing the metal to the inert zero valent form [135]. In this study, *merA* was cloned and expressed in Arabidopsis and the experiments of Rugh et al [135] was repeated. While the MerA-expressing plants produced in this work showed enhanced tolerance to mercury, tolerance to palladium or gold was not enhanced. Similarly expression of *merA* in *E.coli* conferred resistance to mercury but not gold or palladium. Further studies demonstrated that gold and palladium are not substrates for MerA but rather that they act as inhibitors of MerA. These results contradict the Rugh et al study [135] and a study by Summers and Sugarman [143] which used the absorption spectroscopy technique to demonstrate that gold was a substrate for MerA. No further explanation and verification was reported in by Rugh et al [135].

In the study presented here, the root growth of MerA-expressing lines were actually found to be significantly shorter than the wild type when grown on gold or palladium. This could be due to the presence of the general metal binding sequence MXCXXC in MerA, the metals might bind to the enzyme causing a conformational change, but without further reduction the gold and palladium ions are causing localised toxicity, visualised as a shorter root length of the MerA transgenic lines as compared to the wildtype. To test this hypothesis, the amount of gold or palladium accumulated in the transgenic lines could be compared with the wild type using ICP-MS.

#### **7.4 The use of synthetic peptides to increase metal nanoparticle formation in plants.**

Another interesting approach in Chapter 6, which is still being investigated in the Bruce laboratory, is the use of synthetic biology where short synthetic peptides which have been reported to seed the formation of size-controlled gold [242] and palladium [238, 241] nanoparticles *in vitro*, were tested *in planta*. Recent work published by the Bruce group revealed that Arabidopsis plants were able to synthesise various sizes of palladium nanoparticles after 24 hours of treatment with 10 mM palladium solution [22]. Based on both findings, it was hypothesised that transgenic plants expressing specific short synthetic peptides might be able to finely tune and control the desired size of metal nanoparticles formation *in planta*. Quantitative PCR analysis has confirmed that the transgenic plants are expressing the genes encoding the short peptides. Results obtained from the TEM analysis revealed that the transgenic lines expressing the Epsilon peptide (GASLWWSEKL) contained the highest percentage distribution of gold nanoparticles with a diameter size less than 10 nm, an ideal range of gold nanoparticle size used many catalytic reactions [257]. This is also in agreement with the results obtained from the work done by Tan et al [242] where the Epsilon peptides expressed *in vitro* were able to seed the formation of smaller size gold nanoparticles compared to Alpha, Beta and Delta peptide sequences. Interestingly, it was observed that Epsilon plant lines also contained the lowest percentage distribution of gold nanoparticles with diameter size larger than 30 nm as compared to other transgenic lines tested including wild type plants. Other studies have shown that large gold metal nanoparticles exhibit lower catalytic activity compared to smaller sized gold metal nanoparticles within the range 1 – 10 nm [295-297]. This could be due to the increase in surface areas of the smaller size metal nanoparticles. Catalytic studies with the supported nanoparticles obtained from the transgenic lines are currently still being investigated. As most *in vitro* approaches for forming metal nanoparticles involve strong reducing agent such as NaBH<sub>4</sub>, results presented here in this work offer an exciting and greener approach to synthesising tuneable-sized metal nanoparticles for industrial applications.

## 7.5 Potential involvement of *AtHMA5* in detoxification mechanism of palladium and gold in *Arabidopsis*

Metal transporters play an important role in controlling the homeostasis of metals within plant cells. They also play a crucial part in the detoxification of unwanted or non-essential metals. However, most of the studies conducted are investigating the effect of non-essential metals such as cadmium, lead and chromium that are found in many contaminated areas either as natural deposits or as the results of industrial activity. Noble metals including gold, and the PGMs such as palladium are of lower environmental concern due to their low concentration in the earth and low bioavailability compared to other metals. Nevertheless, these precious metals play a disproportionately larger part in specific industries such as automotive, medical, electrical and jewellery. Thus, it is also important to investigate the plant biochemistry behind the uptake, translocation and detoxification of palladium to provide a better understanding on the effect towards plant growth for future phytomining improvement.

A previous study, along with the results obtained in this work show that gold and palladium cause toxicity to *Arabidopsis* [46]. It was also observed that gold and palladium treatment significantly increased the expression of *AtHMA5* an efflux transporter for copper. HMA5 is highly expressed in the roots of *Arabidopsis* and directly involved in the detoxification mechanism for copper in *Arabidopsis* [79] and *Cucumis sativus* [52], as well as the translocation mechanism of copper in *Oryza sativa* [30]. A P-Type ATPase pump, HMA5 detoxifies excess copper by pumping  $\text{Cu}^+$  against its concentration gradient from the cytosol across the plasma membrane in *Arabidopsis* [79], or via sequestration into the vacuole in cucumber [52]. As *AtHMA5* was highly up regulated when exposed to gold and palladium, it was hypothesised that *AtHMA5* could also be involved in the detoxification of gold and palladium in plant. The hypothesis was further investigated by looking at the growth of an *Arabidopsis hma5-1* mutant knock out and by performing a yeast heterologous study. However, the results here showed that *AtHMA5* is not involved in the detoxification mechanism of gold and palladium in plant.

There are a number of factors that can be related to this observation. One of the reasons could be the presence of heavy metal ATPase 7 (*AtHMA7*) that has high sequence homology to *AtHMA5*. It was shown that *AtHMA7* was also up regulated when the plants were exposed to palladium. It could be that *AtHMA7* is possibly involved in detoxifying palladium. It would be interesting to see the growth sensitivity of plants lacking *AtHMA5* and *AtHMA7* when expose to gold and palladium.

Another factor that needs to be considered is the involvement of metal chaperones in delivering metals to the active site of the transporter. It has previously been shown using yeast two-hybrid experiments that *AtHMA5* interacts with metallochaperones such as *AtATX1* by delivering the chelated excess copper ions to the metal binding sites of the transporter to be pumped out of the cell. Interestingly, a recent study conducted by Shin et al [293] revealed that the high transcription levels of *AtHMA5* did not increase the *atx1* mutant plant tolerance in response to excess copper suggesting a direct involvement of *AtATX1* in copper delivery to *AtHMA5*. Since studies with *hma5-1* mutant lines and yeast complementation assays did not show any direct involvement of *AtHMA5* in detoxification mechanism of gold and palladium, a hypothesis that can be further tested is whether metallochaperones are involved in the intracellular delivery of gold and palladium ions. Other potential metallochaperone candidates that could be investigated are the heavy metal associated isoprenylated plant proteins (HIPPs). These flexible glycine-rich proteins are characterised by the presence of one or two heavy metal binding domain and an isoprenylation motif resulted from the addition of a C-terminal hydrophobic anchor that is important for interaction with other membranes or proteins [298]. Not much is known about these proteins as only few HIPPs have been studied so far. Interestingly, recent work on *AtHIPP06* and *AtHIPP26* had revealed their function in increasing plant tolerance to cadmium but not towards copper and zinc, [298, 299]. It was hypothesised that HIPPs protect the plant by trapping cadmium ions in the cytosol preventing the metal from binding to other essential proteins [299].

## 7.6 Future directions.

For future work on the use of willow and miscanthus in phytomining precious metals, the uptake and accumulation capacity of the willow Green Dicks and miscanthus needs to be further characterised. As miscanthus was only tested on a single concentration of palladium (100 mg/kg), the growth of miscanthus on different palladium concentrations also need to be further characterised, as miscanthus showed high uptake and accumulation of palladium in the shoots as well as tolerance to high palladium and cyanide treatment. It would also be interesting to investigate the uptake capacity of miscanthus when grown on palladium concentrations more akin to those found on mine waste areas (0.7 - 1 mg/kg). As a single cyanide treatment was found to increase palladium translocation onto above ground tissue, it is also important to characterise the optimum dose and concentration of cyanide to maximize palladium accumulation as well as minimizing its effect on plant growth and also the environment. The low catalytic activity could be improved by maximising the amount of palladium accumulated in the aerial tissue of the plants. This can be achieved by optimising the amount of cyanide dose given to the plants grown on mine wastes.

Further characterisation on the uptake and nanoparticle formation of palladium are now currently being investigated. As for gold nanoparticles, the difference observed on the size of gold nanoparticles formed within the epsilon plant lines could be further verified by comparing its performance as a catalyst with other synthetic transgenic plant lines as well as wild type. Since whole plants were exposed to gold solution and investigated, it would be interesting if similar results could be obtained when the plants are grown hydroponically where only the root parts are exposed to the media solution containing metals for a longer period of time. By doing this, subcellular nanoparticles distribution within plant tissues could be investigated to see if expressing these peptides could increase the uptake and translocation of gold nanoparticles into the aerial tissues of plant and therefore increasing plant tolerance to gold. It is also important to repeat this experiments *in vivo* by using commercially synthesised peptides to verify the results of Tan et al.

While the results presented here for AtHMA5 indicate that gold and palladium interact with this protein, AtHMA5 does not have activity towards these metals. An important next step towards identifying the transporters involved in gold and palladium uptake would be to perform a screen of mutant Arabidopsis library. The screen could be initially focused on transporter mutants, but later broadened to

hopefully identify contributing components of the uptake and detoxification pathways. These studies would enable further knowledge to be gained on the biological mechanisms behind the uptake of gold, palladium and related metals. Such an understanding could then pave the way for manipulating the levels of these industrially important metals.

## Appendix

**Table A1:** Elemental composition of synthetic ore material (\*, below 5 ppm limit of detection; n = 5 biological replicates  $\pm$  s.e.m.).

<b>Major elements (% wt)</b>											
	Na <sub>2</sub> O	MgO	Al <sub>2</sub> O <sub>3</sub>	SiO <sub>2</sub>	P <sub>2</sub> O <sub>5</sub>	K <sub>2</sub> O	CaO	TiO <sub>2</sub>	MnO	Fe <sub>2</sub> O <sub>3</sub>	
	Na	Mg	Al	Si	P	K	Ca	Ti	Mn	Fe	
Sand	0.34 $\pm$ 0.04	0.35 $\pm$ 0.03	13.4 $\pm$ 0.4	85 $\pm$ 0.9	0.07 $\pm$ 0.00	6.1 $\pm$ 0.1	0.00 $\pm$ 0.00	0.13 $\pm$ 0.01	0.01 $\pm$ 0.00	1.26 $\pm$ 0.07	
Gravel	0.01 $\pm$ 0.00	0.29 $\pm$ 0.01	29.6 $\pm$ 0.8	67 $\pm$ 0.5	0.04 $\pm$ 0.00	1.8 $\pm$ 0.0	0.00 $\pm$ 0.00	0.11 $\pm$ 0.01	0.01 $\pm$ 0.00	0.72 $\pm$ 0.02	
<b>Trace elements (ppm)</b>											
	V	Cr	Co	Ni	Cu	Zn	Rb	Sr	Y	Zr	Pb
Sand	*	*	*	*	*	22 $\pm$ 0.0	498 $\pm$ 6	40 $\pm$ 1.5	33 $\pm$ 1.7	92 $\pm$ 4.6	8.7 $\pm$ 0.6
Gravel	*	*	*	*	7.3 $\pm$ 0.6	20 $\pm$ 0.6	252 $\pm$ 21	32 $\pm$ 6.6	19 $\pm$ 4.7	90 $\pm$ 14.9	6.5 $\pm$ 0.7

**Table A2:** Analysis for Au and PGMs (RDL = Reportable Detection Limit) (Results from Dr Chris Anderson, Massey University, NZ)

Element	Concentration (ppb)	RDL
Au	19000	1
Ir	<1	1
Os	<56	56
Pd	22000	20
Pt	1700	2
Rh	<5	5
Ru	<150	150

Appendix

**Table A3:** Levels of metals in Super Willow grown on mine waste materials containing 20 mg/kg palladium (Pd). After 4 weeks, plants were dosed with 100 mg/kg cyanide (in the form of cyanide), then harvested after seven days. (n/d, not detected; n = 5 biological replicates  $\pm$  s.e.m.).

Metal	Metals in leaf tissues (mg/kg)			Stem tissues (mg/kg)		
	No cyanide	+ cyanide	Fold change	No cyanide	+ cyanide	Fold change
Zn	80 $\pm$ 9	260 $\pm$ 58	3.25	50 $\pm$ 4.8	43 $\pm$ 2.4	0.88
Pd	1.4 $\pm$ 0.21	90 $\pm$ 33	64.77	0.29 $\pm$ 0.01	14 $\pm$ 3.6	49
Cd	0.62 $\pm$ 0.15	1.89 $\pm$ .032	3.06	0.92 $\pm$ 0.12	1.37 $\pm$ 0.40	1.49
Pt	n/d	0.06 $\pm$ 9.12	-	n/d	n/d	-
Au	n/d	6.4 $\pm$ 9.12	-	n/d	18 $\pm$ 3.6	-
Pb	6.5 $\pm$ 2.22	42 $\pm$ 8.33	6.52	7.6 $\pm$ 1.8	13 $\pm$ 2.3	1.79

Appendix

**Table A4:** Quantitative phase analysis on mine feed

<b>Mineral</b>	<b>Ideal Formula</b>	<b>Feed (wt.%)</b>
Quartz	SiO <sub>2</sub>	6.8
Clinocllore	(Mg,Fe <sup>2+</sup> ) <sub>5</sub> Al(Si <sub>3</sub> Al)O <sub>10</sub> (OH) <sub>8</sub>	10.7
Biotite	K(Mg,Fe) <sub>3</sub> (AlSi <sub>3</sub> O <sub>10</sub> )(OH) <sub>2</sub>	1.5
Actinolite	Ca <sub>2</sub> (Mg,Fe) <sub>5</sub> Si <sub>8</sub> O <sub>22</sub> (OH) <sub>2</sub>	40.1
Talc	Mg <sub>3</sub> Si <sub>4</sub> O <sub>10</sub> (OH) <sub>2</sub>	3.9
Plagioclase	NaAlSi <sub>3</sub> O <sub>8</sub> – CaAl <sub>2</sub> Si <sub>2</sub> O <sub>8</sub>	8.7
Andesine (Plagioclase)	(Na,Ca)(Si,Al) <sub>4</sub> O <sub>8</sub>	25.0
Ankerite- Dolomite	Ca(Fe <sup>2+</sup> ,Mg,Mn)(CO <sub>3</sub> ) <sub>2</sub> - CaMg(CO <sub>3</sub> ) <sub>2</sub>	1.4
Ulvöspinel ?	Fe <sup>2+</sup> <sub>2</sub> TiO <sub>4</sub>	0.7
Pyrite	FeS <sub>2</sub>	0.7
Chalcopyrite	CuFeS <sub>2</sub>	0.5
Pentlandite	(Fe,Ni) <sub>9</sub> S <sub>8</sub>	-
Millerite	NiS	-
Merenskyite ?	(Pd,Pt)(Te,Bi) <sub>2</sub>	-
Total		100.0

**Table A5:** Elemental composition of mine waste materials measured by LiBO<sub>2</sub>/Li<sub>2</sub>B<sub>4</sub>O<sub>7</sub> fusion ICP-MS analysis

<b>Element</b>	<b>Concentration (ppm)</b>
Ba	82
Be	1
Ce	5.8
Co	78.3
Cs	2.2
Dy	0.45
Er	0.31
Eu	0.2
Ga	10.4
Gd	0.58
Hf	0.7
Ho	0.14
La	2.9
Lu	0.07
Nb	0.9
Nd	2.1
Pr	0.66
Rb	12.1
Sm	0.42
Sn	<1
Sr	178.9
Ta	<0.1
Tb	0.1
Th	1
Tm	0.08
U	0.1
V	106
W	1.1
Y	3.4
Yb	0.42
Zr	21.1

**Table A6:** Elemental composition of mine waste materials measured by leaching in hot (95°C) Aqua Regia for ICP-MS

<b>Element</b>	<b>Concentration (ppm)</b>
Ag	2.7
As	3.7
Au	23250
Bi	0.5
Cd	0.1
Cu	1157
Hg	<0.01
Mo	5
Ni	1051
Pb	3.3
Sb	2.3
Se	5.8
Tl	0.1
Zn	20

**Abbreviations**

μM	Micro molar
½ MS (A)	half strength Murashige and Skoog medium (Agar)
A	Alanine
ABC	ATP binding cassette
ADP	Adenine diphosphate
ANOVA	Analysis of variance
ArsC	Arsenic reductase
<i>At</i>	<i>Arabidopsis thaliana</i>
ATP	Adenine triphosphate
AU\$	Australian dollar
CaCl <sub>2</sub>	Calcium chloride
CaMV-35S	Cauliflower mosaic virus 35S promoter
CAX	Calcium exchanger
<i>Cc</i>	<i>Cajanus cajan</i>
cDNA	Complementary DNA
CN	Cyanide
CO	Carbon monoxide
Col-0	Columbia-0
COPT	Copper transporters
Cot1	Cobalt toxicity 1
<i>Cs</i>	<i>Cucumis sativus</i>
CTAB	Cetrimonium bromide
CuSO <sub>4</sub>	Copper sulphate
DAB	Diaminobenzidine
DAPI	Diamindino-2-phenylindole
DTT	Dithiothreitol
DNA	Deoxyribonucleic acid
E	Glutamate
ECS	Glutamylcysteine synthetase
EDDS	Ethylenediamine-N,N'-disuccinic acid
EDTA	Ethylenediaminetetraacetic acid

## Abbreviations

EDX	Energy dispersive X-ray spectroscopy
EPR	Electron paramagnetic resonance
F	Phenylalanine
FAD	Flavin adenine dinucleotide
FPLC	Fast protein liquid chromatography
FRO	Ferric reduction oxidase
G	Glycine
g	Gram
GC-FID	Gas chromatography flame ionisation detector
GSH	Glutathione
GWAS	Genome-wide association study
H	Histidine
h	Hour
H <sub>3</sub> BO <sub>3</sub>	Boric acid
Ha	Hectare
HC	Hydrocarbon
HEDTA	N-hydroxyethyl-EDTA
HEPES	4-(2-hydroxyethyl)-1-piperazineethanesulfonic acid
Hg(SR) <sub>2</sub>	Mercury-thiol sulphur complex
HgCl <sub>2</sub>	Mercury chloride
HMA	Heavy metal ATPase
HSC	Heat shock cognate
I	Isoleucine
IAA	Iso amyl alcohol
ICP-MS	Inductive coupled plasma mass spectrometry
IPTG	Isopropyl thio-β-D-galacto-pyranoside
IRT	Iron-regulated transporters
K	Kelvin
K	Lysine
K <sub>2</sub> PdCl <sub>4</sub>	Potassium tetrachloropalladate
KAuCl <sub>4</sub>	Potassium tetrachloroaurate
KCN	Potassium cyanide

## Abbreviations

kDa	Kilodalton
keV	Kiloelectronvolt
kg	Kilogram
KH <sub>2</sub> PO <sub>4</sub>	Monopotassium phosphate
KNO <sub>3</sub>	Potassium nitrate
L	Leucine
L	Litre
LB	Luria bertani
LPD	Lipoamide dehydrogenase
MALDI TOF	Matrix-assisted laser desorption ionization time-of-flight
MerA	Mercuric reductase
<i>merA</i>	Mercuric reductase gene
MerB	Organomercury lyase
mg	Milligram
MgSO <sub>4</sub>	Magnesium sulphate
mL	Milli litre
mM	Milli molar
Mmol	Milli mole
mmol.m <sup>-2</sup> .s <sup>-1</sup>	Millimole. Per meter squared. Per second
MnSO <sub>4</sub>	Manganase (II) sulfate
MT	Metallothionein
MTP	Metal tolerance proteins
N	Asparagine
Na <sub>2</sub> MoO <sub>4</sub>	Sodium molybdate
NaBH <sub>4</sub>	Sodium borohydride
NADPH	Nicotinamide adenine dinucleotide phosphate
NaOH	Sodium hydroxide
NaPH <sub>2</sub> O <sub>2</sub>	Sodium hypophosphite
NAS	Nicotinamine synthase
NASC	European arabidopsis stock centre
ng	Nanogram
NH <sub>4</sub> NO <sub>3</sub>	Ammonium nitrate

## Abbreviations

NH <sub>4</sub> SCN	Ammonium thiocyanate
NLMWOA	Natural, low molecular weight organic acids
nm	nanometer
NO <sub>x</sub>	Nitrogen oxide
NRAMP	Natural resistance associated macrophage proteins
NSS	Noran system six
NTA	Nitrilotriacetic acid
ocs	Octopine synthase
Os	<i>Oryza sativa</i>
Oz	Ounce
P	Proline
PAH	Polycyclic aromatic hydrocarbon
PC	Phytochelatin
PCR	Polymerase chain reaction
PCS	Phytochelatin synthase
PdNO <sub>3</sub>	Palladium nitrate
PGM	Platinum group metal
PMSF	Phenylmethylsulfonyl fluoride
Ppb	Parts per billion
Ppm	Parts per million
Q	Glutamine
qPCR	Quantitative PCR
QTL	Quantitative trait locus
R	Arginine
RNA	Ribonucleic acid
S	Serine
SD	Standard deviation
SDS PAGE	Sodium dodecyl sulphate polyacrylamide gel electrophoresis
SOM	Synthetic ore material
Sp.	Species
T	Threonine
TAIR	The Arabidopsis information resource

## Abbreviations

TCA	Tricarboxylic acid cycle
T-DNA	Transfer DNA
TEM	Transmission electron microscopy
TIP	Tonoplast intrinsic proteins
USD	United States dollar
V	Valine
v/v	Volume per volume
W	Tryptophan
w/m <sup>2</sup>	watt per meter squared
w/w	weight per weight
Y	Tyrosine
YCF	Yeast cadmium factor
YSD	Yeast synthetic drop-out
YSL	Yellow stripe1-like proteins
ZIP	Zinc-regulated transporters
ZnSO <sub>4</sub>	Zinc sulphate
Zrc1	Zinc resistance conferring 1
ΔΔCt	Double delta threshold cycle
μF	Microfarad
μmoles.m <sup>-2</sup> .s <sup>-1</sup>	Micromole. Per meter squared. Per second

## References

1. Quandl. Metal Prices. 2012 [cited 2016; Available from: <https://www.quandl.com/collections/markets/>.
2. Canada, E., Overview of Reviewed Facility-Reported Data 2014.
3. Canada, E., Summary Report: Reviewed 2011 NPRI Facility-Level Data. 2011.
4. Nickel, M.N., Annual Report 2013. 2013.
5. Asif, Z. and Z. Chen, Environmental management in North American mining sector. *Environmental Science and Pollution Research*, 2016. **23**(1): p. 167-179.
6. Johnson MS, B.A., Prevention of heavy metal pollution from mine wastes by vegetative stabilisation. *Trans Inst Min Metall A.*, 1977(86): p. 47–55.
7. Krzaklewski, W. and M. Pietrzykowski, Selected Physico-Chemical Properties of Zinc and Lead Ore Tailings and their Biological Stabilisation. *Water, Air, and Soil Pollution*, 2002. **141**(1): p. 125-141.
8. Mendez, M.O., E.P. Glenn, and R.M. Maier, Phytostabilization Potential of Quailbush for Mine Tailings. *Journal of Environmental Quality*, 2007. **36**(1): p. 245-253.
9. Gil-Loaiza, J., et al., Phytostabilization of mine tailings using compost-assisted direct planting: Translating greenhouse results to the field. *Science of The Total Environment*, 2016. **565**: p. 451-461.
10. Anderson, R., Agouron Day 1: Introduction and Kam Kotia Mine Tailings. 2011.
11. Bardon, J., McArthur River Mine tailings dam. 2015: Australia.
12. Hill, D., Guidelines for Assessing the Design, Size and Operation of Sedimentation Ponds Used in Mining. Ministry of environment, lands, and parks cariboo region, williams lake, British Columbia, 1996: p. 2-17.
13. commission, E., Reference document on best available techniques for; management of tailings and waste-rock in mining activities. 2009. p. 12-16.
14. Report, M.W.C., Two million tonnes a day; a mine waste primer. 2009: p. 1-10.
15. Breitenbach, A.J., Backfilling depleted open pit mines with lined landfills, tailings impoundments, and ore heap leach pads for reduced closure costs, in *Geo Americas 2008 2008*, Geosynthetics in mining Cancun, Mexico.
16. DME, Guidelines on the safe design and operating standards for tailings storage. 1999.
17. Commission, E., Draft reference document on best available techniques for management of tailings and waste-rock in mining activities. European Commission. 2004: Edificio EXPO, Seville, Spain. p. 562-563.
18. Engels, J. Water Management Considerations for Conventional Storage. 2016; Available from: <http://www.tailings.info/technical/water.htm>.
19. Engels, J. In Pit tailings storage. 2016; Available from: <http://www.tailings.info/storage/inpit.htm>.
20. Engels, J. Backfill of Tailings to Underground Workings. 2016; Available from: <http://www.tailings.info/storage/backfill.htm>.
21. Sheoran, V., A.S. Sheoran, and P. Poonia, Phytomining: A review. *Minerals Engineering*, 2009. **22**(12): p. 1007-1019.
22. Parker, H.L., et al., Supported palladium nanoparticles synthesized by living plants as a catalyst for suzuki-miyaura reactions. *PLoS One*, 2014. **9**(1): p. e87192.
23. Hunt, A.J., T.J. Farmer, and J.H. Clark, CHAPTER 1 Elemental Sustainability and the Importance of Scarce Element Recovery, in *Element Recovery and Sustainability*. 2013, The Royal Society of Chemistry. p. 1-28.

## References

24. Kalidindi, S.B. and B.R. Jagirdar, Nanocatalysis and Prospects of Green Chemistry. *ChemSusChem*, 2012. **5**(1): p. 65-75.
25. Reck, B.K., et al., Anthropogenic Nickel Cycle: Insights into Use, Trade, and Recycling. *Environmental Science & Technology*, 2008. **42**(9): p. 3394-3400.
26. R. Rumpold, J.A., Recycling of Platinum Group Metals From Automotive Catalysts by an Acidic Leaching Process, in *Platinum 2012*. 2012, The Southern African Institute of Mining and Metallurgy.
27. Hunt, A.J., et al., Phytoextraction as a tool for green chemistry. *Green Processing and Synthesis*, 2014. **3**(1): p. 3-22.
28. Clemens, S., Molecular mechanisms of plant metal tolerance and homeostasis. *Planta*, 2001. **212**(4): p. 475-486.
29. Clemens, S., M.G. Palmgren, and U. Krämer, A long way ahead: understanding and engineering plant metal accumulation. *Trends in Plant Science*, 2002. **7**(7): p. 309-315.
30. Deng, F., et al., A member of the heavy metal P-type ATPase OsHMA5 is involved in xylem loading of copper in rice. *Plant Physiol*, 2013. **163**(3): p. 1353-62.
31. Mari, S., et al., Root-to-shoot long-distance circulation of nicotianamine and nicotianamine–nickel chelates in the metal hyperaccumulator *Thlaspi caerulescens*. *Journal of Experimental Botany*, 2006. **57**(15): p. 4111-4122.
32. Shah, K. and J.M. Nongkynrih, Metal hyperaccumulation and bioremediation. *Biologia Plantarum*, 2007. **51**(4): p. 618-634.
33. Schützendübel, A. and A. Polle, Plant responses to abiotic stresses: heavy metal-induced oxidative stress and protection by mycorrhization. *J Exp Bot*, 2002. **53**(372): p. 1351-65.
34. Nagajyoti, P.C., K.D. Lee, and T.V.M. Sreekanth, Heavy metals, occurrence and toxicity for plants: a review. *Environmental Chemistry Letters*, 2010. **8**(3): p. 199-216.
35. Lewis, S., M.E. Donkin, and M.H. Depledge, Hsp70 expression in *Enteromorpha intestinalis* (Chlorophyta) exposed to environmental stressors. *Aquatic Toxicology*, 2001. **51**(3): p. 277-291.
36. Stadtman, E.R., Oxidation of Free Amino Acids and Amino Acid Residues in Proteins by Radiolysis and by Metal-Catalyzed Reactions. *Annual Review of Biochemistry*, 1993. **62**(1): p. 797-821.
37. Hegedüs, A., S. Erdei, and G. Horváth, Comparative studies of H<sub>2</sub>O<sub>2</sub> detoxifying enzymes in green and greening barley seedlings under cadmium stress. *Plant Science*, 2001. **160**(6): p. 1085-1093.
38. Coleman, J.R., Carbonic Anhydrase and Its Role in Photosynthesis, in *Photosynthesis: Physiology and Metabolism*, R.C. Leegood, T.D. Sharkey, and S. von Caemmerer, Editors. 2000, Springer Netherlands: Dordrecht. p. 353-367.
39. Prask, J.A. and D.J. Plocke, A Role for Zinc in the Structural Integrity of the Cytoplasmic Ribosomes of *Euglena gacilis*. *Plant Physiol*, 1971. **48**(2): p. 150-5.
40. Wenzel, W.W., et al., Rhizosphere characteristics of indigenously growing nickel hyperaccumulator and excluder plants on serpentine soil. *Environmental Pollution*, 2003. **123**(1): p. 131-138.
41. Zornoza, P., S. Robles, and N. Martin, Alleviation of nickel toxicity by ammonium supply to sunflower plants. *Plant and Soil*, 1999. **208**(2): p. 221-226.
42. Shaw, B.P., S.K. Sahu, and R.K. Mishra, Heavy Metal Induced Oxidative Damage in Terrestrial Plants, in *Heavy Metal Stress in Plants: From Biomolecules to Ecosystems*, M.N.V. Prasad, Editor. 2004, Springer Berlin Heidelberg: Berlin, Heidelberg. p. 84-126.

## References

43. Das, P., S. Samantaray, and G.R. Rout, Studies on cadmium toxicity in plants: a review. *Environ Pollut*, 1997. **98**(1): p. 29-36.
44. Hernandez, L.E., R. Carpena-Ruiz, and A. Gárate, Alterations in the mineral nutrition of pea seedlings exposed to cadmium. *Journal of Plant Nutrition*, 1996. **19**(12): p. 1581-1598.
45. Mukherji S, M.P., Toxic effects of lead growth and metabolism of germinating rice (*Oryza sativa* L.) seeds mitosis of onion (*Allium cepa*) root tip cells. *India Journal of Experimental Biology*, 1976. **14**: p. 519-521.
46. Taylor, A., Gold uptake and tolerance in *Arabidopsis*, in Department of Biology. 2011, University of York.
47. Taylor, A.F., et al., Investigating the Toxicity, Uptake, Nanoparticle Formation and Genetic Response of Plants to Gold. *PLoS ONE*, 2014. **9**(4): p. e93793.
48. Ronchini, M., et al., Palladium uptake by *Pisum sativum*: partitioning and effects on growth and reproduction. *Environ Sci Pollut Res Int*, 2015. **22**(10): p. 7600-11.
49. Battke, F., et al., Palladium exposure of barley: uptake and effects. *Plant Biol (Stuttg)*, 2008. **10**(2): p. 272-6.
50. Desbrosses-Fonrouge, A.-G., et al., *Arabidopsis thaliana* MTP1 is a Zn transporter in the vacuolar membrane which mediates Zn detoxification and drives leaf Zn accumulation. *FEBS Letters*, 2005. **579**(19): p. 4165-4174.
51. Dräger, D.B., et al., Two genes encoding *Arabidopsis halleri* MTP1 metal transport proteins co-segregate with zinc tolerance and account for high MTP1 transcript levels. *The Plant Journal*, 2004. **39**(3): p. 425-439.
52. Migocka, M., et al., Functional and Biochemical Characterization of Cucumber Genes Encoding Two Copper ATPases CshMA5.1 and CshMA5.2. *J Biol Chem*, 2015. **290**(25): p. 15717-29.
53. Park, J., et al., The phytochelatin transporters AtABCC1 and AtABCC2 mediate tolerance to cadmium and mercury. *The Plant Journal*, 2012. **69**(2): p. 278-288.
54. Grill, E., E.L. Winnacker, and M.H. Zenk, Phytochelatins: the principal heavy-metal complexing peptides of higher plants. *Science*, 1985. **230**(4726): p. 674-6.
55. Pilon-Smits, E. and M. Pilon, Phytoremediation of Metals Using Transgenic Plants. *Critical Reviews in Plant Sciences*, 2002. **21**(5): p. 439-456.
56. Csiszár, J., et al., Glutathione-Related Enzyme System: Glutathione Reductase (GR), Glutathione Transferases (GSTs) and Glutathione Peroxidases (GPXs), in Redox State as a Central Regulator of Plant-Cell Stress Responses, D.K. Gupta, J.M. Palma, and F.J. Corpas, Editors. 2016, Springer International Publishing: Cham. p. 137-158.
57. Gill, S.S. and N. Tuteja, Reactive oxygen species and antioxidant machinery in abiotic stress tolerance in crop plants. *Plant Physiology and Biochemistry*, 2010. **48**(12): p. 909-930.
58. Cobbett, C.S., A family of phytochelatin synthase genes from plant, fungal and animal species. *Trends in Plant Science*. **4**(9): p. 335-337.
59. Maitani, T., et al., The Composition of Metals Bound to Class III Metallothionein (Phytochelatin and Its Desglycyl Peptide) Induced by Various Metals in Root Cultures of *Rubia tinctorum*. *Plant Physiol*, 1996. **110**(4): p. 1145-1150.
60. Schmöger, M.E.V., M. Oven, and E. Grill, Detoxification of Arsenic by Phytochelatins in Plants. *Plant Physiology*, 2000. **122**(3): p. 793-802.
61. Howden, R., et al., Cadmium-sensitive, *cad1* mutants of *Arabidopsis thaliana* are phytochelatin deficient. *Plant Physiol*, 1995. **107**(4): p. 1059-66.
62. Bennett, L.E., et al., Analysis of transgenic Indian mustard plants for phytoremediation of metal-contaminated mine tailings. *J Environ Qual*, 2003. **32**(2): p. 432-40.

## References

63. Brunetti, P., et al., Cadmium tolerance and phytochelatin content of *Arabidopsis* seedlings over-expressing the phytochelatin synthase gene AtPCS1. *J Exp Bot*, 2011. **62**(15): p. 5509-19.
64. Song, W.-Y., et al., Phytochelatin–metal(loid) transport into vacuoles shows different substrate preferences in barley and *Arabidopsis*. *Plant, Cell & Environment*, 2014. **37**(5): p. 1192-1201.
65. R. Benatti, M., et al., Metallothionein deficiency impacts copper accumulation and redistribution in leaves and seeds of *Arabidopsis*. *New Phytologist*, 2014. **202**(3): p. 940-951.
66. Guo, W.J., M. Meetam, and P.B. Goldsbrough, Examining the Specific Contributions of Individual *Arabidopsis* Metallothioneins to Copper Distribution and Metal Tolerance. *Plant Physiol*, 2008. **146**(4): p. 1697-706.
67. Gautam, N., et al., Genome-wide identification of rice class I metallothionein gene: tissue expression patterns and induction in response to heavy metal stress. *Funct Integr Genomics*, 2012. **12**(4): p. 635-47.
68. Nath, S., et al., Arsenic stress in rice: Redox consequences and regulation by iron. *Plant Physiology and Biochemistry*, 2014. **80**: p. 203-210.
69. Sekhar, K., et al., Metallothionein 1 (CcMT1) of pigeonpea (*Cajanus cajan*, L.) confers enhanced tolerance to copper and cadmium in *Escherichia coli* and *Arabidopsis thaliana*. *Environmental and Experimental Botany*, 2011. **72**(2): p. 131-139.
70. de la Fuente, J.M., et al., Aluminum tolerance in transgenic plants by alteration of citrate synthesis. *Science*, 1997. **276**(5318): p. 1566-8.
71. Anoop, V.M., et al., Modulation of citrate metabolism alters aluminum tolerance in yeast and transgenic canola overexpressing a mitochondrial citrate synthase. *Plant Physiol*, 2003. **132**(4): p. 2205-17.
72. Zhou, G., et al., Enhancing the aluminium tolerance of barley by expressing the citrate transporter genes SbMATE and FRD3. *Journal of Experimental Botany*, 2014.
73. Pianelli, K., et al., Nicotianamine Over-accumulation Confers Resistance to Nickel in *Arabidopsis thaliana*. *Transgenic Research*, 2005. **14**(5): p. 739-748.
74. Romkens, P., et al., Potentials and drawbacks of chelate-enhanced phytoremediation of soils. *Environmental Pollution*, 2002. **116**(1): p. 109-121.
75. do Nascimento, C.W.A., D. Amarasiriwardena, and B. Xing, Comparison of natural organic acids and synthetic chelates at enhancing phytoextraction of metals from a multi-metal contaminated soil. *Environmental Pollution*, 2006. **140**(1): p. 114-123.
76. Lee, S. and B.S. Kang, Phytochelatin is not a primary factor in determining copper tolerance. *Journal of Plant Biology*, 2005. **48**(1): p. 32-38.
77. Eren, E. and J.M. Arguello, *Arabidopsis* HMA2, a divalent heavy metal-transporting P(1B)-type ATPase, is involved in cytoplasmic Zn<sup>2+</sup> homeostasis. *Plant Physiol*, 2004. **136**(3): p. 3712-23.
78. Hussain, D., et al., P-Type ATPase Heavy Metal Transporters with Roles in Essential Zinc Homeostasis in *Arabidopsis*. *The Plant Cell*, 2004. **16**(5): p. 1327-1339.
79. Andres-Colas, N., et al., The *Arabidopsis* heavy metal P-type ATPase HMA5 interacts with metallochaperones and functions in copper detoxification of roots. *Plant J*, 2006. **45**(2): p. 225-36.
80. Boutigny, S., et al., HMA1 and PAA1, two chloroplast-envelope PIB-ATPases, play distinct roles in chloroplast copper homeostasis. *Journal of Experimental Botany*, 2014. **65**(6): p. 1529-1540.
81. Kim, Y.-Y., et al., AtHMA1 contributes to the detoxification of excess Zn(II) in *Arabidopsis*. *The Plant Journal*, 2009. **58**(5): p. 737-753.

## References

82. Gravot, A., et al., AtHMA3, a plant P1B-ATPase, functions as a Cd/Pb transporter in yeast. *FEBS Letters*, 2004. **561**(1–3): p. 22-28.
83. Courbot, M., et al., A major quantitative trait locus for cadmium tolerance in *Arabidopsis halleri* colocalizes with HMA4, a gene encoding a heavy metal ATPase. *Plant Physiol*, 2007. **144**(2): p. 1052-65.
84. Sautron, E., et al., HMA6 and HMA8 are two chloroplast Cu<sup>+</sup>-ATPases with different enzymatic properties. *Biosci Rep*, 2015.
85. Sievers, F., et al., Fast, scalable generation of high-quality protein multiple sequence alignments using Clustal Omega. *Mol Syst Biol*, 2011. **7**: p. 539.
86. Verret, F., et al., Overexpression of AtHMA4 enhances root-to-shoot translocation of zinc and cadmium and plant metal tolerance. *FEBS Lett*, 2004. **576**(3): p. 306-12.
87. Mills, R.F., et al., The plant P1B-type ATPase AtHMA4 transports Zn and Cd and plays a role in detoxification of transition metals supplied at elevated levels. *FEBS Letters*, 2005. **579**(3): p. 783-791.
88. Morel, M., et al., AtHMA3, a P(1B)-ATPase Allowing Cd/Zn/Co/Pb Vacuolar Storage in *Arabidopsis*. *Plant Physiol*, 2009. **149**(2): p. 894-904.
89. Kobayashi, Y., et al., Amino acid polymorphisms in strictly conserved domains of a P-type ATPase HMA5 are involved in the mechanism of copper tolerance variation in *Arabidopsis*. *Plant Physiol*, 2008. **148**(2): p. 969-80.
90. Cunningham, S.D. and D.W. Ow, Promises and Prospects of Phytoremediation. *Plant Physiol*, 1996. **110**(3): p. 715-719.
91. Watanabe, M.E., Phytoremediation on the brink of commercialization. *Environ Sci Technol*, 1997. **31**(4): p. 182A-6A.
92. Anderson, C.W.N., et al., Phytomining for nickel, thallium and gold. *Journal of Geochemical Exploration*, 1999. **67**(1–3): p. 407-415.
93. Chaney, R.L., et al., Method for phytomining of nickel, cobalt and other metals from soil. 1998, US Patent. p. 711,784.
94. Wilson-Corral, V., C.W.N. Anderson, and M. Rodriguez-Lopez, Gold phytomining. A review of the relevance of this technology to mineral extraction in the 21st century. *Journal of Environmental Management*, 2012. **111**: p. 249-257.
95. Robinson, B.H., et al., The potential of the high-biomass nickel hyperaccumulator *Berkheya coddii* for phytoremediation and phytomining. *Journal of Geochemical Exploration*, 1997. **60**(2): p. 115-126.
96. Robinson, B.H., et al., The nickel hyperaccumulator plant *Alyssum bertolonii* as a potential agent for phytoremediation and phytomining of nickel. *Journal of Geochemical Exploration*, 1997. **59**(2): p. 75-86.
97. Robinson, B.H., R.R. Brooks, and B.E. Clothier, Soil Amendments Affecting Nickel and Cobalt Uptake by *Berkheya coddii*: Potential Use for Phytomining and Phytoremediation. *Annals of Botany*, 1999. **84**(6): p. 689-694.
98. Raskin, I., et al., Bioconcentration of heavy metals by plants. *Current Opinion in Biotechnology*, 1994. **5**(3): p. 285-290.
99. Baker, A.J.M., et al., Environmental biotechnology in waste treatment and recycling The possibility of in situ heavy metal decontamination of polluted soils using crops of metal-accumulating plants. *Resources, Conservation and Recycling*, 1994. **11**(1): p. 41-49.
100. McGrath, S.P. and F.J. Zhao, Phytoextraction of metals and metalloids from contaminated soils. *Curr Opin Biotechnol*, 2003. **14**(3): p. 277-82.
101. Fischerova, Z., et al., A comparison of phytoremediation capability of selected plant species for given trace elements. *Environ Pollut*, 2006. **144**(1): p. 93-100.
102. Keeling, S.M., et al., Nickel and Cobalt Phytoextraction by the Hyperaccumulator *Berkheya coddii*: Implications for Polymetallic

## References

- Phytomining and Phytoremediation. International Journal of Phytoremediation, 2003. **5**(3): p. 235-244.
103. Greger, M. and T. Landberg, Cadmium accumulation in *Salix* in relation to cadmium concentration in the soil. null. Vol. null. 1995. null.
  104. Kuzovkina, Y.A., M. Knee, and M.F. Quigley, Cadmium and copper uptake and translocation in five willow (*Salix L.*) species. Int J Phytoremediation, 2004. **6**(3): p. 269-87.
  105. Meers, E., et al., Potential of five willow species (*Salix spp.*) for phytoextraction of heavy metals. Environmental and Experimental Botany, 2007. **60**(1): p. 57-68.
  106. Nissim, W.G., et al., Early response of willow to increasing silver concentration exposure. Int J Phytoremediation, 2014. **16**(7-12): p. 660-70.
  107. Bang, J., et al., Phytoremediation of Heavy Metals in Contaminated Water and Soil Using *Miscanthus sp.* Goedae-Uksae 1. International Journal of Phytoremediation, 2015. **17**(6): p. 515-520.
  108. Korzeniowska, J. and E. Stanislawska-Glubiak, Phytoremediation potential of *Miscanthus x giganteus* and *Spartina pectinata* in soil contaminated with heavy metals. Environ Sci Pollut Res Int, 2015. **22**(15): p. 11648-57.
  109. Pidlisnyuk, V., et al., Sustainable Land Management: Growing *Miscanthus* in Soils Contaminated with Heavy Metals. Journal of Environmental Protection, 2014. **Vol.05No.08**: p. 8.
  110. Pidlisnyuk, V., et al., *Miscanthus* as a Productive Biofuel Crop for Phytoremediation. Critical Reviews in Plant Sciences, 2014. **33**(1): p. 1-19.
  111. Sun, Y.Y., et al., Phytoremediation of soils contaminated with phenanthrene and cadmium by growing willow (*Salix x aureo-pendula CL 'j1011'*). Int J Phytoremediation, 2016. **18**(2): p. 150-6.
  112. Wang, W., et al., Effect of heavy metals combined stress on growth and metals accumulation of three *Salix* species with different cutting position. Int J Phytoremediation, 2016. **18**(8): p. 761-7.
  113. Zhivotovsky, O.P., et al., Lead uptake and translocation by willows in pot and field experiments. Int J Phytoremediation, 2011. **13**(8): p. 731-49.
  114. Greger, M. and T. Landberg, Use of Willow in Phytoextraction. International Journal of Phytoremediation, 1999. **1**(2): p. 115-123.
  115. Arduini, I., et al., Response of *miscanthus* to toxic cadmium applications during the period of maximum growth. Environmental and Experimental Botany, 2006. **55**(1-2): p. 29-40.
  116. Arduini, I., et al., Low cadmium application increase *miscanthus* growth and cadmium translocation. Environmental and Experimental Botany, 2004. **52**(2): p. 89-100.
  117. Iqbal, M., A. Bermond, and I. Lamy, Impact of *miscanthus* cultivation on trace metal availability in contaminated agricultural soils: Complementary insights from kinetic extraction and physical fractionation. Chemosphere, 2013. **91**(3): p. 287-294.
  118. Bosiacki, M., Influence of increasing nickel content in soil on *Miscanthus x giganteus* Greef and Deu. Yielding and on the content of nickel in above-ground biomass, Archives of Environmental Protection. 2015. p. 72.
  119. Gleason, M.L., et al., Effects of stem density upon sediment retention by salt marsh cord grass, *Spartina alterniflora loisel.* Estuaries, 1979. **2**(4): p. 271-273.
  120. Martínez Domínguez, D., R. Torronteras Santiago, and F. Córdoba Garcí a, Modulation of the antioxidative response of *Spartina densiflora* against iron exposure. Physiologia Plantarum, 2009. **136**(2): p. 169-179.
  121. Blaylock, M.J., et al., Enhanced Accumulation of Pb in Indian Mustard by Soil-Applied Chelating Agents. Environmental Science & Technology, 1997. **31**(3): p. 860-865.

## References

122. Huang, J.W., et al., Phytoremediation of Lead-Contaminated Soils: Role of Synthetic Chelates in Lead Phytoextraction. *Environmental Science & Technology*, 1997. **31**(3): p. 800-805.
123. Anderson, C.W.N., et al., Harvesting a crop of gold in plants. *Nature*, 1998. **395**(6702): p. 553-554.
124. Anderson, C., F. Moreno, and J. Meech, A field demonstration of gold phytoextraction technology. *Minerals Engineering*, 2005. **18**(4): p. 385-392.
125. Anderson, C.W., et al., In vivo effect of copper and silver on synthesis of gold nanoparticles inside living plants. *ACS Sustainable Chemistry & Engineering*, 2013. **1**(6): p. 640-648.
126. Anderson, C.W.N., Stewart, R.B., Moreno, F.N., Wreesmann, C.T., Gardea-Torresday, J.L., Robinson, B., Meech, J.A., Gold phytomining. Novel developments in a plant-based mining system. *Gold 2003 Conference*, World Gold Council, Vancouver, 2003: p. 35-45.
127. Duo, L.-A., Y.-B. Gao, and S.-L. Zhao, Heavy Metal Accumulation and Ecological Responses of Turfgrass to Rubbish Compost with EDTA Addition. *Journal of Integrative Plant Biology*, 2005. **47**(9): p. 1047-1054.
128. Meers, E., et al., Chemically assisted phytoextraction: a review of potential soil amendments for increasing plant uptake of heavy metals. *Int J Phytoremediation*, 2008. **10**(5): p. 390-414.
129. Krishnamurti, G.S.R., et al., Kinetics of cadmium release from soils as influenced by organic acids: Implication in cadmium availability. *Journal of Environmental Quality*, 1997. **26**(1): p. 271-277.
130. Meers, E., et al., Enhanced phytoextraction: In search of EDTA alternatives. *International Journal of Phytoremediation*, 2004. **6**(2): p. 95-109.
131. Tandy, S., R. Schulin, and B. Nowack, Uptake of Metals during Chelant-Assisted Phytoextraction with EDDS Related to the Solubilized Metal Concentration. *Environmental Science & Technology*, 2006. **40**(8): p. 2753-2758.
132. Quartacci, M.F., et al., Phytoextraction of metals from a multiply contaminated soil by Indian mustard. *Chemosphere*, 2006. **63**(6): p. 918-925.
133. Kayser, A., et al., Enhancement of Phytoextraction of Zn, Cd, and Cu from Calcareous Soil: The Use of NTA and Sulfur Amendments. *Environmental Science & Technology*, 2000. **34**(9): p. 1778-1783.
134. Chiu, K.K., Z.H. Ye, and M.H. Wong, Enhanced uptake of As, Zn, and Cu by *Vetiveria zizanioides* and *Zea mays* using chelating agents. *Chemosphere*, 2005. **60**(10): p. 1365-1375.
135. Rugh, C.L., et al., Mercuric ion reduction and resistance in transgenic *Arabidopsis thaliana* plants expressing a modified bacterial *merA* gene. *Proc Natl Acad Sci U S A*, 1996. **93**(8): p. 3182-7.
136. Pulford, I.D. and C. Watson, Phytoremediation of heavy metal-contaminated land by trees--a review. *Environ Int*, 2003. **29**(4): p. 529-40.
137. Hirschi, K.D., et al., Expression of *Arabidopsis* CAX2 in tobacco. Altered metal accumulation and increased manganese tolerance. *Plant Physiol*, 2000. **124**(1): p. 125-33.
138. Bhuiyan, M.S.U., et al., Overexpression of *AtATM3* in *Brassica juncea* confers enhanced heavy metal tolerance and accumulation. *Plant Cell, Tissue and Organ Culture (PCTOC)*, 2011. **107**(1): p. 69-77.
139. Dhankher, O.P., et al., Engineering tolerance and hyperaccumulation of arsenic in plants by combining arsenate reductase and [gamma]-glutamylcysteine synthetase expression. *Nat Biotech*, 2002. **20**(11): p. 1140-1145.

## References

140. Bizily, S.P., et al., Phytoremediation of methylmercury pollution: merB expression in *Arabidopsis thaliana* confers resistance to organomercurials. *Proc Natl Acad Sci U S A*, 1999. **96**(12): p. 6808-13.
141. Bizily, S.P., C.L. Rugh, and R.B. Meagher, Phytodetoxification of hazardous organomercurials by genetically engineered plants. *Nat Biotech*, 2000. **18**(2): p. 213-217.
142. Rugh, C.L., et al., Development of transgenic yellow poplar for mercury phytoremediation. *Nat Biotech*, 1998. **16**(10): p. 925-928.
143. Summers, A.O. and L.I. Sugarman, Cell-free mercury(II)-reducing activity in a plasmid-bearing strain of *Escherichia coli*. *J Bacteriol*, 1974. **119**(1): p. 242-9.
144. Survey, U.G., Mineral Commodity Summaries 2015. 2015. p. 196.
145. Survey, U.G., Global Mine Production of Palladium From 2010 to 2015, by Country, in USGS-Mineral Commodity Summaries. 2016. p. 127.
146. Matthey, J., Platinum Group Metals Market Report November 2015. 2015.
147. G. J. K. Acres, B.J.C., Platinum Catalysts for Exhaust Purification. *Platinum Metals Review*, 1972. **16**(3): p. 74.
148. Twigg, M.V., Twenty-Five Years of Autocatalysts. *Platinum Metals Review*, 1999. **43**(4): p. 168-171.
149. Golunski, S., Why Use Platinum in Catalytic Converters ? *Platinum Metals Review*, 2007. **51**(3): p. 162.
150. Picquet, M., Organometallics as Catalysts in the Fine Chemical Industry. *Platinum Metals Review*, 2013. **57**(4): p. 272-280.
151. Colon, P., N. Pradelle-Plasse, and J. Galland, Evaluation of the long-term corrosion behavior of dental amalgams: influence of palladium addition and particle morphology. *Dental Materials*, 2003. **19**(3): p. 232-239.
152. Ferrier, G.G., A.R. Berzins, and N.M. Davey, The Production of Palladium Powders for Electronic Applications. *Platinum Metals Review*, 1985. **29**(4): p. 175-179.
153. Nassar, N.T., Limitations to elemental substitution as exemplified by the platinum-group metals. *Green Chemistry*, 2015. **17**(4): p. 2226-2235.
154. Chaney, R., Plant uptake of inorganic waste constituents. 1983.
155. Harris, A.T., et al., Indicative assessment of the feasibility of Ni and Au phytomining in Australia. *Journal of Cleaner Production*, 2009. **17**(2): p. 194-200.
156. Harris, A.T. and R. Bali, On the formation and extent of uptake of silver nanoparticles by live plants. *Journal of Nanoparticle Research*, 2007. **10**(4): p. 691-695.
157. Nemitandani, T., et al., The potential of *Berkheya coddii* for phytoextraction of nickel, platinum, and palladium contaminated sites. *Toxicological & Environmental Chemistry*, 2006. **88**(2): p. 175-185.
158. Nkrumah, P.N., et al., Current status and challenges in developing nickel phytomining: an agronomic perspective. *Plant and Soil*, 2016. **406**(1): p. 55-69.
159. Broadhurst, C.L. and R.L. Chaney, Growth and Metal Accumulation of an *Alyssum murale* Nickel Hyperaccumulator Ecotype Co-cropped with *Alyssum montanum* and Perennial Ryegrass in Serpentine Soil. *Frontiers in Plant Science*, 2016. **7**(451).
160. van der Ent, A., et al., Agromining: farming for metals in the future? *Environ Sci Technol*, 2015. **49**(8): p. 4773-80.
161. Rodrigues, J., et al., Life cycle assessment of agromining chain highlights role of erosion control and bioenergy. *Journal of Cleaner Production*, 2016. **139**: p. 770-778.

## References

162. Cordos, E., et al., Evaluation of soil pollution with copper, lead, zinc and cadmium in the mining area Baia Mare. REVISTA DE CHIMIE-BUCHAREST-ORIGINAL EDITION-, 2007. **58**(5): p. 470.
163. Mudder, T. and M. Botz, Cyanide and society: a critical review. ejmp & ep (European Journal of Mineral Processing and Environmental Protection), 2004. **4**(1): p. 62-74.
164. Leduc G, P.R., McCracken IR, The effects of cyanides on aquatic organisms with emphasis upon freshwater fishes. 1982.
165. Da Rosa CD, L.J., Golden Dreams, Poisoned Streams. Mineral Policy Center, Washington DC, 1997.
166. Larsen, M., S. Trapp, and A. Pirandello, Removal of cyanide by woody plants. Chemosphere, 2004. **54**(3): p. 325-333.
167. Peiser, G.D., et al., Formation of cyanide from carbon 1 of 1-aminocyclopropane-1-carboxylic acid during its conversion to ethylene. Proc Natl Acad Sci U S A, 1984. **81**(10): p. 3059-63.
168. Larsen, M., A.S. Ucisik, and S. Trapp, Uptake, metabolism, accumulation and toxicity of cyanide in Willow trees. Environ Sci Technol, 2005. **39**(7): p. 2135-42.
169. Larsen, M. and S. Trapp, Uptake of iron cyanide complexes into willow trees. Environ Sci Technol, 2006. **40**(6): p. 1956-61.
170. Yu, X.Z. and J.D. Gu, Uptake, accumulation and metabolic response of ferricyanide in weeping willows. J Environ Monit, 2009. **11**(1): p. 145-52.
171. Ebbs, S., et al., Transport and metabolism of free cyanide and iron cyanide complexes by willow. Plant, Cell & Environment, 2003. **26**(9): p. 1467-1478.
172. Yu, X., S. Trapp, and P. Zhou, Phytotoxicity of cyanide to weeping willow trees. Environ Sci Pollut Res Int, 2005. **12**(2): p. 109-13.
173. Bjarnholt, N., et al., Leaching of cyanogenic glucosides and cyanide from white clover green manure. Chemosphere, 2008. **72**(6): p. 897-904.
174. Evangelou, M.W., et al., Metal uptake and allocation in trees grown on contaminated land: implications for biomass production. Int J Phytoremediation, 2013. **15**(1): p. 77-90.
175. Punshon, T. and N. Dickinson, Heavy Metal Resistance and Accumulation Characteristics in Willows. International Journal of Phytoremediation, 1999. **1**(4): p. 361-385.
176. Didier, T., et al., Prospects of *Miscanthus x giganteus* for PAH phytoremediation: A microcosm study. Industrial Crops and Products, 2012. **36**(1): p. 276-281.
177. Balsamo, R.A., et al., Utilization of grasses for potential biofuel production and phytoremediation of heavy metal contaminated soils. Int J Phytoremediation, 2015. **17**(1-6): p. 448-55.
178. Wang, Q., et al., Model optimization of cadmium and accumulation in switchgrass (*Panicum virgatum* L.): potential use for ecological phytoremediation in Cd-contaminated soils. Environmental science and pollution research international, 2015. **22**(21): p. 16758-16771.
179. Landberg, T. and M. Greger, Appl. Geochem., 1996. **11**(null): p. 175.
180. Landberg, T., et al., Willow vegetation filters for municipal wastewaters and sludges. null. Vol. null. 1994. 133.
181. Kim, S.J., et al., Analysis of the biomass content of various *Miscanthus* genotypes for biofuel production in Korea. Industrial Crops and Products, 2012. **38**: p. 46-49.
182. Pyter, R., et al., Agronomic Experiences with *Miscanthus x giganteus* in Illinois, USA, in Biofuels: Methods and Protocols, R.J. Mielenz, Editor. 2009, Humana Press: Totowa, NJ. p. 41-52.
183. Vassilev, A., et al., The Use of Plants for Remediation of Metal-Contaminated Soils. TheScientificWorldJOURNAL, 2004. **4**: p. 9-34.

## References

184. Richard Lord, J.A., Andy Lane, Jonathan Scurlock, Graham Street, Biomass, Remediation, re-Generation (BioReGen Life Project): Reusing brownfield sites for renewable energy crops, in GeoCongress. 2008, ASCE Geotechnical Special Publication: New Orleans. p. pp527-534.
185. Witters, N., et al., Phytoremediation, a sustainable remediation technology? II: Economic assessment of CO<sub>2</sub> abatement through the use of phytoremediation crops for renewable energy production. *Biomass and Bioenergy*, 2012. **39**: p. 470-477.
186. Naidu, S.L., et al., Cold tolerance of C<sub>4</sub> photosynthesis in *Miscanthus x giganteus*: adaptation in amounts and sequence of C<sub>4</sub> photosynthetic enzymes. *Plant Physiol*, 2003. **132**(3): p. 1688-97.
187. Techer, D., et al., Contribution of *Miscanthus x giganteus* root exudates to the biostimulation of PAH degradation: an in vitro study. *Sci Total Environ*, 2011. **409**(20): p. 4489-95.
188. Utmazian, M.N.D.S, Wieshammer, G., Vega, R., Wenzel, W.W. Hydroponic screening for metal resistance and accumulation of cadmium and zinc in twenty clones of willows and poplars. *Environmental Pollution*. 2007. **148**(1): p. 155-165.
189. Mleczek, M., et al., Hydroponic estimation of heavy metal accumulation by different genotypes of *Salix*. *Journal of Environmental Science and Health, Part A*, 2010. **45**(5): p. 569-578.
190. Theron, A.J., et al., Effects of platinum and palladium ions on the production and reactivity of neutrophil-derived reactive oxygen species. *Free Radic Biol Med*, 2004. **36**(11): p. 1408-17.
191. Liu, T.Z., et al., Palladium or platinum exacerbates hydroxyl radical mediated DNA damage. *Free Radic Biol Med*, 1997. **23**(1): p. 155-61.
192. Hideg, É., C. Spetea, and I. Vass, Singlet oxygen and free radical production during acceptor- and donor-side-induced photoinhibition. *Biochimica et Biophysica Acta (BBA) - Bioenergetics*, 1994. **1186**(3): p. 143-152.
193. Vass, I., Molecular mechanisms of photodamage in the Photosystem II complex. *Biochimica et Biophysica Acta (BBA) - Bioenergetics*, 2012. **1817**(1): p. 209-217.
194. Chen, M., et al., Toxic effect of palladium on embryonic development of zebrafish. *Aquat Toxicol*, 2015. **159**: p. 208-16.
195. García-Sánchez, S., I. Bernales, and S. Cristobal, Early response to nanoparticles in the *Arabidopsis* transcriptome compromises plant defence and root-hair development through salicylic acid signalling. *BMC Genomics*, 2015. **16**(1): p. 1-17.
196. Wang, Z., et al., CuO Nanoparticle Interaction with *Arabidopsis thaliana*: Toxicity, Parent-Progeny Transfer, and Gene Expression. *Environmental Science & Technology*, 2016. **50**(11): p. 6008-6016.
197. Jing Chen , K.H., A new technique for extraction of platinum group metals by pressure cyanidation. *Hydrometallurgy*, 2006. **82**(3-4): p. 16-171.
198. Han, K.N. and X. Meng, Recovery of platinum group metals and rhenium from materials using halogen reagents. 1996, Google Patents.
199. Schoeman, E.a.B., S.M. and Akdogan, G. and Eksteen, J. J, The Recovery of Platinum, Palladium, and Gold from a Cyanide Heap Solution, with use of Ion Exchange Resins, in *The 5th International Platinum Conference*, H.W. Glen, Editor. 2013, The South African Institute of Mining & Metallurgy: Sun City, Africa. p. pp. 729-742.
200. Hung, C.-H. and S.G. Pavlostathis, Aerobic biodegradation of thiocyanate. *Water Research*, 1997. **31**(11): p. 2761-2770.
201. Douglas Gould, W., et al., A critical review on destruction of thiocyanate in mining effluents. *Minerals Engineering*, 2012. **34**: p. 38-47.

## References

202. Castric, P.A., K.J. Farnden, and E.E. Conn, Cyanide metabolism in higher plants. V. The formation of asparagine from -cyanoalanine. *Arch Biochem Biophys*, 1972. **152**(1): p. 62-9.
203. Boucabeille, C., et al., Microbial degradation of metal complexed cyanides and thiocyanate from mining wastewaters. *Environmental Pollution*, 1994. **84**(1): p. 59-67.
204. Hutchinson, M., K.I. Johnstone, and D. White, The Taxonomy of certain Thiobacilli. *Microbiology*, 1965. **41**(3): p. 357-366.
205. Bakos, I., A. Paszternák, and D. Zitoun, Pd/Ni Synergistic Activity for Hydrogen Oxidation Reaction in Alkaline Conditions. *Electrochimica Acta*, 2015. **176**: p. 1074-1082.
206. Mallikarjuna, K., et al., Palladium nanoparticles: Single-step plant-mediated green chemical procedure using Piper betle leaves broth and their anti-fungal studies. *International Journal of Chemical and Analytical Science*, 2013. **4**(1): p. 14-18.
207. Sheny, D.S., D. Philip, and J. Mathew, Rapid green synthesis of palladium nanoparticles using the dried leaf of *Anacardium occidentale*. *Spectrochimica Acta Part A: Molecular and Biomolecular Spectroscopy*, 2012. **91**: p. 35-38.
208. Sathishkumar, M., et al., Phyto-crystallization of palladium through reduction process using *Cinnamom zeylanicum* bark extract. *Journal of Hazardous Materials*, 2009. **171**(1-3): p. 400-404.
209. Gardea-Torresdey, J.L., et al., Use of ICP and XAS to determine the enhancement of gold phytoextraction by *Chilopsis linearis* using thiocyanate as a complexing agent. *Anal Bioanal Chem*, 2005. **382**(2): p. 347-52.
210. Vert, G., et al., IRT1, an Arabidopsis transporter essential for iron uptake from the soil and for plant growth. *Plant Cell*, 2002. **14**(6): p. 1223-33.
211. Eide, D., et al., A novel iron-regulated metal transporter from plants identified by functional expression in yeast. *Proceedings of the National Academy of Sciences of the United States of America*, 1996. **93**(11): p. 5624-5628.
212. van der Zaal, B.J., et al., Overexpression of a Novel Arabidopsis Gene Related to Putative Zinc-Transporter Genes from Animals Can Lead to Enhanced Zinc Resistance and Accumulation. *Plant Physiology*, 1999. **119**(3): p. 1047-1056.
213. Song, W.Y., et al., Engineering tolerance and accumulation of lead and cadmium in transgenic plants. *Nat Biotechnol*, 2003. **21**(8): p. 914-9.
214. Ledwidge, R., et al., NmerA of Tn501 Mercuric Ion Reductase: Structural Modulation of the pKa Values of the Metal Binding Cysteine Thiols. *Biochemistry*, 2010. **49**(41): p. 8988-8998.
215. Zhang, W.-H. and S.D. Tyerman, Inhibition of Water Channels by HgCl<sub>2</sub> in Intact Wheat Root Cells. *Plant Physiology*, 1999. **120**(3): p. 849-858.
216. Ruiz, O.N. and H. Daniell, Genetic engineering to enhance mercury phytoremediation. *Curr Opin Biotechnol*, 2009. **20**(2): p. 213-9.
217. Barkay, T., S.M. Miller, and A.O. Summers, Bacterial mercury resistance from atoms to ecosystems. *FEMS Microbiol Rev*, 2003. **27**(2-3): p. 355-84.
218. Freedman, Z., C. Zhu, and T. Barkay, Mercury resistance and mercuric reductase activities and expression among chemotrophic thermophilic Aquificae. *Appl Environ Microbiol*, 2012. **78**(18): p. 6568-75.
219. Tezuka, T. and K. Tonomura, Purification and properties of an enzyme catalyzing the splitting of carbon-mercury linkages from mercury-resistant *Pseudomonas* K-62 strain. I. Splitting enzyme 1. *J Biochem*, 1976. **80**(1): p. 79-87.
220. Fox, B.S. and C.T. Walsh, Mercuric reductase: homology to glutathione reductase and lipoamide dehydrogenase. Iodoacetamide alkylation and sequence of the active site peptide. *Biochemistry*, 1983. **22**(17): p. 4082-8.

## References

221. Fox, B. and C.T. Walsh, Mercuric reductase. Purification and characterization of a transposon-encoded flavoprotein containing an oxidation-reduction-active disulfide. *J Biol Chem*, 1982. **257**(5): p. 2498-503.
222. Parkhill, J., et al., Construction and characterization of a mercury-independent MerR activator (MerRAC): transcriptional activation in the absence of Hg(II) is accompanied by DNA distortion. *EMBO J*, 1993. **12**(2): p. 413-21.
223. Ledwidge, R., et al., NmerA of Tn501 mercuric ion reductase: structural modulation of the pKa values of the metal binding cysteine thiols. *Biochemistry*, 2010. **49**(41): p. 8988-98.
224. Ledwidge, R., et al., NmerA, the metal binding domain of mercuric ion reductase, removes Hg<sup>2+</sup> from proteins, delivers it to the catalytic core, and protects cells under glutathione-depleted conditions. *Biochemistry*, 2005. **44**(34): p. 11402-16.
225. Johs, A., et al., Structural characterization of intramolecular Hg(2+) transfer between flexibly linked domains of mercuric ion reductase. *J Mol Biol*, 2011. **413**(3): p. 639-56.
226. Lian, P., et al., X-ray structure of a Hg<sup>2+</sup> complex of mercuric reductase (MerA) and quantum mechanical/molecular mechanical study of Hg<sup>2+</sup> transfer between the C-terminal and buried catalytic site cysteine pairs. *Biochemistry*, 2014. **53**(46): p. 7211-22.
227. Schiering, N., et al., Structure of the detoxification catalyst mercuric ion reductase from *Bacillus* sp. strain RC607. *Nature*, 1991. **352**(6331): p. 168-72.
228. Heaton, A.C., et al., Toward detoxifying mercury-polluted aquatic sediments with rice genetically engineered for mercury resistance. *Environ Toxicol Chem*, 2003. **22**(12): p. 2940-7.
229. Gleave, A.P., A versatile binary vector system with a T-DNA organisational structure conducive to efficient integration of cloned DNA into the plant genome. *Plant Mol Biol*, 1992. **20**(6): p. 1203-7.
230. Livak, K.J. and T.D. Schmittgen, Analysis of relative gene expression data using real-time quantitative PCR and the 2(-Delta Delta C(T)) Method. *Methods*, 2001. **25**(4): p. 402-8.
231. Miller, S.M., et al., Two-electron reduced mercuric reductase binds Hg(II) to the active site dithiol but does not catalyze Hg(II) reduction. *J Biol Chem*, 1986. **261**(18): p. 8081-4.
232. Giovanella, P., et al., Mercury (II) removal by resistant bacterial isolates and mercuric (II) reductase activity in a new strain of *Pseudomonas* sp. B50A. *N Biotechnol*, 2016. **33**(1): p. 216-23.
233. Marshall, J.L., J.E. Booth, and J.W. Williams, Characterization of the covalent mercury (II)-NADPH complex. *J Biol Chem*, 1984. **259**(5): p. 3033-6.
234. Rinderle, S.J., J.E. Booth, and J.W. Williams, Mercuric reductase from R-plasmid NR1: characterization and mechanistic study. *Biochemistry*, 1983. **22**(4): p. 869-76.
235. Gachhui, R., et al., Studies on mercury-detoxicating enzymes from a broad-spectrum mercury-resistant strain of *Flavobacterium rigense*. *Folia Microbiologica*. **42**(4): p. 337-343.
236. Crookes-Goodson, W.J., J.M. Slocik, and R.R. Naik, Bio-directed synthesis and assembly of nanomaterials. *Chemical Society Reviews*, 2008. **37**(11): p. 2403-2412.
237. Brown, S., M. Sarikaya, and E. Johnson, A genetic analysis of crystal growth. *J Mol Biol*, 2000. **299**(3): p. 725-35.

## References

238. Chiu, C.-Y., Y. Li, and Y. Huang, Size-controlled synthesis of Pd nanocrystals using a specific multifunctional peptide. *Nanoscale*, 2010. **2**(6): p. 927-930.
239. Dickerson, M.B., K.H. Sandhage, and R.R. Naik, Protein- and Peptide-Directed Syntheses of Inorganic Materials. *Chemical Reviews*, 2008. **108**(11): p. 4935-4978.
240. Naik, R.R., et al., Biomimetic synthesis and patterning of silver nanoparticles. *Nat Mater*, 2002. **1**(3): p. 169-72.
241. Pacardo, D.B., et al., Biomimetic synthesis of Pd nanocatalysts for the Stille coupling reaction. *ACS Nano*, 2009. **3**(5): p. 1288-96.
242. Tan, Y.N., J.Y. Lee, and D.I. Wang, Uncovering the design rules for peptide synthesis of metal nanoparticles. *J Am Chem Soc*, 2010. **132**(16): p. 5677-86.
243. Slocik, J.M., M.O. Stone, and R.R. Naik, Synthesis of gold nanoparticles using multifunctional peptides. *Small*, 2005. **1**(11): p. 1048-52.
244. Reiss, B.D., et al., Biological Routes to Metal Alloy Ferromagnetic Nanostructures. *Nano Letters*, 2004. **4**(6): p. 1127-1132.
245. Ahmad, G., et al., Rapid Bioenabled Formation of Ferroelectric BaTiO<sub>3</sub> at Room Temperature from an Aqueous Salt Solution at Near Neutral pH. *Journal of the American Chemical Society*, 2008. **130**(1): p. 4-5.
246. Coppage, R., et al., Exploiting Localized Surface Binding Effects to Enhance the Catalytic Reactivity of Peptide-Capped Nanoparticles. *Journal of the American Chemical Society*, 2013. **135**(30): p. 11048-11054.
247. Lim, B., et al., Pd-Pt bimetallic nanodendrites with high activity for oxygen reduction. *Science*, 2009. **324**(5932): p. 1302-5.
248. Tan, Y.N., J.Y. Lee, and D.I.C. Wang, Uncovering the Design Rules for Peptide Synthesis of Metal Nanoparticles. *Journal of the American Chemical Society*, 2010. **132**(16): p. 5677-5686.
249. Coppage, R., et al., Determining Peptide Sequence Effects That Control the Size, Structure, and Function of Nanoparticles. *ACS Nano*, 2012. **6**(2): p. 1625-1636.
250. Iravani, S., Green synthesis of metal nanoparticles using plants. *Green Chemistry*, 2011. **13**(10): p. 2638-2650.
251. Bennett, J.A., et al., Palladium supported on bacterial biomass as a novel heterogeneous catalyst: A comparison of Pd/Al<sub>2</sub>O<sub>3</sub> and bio-Pd in the hydrogenation of 2-pentyne. *Chemical Engineering Science*, 2010. **65**(1): p. 282-290.
252. Singaravelu, G., et al., A novel extracellular synthesis of monodisperse gold nanoparticles using marine alga, *Sargassum wightii* Greville. *Colloids Surf B Biointerfaces*, 2007. **57**(1): p. 97-101.
253. De Corte, S., et al., Bio-palladium: from metal recovery to catalytic applications. *Microbial biotechnology*, 2012. **5**(1): p. 5-17.
254. Yang, C., et al., Viral-templated palladium nanocatalysts for Suzuki coupling reaction. *Journal of Materials Chemistry*, 2011. **21**(1): p. 187-194.
255. Galloway, J.M. and S.S. Staniland, Protein and peptide biotemplated metal and metal oxide nanoparticles and their patterning onto surfaces. *Journal of Materials Chemistry*, 2012. **22**(25): p. 12423-12434.
256. Kim, J., et al., Peptide-mediated shape- and size-tunable synthesis of gold nanostructures. *Acta Biomaterialia*, 2010. **6**(7): p. 2681-2689.
257. Hvolbæk, B., et al., Catalytic activity of Au nanoparticles. *Nano Today*, 2007. **2**(4): p. 14-18.
258. Wilson, O.M., et al., Effect of Pd Nanoparticle Size on the Catalytic Hydrogenation of Allyl Alcohol. *Journal of the American Chemical Society*, 2006. **128**(14): p. 4510-4511.

## References

259. Rima J. Isaifan, S.N., Elena A. Baranova, Particle size effect on catalytic activity of carbon-supported Pt nanoparticles for complete ethylene oxidation. *Applied Catalysis A: General*, 2013. **464-465**: p. 87-94.
260. Arrivault, S., T. Senger, and U. Kramer, The Arabidopsis metal tolerance protein AtMTP3 maintains metal homeostasis by mediating Zn exclusion from the shoot under Fe deficiency and Zn oversupply. *Plant J*, 2006. **46**(5): p. 861-79.
261. Loque, D., et al., Tonoplast intrinsic proteins AtTIP2;1 and AtTIP2;3 facilitate NH<sub>3</sub> transport into the vacuole. *Plant Physiol*, 2005. **137**(2): p. 671-80.
262. Schuler, M.A. and D. Werck-Reichhart, Functional genomics of P450s. *Annu Rev Plant Biol*, 2003. **54**: p. 629-67.
263. Dixon, D.P. and R. Edwards, Glutathione transferases. *Arabidopsis Book*, 2010. **8**: p. e0131.
264. Reith, F., et al., Mechanisms of gold biomineralization in the bacterium *Cupriavidus metallidurans*. *Proc Natl Acad Sci U S A*, 2009. **106**(42): p. 17757-62.
265. Hruz, T., et al., Genevestigator V3: A Reference Expression Database for the Meta-Analysis of Transcriptomes. *Advances in Bioinformatics*, 2008. **2008**: p. 420747.
266. Petris, M.J., et al., Copper-regulated Trafficking of the Menkes Disease Copper ATPase Is Associated with Formation of a Phosphorylated Catalytic Intermediate. *Journal of Biological Chemistry*, 2002. **277**(48): p. 46736-46742.
267. Hirayama, T., et al., RESPONSIVE-TO-ANTAGONIST1, a Menkes/Wilson Disease, 2013;Related Copper Transporter, Is Required for Ethylene Signaling in Arabidopsis. *Cell*. **97**(3): p. 383-393.
268. Binder, B.M., F.I. Rodríguez, and A.B. Bleecker, The Copper Transporter RAN1 Is Essential for Biogenesis of Ethylene Receptors in Arabidopsis. *The Journal of Biological Chemistry*, 2010. **285**(48): p. 37263-37270.
269. Yon Rhee, S., et al., The Arabidopsis Information Resource (TAIR): a model organism database providing a centralized, curated gateway to Arabidopsis biology, research materials and community. *Nucleic Acids Research*, 2003. **31**(1): p. 224-228.
270. Sievers, F., et al., Fast, scalable generation of high-quality protein multiple sequence alignments using Clustal Omega. *Molecular Systems Biology*, 2011. **7**: p. 539-539.
271. Birnbaum, K., et al., A gene expression map of the Arabidopsis root. *Science*, 2003. **302**(5652): p. 1956-60.
272. Völlmecke, C., et al., The ATPases CopA and CopB both contribute to copper resistance of the thermoacidophilic archaeon *Sulfolobus solfataricus*. *Microbiology*, 2012. **158**(6): p. 1622-1633.
273. Kumari, M., G.J. Taylor, and M.K. Deyholos, Transcriptomic responses to aluminum stress in roots of *Arabidopsis thaliana*. *Molecular Genetics and Genomics*, 2008. **279**(4): p. 339-357.
274. del Pozo, T., V. Cambiazo, and M. González, Gene expression profiling analysis of copper homeostasis in *Arabidopsis thaliana*. *Biochemical and Biophysical Research Communications*, 2010. **393**(2): p. 248-252.
275. Forbes, J.R. and D.W. Cox, Functional characterization of missense mutations in ATP7B: Wilson disease mutation or normal variant? *Am J Hum Genet*, 1998. **63**(6): p. 1663-74.
276. Korshunova, Y.O., et al., The IRT1 protein from *Arabidopsis thaliana* is a metal transporter with a broad substrate range. *Plant Mol Biol*, 1999. **40**(1): p. 37-44.

## References

277. Rogers, E.E., D.J. Eide, and M.L. Guerinot, Altered selectivity in an Arabidopsis metal transporter. *Proc Natl Acad Sci U S A*, 2000. **97**(22): p. 12356-60.
278. Besson-Bard, A., et al., Nitric Oxide Contributes to Cadmium Toxicity in Arabidopsis by Promoting Cadmium Accumulation in Roots and by Up-Regulating Genes Related to Iron Uptake. *Plant Physiol*, 2009. **149**(3): p. 1302-15.
279. Connolly, E.L., J.P. Fett, and M.L. Guerinot, Expression of the IRT1 Metal Transporter Is Controlled by Metals at the Levels of Transcript and Protein Accumulation. *Plant Cell*, 2002. **14**(6): p. 1347-57.
280. Baloun, J., et al., Characterization of the HMA7 gene and transcriptomic analysis of candidate genes for copper tolerance in two *Silene vulgaris* ecotypes. *Journal of Plant Physiology*, 2014. **171**(13): p. 1188-1196.
281. Finazzi, G., et al., Ions channels/transporters and chloroplast regulation. *Cell Calcium*, 2015. **58**(1): p. 86-97.
282. Salt, D.E., I. Baxter, and B. Lahner, Ionomics and the Study of the Plant Ionome. *Annual Review of Plant Biology*, 2008. **59**(1): p. 709-733.
283. Danku, J.M.C., et al., Large-Scale Plant Ionomics, in *Plant Mineral Nutrients: Methods and Protocols*, J.M.F. Maathuis, Editor. 2013, Humana Press: Totowa, NJ. p. 255-276.
284. Lahner, B., et al., Genomic scale profiling of nutrient and trace elements in *Arabidopsis thaliana*. *Nat Biotech*, 2003. **21**(10): p. 1215-1221.
285. Hu, S., P. Furst, and D. Hamer, The DNA and Cu binding functions of ACE1 are interdigitated within a single domain. *New Biol*, 1990. **2**(6): p. 544-55.
286. Evans, C.F., D.R. Engelke, and D.J. Thiele, ACE1 transcription factor produced in *Escherichia coli* binds multiple regions within yeast metallothionein upstream activation sequences. *Molecular and Cellular Biology*, 1990. **10**(1): p. 426-429.
287. Culotta, V.C., W.R. Howard, and X.F. Liu, CRS5 encodes a metallothionein-like protein in *Saccharomyces cerevisiae*. *J Biol Chem*, 1994. **269**(41): p. 25295-302.
288. Cizewski Culotta, V., et al., A Physiological Role for *Saccharomyces cerevisiae* Copper/Zinc Superoxide Dismutase in Copper Buffering. *Journal of Biological Chemistry*, 1995. **270**(50): p. 29991-29997.
289. Southron, J.L., U. Basu, and G.J. Taylor, Complementation of *Saccharomyces cerevisiae* ccc2 mutant by a putative P1B-ATPase from *Brassica napus* supports a copper-transporting function. *FEBS Letters*, 2004. **566**(1-3): p. 218-222.
290. Yuan, D.S., et al., The Menkes/Wilson disease gene homologue in yeast provides copper to a ceruloplasmin-like oxidase required for iron uptake. *Proc Natl Acad Sci U S A*, 1995. **92**(7): p. 2632-6.
291. Weissman, Z., et al., The high copper tolerance of *Candida albicans* is mediated by a P-type ATPase. *Proc Natl Acad Sci U S A*, 2000. **97**(7): p. 3520-5.
292. Kaler, S.G., ATP7A-related copper transport diseases emerging concepts and future trends. *Nat Rev Neurol*, 2011. **7**(1): p. 15-29.
293. Shin, L.J., J.C. Lo, and K.C. Yeh, Copper chaperone antioxidant protein1 is essential for copper homeostasis. *Plant Physiol*, 2012. **159**(3): p. 1099-110.
294. Australia, M.C.o., Fact Sheet - Cyanide and Its Use By The Minerals Industry. 2005. p. 1-3.
295. Shimizu, K.-i., et al., Chemoselective Hydrogenation of Nitroaromatics by Supported Gold Catalysts: Mechanistic Reasons of Size- and Support-Dependent Activity and Selectivity. *The Journal of Physical Chemistry C*, 2009. **113**(41): p. 17803-17810.

## References

296. Lin, C., et al., Size effect of gold nanoparticles in catalytic reduction of p-nitrophenol with NaBH<sub>4</sub>. *Molecules*, 2013. **18**(10): p. 12609-20.
297. Boca, S.C., C. Farcau, and S. Astilean, The study of Raman enhancement efficiency as function of nanoparticle size and shape. *Nuclear Instruments and Methods in Physics Research Section B: Beam Interactions with Materials and Atoms*, 2009. **267**(2): p. 406-410.
298. de Abreu-Neto, J.B., et al., Heavy metal-associated isoprenylated plant protein (HIPPP): characterization of a family of proteins exclusive to plants. *FEBS Journal*, 2013. **280**(7): p. 1604-1616.
299. Tehseen, M., et al., Metallochaperone-like genes in *Arabidopsis thaliana*. *Metallomics*, 2010. **2**(8): p. 556-564.